SHEAR STRENGTH OF LIGHTLY REINFORCED CONCRETE BEAMS

by

Michael N. Palaskas

David Darwin

A Report on a Research Project Sponsored by

ARMCO INC.

University of Kansas

Lawrence, Kansas

September 1980

ACKNOWLEDGEMENTS

This report is based on a thesis submitted by Michael N. Palaskas in partial fulfillment of the requirements for the Ph.D. degree. The support of Mr. Palaskas' graduate study by University of Kansas General Research allocation #3215-X038 and the Department of Civil Engineering is gratefully acknowledged.

ARMCO INC. donated the reinforcing steel and funded the reproduction of this report.

Copies of the original load-displacement and load-strain data may be obtained for the price of reproduction from the second author by requesting "Data File SM3."

TABLE OF CONTENTS

LIST OF TABLES

LIST OF FIGURES

CHAPTER 1

INTRODUCTION

1.1 General

One of the modes of failure that can occur in a reinforced concrete structure during its lifetime, is the so-called "shear failure." Such failures reduce the strength of structural elements below their flexural capacity and result in a large reduction in ductility. For this reason shear failures are considered undesirable.

Since the beginning of this century, many investigators have experimentally studied reinforced concrete beams. The results are numerous, but not conclusive enough to develop a universally accepted solution to the shear capacity problem. The absence of a general solution is excellent evidence of the tremendous difficulty involved in solving the problem. Most of the investigations have been unrelated, and unfortunately there has been no systematic overall approach to the test programs. In fact, many times the test specimens have not been representative of those used in real structures.

In spite of this extensive experimental research, there are some areas which have not received much attention until the past decade. One of these areas is the behavior of normally proportioned reinforced concrete beams with small amounts of shear reinforcement and low to optimum percentages of longitudinal reinforcement. It is this category of beams which is the primary interest of this investigation.

1.2 Previous Work

1.2.1 Background

Researchers of the late 1800's were divided over the issue of the

mechanism of the shear failure of reinforced concrete members. Some believed that the cause of shear failure was horizontal shear, others believed it was diagonal tension (2,19).

For a decade, the two groups continued the discussion of the mechanism of shear failure until E. Mörsch, from Germany, resolved this issue (2,19,33). By testing a number of reinforced concrete beams, Mörsch found that diagonal tension was the controlling factor.

After the acceptance of Mörsch's theory, the early specifications in the United States considered the nominal shearing stress, $v = \frac{V}{b_w jd}$ (in which v = nominal shear stress, psi, V = shear force, pounds, b_w = web width, inches, and jd = internal moment arm, inches), to be a measure of diagonal tension and restricted the stress, v, to values less than certain fractions of the cylinder strength, f'_c (2). In 1909 A. N. Talbot pointed out the fallacies of such a procedure (2,40). Testing 106 beams without shear reinforcement, Talbot demonstrated (40) that the main variables affecting the shear strength of reinforced concrete beams without shear reinforcement were the concrete strength, the ratio of beam length to depth, and the percentage of longitudinal reinforcement.

Talbot's findings were ignored until the early 1950's, when A. P. Clark (11) introduced an expression for the effect of the shear-span to depth ratio, a/d, on shear strength. Clark expressed Talbot's findings as:

$$v_n = 7000\ \rho_w + 0.12 f'_c\ d/a + 2500\ \sqrt{\rho_v} \qquad (1.1)$$

in which ρ_w = percentage of longitudinal steel ($\rho_w = A_s/b_w d$), a/d = shear-span, a, to effective depth, d, ratio, ρ_v = ratio of shear reinforcement

($\rho_v = \frac{A_v}{b_w S}$), A_v = area of a stirrup, in^2, A_s = area of longitudinal reinforcement, in^2, and S = stirrup spacing along the axis of the beam, inches.

The a/d ratio provided a way to account for the effect of horizontal flexural tension on shear strength. Unfortunately, the shear-span could not be defined for generalized cases of loading. This handicap was overcome in the early 1950's when researchers at the University of Illinois expressed the shear-span to depth ratio in the modified form of M/Vd, involving bending moment, M, shear force, V, and effective depth, d (2,3). For the case of simple beams with concentrated loads, it is obvious that the term M/Vd is synonymous with the a/d ratio.

From the early 1950's to the present, researchers have made numerous shear tests and found that some other variables influence the shear strengtn of concrete beams (2,3). Among the variables are the type of loading and the type of cross section. The ACI-ASCE Committee on Shear and Diagonal Tension chose to express the shear capacity of reinforced concrete beams without stirrups as a function of the square root of the cylinder strengtn, the shear-span to depth ratio, and the percentage of longitudinal reinforcement (3,5). For beams with web reinforcement, the committee concluded that both the web reinforcement and the concrete contribute to the shear capacity of a member. They found that the nominal shear stress in the concrete at diagonal tension cracking correlated well the concrete contribution at the failure load. The following equation was selected to express the ultimate capacity of reinforced concrete beams in shear.

$$v_n = v_c + r\rho_v f_{vy} \qquad (1.2)$$

in which

v_n = nominal (ultimate) strength, psi, $r = (\sin\alpha + \cos\alpha)$,

α = inclination of web reinforcement to longitudinal axis,

f_{vy} = yield point of web reinforcement, psi, and

v_c = shear stress carried by the concrete equal to shear at diagonal tension cracking, psi.

In the United States design practice, two expressions are given for the shear stress at diagonal tension cracking (5):

$$v_c = 1.9\sqrt{f'_c} + 2500 \frac{\rho_w V_u d}{M_u} \tag{1.3}$$

or, more conservatively,

$$v_c = 2\sqrt{f'_c} \tag{1.4}$$

in which

V_u = factored shear at the section, and

M_u = factored moment at the section.

The expression $r\,\rho_v f_{vy}$ was derived using the truss analogy for beams at failure, assuming that the web reinforcement yields and that diagonal cracks have a horizontal projection equal to the effective depth of the beam.

To insure ductility, the committee set a minimum value of shear reinforcement, $\rho_v f_{vy}$, equal to 50 psi.

The key shortcoming of this procedure is that it does not accurately represent the effects of the various parameters on shear strength and thus

results in a variable factor of safety in the applicable range of the equation. It has been retained in the ACI Building Code (5) because of its relative simplicity and because it has generally provided conservative designs.

One equation, which predicts the diagonal tension cracking stress with good accuracy, was derived by Zsutty (42):

$$v_c = 59 \left(f'_c \rho_w \frac{d}{a}\right)^{1/3} \tag{1.5}$$

This equation was derived using the techniques of dimensional analysis and statictical regression analysis applied to existing shear test data.

The mechanism of shear transfer in reinforced concrete beams with stirrups is not yet completely understood. It is believed that shear is carried to the supports of the beam in five different ways (3,11,13,14,15, 22,32,41,42).

1. shear force in the uncracked concrete,
2. tension forces in the shear reinforcement,
3. forces due to arch action,
4. dowel forces in the flexural reinforcement, and
5. friction forces along the crack.

The relative contribution to shear transfer of these mechanisms depends on such factors as, (3)

1. the geometry of the beam,
2. the type of concrete,
3. the type, amount and detailing of reinforcement,
4. the type, stage and location of loading, and

5. the type of supports.

Fig. 1.1 illustrates qualitatively the relative contributions of the various mechanisms to shear resistance as a function of load.

1.2.2 Rational Approaches

Many researchers have attempted to develop rational solutions to the shear capacity problem (7,8,9,12,16,20,21,22,23,27,30,31,33,34,37,38,39, 43). For beams with stirrups, the major concern of this study, most of the theories can be classified under a few categories.

Modified Truss Analogy

This theory is attributed to Ritter and Mörsch (2,19,33,38). They assume that beams resemble a truss after shear cracking. The top and bottom chords of the truss are the concrete compression zone and longitudinal reinforcement, respectively. The diagonal and vertical struts consist of the beam web and shear reinforcement. The assumption that all shear is carried by the shear reinforcement does not agree well with test data.

North American design methods, as represented by Eqs. (1.2)-(1.4), recognize the contribution of the concrete (5). It is assumed that part of the applied shear is carried by the concrete, and the rest is carried by the shear reinforcement. The concrete contribution has been determined experimentally and thus has an empirical, rather than a rational basis. Failure is assumed to take place after yielding of the shear reinforcement and along a plane oriented at about 45° to the axis of the beam.

The main weaknesses of this method are its inability to accurately express the effects of the percentage of the longitudinal reinforcement and shear-span to depth ratio on the shear capacity of reinforced concrete beams, and the assumption of a constant horizontal crack projection

equal to the effective depth of the beam. For these reasons, the margin of safety provided by this expression is variable.

Plane of Minimum Resistance

The developer of this theory, M.S. Borishansky (7), rationalized that failure can occur along any inclined plane of the beam, if the total shear resistance along that plane is a minimum. It is assumed that after shear cracking, shear is carried by both the stirrups and the concrete. At failure all stirrups along the crack yield. The concrete capacity is not constant, but is a function of the beam depth to crack projection ratio. The capacity versus crack projection relation for the concrete was obtained experimentally.

$$V_c = 0.15\, b_w d\, R_b/z \tag{1.6}$$

in which,

b_w = web width, cm,

d = effective depth, cm,

R_b = design cube strength, kgf/cm^2, and

z = horizontal crack projection, cm.

The stirrup capacity is, also, a function of the crack projection and is expressed as:

$$V_s = \frac{A_v}{s} f_{vy}\, z \tag{1.7}$$

in which,

f_{vy} = yield stress of shear reinforcement, kgf/cm^2,

A_v = area of the vertical stirrups, cm^2, and

s = spacing of stirrups along the axis of beam, cm.

For the case of a beam loaded with concentrated loads, the ultimate shear capacity is:

$$V_n = V_c + V_s = 0.15\ b_w d^2 R_b / z + \frac{A_v}{s} f_{vy}\ z \qquad (1.8)$$

The size of the crack, z, for which the expression of the ultimate shear, V_n, is a minimum can be found after differentiation of Eq. (1.8) with respect to crack projection, z. Using this mathematical technique, Borishansky, obtained the following equation:

$$V_n = 2\sqrt{0.15 b_w d^2 R_b A_v\ f_{vy}/s} \qquad (1.9)$$

The introduction of the variable crack inclination in this method is compatible with the test results reported by a number of investigators (17,22,24,35,37). In contrast, the concrete capacity term is entirely empirical and independent of the percentage of longitudinal reinforcement, ρ_w. This is a weakness in the theory, since ρ_w has been proven experimentally to have an appreciable effect on the shear capacity of reinforced concrete beams (11).

Shear-Compression Theory

The development of this theory is credited to many different investigators (27,30,37,43). One of the most complete approaches is the one developed by Regan (37). In his approach, Regan states that failure is caused by the normal stresses in the compression zone of the beam. He

obtained these stresses using equilibrium equations and an approximate compatibility equation. The compatibility equation relates the total deformations of the concrete and the tension steel, between two planes at the ends of the shear crack, with an average neutral axis depth, as shown in Fig. 1.2. The final equation of ultimate shear capacity is too complex to be practical for design. This is recognized and Regan recommends a graphical or another simplified approach.

The main handicap of the shear-compression failure theories is that they always predict failures caused by crushing of the concrete. Many rectangular beams, and most T-beams, fail in a mode different than compression. These types of failures have been defined as "shearing" failures (35). However, for reinforced concrete beams that fail in the shear-compression mode, this theory satisfactorily predicts the ultimate shear capacity.

Arch Theory

In the "remaining arch" theory (20,21,22,23), it is assumed that cracks generate and propagate perpendicular to the principal tensile stress trajectories and parallel to the principal compressive trajectories in a beam, as shown in Fig. 1.3a. After cracking, the beam is transformed into a number of tied arches, and the applied shear is carried to the beam support by arch action. Only the outside arch is supported directly by the beam supports. The remaining arches are hanging arches. Kani (20,21, 22,23) states that the cause of premature shear failure is not the shear force, but the compression arch forces. Failure is caused by the reduction of the compression arch capacity due to the loss of the supports of the internal hanging arches, as shown in Figs. 1.3 b,c,d. The primary

function of stirrups is to act as the hanging supports of the internal, arches, thus retaining the flexural capacity of the beam. The arch theory provides quantitative results for beams without stirrups. However, it is a qualitative theory for beams with stirrups, and remains impractical for design.

Diagonal Compression Field Theory

Diagonal compression field theory (8,12,16,34) uses a truss model with a variable inclination of the concrete diagonals, as shown in Fig. 1.4. The truss model is approximated with compression and tension chords consisting of the concrete compression zone and the longitudinal reinforcement, respectively. The stirrups represent the posts of the truss, and the continuous diagonal compression field represents the diagonals.

One mode of failure is due to crushing of the concrete in the continuous diagonal compression field, while the shear reinforcement yields, or is still elastic. The other mode of failure is due to yielding of the shear or flexural reinforcement, or both, while the concrete in the continuous diagonal compression field is still intact. In all cases, it is assumed that the top chord of the truss (the compression zone of the beam) has adequate strength to carry the applied loads. This strength is determined from the equations of pure bending.

This represents a weakness in the diagonal compression field theory, since it has been found that combined flexural and shear stresses have an appreciable effect on the capacity of concrete. In addition, it has been observed that in regions of high bending and shear stresses, cracks propagate higher in the compression zone of the beam than they do in regions subject to pure flexure. For these reasons, the capacity of the

compression zone in reinforced concrete beams is significantly reduced when shear forces are present. A rational theory should incorporate this strengtn reduction.

1.2.3 Experimental Work That Impacts on This Study

In 1968 Rajagopalan and Ferguson (36) showed, after testing ten rectangular beams without stirrups and with low percentages of longitudinal reinforcement, that the present code provisions (Eqs. (1.3) and (1.4) are unconservative for low percentages of longitudinal reinforcement. They found that the expression

$$v_c = (0.8 + 100\rho_w)\sqrt{f'_c} \tag{1.9}$$

conservatively represents the shear strength of reinforced concrete beams without stirrups and with a reinforcing ratio, ρ_w, less than 1.2 percent. In the recent "Suggested Revisions to Shear Provisions of ACI Code, 318-71" (4) by ACI-ASCE Committee 426, a similar expression

$$v_c = (0.8 + 120\rho_w)\sqrt{f'_c} \tag{1.10}$$

was recommended.

According to the findings of Bresler and Scordelis (10) in 1963 and Haddadin, Hong, and Mattock (17) in 1971, the effect of the first shear reinforcement on the shear strength of beams is about 75 percent higher than the strength calculated using the ACI Code provisions (5). Beams in these two studies had flexural reinforcing ratios, ρ_w, in excess of 1.8 percent.

In spite of the extensive use of concrete beams with small amounts of shear and longitudinal reinforcement, no experimental work has been performed to determine the shear strength of these beams. Tests on beams of this type are needed and will yield valuable information about the behavior and shear capacity of these commonly used reinforced concrete members.

1.3 Object and Scope

The objectives of this study are to experimentally investigate the behavior of reinforced concrete beams with low amounts of both flexural and shear reinforcement and to develop a useful representation of the shear strength of reinforced concrete beams.

The tests consist of fifteen simply supported T-beams loaded to failure. The major variables in the study are the flexural reinforcing ratio, ρ_w, and amount of shear reinforcement, $\rho_v f_{vy}$. The test results are analyzed and compared with the provisions of the ACI Building Code (5).

A failure model is developed that incorporates the observed shear behavior of reinforced concrete beams and helps explain how shear strength is effected by flexural reinforcing ratio, concrete strength, shear-span to depth ratio, and shear reinforcement.

CHAPTER 2

EXPERIMENTAL WORK

2.1 General

The main purpose of this work is to determine the ultimate shear capacity of slender reinforced concrete beams with small amounts of shear and longitudinal reinforcement. This can be achieved only with a clear shear mode failure of the selected specimens. Therefore, care was taken in the design of the specimens to eliminate all other possible modes of failure. A description of the materials and the procedures used during this experimental work is presented.

2.2 Test Specimens

The test specimens (Fig. 2.1) consisted of fifteen concrete T-beams, eleven with stirrups and four without. The geometry of these specimens was selected to closely resemble members in actual structures. In this manner, the size effect was eliminated. All beams had the same cross section: web width = 7½ inches; total depth = 18 inches; flange width = 24 inches; and flange thickness = 4 inches. The span of the beams was 13'-2", and the length was 20'-0". The 3'-5" overhangs at the ends of the beams increased the embedment and prevented slippage of the reinforcing steel. Non-prestressed, prestressing strands were selected for the longitudinal reinforcement to prevent flexural failures in the test specimens. The use of the high strength steel also allowed high strains to be obtained in the flexural steel, as would occur in continuous reinforced concrete beams undergoing moment redistribution following the formation of one or more plastic hinges.

The beams were divided in three series, as a function of the quantity of the longitudinal reinforcement. Five strands were used for each beam to

eliminate the effect of the arrangement of the longitudinal reinforcement on the shear capacity of the beams. The smooth wire stirrups were spaced at a distance of about half the effective depth of the beam. The amount of longitudinal steel was controlled using different diameter strands, 1/2 inch, 7/16 inch and 0.6 inch for series A, B, and C, respectively. The amount of shear reinforcement, $\rho_v f_{vy}$, varied from 0 to about 110 psi, using different sizes of smooth wire (0.132, 0.186, 0.229 or 0.244 inches in diameter). The flange reinforcement in all beams consisted of two #4 longitudinal bars and #3 transverse bars, spaced as shown in Fig. 2.1. Information on the shear and longitudinal reinforcing steels is summarized in Table 2.1.

2.3 Material Properties and Sizes

2.3.1 Concrete

Concrete was supplied by a local ready mix plant. The concrete was air entrained. Type I cement was used. The nominal size of coarse aggregate was 3/4 inch (locally described as "1/2 inch aggregate").

Mix proportions, compressive strengths and moduli of rupture are presented in Table 2.2. A typical stress-strain curve is shown in Fig. 2.2.

2.3.2 Steel

Three different types of reinforcement were used in the test specimens: prestressing strands, deformed bars and smooth wire.

The flexural steel in all beams was non-prestressed, ASTM A416, Grade 270 Seven-Wire Stress-Relieved Strand. Typical force-strain diagrams for these strands are shown in Figs. 2.3, 2.4 and 2.5.

The flange reinforcement was ASTM A615, Grade 60 deformed billet steel bars.

The stirrups were low carbon smooth wires with a diameter of 0.132, 0.186, 0.229 or 0.244 inches. All wires were annealed in order to obtain

a yield stress close to the design yield stress obtained with deformed reinforcing bars. The wires were supplied in coils because of the manufacturing process. The wire was straightened with a roller. During rolling, residual stresses were introduced. For this reason, the stress-strain curve of these wires was not linear up to the yield point. To obtain a well defined yield point on the stress-strain diagram, all wires were loaded to the yield stress (preyielded). In this manner, a well defined yield plateau was obtained, as shown in Fig. 2.6. Due to work hardening during preyielding, strain aging occurred in the wires. To obtain the actual yield and ultimate loads of the wires on the day of the test, two wire specimens were tested after the failure of each beam. The preyielding loads, as well as the yield and ultimate loads on the day of testing, are presented in Table 2.1.

2.4 Specimen Preparation

The beams were prepared in four stages: (1) fabrication of the reinforcing cage, (2) installation of gages on the reinforcing steel, (3) casting and curing of the concrete, and (4) preparation for the test.

As soon as the stress relieved strand was received, it was flame cut into the desired lengths and stored outside of the laboratory, exposed to the weather. This treatment provided the strands with a uniform coat of rust which improved the bond and prevented slippage of the strands during the tests.

After preyielding, the stirrups were cut to length, bent to shape using a one inch diameter pin, and welded to form a closed loop. The only possible failure mode of the stirrups was by yielding of the stirrups themselves, since slippage of the anchorage was prevented. The strands,

reinforcing bars, and smooth wire stirrups were assembled to form a cage using commercially available wire ties.

Following the fabrication of the reinforcing steel, strain gages were installed on the stirrups and strands, as shown in Fig. 2.7. Information on the gage types and the installation procedures is presented in Appendix B.

Prior to casting the concrete, the plywood form was oiled and sealed, and the reinforcing cage was secured in the form using commercially available steel chairs and form ties. The concrete was placed in two layers (web and flange) with the aid of a cubic yard concrete bucket and an internal vibrator. Ten cylinders and two flexure specimens were made for each test. The forms were removed after three days (except for beams C00 and C50-one day) and covered with a polyethylene sheet. The beam and the control specimens were wet cured together until the compressive strength was at least 3000 psi.

When the concrete compressive strength reached 3000 psi, the beam was lifted to the test supports with a 3 ton capacity crane. For alignment of the beam and uniform bearing stresses at the supports, a quick set gypsum cement grout, Hydrostone, was used. Hydrostone, also, was used to align and secure the loading beam bearing plates on top of the beam. Next, a coat of white wash, made of Hydrostone, was applied to one side of the beam. After drying, the location of neutral axis and the locations of the shear and tensile steel were marked. For comparison, stirrup "locations" were also marked on beams without shear reinforcement. The marking was followed by the installation of the paper gages on the top of the beam, as shown in Fig. 2.7. Finally, the loading system (loading beams, load rods

and hydraulic jacks) were installed.

2.5 Test Equipment

The load was applied to the beam with the aid of a Satec pumping console assembly (an electrically powered, 3000 psi capacity hydraulic loading system) and four 60-ton Enerpac hydraulic jacks. The jacks, located below the structural test floor, pulled on four one-inch diameter steel rods attached to two wide flange beams attached to the test specimens (Fig. 2.8). The one-inch steel rods served as load cells. Two 1/4-inch strain gages were installed on each rod, and then the rods were calibrated within one percent of the total load. In this manner, monitoring of the applied loads was possible with the aid of a strain indicator.

The beam supports were one 6 inch roller and one bolster (Fig. 2.8). To reduce the friction in the bolster, 1/32 inch teflon sheets were inserted between the bearing surfaces of the bolster.

A Vishay Model 220 Data Logging System was used to read the specimen strain gages and one hand operated Budd Instrument P-350 strain indicator was used to obtain the strains in the four loading rods. This combination of strain recorders was used for all beams, except C00 and C75. For these beams, hand operated Budd Instrument P-350 strain indicators were used for all gages.

Three 0.001 inch scale dial gages and one LVDT were used to monitor the deflections.

Four techniques were used to determine the shear cracking loads. These techniques used data obtained from the cracking patterns, the stirrup strain gages, the concrete strain gages, and four 0.0001 inch scale dial gages installed on specially constructed "shear cracking frames"(6) to

measure the increase in beam depth.

2.6 Test Procedure

One dial gage and the LVDT were placed at the center of the span. Two other dial gages were placed at the load points, shown in Fig. 2.8. The four shear cracking frames were secured at the locations of the third and fourth stirrups from the center line of the span, on both sides of the beam. The dial gages were adjusted and the strain gages and the LVDT were connected and balanced.

To check the equipment, all beams were loaded to about one-third of the calculated flexural cracking load and unloaded. The readings of all strain and dial gages were then recorded for zero load. The load was then applied incrementally until the beam failed. The size of the load increments was reduced around the calculated flexural cracking, shear cracking and failure loads. The smallest increments in total load were about 1250 pounds and the largest were about 5000 pounds. At each increment, all strain and dial gage readings were recorded, while the applied load was kept constant. Following the readings, the beam was inspected, and all cracks were marked. The value of the total applied load was inscribed at the end of each crack. In this way, a complete crack propagation history was available from photographs taken during and after the test. In addition, a time log of all actions and observations was kept.

Cracks were marked until very little additional cracking was observed. After failure, all additional cracks were marked, and detailed photographs were taken. The beam tests were followed by tests of the remaining concrete cylinders, flexure specimens and stirrup tension specimens.

The average time for a test, from initial loading to failure, was about one hour and forty-five minutes.

2.7 Results and Observations

Geometric and material information (dimensions, concrete strength, shear-span to depth ratio, percentage of longitudinal reinforcement, and amount of shear reinforcement), the flexural cracking stress and the ultimate shear capacity, $V_{n\ test}$, are presented for each beam in Table 2.3.

Using the photographs which were taken during and after the tests, the complete crack pattern for each beam has been reproduced, except for beams #1 and #2*, in Figs. 2.9-2.13. The heavy crack line represents the failure crack. The numbers represent the total load, to the nearest kip, at which the crack formed.

The deflection dial gage readings are plotted versus the applied load in Figs. 2.14-2.28. The recorded readings of the steel and concrete strain gages are plotted versus the total applied load in Figs. 2.29-2.76. The shear frame dial gage readings are plotted versus the applied load in Figs. 2.77-2.87.

A description of the behavior of a typical beam from the beginning of a test to the time of failure follows:

In the first stages of loading, the beams were free of cracks. Since the stresses were very small and the full section participated in carrying the load, the deflection was small and proportional to the applied load. At a load close to the calculated flexural cracking load (obtained using the ACI (5) modulus of rupture), the first cracks were observed and a

---

* Beams #1 and #2 served as preliminary tests, and complete crack patterns were not obtained.

considerable increase in deflection occurred. These cracks always initiated in the region of pure flexure and extended vertically up to the neutral axis of the uncracked section of the beam. With increasing load, more flexural cracks developed in both the center and the shear span regions of the beam. Cracks in the two regions propagated differently. Cracks in the pure moment section were always vertical, while cracks in the shear span curved toward the point of the applied load, as soon as they entered the area between the level of the tension reinforcement and the neutral axis.

The trend of cracking was almost the same in all beams, except that the number and the size of the cracks seemed to depend on the amount of the flexural reinforcement. Compared to the other series, the beams in Series B (ρ_w = 0.5 percent) exhibited fewer and wider cracks. In contrast, the other series (ρ_w = 0.66 and 0.94 percent) exhibited a greater number of cracks of smaller width. The cracks in the Series C beams (ρ_w = 0.94 percent) were so narrow that additional light was required in order to locate them.

This trend of flexural cracking continued until "shear cracking" began. Shear cracking was accompanied by an increase in stirrup strain and beam depth and a decrease in the compressive strain in the concrete within the shear span. The shear cracks were extensions of the flexural cracks and initiated close to the midheight of the beam. They propagated at an inclination flatter than 45° in two directions, toward the flange and toward the flexural reinforcement. When the bottom end of the crack reached the flexural reinforcement, it continued to propagate with increasing load along the reinforcement for a distance at least equal

to one stirrup spacing. The other end of the crack propagated until it reached the bottom of the flange. From there on, two possible crack paths were observed. For most beams, the crack extended horizontally along the junction of the flange and the web. In a few cases, the crack remained fairly stable after it reached the bottom of the flange, until failure occurred. For beams with the first type of crack path, the crack entered the flange at failure or at a load stage prior to failure. In both cases, failure occurred with a sudden extension of the crack toward the point of loading. The only exception to this failure mode was beam C75. In this beam, the failure crack in the flange was a horizontal crack extending along the total length of the shear span of the beam.

In all cases, the mode of failure was a tensile failure of the flange with no signs of crushing of the concrete. The location of the failure shear crack, (i.e., the horizontal projection of the crack within the shear span) was erratic: sometimes closer to the support, sometimes closer to the applied load, and at other times in the center of the shear span. For the beams without stirrups, the failure crack was always the crack closest to the support. In beams with stirrups, the failure crack was either the crack closest to the support (beams A50a, B50), or an interior crack (beams A25, A25a , A50, C25, C75). In three beams with stirrups (beams A75, B25, C50), failure occurred along a double inclined shear crack.

CHAPTER 3

EVALUATION OF EXPERIMENTAL RESULTS

3.1 General

It is of primary interest in this report to examine how the amount of flexural steel, ρ_w, and web reinforcement, $\rho_v f_{vy}$, affect the behavior of reinforced concrete beams, with special emphasis on shear cracking and ultimate shear capacity.

A description of the findings and a comparison with the current provisions of the ACI Building Code (5) follow.

3.2 Evaluation of Results

3.2.1 Flexural Cracking

The parameter which has the greatest effect on the deflection of these reinforced concrete beams, after flexural cracking, is the amount of longitudinal reinforcement. For the same load, much more deflection was recorded for the beams in Series B (ρ_w about 0.5%) than for the beams in Series C (ρ_w about .94%). This difference is apparent in Figs. 2.14-2.28.

The flexural cracking loads were obtained using the load-deflection curves (Figs. 2.14-2.28) and the load-strain curves for strain gages #1 and #2 (Figs. 2.29-2.76). These loads are in good agreement with the flexural cracking loads calculated using the transformed cross section and $7.5\sqrt{f'_c}$ for the modulus of rupture, f_r, as recommended in the ACI Building Code (5). The calculated stress at flexural cracking varied between $6.18\sqrt{f'_c}$ and $7.57\sqrt{f'_c}$.

3.2.2 Shear Cracking

Four methods were used to determine the shear cracking load. These approaches were based on the stirrup strains, the concrete strains, the increase in beam depth following crack formation, and the cracking patterns. The four methods were used to provide detailed information on beam behavior and to compare procedures for defining "shear cracking." The details of this portion of the study are presented in Reference 6.

The shear cracking load is considered to be the load at which significant changes in the load carrying mechanisms occur, resulting in the redistribution of stresses within the beam. Using this criterion, the objective is to determine the load at which this change occurs. The techniques for analyzing the data are summarized below:

The concrete strain data (Figs. 2.29-2.76) indicates that an appreciable change (reduction) in the compressive strain occurs in the extreme compression fiber within the shear span at a load coinciding with the formation of diagonal cracks. This load is defined as the shear cracking load.

The shear cracking loads are obtained from stirrup strain and depth increase data using Figs. 2.29-2.87. These load-strain and load-depth increase curves show essentially no reading up to a load of 1.5 to 2 times the flexural cracking load. However, in most of the beams, small readings were recorded before the formation of the first shear cracks due to inclined flexural cracks within the shear-span. To obtain the shear cracking load from these figures, the portion of the graph which shows a marked increase in strain or depth is extended back until it intersects the load axis, as illustrated in Fig. 3.1. The point of intersection is defined as the

shear cracking load.

The shear cracking load obtained from the crack patterns (Figs. 2.9-2.13), is assumed to be the load at which a crack forms at the level of the neutral axis (the centroid of the uncracked transformed cross section) at an angle of 45° or less to the longitudinal axis of the beam.

The shear cracking stresses obtained using the four methods are presented in Table 3.1. Results are not available for beams #1 and #2, since these beams were not fully instrumented.

To help reduce the effect of the variable concrete strength, the results are normalized with respect to $(f'_c)^{1/2}$ and $(f'_c)^{1/3}$ in Figs. 3.2 and 3.3 (6). The results are, also, compared with the predictive equations, Eqs (1.3) (1.5) and (1.9), presented by the ACI Building Code (5), Zsutty (42) and Rajagopalan and Ferguson (36), respectively. Presented in this form, the results obtained using the stirrup and concrete strains exhibit much less scatter than the cracking loads obtained using the depth increase and the cracking patterns. Both the stirrup and the concrete strains appear to be more sensitive to the change in the load carrying mechanisms at shear cracking than do the other two procedures.

The shear cracking loads obtained using the concrete and stirrup strains match each other quite well. The values obtained from the depth increase data are equal to or greater than the values obtained from the stirrup and concrete strains. The shear cracking loads obtained from the crack patterns do not show a consistent relationship to the loads obtained from the stirrup and concrete strains.

Overall, the comparison indicates that the loads obtained using the concrete and stirrup strains provide a good indication of the true shear

cracking load of the beam, while the other two methods are not as accurate.

3.2.3 Stirrup Effectiveness

According to the ACI Building Code (5), the contribution of stirrups to the ultimate shear capacity of reinforced concrete beams is expressed as the product of a coefficient, r, and the amount of shear reinforcement, $\rho_v f_{vy}$ ($v_s = r\ \rho_v f_{vy}$). For beams with vertical stirrups, r is equal to one. The contribution of concrete to the ultimate shear capacity is assumed to be equal to the shear cracking stress of the beam, v_c. In this investigation, the shear cracking loads were measured for thirteen of the T-beams tested, and therefore, the stirrup contribution to shear capacity is known for each of these beams.

The stirrup effectiveness factor is defined as the ratio of the stirrup contribution from the tests ($v_n - v_c$) divided by the predicted stirrup capacity according to the ACI Building Code ($\rho_v f_{vy}$). The test stirrup contributions are plotted versus the ACI code stirrup contribution, $\rho_v f_{vy}$, in Figs. 3.4a to 3.4d, for the different methods used to obtain v_c.

Using linear regression analysis, it was found (6) that the stirrup contribution can be expressed reasonably well by the expression:

$$v_n - v_c = 1.5\ \rho_v f_{vy} + c \qquad (3.1)$$

in which

$$c = 2\text{-}8 \text{ psi}.$$

In Figs. 3.4b and 3.4c, it is shown that the correlation coefficient in

this analysis is 0.96 and 0.97 for the cases in which the shear cracking stress is determined from the concrete and stirrup strains, the two methods which appear to be the most reliable methods for the determination of the shear cracking loads.

The stirrup effectiveness factor (neglecting the small value of c) of 1.5 is smaller than the factors 1.80 and 1.75 which were reported by Bresler and Scordelis (10) and Haddadin, Hong and Mattock (17). The reason for this difference probably lies in the different type and amount of longitudinal reinforcement that was used in this study. Only strands were used in this investigation as longitudinal reinforcement, in amounts which never exceeded one percent. Flexural reinforcement in excess of 1.8 percent were used by the other investigators. Both the lower percentage of flexural reinforcing steel and the lower bond strength obtained with the strands, as compared with the reinforcing bars, could have contributed to the lower stirrup effectiveness exhibited in these tests.

3.3 Comparison with Design Equations

3.3.1 Shear Cracking Stress

The shear cracking stresses obtained using the concrete and stirrup strains are compared with loads predicted by Eqs. (1.3) and (1.4) from the ACI Building Code (5), Eq. (1.5) proposed by Zsutty (42) and Eq. (1.9) recommended by Rajagopalan and Ferguson (36), in Table 3.2 and Figs. 3.2b, c and 3.3b, c. The ACI equations provide an unconservative estimate of the shear cracking load for the T-beams tested in this study. Much better predictions are obtained using Eq. (1.5) by Zsutty (42) and Eq. (1.9) by Rajagopalan and Ferguson (36).

3.3.2 Ultimate Shear Stress

A summary of the nominal (ultimate) shear stress obtained from the tests and the values predicted by the current ACI code procedures (Eqs. (1.2), (1.3) and (1.4)) are presented in Table 3.3. These results are compared in Fig. 3.5.

A comparison of Figs. 3.2b, c, 3.3b, c and 3.5 indicates that there is a better agreement between the test results and the calculated values for nominal shear strength than there is for the shear carcking stress. The reason for the improved agreement in the case of shear strength is that, while the ACI equations (Eqs. (1.3) and (1.4)) overestimate the contribution of the concrete to the shear strength for beams with longitudinal reinforcement ratios less than about one percent, they underestimate the contribution of the stirrups (Eq. (1.2)). The two errors appear to counterbalance each other. The net result is a good agreement between the calculated nominal shear capacity and the experimental shear capacity obtained in this study. This coincidence will not be true for the whole range of percentages of longitudinal reinforcement, ρ_w, to which the ACI equation, Eq. (1.3), applies. The application of Eq. (1.2) gives a different margin of safety in beams with different amounts of longitudinal and shear reinforcement. The result is that in the case of beams with very low amounts of longitudinal and shear reinforcement , the ACI (5) procedure could predict shear capacity values a little on the unsafe side, while in beams with large percentages of longitudinal reinforcement the procedure is overconservative. It should be noted that in the case of T-beams with small amounts of shear and longitudinal reinforcement, it appears that the ACI procedure is safe and in good agreement with the shear strength obtained during these tests. Of the beams with stirrups, only one beam, B25,

failed at a load less than that predicted by the ACI (5) procedure.

3.4 Design Implications and Recommendations

3.4.1 Beams with Stirrups

The test results indicate that beams with stirrups containing amounts of longitudinal reinforcement close to minimum, exhibit a reduction in shear strength, relative to the ACI Code equations, when they are compared to beams with larger amounts of longitudinal reinforcement. It appears that the application of the current ACI Code procedure for the ultimate shear capacity for this type of beams loses the typical conservatism which is present for beams with flexural steel greater than about 1.2 percent. In fact, for beams with percentages of longitudinal reinforcement close to minimum permitted by the ACI Code (5), the current ACI procedure may be slightly unconservative.

The tests performed during this investigation do not point to any alarming deficiency in the shear strength of this type of beam, compared to the shear strength predicted by the current ACI procedure. In addition, the number of tests is too few to warrant a recommendation to change the present ACI procedures. However, it appears that the use of a shear cracking equation similar to that proposed by Zsutty, Eq. (1.5), would result in a consistently conservative shear strength prediction along the whole range of percentages of longitudinal reinforcement to which the ACI code, Eq. (1.2), applies.

In spite of the beneficial effect that the change would produce on the margin of safety, it seems reasonable to suggest that in the case of beams with stirrups, a reduction in the ACI code (5) concrete capacity term, V_c, without any increase in the stirrup capacity term, V_s, is

neither necessary nor desirable at the present time.

3.4.2 Beams without Stirrups

For beams without stirrups, the ACI Code (5), Eqs. (1.3) and (1.4), seems to be unconservative for beams with amounts of longitudinal reinforcement less than about 1.2 percent. However, the deficiency in shear strength does not really present a problem. The allowable shear capacity for beams without stirrups in the ACI Code is not limited by Eqs. (1.3) and (1.4), but by the quantity $\sqrt{f'_c}$. The ACI Code requires that the minimum amount of shear reinforcement must be provided whenever the applied shear, v_u, exceeds $\phi\sqrt{f'_c}$. This additional Code requirement is an adequate safeguard (6), since beams without shear reinforcement exhibit a shear strength greater than $\sqrt{f'_c}$. In addition, shear capacity should be well in excess of $\sqrt{f'_c}$ in locations of low moment (where longitudinal reinforcement may be reduced) due to the strengthening effect of low shear-span to depth ratios (low $\frac{a}{d}$ or M/Vd) on v_c.

CHAPTER 4

ULTIMATE STRENGTH MODEL FOR BEAMS WITH STIRRUPS

4.1 General

A universally accepted explanation of the manner in which loads are carried to the supports of shear-critical reinforced concrete beams, with or without stirrups, has not been developed; and in spite of the large amount of work accomplished to date, the manner in which stirrups influence the shear transfer mechanisms is not yet completely understood.

In this study, a relatively simple semianalytical model is used to explain the relative contribution of the various shear transfer mechanisms in reinforced concrete beams on both a qualitative and a quantitative basis.

4.2 Analytical Model

4.2.1 The model

A complete analytical approach to the ultimate shear capacity problem of reinforced concrete beams with shear cracks is a task of tremendous complexity. Considering this complexity (composite material, nonlinear properties and geometric discontinuities), it is concluded that a realistic approach to the ultimate shear capacity problem is an approach which is based on both the basic principles of mechanics and test results and observations.

The model utilizes the truss analogy, as shown in Fig. 4.1. It is assumed that in beams with stirrups, the shear forces are carried to the supports by four distinct shear transfer mechanisms: shear forces in the concrete compression zone, V_{cz}, dowel forces, V_d, interface or friction

forces along the cracks, V_{ay}, and tension forces in the shear reinforcement, V_s.

At failure, the shear capacity of a reinforced concrete beam is expressed as

$$V_n = V_{cz} + V_{ay} + V_d + V_s \tag{4.1a}$$

which can be written as,

$$V_n = V_c + V_s \tag{4.1.b}$$

in which V_c ($V_{cz} + V_{ay} + V_d$) is the total shear carried by the concrete.

It has been found from tests (3,14,41) that the four main parameters which affect the shear capacity of reinforced concrete beams are: the concrete strength, the percentage of longitudinal reinforcement, the shear-span to depth ratio and the amount of shear reinforcement.

For simplicity, this model is developed for rectangular beams with vertical stirrups and shear-span to depth ratios greater that 2.5. In this type of beam, the effect of the shear-span to depth ratio is not as large as in the case of short beams, but is still significant. The ultimate shear capacity, then, is expressed as a function of all four parameters.

4.2.2 Overview of Method

The purpose of this section is to give an overview of the method which is presented in the following sections. Expressions are derived for the shear capacity of the compression zone, V_{cz}. V_{cz} depends on the

size of the compression zone, the shear stress distribution in the compression zone, and the shear strength of the concrete. The size of the compression zone can be determined if the location of the tip of the failure shear crack is known. As a first step, the location of the tip of the failure crack is determined. Following this derivation, expressions are obtained for the average shear stress in the compression zone at failure. Then the compression zone capacity, V_{cz}, is presented as a function of the concrete strength, f'_c, shear-span to depth ratio, a/d, percentage of longitudinal reinforcement, ρ_w, and amount of shear reinforcement, $\rho_v f_{vy}$.

Using experimental data for reinforced concrete beams without stirrups (10,24,32,33), the total contribution of the dowel force, V_d, plus the interface shear , V_{ay}, is expressed approximately as a function of shear-span to depth ratio and percentage of longitudinal reinforcement.

In this manner, the ultimate concrete capacity, V_c, for beams without stirrups is expressed as a function of three independent variables: concrete strength, shear-span to depth ratio, and percentage of longitudinal reinforcement. The predicted concrete capacity is compared with predictive expressions presented by other investigators.

For beams with stirrups, it is assumed that the relative contribution of the compression zone, dowel shear, and interface shear are the same as in the case of similar beams without stirrups. The contribution of the stirrups is obtained with the simplifying assumption that the failure shear crack is inclined at 30° to the axis of the beam, as shown in Fig. 4.2. The model is used to help determine the effect of the shear reinforcement on the concrete shear capacity, V_c, and on the total nominal

shear capacity, V_n, of rectangular beams. Comparisons are made with experimental results for both rectangular beams and T-beams.

In the process of developing the model, a number of approaches were tried, which did not work. One model was based on the assumption that the inclined crack does not have any effect on the size of the compression zone. This model determined the depth of the compression zone as if the beam were in pure bending. The compression zone was very large, and the predicted compression zone shear capacity was greater than the total shear strength measured experimentally in reinforced concrete beams. Following another approach, the effect of the inclined crack on the size of the compression zone was incorporated, but the dowel and interface shears were ignored. The ultimate shear capacities predicted with this model were always smaller than the shears obtained from tests of rectangular reinforced concrete beams. An improved version of the last approach, in which the effects of the dowel and interface shears are included, is the model presented in the following sections. A key aspect of the model, as compared to others, is that it isolates the effect of the inclined crack on the size of the compression zone. In the development of this model, the main parameters found to influence the ultimate shear capacity of beams (concrete strength, shear-span to depth ratio, percentage of longitudinal reinforcement, amount of shear reinforcement) are included.

While quantitative results are obtained, the model should be considered primarily as a qualitative model, because of a number of limitations. For simplicity, crack depth is based on zero tensile strength. In addition, the nonlinear material behavior of concrete and the effect of shear stresses on the nominal stress-strain curve are, also, ignored. These

limitations affect the accuracy of the quantitative results. However, the model explains some important aspects of shear behavior and illustrates how the controlling parameters work.

4.3 Concrete Capacity

4.3.1 Compression Zone Capacity, V_{cz}

The shear force carried by the intact concrete compression zone depends on the area of the zone and the average shear stress in the zone at failure. The first task, then, is to determine the depth of the compression zone.

Depth of Compression Zone: It has been found experimentally (1) that the neutral axis in beams subject to combined bending and shear is located much higher than in beams subject to pure bending. The depth of the compression zone in the case of combined bending and shear may be as low as 0.357 the compression zone depth in beams under pure bending.

In the case of pure bending, the planarity assumption (planes before bending remain plane after bending) holds reasonably well. An expression can be derived relating the effective depth, the depth of the neutral axis and strains in the extreme compression fiber and flexural steel. This expression, together with the equilibrium equations, defines the location of the neutral axis of the beam. For beams subject to bending and shear, a compatibility equation cannot be accurately formulated at an isolated cross section within the beam due to the geometric discontinuity caused by the inclined cracks. In this case, the region of the beam traversed by the diagonal cracks must be investigated.

To investigate this region and determine the effect of the diagonal cracks on the location of the neutral axis, a procedure is developed to

convert a beam with a single diagonal crack into an equivalent beam with a vertical crack in order to use conventional expressions for determining the depth of the neutral axis.

In Fig. 4.2, two beams are shown; one beam is subject to bending and shear, the other to pure bending. For an elastic material, if the strains at the extreme compression fiber (plane 1-1 in Fig. 4.2) and the location of the neutral axis are the same for both beams, then the normal stresses in the concrete, the resultant compressive force and its point of application are, also, the same. Thus, in terms of the concrete, the beams are equivalent. However, due to the geometry of the crack, the strain in the flexural steel for the beam in bending and shear is smaller than the strain for the beam in pure bending. Since the tension forces, T_2, must be the same in the beams, the amount of flexural steel in the equivalent beam must be smaller.

The ratio of the flexural steel in the equivalent beam to the steel in the beam with the diagonal crack is defined as the "geometric and shear softening effect factor", F_s. This softening factor is determined from the analysis of the deformations of the concrete region bounded by the top of the beam, the diagonal crack and the two planes, 1-1 and 2-2, through the ends of the shear crack, as shown in Fig. 4.2a.

The following notation is illustrated in the figure:

z = horizontal projection of shear crack,

C = concrete compressive force,

T_i = tensile force in flexural steel, $i = 1,2$,

H_x = depth of concrete zone at location x,

A_s = flexural steel in beam under bending and shear,

A_{sb} = flexural steel in equivalent beam under pure bending that produces neutral axis location equivalent to neutral axis in beam under bending and shear,

Y_x = location of neutral axis at plane x, equal to kd at plane 1-1,

Y_{cx} = point of application of compression force, C, from the extreme compressive fiber of beam at section x,

y_x = distance from point of application of resultant, C, to the level of flexural steel at section x,

M_1 = applied moment at section 1,

M_2 = applied moment at section 2,

M_x = applied moment at section x,

M_b = moment for the pure bending case,

ε_{sx} = strain at level of flexural steel at location x, and

ε_{cx} = strain in extreme compressive fiber of concrete at location x.

Reasonable simplicity is preserved in the derivation of the expression for the softening factor with the following assumptions:

1. Stresses and strains are linearly related in the concrete.
2. Planes 1-1 and 2-2 of the beam in Fig. 4.2a, remain plane after loading.
3. The neutral axis passes through the tip of the shear crack.
4. The compression force, C, is the same for both beams.
5. Dowel and interface shears are present and act at the intersection of the shear crack with the flexural steel, as shown in Fig. 4.2a.
6. The inclined force shown in Fig. 4.2a acts parallel to the diagonal crack.

7. No dowel forces exist in the shear reinforcement.
8. For the concrete region only, planes before loading remain plane after loading.
9. The angle of the crack, θ, is constant and equal to 30°.
10. The shear crack is a parabola: $H_x = d - d(1-k)\ (1-x/z)^{\frac{1}{2}}$.

As a first step, the point of application of the resultant, C, is found for a section, x, between planes 1-1 and 2-2, as shown in Fig. 4.2c. Then the stresses in the concrete at the top of the beam and at the crack level are obtained at x. Since the stresses, and therefore the strains, are known, the location of the neutral axis and the strains at the boundaries of the concrete (top of beam and crack level) are determined. Then the deformation at the level of the flexural steel is obtained between planes 1-1 and 2-2. The softening factor ($F_s = A_{sb}/A_s$) is equal to the ratio of the steel strain at plane 2-2 to the steel strain in the equivalent beam. F_s is found as follows.

The applied moment at x is

$$M_x = V_n(a-x) = M_1 - V_n x \tag{4.2}$$

The internal moment at x is

$$M_x = T_2 y_x + V_s(z-x)^2/2z + (V_d+V_{ay})\ (z-x) \tag{4.3}$$

From the equilibrium of the external and internal moments,

$$y_x = [M_1 - V_n x - V_s(z-x)^2/2z - (V_d+V_{ay})\ (z-x)]/T_2 \tag{4.4}$$

Defining K_1 as the ratio of dowel shear plus interface shear to the total shear carried by the concrete ($\frac{V_d+V_{ay}}{V_c}$) and K_2 as the ratio of the shear carried by the stirrups to the nominal shear force (V_s/V_n), y_x can be expressed as

$$y_x = \frac{[2-K_2z/a+2K_2x/a-2x/a-K_2x^2/za-2(1-K_2)K_1z/a+2(1-K_2)K_1x/a](3-k)d}{2[3-1.5K_2z/a-3(1-K_2)K_1z/a]} \tag{4.5}$$

Substituting $z = (d-kd)/\tan\theta$ and $y_x = d-Y_{cx}$, solving for Y_{cx}, and simplifying:

$$Y_{cx} = d - \{[2a\tan\theta-(1-k)K_2d+2K_2(1-k)d\frac{x}{z}-2(1-k)d\frac{x}{z}$$

$$-K_2(1-k)d(\frac{x}{z})^2-2(1-K_2)K_1(1-k)d+2(1-K_2)(1-k)K_1d\frac{x}{z}](3-k)d\}/ \tag{4.6}$$

$$2[3a\tan\theta-1.5K_2(1-k)d-3(1-K_2)K_1(1-k)d]$$

The strain in the extreme compressive fiber of the concrete is

$$\varepsilon_{cx} = \frac{4C}{E_cb_wH_x} - \frac{6(H_x/2-Y_{cx})C}{E_cb_wH_x^2} \tag{4.7}$$

The neutral axis depth Y_x is

$$Y_x = \varepsilon_{cx}/[\varepsilon_{cx}-(4C/E_cb_wH_x + 6(H_x/2-Y_{cx})C/E_cb_wH_x^2)] \tag{4.8}$$

The strain at the level of the steel is

$$\varepsilon_{sx} = (d-Y_x)\varepsilon_{cx}/Y_x \tag{4.9}$$

The total elongation of the steel is

$$\Delta_s = \int_0^z (\varepsilon_{sx})dx \tag{4.10}$$

and the average strain in the steel is

$$\varepsilon_{sav} = \frac{\Delta_s}{z} \tag{4.11}$$

The strain in the steel is not constant between planes 1-1 and 2-2. At plane 2-2 the steel strain is approximated as

$$\varepsilon_{s2} = \varepsilon_{sav} - \frac{[(V_{ay}+V_d)+V_s]z}{2d(1-k)A_sE_s} \tag{4.12}$$

The variation of ε_{s2} from ε_{sav} is based on the assumption that the strains in the steel vary linearly between planes 1-1 and 2-2, due to the inclined force shown in Fig. 4.2a.

The strain in the steel in the equivalent beam is

$$\varepsilon_{sb} = \frac{2(1-k)C}{E_c b_w k} \tag{4.13}$$

From equilibrium ($T_2 = C = T_{2b}$)

$$A_{sb}\,\varepsilon_{sb}\,E_s = A_s\varepsilon_{s2}E_s \tag{4.14}$$

Substituting the expressions for ε_{sb}, ε_{s2} and E_c ($57000\sqrt{f'_c}$ psi) and the value for E_s(29,000,000 psi) into Eq. (4.14), and solving for A_{sb} gives

$$A_{sb} = A_s \left[\frac{\varepsilon_{sav}}{\varepsilon_{sb}} - \frac{(3k^2-k^3)(1-K_2)K_1+K_2)\sqrt{f'_c}}{6105(1-k)^2\ [\tan\theta a/d(1-k)-K_2/2-(1-K_2)K_1]\rho_w} \right] \quad (4.15a)$$

$$A_{sb} = A_s . F_s \quad (4.15b)$$

where ρ_w is the percentage of flexural reinforcement in the beam with the diagonal crack, and the quantity in the brackets is the softening factor, F_s.

For a given equivalent reinforcing ratio, $\rho_w^*(=F_s\rho_w)$, and modular ratio, $n(=E_s/E_c)$, the depth of the neutral axis can be obtained.

$$k = \sqrt{2n\rho_w^* + (n\rho_w^*)^2} - n\rho_w^* \quad (4.16)$$

Equations (4.15) and (4.16) are solved simultaneously for k and F_s using an iterative technique. The depth of the neutral axis and the softening factor can be determined for any reinforced concrete beam for which the ratios, K_1, K_2, and the angle of diagonal crack, θ, are known.

Average stress at failure: For a given depth of the neutral axis, kd, the capacity, V_{cz}, can be found if the average shear stress in the compression zone is known at failure. To obtain the average shear stress, an equation is derived for the shear stress at a point within the compression zone of a reinforced concrete beam subject to bending and shear. The assumed forces and strains are shown in Fig. 4.3, in which:

Y = distance to neutral axis from tne top of the beam,

Y_c = distance of resultant C from the top of the beam,

$\bar{y}$ = distance of resultant C from the neutral axis,

ε_u = strain corresponding to maximum stress on the stress-strain

developed by Kupfer and Gerstle (25) for combined tension and compression is used (Fig. 4.5). Using this criterion, the principal tensile stress at failure, σ_1, is expressed as

$$\sigma_1 = (1 + 2/3 \frac{\sigma_2}{f'_c}) f'_t \tag{4.25}$$

in which f'_t is the tensile strength of the concrete (assumed equal to $5\sqrt{f'_c}$). For a normal stress, σ, and a shear stress, τ, acting as shown in Fig. 4.6, the failure criterion is expressed as

$$\tau = \left[\frac{f'^2_t + \frac{\sigma^2}{4} + \frac{f'^2_t \sigma^2}{9f'^2_c} - \frac{f'_t \sigma^2}{3f'_c} + \frac{2f'^2_t \sigma}{3f'_c} - f'_t \sigma}{(1 + \frac{2f'_t}{3f'_c})^2} - \frac{\sigma^2}{4} \right]^{\frac{1}{2}} \tag{4.26}$$

Eq. (4.26) is plotted in Fig. 4.6 for 4000 psi concrete.

The variation of shear strength with y is shown in Fig. 4.4 for a strain ratio, w = 0.6. Fig. 4.4 suggests that failure initiates at an interior point, close to the center of the compression zone.

Using this procedure, the average shear stress within the compression zone at failure, τ_{av}, can be accurately approximated (within 3 percent) as

$$\tau_{av} = K_3 (f'_c)^{.75} \tag{4.27}$$

The constant , K_3, depends on the strain ratio, w. The values of τ_{av} obtained from this analysis are shown in Table 4.1 for different concrete strengths and strain ratios. The representative constant, K_3, for each

strain ratio, w, is also shown.

After the examination of the results and comparison with test data (26), a constant value for $K_3 = 0.75$ was selected as reasonably representative. The value of average shear stress within the compression zone at failure is therefore:

$$\tau_{av} = 0.75(f'_c)^{.75} \tag{4.28}$$

The shear capacity of the compression zone is:

$$V_{cz} = b_w kd\ \tau_{av} = 0.75k(f'_c)^{.75} b_w d \tag{4.29a}$$

or in terms of nominal stress,

$$v_{cz} = \frac{V_{cz}}{b_w d} = 0.75k(f'_c)^{.75} \tag{4.29b}$$

4.3.2 Dowel and Interface Shear Capacity

Based on the simplified model described above, the "contribution" of the dowel and interface shear to the nominal shear capacity of rectangular reinforced concrete beams without stirrups is obtained using an analysis of the experimental data obtained from a number of investigators (10, 24,35,36). Using Eqs. (4.15), (4.16) and (4.29), the factor, K_1, is determined for each beam with an iterative procedure.

The procedure consists of selecting a value for $K_1 (= (V_d + V_{ay})/V_c)$ and obtaining the values for k (Eqs. (4.15 and 4.16)), V_{cz} (Eq. (4.29)), and finally

$$V_c = \frac{V_{cz}}{1-K_1} \tag{4.30}$$

for the particular beam under consideration. The value of V_c from Eq. (4.30) is then compared with the test value. K_1 is modified until the solution converges.

As shown in Fig. 4.7, K_1 can be expressed reasonably well as a function of only two independent variables, shear-span to depth ratio, a/d, and percentage of longitudinal reinforcement, ρ_w, in the following form (based on a least squares fit of the calculated values of K_1 versus a/d):

$$K_1 = 1 - [-.33+.29\ a/d\ -.033(a/d)^2+.0015(a/d)^3]\ (100\rho_w)^{.25} \tag{4.31}$$

Fig. 4.7 and Eq. (4.31) indicate that the relative contribution of dowel shear and aggregate interlock to total shear strength decrease with increasing values of a/d and ρ_w. Conversely, the relative contribution of the compression zone increases. Eqs. (4.15), (4.16) and (4.29) can now be used in conjunction with Eqs. (4.31) and (4.30) to obtain the softening factor, F_s, the neutral axis location at the top of the diagonal crack, k , and the concrete compression zone capacity, V_{cz}, for different values of concrete strength, shear-span to depth ratio, and percentage of longitudinal reinforcement. These values are presented in Figs. 4.8, 4.9 and 4.10. These figures suggest that the size of the compression zone, and therefore the shear capacity of the compression zone, strongly depends on the shear-span to depth ratio and percentage of longitudinal reinforcement. Concrete strength has a smaller, but still significant, effect on the compression zone shear capacity of the model.

4.3.3 Concrete Capacity V_c

For beams without stirrups, the nominal shear capacity, V_c, is expressed as

$$V_c = V_{cz}/(1-K_1) \tag{4.30}$$

Eq. (4.30) is a function of concrete strength, shear-span to depth ratio and percentage of longitudinal reinforcement and can be used to predict the nominal (ultimate) shear capacity for rectangular beams without stirrups. The predicted shear capacities are shown in Fig. 4.11 in terms of shear stress, v_c. The curves are similar to the curves obtained using Eq. (1.5), proposed by Zsutty. For comparison, v_c is plotted versus the percentage of longitudinal reinforcement (Fig. 4.12), for f'_c = 4000 psi and a/d = 4, and compared with shear capacities from other predictive relations (5,36,42).

Figs. 4.11 and 4.12 suggest that the concrete shear capacity is an increasing function of both concrete strength and percentage of longitudinal reinforcement, and a decreasing function of shear-span to depth ratio. The proposed model, therefore, matches observed behavior on at least a qualitative basis. Unfortunately, the model seems to show a much stronger effect of ρ_w on v_c than obtained by Zsutty based on a statistical analysis. This over-sensitivity of the model is likely due to the fact that it ignores the nonlinear, softening behavior of the concrete within the compression zone. It is, also, important to note that even the qualitative match requires the use of Eq. (4.31) based on test results.

The predicted shear capacities are compared with the test results used to develop the model in Fig. 4.13.

4.4 Capacity of Shear Reinforcement, V_s

The contribution of stirrups to the shear capacity of the model can be evaluated only if both the stress in the stirrups and the number of stirrups

crossed by the shear crack at failure are known. The stirrups which cross the shear crack can be assumed to yield. Yielding of the stirrups has been reported by many investigators (10,17,35,37), and was observed in all eleven T-beams with stirrups tested in this investigation. The horizontal crack projection, z, can be evaluated if the inclination, θ, of the assumed parabolic crack to the axis of the beam is known. In this investigation, the inclination, θ, is assumed to be 30°. This is close to the optimum value of 31° adopted by the CEB (comité Euro-International du Bèton) as proposed by Grob and Thurlimann (16). The horizontal projection of the shear crack is expressed as:

$$z = (d-kd) \cot 30 = (1-k)\, d \cot 30 \qquad (4.32)$$

The stirrup shear capacity then is:

$$V_s = 1.73(1-k)\rho_v f_{vy}\, b_w d \qquad (4.33)$$

This representation for V_s results in a somewhat reduced effectiveness of the shear reinforcement as the depth of the neutral axis, k, increases.

For beams with stirrups it is assumed that the variation of the factor K_1 ($= (V_{ay}+V_d)/V_c$) is the same as in similar beams without stirrups. The shear capacities, V_{cz}, $(V_{ay}+V_d)$, and V_c are again obtained but are now based on four independent variables: concrete strength, shear-span to depth ratio, percentage of longitudinal reinforcement, and amount of shear reinforcement $\rho_v f_{vy}$ (factor K_2). The variation of shear capacity, along with the individual components of v_n, is presented in Fig. 4.14 as a function of $\rho_v f_{vy}$ for f'_c = 4000 psi, ρ_w = 1.0% and a/d = 4.0.

The results indicate that the presence of shear reinforcement causes an increase in the contribution of the concrete to the shear capacity of the model, in addition to the direct contribution obtained from Eq. (4.33). The concrete capacity, V_c, increases quickly as the amount of shear

reinforcement, $\rho_v f_{vy}$, increases from 0 to about 150 psi, and then remains approximately constant with the further increase in the amount of shear reinforcement.

4.5 Effectiveness of Shear Reinforcement

The nominal (ultimate) shear capacity of reinforced concrete beams with stirrups is

$$V_n = V_c + V_s \tag{4.1b}$$

or in terms of stresses,

$$v_n = v_c + v_s = v_c + r\rho_v f_{vy} \tag{4.34a}$$

in which r is defined as the effectiveness factor of the shear reinforcement.

When the nominal shear, v_n, is expressed in the form

$$v_n = v_c^* + r\rho_v f_{vy} \tag{4.34b}$$

in which v_c^* is the ultimate shear capacity for a similar beam without stirrups, the effectiveness factor, r, varies considerably as a function of the amount of the shear reinforcement. As it is shown in Fig. 4.15, the effectiveness factor is larger in beams with small shear-span to depth ratios, small amounts of flexural and shear reinforcement and higher concrete strengths.

Fig. 4.15 shows that the effectiveness factor for a beam with a/d = 4, ρ_w=.02, f_c' = 4000 and $\rho_v f_{vy}$ close to the minimum is about 1.65. This

value is reasonably compatible with the effectiveness factors (1.8, 1.75) reported by other investigators (10,17). It is of interest to note that the effectiveness factors obtained for the model are based on a constant crack inclination, $\theta = 30\ °$, which is not necessarily justified.

In Fig. 4.16, the nominal shear stress is plotted for a constant percentage of flexural reinforcement and two shear-span to depth ratios. In the same figure, experimental results for T-beams (17) are also shown. Examination of Fig. 4.16 suggests that there is a reasonable agreement between the test results and the values of v_n predicted by the model. The model appears to be unconservative for beams with small shear-span to depth ratios and larger amounts of shear reinforcement. This weakness in the model is in all likelihood due to the use of an average failure shear (τ_{av}) within the compression zone of the model, which is independent of the actual loading on the beam.

In Fig. 4.17, the nominal shear stress is plotted for a shear-span to depth ratio of 4 and different amounts of longitudinal reinforcement. This figure suggests that the effect of the percentage of longitudinal reinforcement on the ultimate shear capacity is more pronounced in beams with small amounts of shear reinforcement and tends to diminish with increasing amounts of shear reinforcement. The severity of this behaivor in the model seems to be somewhat unrealistic, and experimental evidence does not exist showing the convergence in v_n illustrated in Fig. 4.17.

4.6 Comparison of Predicted and Experimental Shear Capacities

The shears predicted by the proposed procedure are compared with test results (10,17,24,35) for beams with stirrups in Figs. 4.18 and 4.19 and Tables 4.2 and 4.3, for rectangular beams and T-beams, respectively.

It appears that the proposed procedure is somewhat better for rectangular beams than for T-beams. The predicted ultimate shear capacities are more conservative in the case of T-beams. For rectangular beams, the means of the ratios of the test results to the predicted values of shear strength are .75, 1.01 and 1.04, with coefficient of variation of 6.87%, 10.08% and 5.86% for beams from references 24, 35 and 10, respectively. The ratio of .75 is obtained from the tests by Krefeld and Thurston (24). In their tests, Krefeld and Thurston did not use compression reinforcement; therefore, there is a possibility that these beams failed at smaller loads compared to the beams tested by the other investigators (10,35) due to insufficient anchorage of the stirrups.

For the T-beams, the mean values of the ratios of test to predicted shear strengths are 0.89, 1.14 and 1.26, with coefficients of variation of 5.36%, 9.17% and 13.41% for the results reported in Chapter 2 of this report, Reference 17, and Reference 35, respectively. The value 0.89 obtained for the test results from this investigation may be the result of the different types of flexural reinforcement used in these T-beams. Since the flexural reinforcement consisted of strands, instead of reinforcing bars, it is possible that the dowel shear, which is normally carried by the flexural reinforement, was reduced, as was the bond strength between the strands and the concrete.

Overall, the mean values of the ratios of experimental shear strength to predicted shear strength are 0.95 for the rectangular beams and 1.15 for the T-beams, with coefficients of variation of 14.70% and 19.74%, respectively.

4.7 Critique of the Model

For the benefit of simplicity, some of the assumptions used in

developing the model are not truly representative of the actual materials being modeled: Concrete stress-strain curves are nonlinear, not linear. The average shear stress at failure is not only a function of the concrete strength, but is also a function of the applied moment. Interface shear is present along the total length of the shear crack. The inclination of the critical shear crack is not constant for all beams.

One of the most apparent inconsistencies in the model is the assumption of zero tensile strength in the concrete, used to determine the depth of the compression zone, while at the same time assuming a tensile strength (Eq. (4.25)) to obtain the shear capacity of the same compression zone.

The overall effect of the simplifying assumptions is to ignore the true stress-strain behavior of the concrete and, therefore, ignore the material softening in combined compression and shear and the accompanying reduction in the depth of the compression zone. This results in too great an increase in the depth of the compression zone, as a function of a/d and ρ_w, and a subsequent overestimation of the concrete capacity. The use of an average failure shear stress within the compression zone, τ_{av}, also prevents the model from exhibiting compression-type failure (and reduced "stirrup effectiveness") for high values of $\rho_v f_{vy}$. Finally, no attempt is made to model the aggregate interlock and dowel shear except through the use of test data.

In spite of these shortcomings, the model provides a qualitative representation of the effects of concrete strength, shear-span to depth ratio, percentage of longitudinal reinforcement and amount of shear reinforcement on the shear capacity of reinforced concrete beams. The qualitative success of the model suggests that the general approach is correct and that a more

accurate model can be obtained by following a similar approach and improving the realism of the stress-strain representation of the concrete.

CHAPTER 5

SUMMARY AND CONCLUSIONS

5.1 Summary

Fifteen lightly reinforced concrete T-beams, eleven with stirrups and four without stirrups were tested to failure. The major variables in the study were the amounts of flexural and shear reinforcement. The flexural steel varied from one-half to one percent, and the shear reinforcement varied from zero to about 110 psi. The test results are analyzed and compared with the ACI Building Code (5) shear design procedures. Design recommendations are presented.

An analytical model is developed which examines the effects of concrete strength, shear-span to depth ratio, percentage of flexural steel and amount of shear reinforcement on the shear capacity of normal ($a/d \geq 2.5$) rectangular reinforced concrete beams. The effects of these parameters on the relative contributions of compression zone capacity, aggregate interlock, dowel shear and stirrup capacity to shear strength are examined.

5.2 Conclusions

1. The test results obtained in this study indicate that reinforced concrete T-beams with small percentages of longitudinal reinforcement and small amounts of shear reinforcement exhibit a reduction in shear capacity relative to the design expressions in the ACI Building Code (5), when compared to similar beams with normal to large percentages of longitudinal reinforcement.
2. The shear capacity of these lightly reinforced T-beams is, in most cases, equal to or greater than the shear capacity predicted by the

current ACI Code (5), and the present ACI procedure appears to be safe for T-beams.

3. For the lightly reinforced concrete T-beams, in this investigation it was found that the stirrups are 1.5 times as effective as predicted by the ACI Code (5).
4. The current procedures for shear design (5) should be retained for reinforced concrete beams both with or without stirrups, until additional tests are performed.
5. The semianalytical model developed in this study is a reasonable qualitative tool for the examination of the effect of concrete strength, shear-span to depth ratio, percentage of flexural steel and amount of shear reinforcement on the ultimate shear capacity of reinforced concrete beams.
6. The model can be used to examine the relative contribution of the different shear transfer mechanisms on shear capacity.
7. The model explains the observed high effectiveness of the first small amounts of shear reinforcement in terms of a greater shear crack projection and an increased compression zone capacity.
8. Due to the simplifying assumptions used, the model overestimates the effect of shear-span to depth ratio and flexural reinforcing ratio on shear strength and cannot account for shear-compression failure.
9. Diagonal cracks must be modeled to properly represent both the concrete and steel contributions to the shear strength of reinforced concrete beams.

5.3 Recommendations for Further Study

The experimental investigation in this study is only a small part of a test program needed to examine the ultimate shear capacity of reinforced concrete beams with small amounts of flexural and shear reinforcement. Additional tests should be carried out on both T-beams and rectangular beams. The effect of concrete strength and shear-span to depth ratio should be examined. In addition, the effect of continuity and type of loading should be investigated. The type of flexural reinforcement used in the future should be high strength deformed reinforcing bars, in order to more accurately represent the flexural steel which is used in practice.

The relatively simple model presented in this study may be improved, but with some loss in simplicity. A better representation of interface shear along the total length of the shear crack should be incorporated in the basic model. The actual nonlinear stress-strain curve for the concrete should be used, and the effect of a variable shear crack inclination on ultimate strength should be studied.

REFERENCES

1. Acharya, D. N. and Kemp, K. O., "Significance of Dowel Forces on the Shear Failure of Rectangular Reinforced Concrete Beams without Web Reinforcement," Journal of the American Concrete Institute, Proc. Vol. 62, No. 10, Oct., 1965, pp. 1265-1279.

2. ACI-ASCE Committee 326, "Shear and Diagonal Tension," Journal of the American Concrete Institute, Proc. Vol. 59, No. 1, Jan. 1962, pp. 1-30, No. 2, Feb., 1962, pp. 277-333, No. 3, March, 1962, pp. 353-395.

3. ACI-ASCE Committee 426, "The Shear Strength of Reinforced Concrete Members," Journal of the Structural Division, ASCE, Vol. 99, No. ST6, Proc. Paper 9791, June, 1973, pp. 1091-1187.

4. ACI-ASCE Committee 426, "Suggested Revisions to Shear Provisions of ACI Code 318-71," Journal of the American Concrete Institute, Proc. Vol. 74, No. 9, Sept., 1977, pp. 458-469.

5. American Concrete Institute, Building Code Requirements for Reinforced Concrete (ACI 318-77), Detroit, Michigan, 1977.

6. Attiogbe, E. K., Palaskas, M. N., and Darwin, D., "Shear Cracking and Stirrup Effectiveness of Lightly Reinforced Concrete Beams," Structural Engineering and Engineering Materials, SM Report No. 1, University of Kansas Center for Research, Inc., Lawrence, Kansas, July 1980.

7. Borishansky, M.S., "Shear Strength of Reinforced Concrete Elements," C.I.B. Congress, Rotterdam, 1959, UDC 624.075.3: 624.012.45, pp. 85-95.

8. Braestrup, M. W. "Plastic Analysis of Shear in Reinforced Concrete," Magazine of Concrete Research, Vol. 26, No. 89, Dec., 1974, pp. 221-228.

9. Bresler, Boris and MacGregor, J. G., "Review of Concrete Beams Failing in Shear," Journal of the Structural Division, ASCE, Vol. 93, No. ST1, Proc. Paper 5106, Feb., 1967, pp. 343-372.

10. Bresler, Boris and Scordelis, A. C., "Shear Strength of Reinforced Concrete Beams," Journal of the American Concrete Institute, Proc. Vol. 60, No. 4, Jan., 1963, pp. 51-74.

11. Clark, A. P., "Diagonal Tension in Reinforced Concrete Beams," Journal of the American Concrete Institute, Proc. Vol. 48, No. 11, Oct., 1951, pp. 145-156.

12. Collins, M. P., "Towards a Rational Theory for Reinforced Concrete

Members in Shear," Journal of the Structural Division, ASCE, Vol. 104, No. ST4, Proc. Paper 13697, Apr., 1978, pp. 649-666.

13. Elstner, R. C., Moody, K. G., Viest, I. M., and Hognestad, E., "Shear Strength of Reinforced Concrete Beams, Part 3-Tests of Restrained Beams with Web Reinforcement," Journal of the American Concrete Institute, Proc. Vol. 51, No. 6, Feb., 1955, pp. 525-539.

14. Fenwick, R. C. and Paulay, T., "Mechanism of Shear Resistance of Concrete Beams," Journal of the Structural Division, ASCE, Vol. 94, No. ST10, Proc. Paper 2325, Oct., 1968, pp. 2325-2350.

15. Gergely, P., "Splitting Cracks Along the Main Reinforcement in Concrete Member," Report to Bureau of Public Roads, U. S. Department of Transportation, Cornell University, Ithaca, N. Y., Apr., 1969.

16. Grob, Josef and Thurlimann, Bruno, "Ultimate Strength and Design of Reinforced Concrete Beams under Bending and Shear," IABSE, Vol. 36-II, 1976, pp. 105-119.

17. Haddadin, M. J., Sheu-Tien Hong, Mattock, A. H., "Stirrup Effectiveness in Reinforced Concrete Beams with Axial Force," Journal of the Structural Division, ASCE, Vol. 97, No. ST9, Proc. Paper 8394, Sept., 1971, pp. 2277-2297.

18. Hognestad, E., "A Study of Combined Bending and Axial Load in Reinforced Concrete Members," Engineering Experiment Station Bulletin Series, No. 399, University of Illinois, Urbana, Illinois, 1951, pp. 128.

19. Hognestad, E., "What Do We Know About Diagonal Tension and Web Reinforcement in Concrete?," Engineering Experiment Station, Circular Series, No. 64, University of Illinois, Urbana, Illinois, Mar., 1952, pp. 47.

20. Kani, G. N. J., "The Riddle of Shear Failure and Its Solution," Journal of the American Concrete Institute, Proc. Vol. 61, No. 4, Apr., 1964, pp. 441-407.

21. Kani, G. N. J.,"Basic Facts Concerning Shear Failure," Journal of the American Concrete Institute, Proc. Vol. 63, No. 6, June, 1966, pp. 675-790.

22. Kani, G. N. J., "A Rational Theory for the Function of Web Reinforcement," Journal of the American Concrete Institute, Proc. Vol. 66, No. 3, March, 1969, pp. 185-197.

23. Kani, M. W., Huggins, M. W., and Wittkopp, R. R., Kani, on Shear in Reinforced Concrete, University of Toronto Press, 1979.

24. Krefeld, W. J. and Thurston, C. W., "Studies of the Shear and Diagonal Tension Strength of Simply Supported Reinforced Concrete Beams," Journal of the American Concrete Institute, Proc. Vol. 63, No. 4, Apr., 1966, pp. 451-475.

25. Kupfer, H. B. and Gerstle, K. H., "Behavior of Concrete Under Biaxial Stresses," Journal of Engineering Mechanics Division, ASCE, Vol. 99, No. EM4, Aug. 1973, pp. 852-866.

26. Kupfer, H. Hilsdorf, H. K. and Rusch, H., "Behavior of Concrete Under Biaxial Stresses," Journal of the American Concrete Institute, Proc. Vol. 66, No. 8, Aug. 1969, pp. 656-666.

27. Laupa, A., Siess, C. P. and Newmark, N., "Strength in Shear of Reinforced Concrete Beams," Engineering Experimental Station Bulletin 428, University of Illinois, Urbana, Illinois, Mar. 1955.

28. Micro-Measurements, "Strain Gage Installations with M-Bond 200 Adhesive," Instruction Bulletin, B-127-5, Measurements Group, Raleigh, North Carolina, May 1976.

29. Micro-Measurements, "Application of M-Coat G and GL Protective Coatings," Instruction Bulletin, B-141, Measurements Group, Raleigh, North Carolina, May 1978.

30. Moody, K., Viest, I. M., Elstner, R. C. and Hognestad, E., "Shear Strength of Reinforced Concrete Beams," Journal of the American Concrete Institute, Proc. Vol. 51, No. 2, Feb., 1955, pp. 525-539, No. 3, Mar., 1955, pp. 697-732.

31. Moore, W. P., Jr., "An Analytical Study of the Effect of Web Reinforcement on the Strength of Reinforced Concrete Beams Subjected to Combined Flexure and Shear," Structural Research Series, No. 282, University of Illinois, Urbana, Illinois, May 1964.

32. Moretto, O., "An Investigation of the Strength of Welded Stirrups in Reinforced Concrete Beams," Journal of the American Concrete Institute, Proc. Vol. 42, No. 2, Nov., 1945, pp. 141-162.

33. Mörsch E., "Versuche über Schubspannugen in Betoneisenträgern," Beton und Eisen Berlin, Vol. 2, No. 4, Oct. 1903, pp. 269-274.

34. Nielsen, M. P., Braestrup, M. W., and Bach, F., "Rational Analysis of Shear in Reinforced Concrete Beams," IABSE Proc. P.-15/78, May 1978, pp. 1-16.

35. Placas, Alexander, and Regan, P. E., "Shear Failure of Reinforced Concrete Beams," Journal of the American Concrete Institute, Proc. Vol. 68, No. 10, Oct. 1971, pp. 763-773.

36. Rajagopalan, K. S., and Ferguson, P. M., "Exploratory Shear Tests Emphasizing Percentage of Longitudinal Steel," Journal of the American Concrete Institute, Proc. Vol. 65, No. 46, Aug. 1968, pp. 634-638.

37. Regan, P. E., "Combined Shear and Bending of Reinforced Concrete Members," Thesis presented to the University of London, England, 1967 in partial fulfillment of the requirements for the degree of Doctor of Philosophy.

38. Ritter, W., "Die Bauweise Hennebique," Schweizerische Bauzeitung, Zurich, Vol, 33, No. 7, Feb. 1899, pp. 59-61.

39. Rusch, H., "Uber die Grenzen der Anwendbarkeit der Fachwekanalogie bei der Berechnung der Schulfestigkeit von Stalbetonbalken," Ehrenbuch Prof. Ing. F. Campus, Amici et Alumni, Belgium, 1964.

40. Talbot, A. N. "Tests of Reinforced Concrete Beams Resistance to Web Stresses," Engineering Experiment Station Bulletin No. 29, University of Illinois, Urbana, Illinois, Jan. 1909, pp. 1-85.

41. Taylor, H. P. J., "Investigation of the Forces Carried Across Cracks in Reinforced Concrete Beams in Shear by Interlock of Aggregate," Cement and Concrete Association, Technical Report 42.477, London, England, 1970.

42. Zsutty, T. C., "Beam Shear Strength Prediction by Analysis of Existing Data," Journal of the American Concrete Institute, Proc. Vol. 65, No. 71, Nov., 1968, pp. 943-951.

43. Zwoyer, E. M. and Siess, C., "Ultimate Strength in Shear of Simply Supported Beams Without Web Reinforcement," Journal of the American Concrete Institute, Proc. Vol. 51, No. 8, Oct. 1954, pp. 181-200.

TABLE 2.1 LONGITUDINAL AND TRANSVERSE REINFORCEMENT

Series	Beam	Longitudinal Reinforcement: Bottom: Type	Area, in^2	Flexural reinforcing + ratio, ρ_w	Flange Type	Transverse Reinforcement: Flange Type	Smooth Wire Stirrups: Diameter in	Spacing in	Shear reinforcing ++ $\rho_v f_{vy}$, psi	Preyielding load, pounds	Yield load, pounds	Ultimate load, pounds
	#2	5-1/2 in		0.693	2 #4 ASTM A615 Grade 60 deformed billet bars f_y = 70,000 psi (see Fig. 2.1)	#3 ASTM A615 Grade 60 deformed billet bars f_y = 61,360 psi (see Fig. 2.1)						
	A00	ASTM A416		0.656								
	A25	270 ksi		0.663			0.132	7	31.8	750	835	1078
A	A25a	stress	0.765	0.668			0.132	7	31.8	750	835	1115
	A50	relieved		0.661			0.186	7	73.9	1650	1940	2125
	A50a	strands		0.658			0.186	7	75.0	1700	1970	2200
	A75			0.655			0.229	7	97.1	2350	2550	3240
	#1			0.699			0.244	7½*	110.2**	1350	1550**	- -
	B00	5-7/16 in		0.488								
	B25	ASTM A416	0.575	0.494			0.132	7	32.4	750	850	1135
B	B50	270 ksi		0.498			0.186	7	76.2	1700	2000	2200
		stress relieved strands										
	C00	5-0.6 in		0.943								
C	C25	ASTM A416	1.090	0.948			0.132	7	32.4	750	950	1120
	C50	270 ksi		0.939			0.186	7	76.2	1700	2000	2210
	C75	stress relieved strands		0.933			0.229	7	103.0	2350	2705	3347

* double stirrups at 7½" were used

** estimated

\+ $\rho_w = \frac{A_s}{b_w d}$

++ $\rho_v f_{vy} = \frac{A_v f_{vy}}{b_w s}$

TABLE 2.2 CONCRETE MIX DESIGN AND STRENGTH

Series	Beam	Coarse aggregate lb/cy*	Fine aggregate lb/cy*	Type I cement lb*	w/c	Slump in	Measured air content %	Age at test, days	Cylinder strength, f'_c, psi	Modulus of rupture. f_r, psi
	#2	1470	1460	564	.473	1½	5.5	21	4750	437
	A00	1510	1500	470	.568	1½	5.0	7	4740	667
	A25	1510	1500	470	.568	1	5.5	16	4720	396
A	A25a	1490	1480	517	.516	¾	2.0	4	4790	664
	A50	1510	1500	470	.568	1½	6.5	18	3810	380
	A50a	1490	1480	517	.516	1¾	4.5	6	4060	512
	A75	1510	1500	470	.568	1¼	3.9	6	4670	550
	#1	1510	1500	470	.568	½	6.0	10	5520	717
	B00	1510	1500	470	.568	¾	4.5	11	4640	567
B	B25	1510	1500	470	.568	1¼	3.8	18	4470	525
	B50	1510	1500	470	.568	1½	6.0	13	4390	585
	C00	1490	1480	517	.516	½	4.4	3	4270	604
C	C25	1490	1480	517	.516	¾	3.3	5	4100	462
	C50	1450	1450	611	.450	1¼	6.5	3	4300	650
	C75	1490	1480	517	.516	1	3.2	9	4260	585

* Based on air content = 5.0%.

TABLE 2.3 SUMMARY OF TEST PROGRAM, FLEXURAL CRACKING STRESSES AND NOMINAL SHEAR STRENGTH

Series	Beam	$\rho_w = \frac{A_s}{b_w d}$ %	$\rho_v f_{vy}$ psi	f'_c psi	a/d	b_w in	d in	*Test flexural cracking stress psi	V_n test kips
A	#2	0.693	- -	4750	4.14	7½	14.72	$7.48\sqrt{f'_c}$	16.244
	A00	0.656	- -	4740	3.92		15.54	$6.54\sqrt{f'_c}$	14.560
	A25	0.663	31.8	4720	3.97		15.38	$6.55\sqrt{f'_c}$	19.275
	A25a	0.668	31.8	4790	4.00		15.26	$6.77\sqrt{f'_c}$	20.772
	A50	0.661	73.9	3810	3.96		15.42	$7.22\sqrt{f'_c}$	25.954
	A50a	0.658	75.0	4060	3.94		15.49	$7.49\sqrt{f'_c}$	24.660
	A75	0.655	97.1	4670	3.92		15.56	$6.83\sqrt{f'_c}$	31.966
	#1	0.699	110.2	5520	4.18		14.60	$6.24\sqrt{f'_c}$	31.275
B	B00	0.488	- -	4640	3.88	7½	15.70	$6.18\sqrt{f'_c}$	16.027
	B25	0.494	32.4	4470	3.93		15.52	$6.38\sqrt{f'_c}$	17.670
	B50	0.498	76.2	4390	3.96		15.39	$7.57\sqrt{f'_c}$	24.050
C	C00	0.943	- -	4270	3.96	7½	15.41	$7.14\sqrt{f'_c}$	13.270
	C25	0.948	32.4	4100	3.98		15.33	$7.23\sqrt{f'_c}$	18.650
	C50	0.939	76.2	4300	3.94		15.47	$7.82\sqrt{f'_c}$	30.150
	C75	0.933	103.0	4260	3.92		15.57	$7.53\sqrt{f'_c}$	31.020

* Based on the uncracked transformed cross section.

*TABLE 3.1 SHEAR CRACKING STRESSES OBTAINED FROM CONCRETE STRAINS, STIRRUP STRAINS, DEPTH INCREASE AND CRACKING PATTERNS

Series	Beam	Diagonal Cracking, psi			
		Concrete strains	Stirrup strains	Depth increase	Cracking patterns
A	#2	- -	- -	- -	- -
	A00	111	- -	- -	89
	A25	112	112	124	112
	A25a	114	114	114	114
	A50	116	112	122	122
	A50a	114	114	114	114
	A75	110	110	116	110
B	#1	- -	- -	- -	- -
	B00	89	- -	- -	100
	B25	93	93	114	104
	B50	98	98	131	98
C	C00	96	- -	- -	73
	C25	114	115	115	114
	C50	115	115	115	115
	C75	116	116	116	94

* From Ref. (6)

TABLE 4.1 AVERAGE SHEAR STRESSES IN THE COMPRESSION ZONE AT FAILURE BASED ON ASSUMED LINEAR STRESS-STRAIN CURVE FOR CONCRETE

w	.5	.6	.7	.8	.9	1.0
f'_c \ K_3	.735	.772	.804	.831	.853	.873
3000	298 (298)	313 (313)	326 (326)	337 (337)	346 (346)	354 (354)
4000	365 (370)	384 (388)	400 (404)	415 (418)	428 (429)	438 (439)
5000	427 (437)	450 (459)	471 (478)	489 (494)	504 (507)	516 (519)
6000	486 (501)	513 (526)	537 (548)	558 (566)	576 (581)	591 (595)

Values in parenthesis are obtained using $\tau_{av} = K_3 f'^{.75}_c$

TABLE 4.2 COMPARISON OF PREDICTED AND EXPERIMENTAL NOMINAL SHEAR STRESS FOR RECTANGULAR BEAMS WITH STIRRUPS

Beams	f'_c psi	b_w in.	d in.	a/d	$100\rho_w$	$\rho_v f_{vy}$	V_{ntest} kips	v_{ntest} psi	v_n^* psi	$\frac{v_{ntest}}{v_n}$
				BRESLER AND SCORDELIS (10)						
A1	3490	12.1	18.35	3.92	1.80	47.2	52.5	236	243	.973
A2	3520	12.0	18.27	4.93	2.28	47.6	55.0	251	231	1.086
B1	3590	9.1	18.15	3.95	2.43	69.2	50.0	303	287	1.054
B2	3360	9.0	18.33	4.91	2.43	70.0	45.0	273	258	1.057
C1	4290	6.1	18.25	3.95	1.80	93.9	35.0	314	324	.971
C2	3450	6.0	18.28	4.93	3.66	95.2	36.5	333	299	1.113
				PLACAS AND REGAN (35)						
R8	3870	6.0	10.7	3.36	1.46	83.5	17.9	279	313	.890
R9	4290	6.0	10.7	3.36	1.46	167.0	23.5	366	446	.821
R10	4295	6.0	10.7	3.36	.97	83.5	16.9	263	291	.903
R11	3800	6.0	10.7	3.36	1.95	83.5	20.1	313	326	.959
R12	4920	6.0	10.0	3.60	4.16	83.5	24.6	410	384	1.067
R13	4680	6.0	10.0	3.60	4.16	167.0	33.6	560	479	1.168
R14	4210	6.0	10.7	3.36	1.46	55.7	20.1	313	267	1.170
R15	4330	6.0	10.0	3.60	4.16	167.0	31.4	523	467	1.121
R16	4580	6.0	10.0	3.60	4.16	167.0	31.4	523	476	1.099
R17	1850	6.0	10.7	3.36	1.46	83.5	15.7	244	251	.975
R20	6230	6.0	10.7	3.36	1.46	83.5	20.2	315	353	.891
R21	6980	6.0	10.0	3.60	4.16	167.0	33.6	560	545	1.027
R22	4280	6.0	10.7	4.50	1.46	83.5	17.9	279	282	.988
R24	4480	6.0	10.0	5.05	4.16	83.5	20.7	345	317	1.089
R25	4470	6.0	10.0	3.60	4.16	83.5	23.5	392	371	1.055
R27	1980	6.0	10.0	3.60	4.16	167.0	21.3	355	355	1.000
R28	4580	6.0	10.0	3.60	4.16	326.0	40.3	672	657	1.022

* predicted

TABLE 4.2 (continued)

KREFELD AND THURSTON (24)

26-1	5820	10.0	17.94	4.01	2.22	79.0	46.5	259	343	.756
29a-1	5630	10.0	17.94	4.01	2.22	53.0	35.9	200	299	.670
29b-1	5460	10.0	17.94	4.01	2.22	53.0	36.0	201	298	.674
29a-2	5390	10.0	17.94	4.01	2.22	62.0	48.7	271	311	.873
29b-2	6000	10.0	17.94	4.01	2.22	62.0	45.5	254	321	.789
29c-2	3500	10.0	17.94	4.01	2.22	62.0	36.3	202	268	.755
29d-2	4410	10.0	17.94	4.01	2.22	62.0	37.1	207	292	.708
29e-2	7030	10.0	17.94	4.01	2.22	62.0	46.4	259	340	.761
29-3	4970	10.0	17.94	4.01	2.22	40.0	43.3	223	266	.837

TABLE 4.3 COMPARISON OF PREDICTED AND EXPERIMENTAL NOMINAL SHEAR STRESS FOR T-BEAMS WITH STIRRUPS

Beams	f'_c psi	b_w in.	d in.	a/d	$100\rho_w$	$\rho_v f_{vy}$	V_{ntest} kips	v_{ntest} psi	v_n^* psi	$\frac{v_{ntest}}{v_n}$
				AUTHOR						
A25	4720	7.5	15.38	3.96	.663	31.8	19.275	167	189	.885
A25a	4790	7.5	15.26	4.00	.668	31.8	20.772	181	183	.991
A50	3810	7.5	15.42	3.96	.661	74.0	25.954	224	247	.907
A50a	4060	7.5	15.49	3.94	.658	75.0	24.660	212	248	.855
A75	4670	7.5	15.56	3.92	.655	97.0	31.966	274	295	.928
#1	5520	7.5	14.60	4.18	.699	106.0	31.275	285	321	.888
B25	4470	7.5	15.52	3.93	.494	32.4	17.670	152	174	.872
B50	4390	7.5	15.39	3.96	.498	76.2	24.05	208	247	.844
C25	4100	7.5	15.33	3.98	.948	32.4	18.650	162	199	.813
C50	4300	7.5	15.47	3.94	.939	76.2	30.150	260	270	.963
C75	4260	7.5	15.57	3.92	.933	103.0	31.020	266	313	.847
				HADDADIN, HONG AND MATTOCK (17)						
B3	4000	7.0	15.00	3.37	3.81	210.0	61.0	581	519	1.118
C2	4027	7.0	15.00	4.25	3.81	95.0	39.0	371	338	1.099
C3	3500	7.0	15.00	4.25	3.81	210.0	58.5	577	448	1.245
D3	4244	7.0	15.00	6.00	3.81	210.0	54.2	516	424	1.218
C4	3730	7.0	15.0	4.25	3.81	393.0	69.8	665	552	1.020

* predicted

TABLE 4.3 (continued)

PLACAS AND REGAN (35)

T1	4050	6.0	10.7	3.36	1.25	83.5	24.7	385	308	1.248
T3	3990	6.0	10.7	3.36	1.46	83.5	23.5	366	316	1.160
T4	4710	6.0	10.7	3.36	1.95	83.5	24.6	383	347	1.103
T5	4890	6.0	10.7	3.36	1.46	167.0	31.4	489	459	1.066
T6	3740	6.0	10.0	3.60	4.16	326.0	46.0	767	618	1.240
T7	3970	6.0	10.4	3.46	3.00	83.5	24.6	394	348	1.131
T8	4530	6.0	10.0	3.60	4.16	83.5	28.0	467	373	1.250
T9	2930	6.0	10.0	3.60	4.16	167.0	34.7	578	409	1.415
T10	4090	6.0	10.7	3.36	1.46	55.7	19.5	304	262	1.158
T13	1850	6.0	10.7	3.36	1.46	83.5	20.2	315	252	1.245
T15	4810	6.0	10.0	7.20	4.16	83.5	23.5	392	291	1.345
T16	4740	6.0	10.0	7.20	4.16	55.7	20.8	347	259	1.338
T17	4790	6.0	10.0	7.20	4.16	167.0	30.1	502	378	1.326
T19	4340	6.0	10.0	5.40	4.16	83.5	25.5	425	305	1.392
T20	4655	6.0	10.0	5.40	4.16	167.0	34.6	577	405	1.423
T25	7840	6.0	10.7	3.36	1.46	83.5	25.8	402	376	1.070
T26	8260	6.0	10.0	3.60	4.16	167.0	40.3	672	575	1.169
T27	1740	6.0	10.0	3.60	4.16	167.0	29.7	495	337	1.467
T31	4495	6.0	10.7	3.36	1.46	83.5	21.3	332	322	1.030
T32	4000	6.0	10.0	3.60	4.16	326.0	48.6	785	658	1.192
T34	4920	6.0	10.0	5.40	4.16	83.5	25.2	420	320	1.311
T35	4880	6.0	10.0	5.40	4.16	83.5	25.8	430	319	1.346
T36	3500	6.0	10.0	3.60	4.16	167.0	40.3	672	434	1.546
T37	4615	6.0	10.0	3.60	4.16	326.0	47.1	785	658	1.192
T38	4380	6.0	10.0	3.60	4.16	326.0	53.8	897	648	1.383

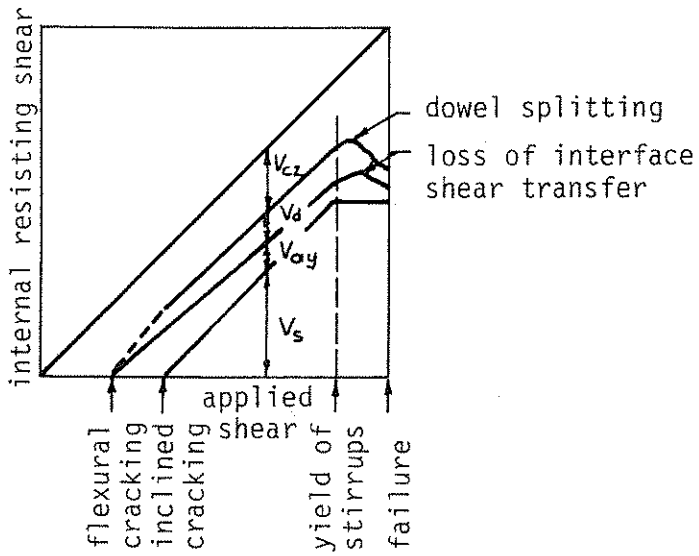

Figure 1.1 Distribution of Internal Shears on Beams with Stirrups (3).

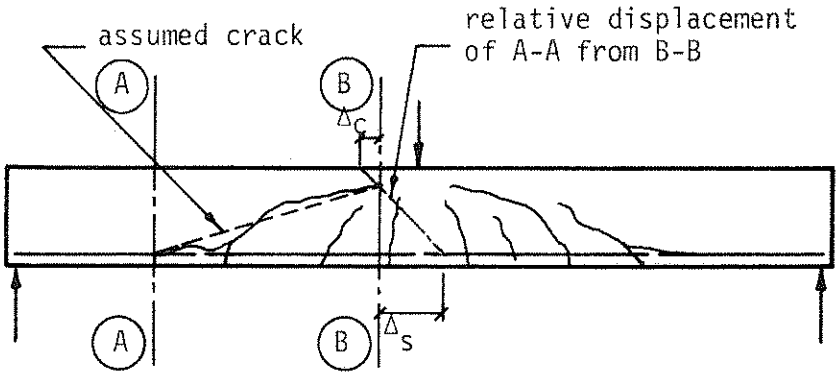

Figure 1.2 Shear Compression Model.

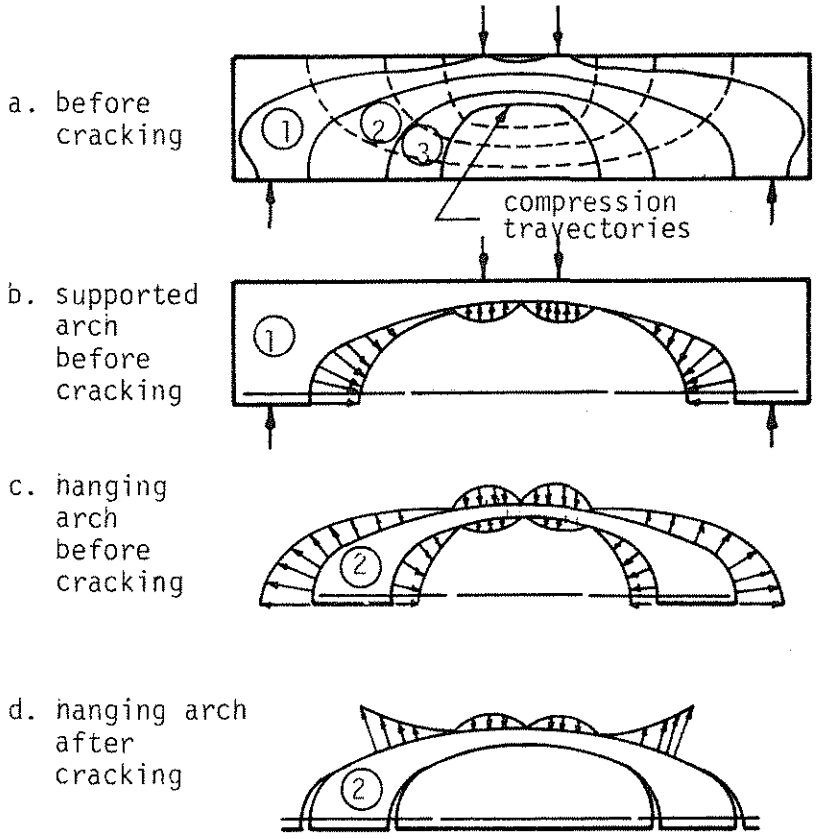

Figure 1.3 Internal Arches in a Reinforced Concrete Beam (22).

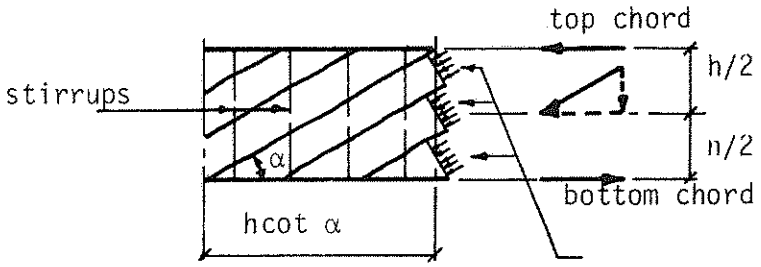

Figure 1.4 Diagonal Compression Field Model (16).

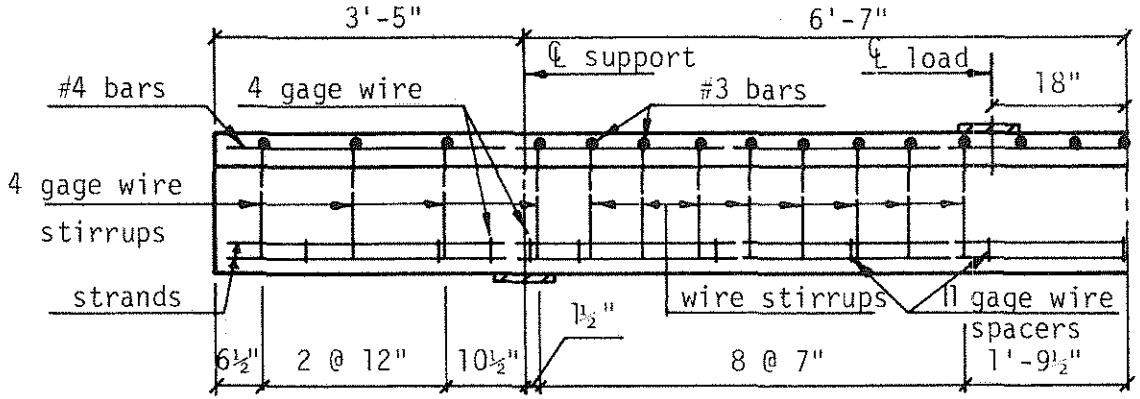

Half Beam Elevation

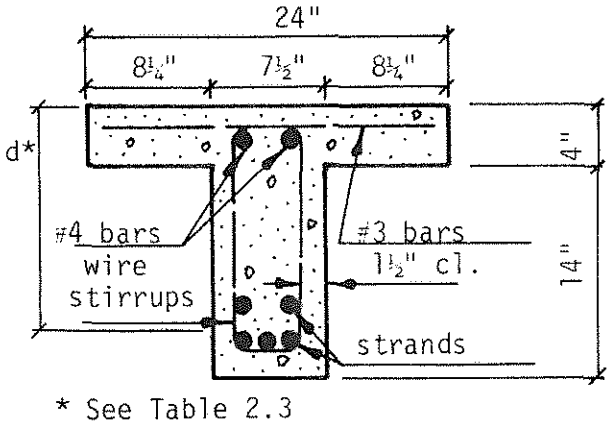

* See Table 2.3

Section at Shear Span

Beams with Stirrups

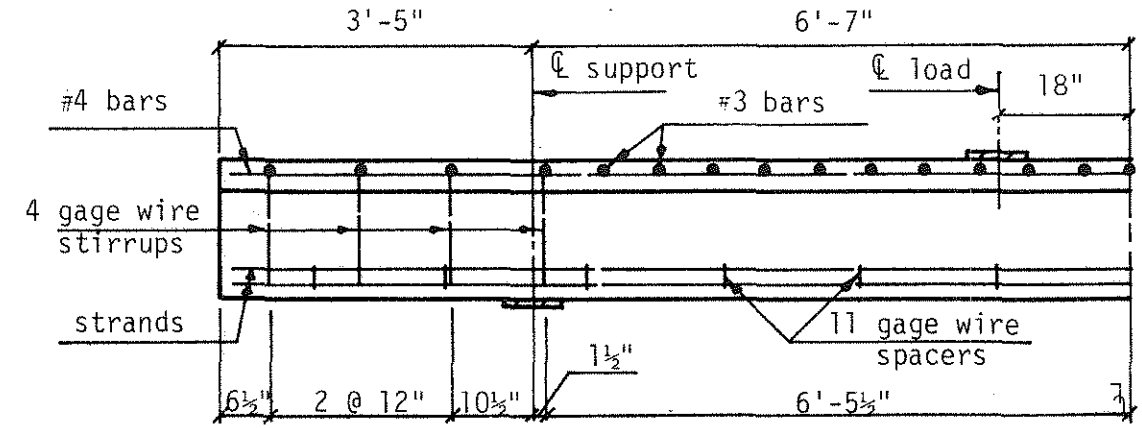

Half Beam Elevation

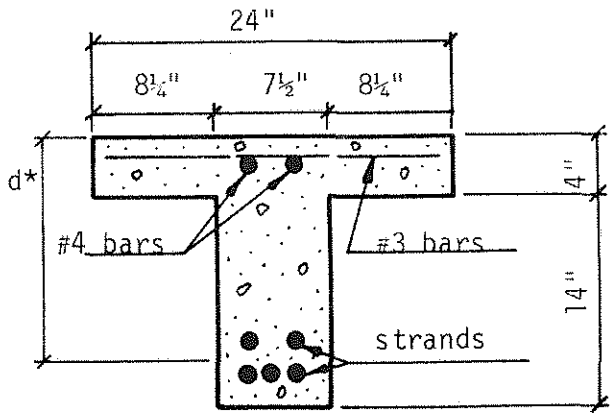

* See Table 2.3

Section at Shear Span

Beams without Stirrups

Figure 2.1 Beam Details

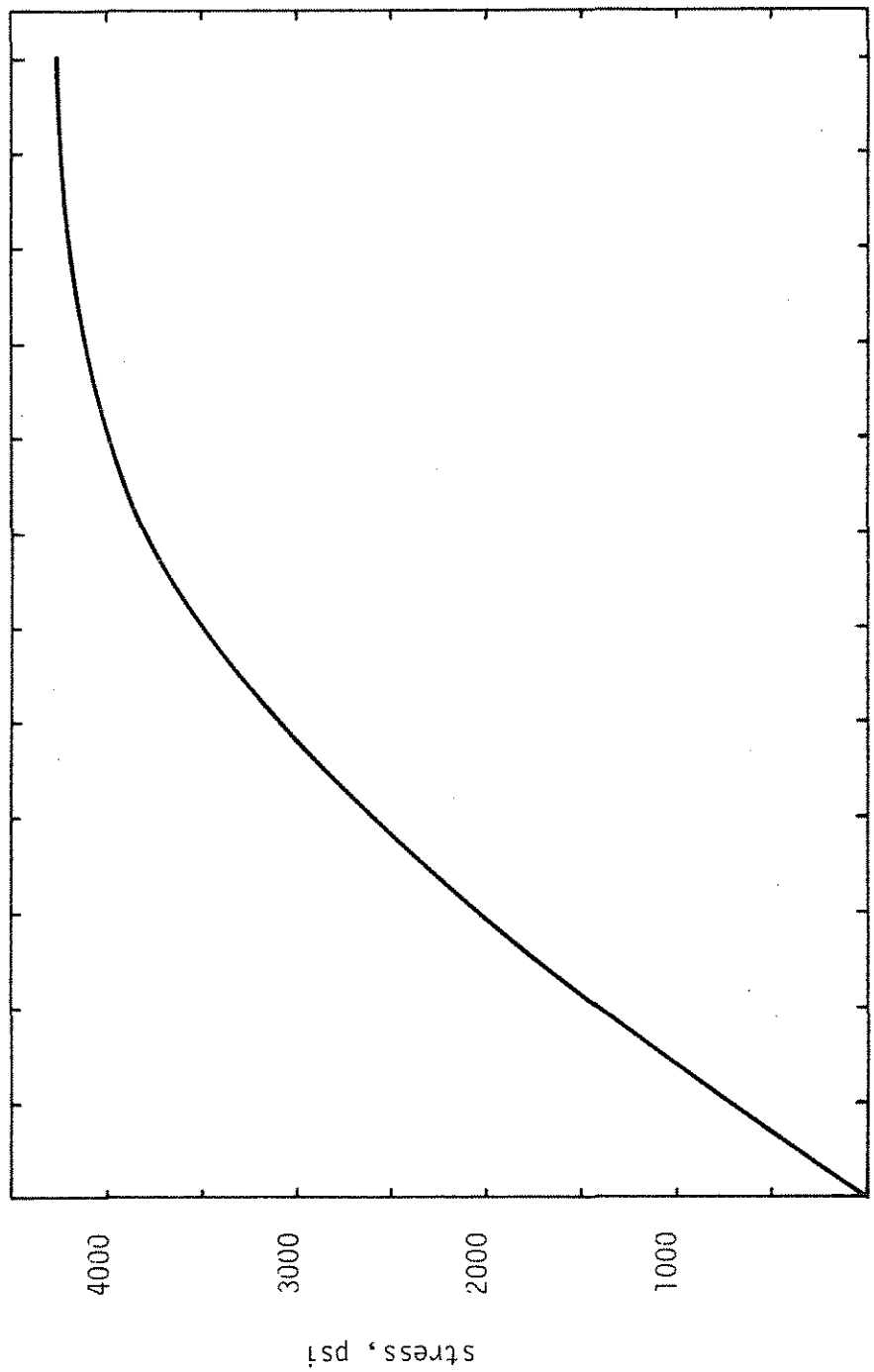

Figure 2.2 Typical Stress-Strain Curve for Concrete.

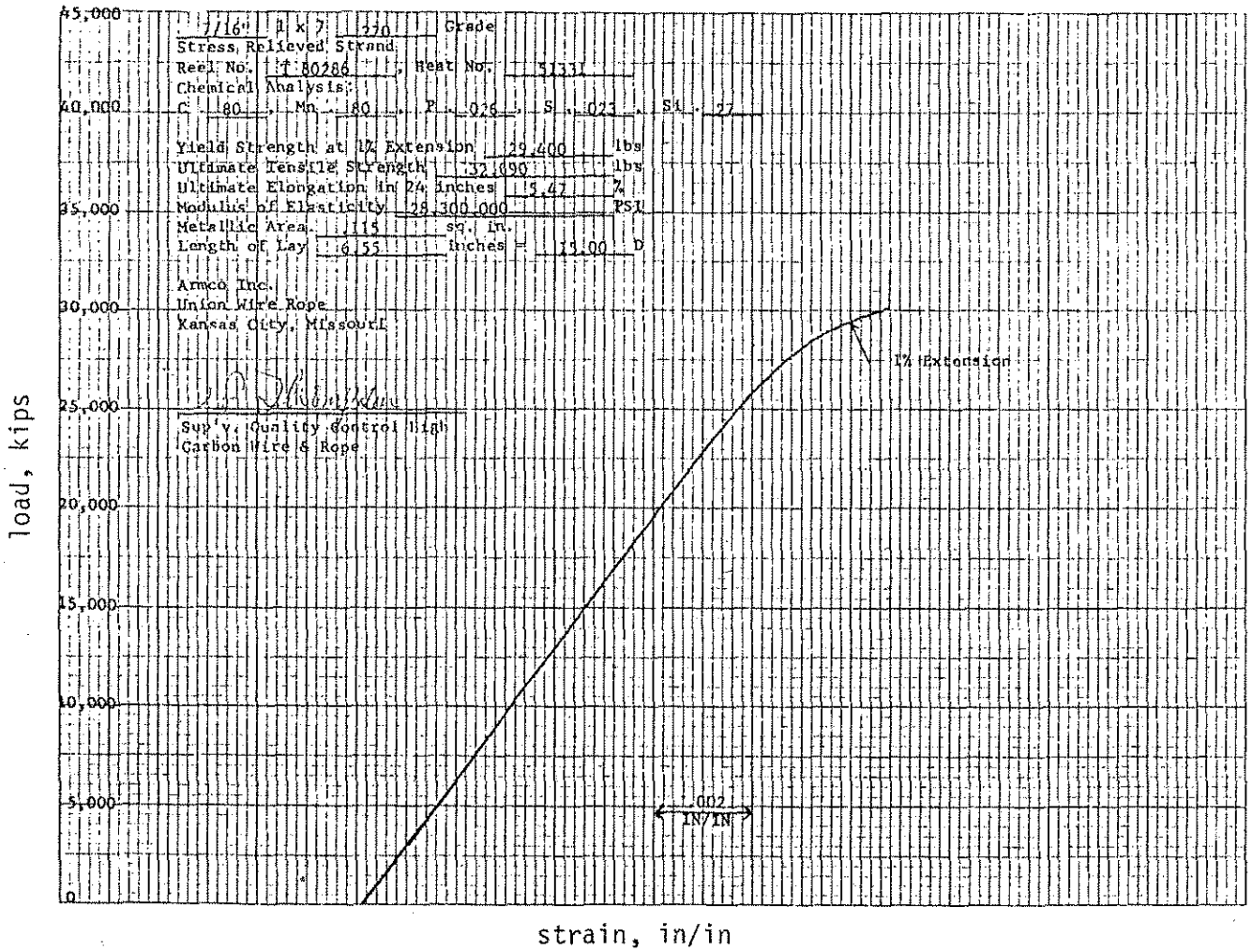

Figure 2.3 Load-Strain Curve, 7/16 inch Diameter Strand.

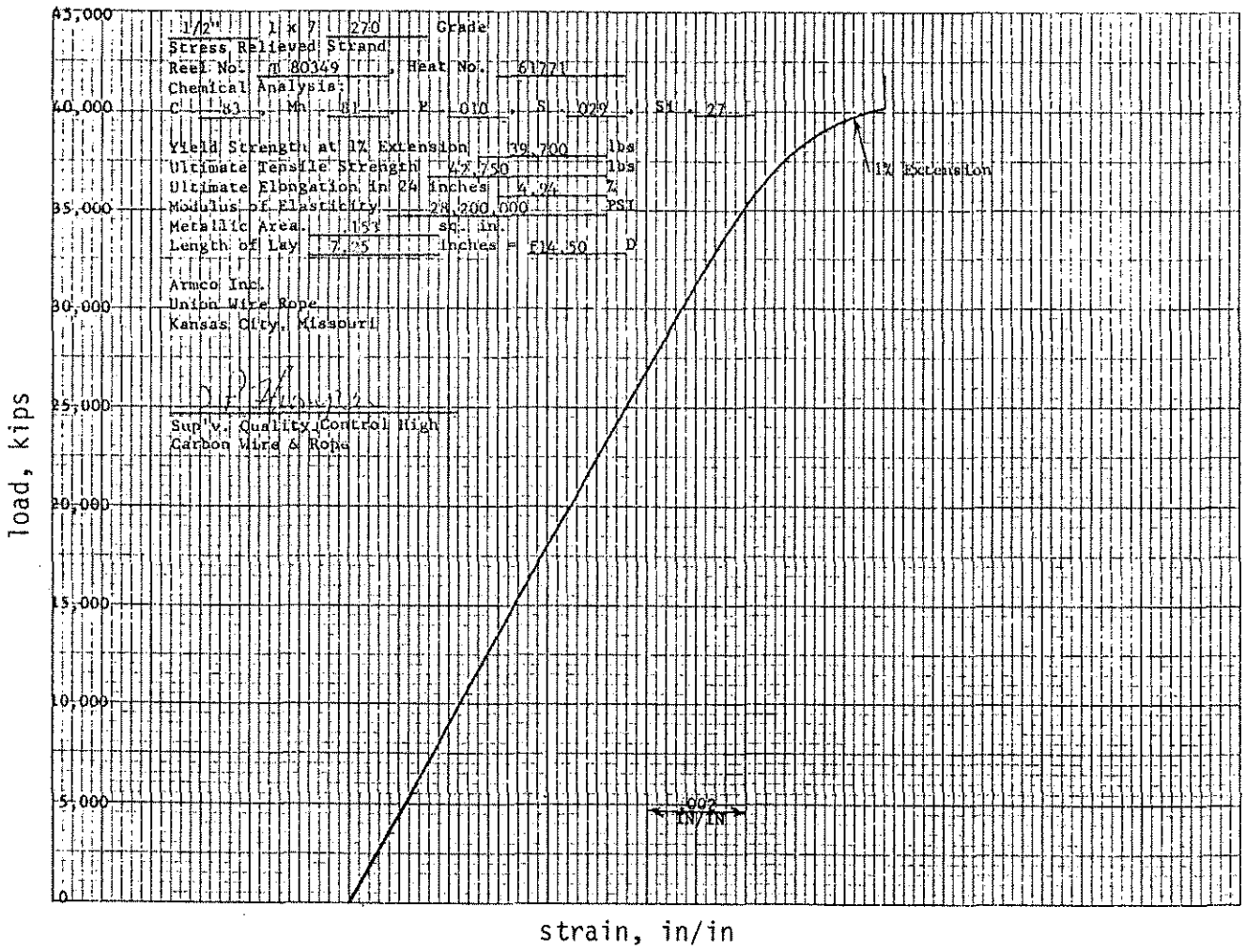

Figure 2.4 Load-Strain Curve, 1/2 inch diameter Strand.

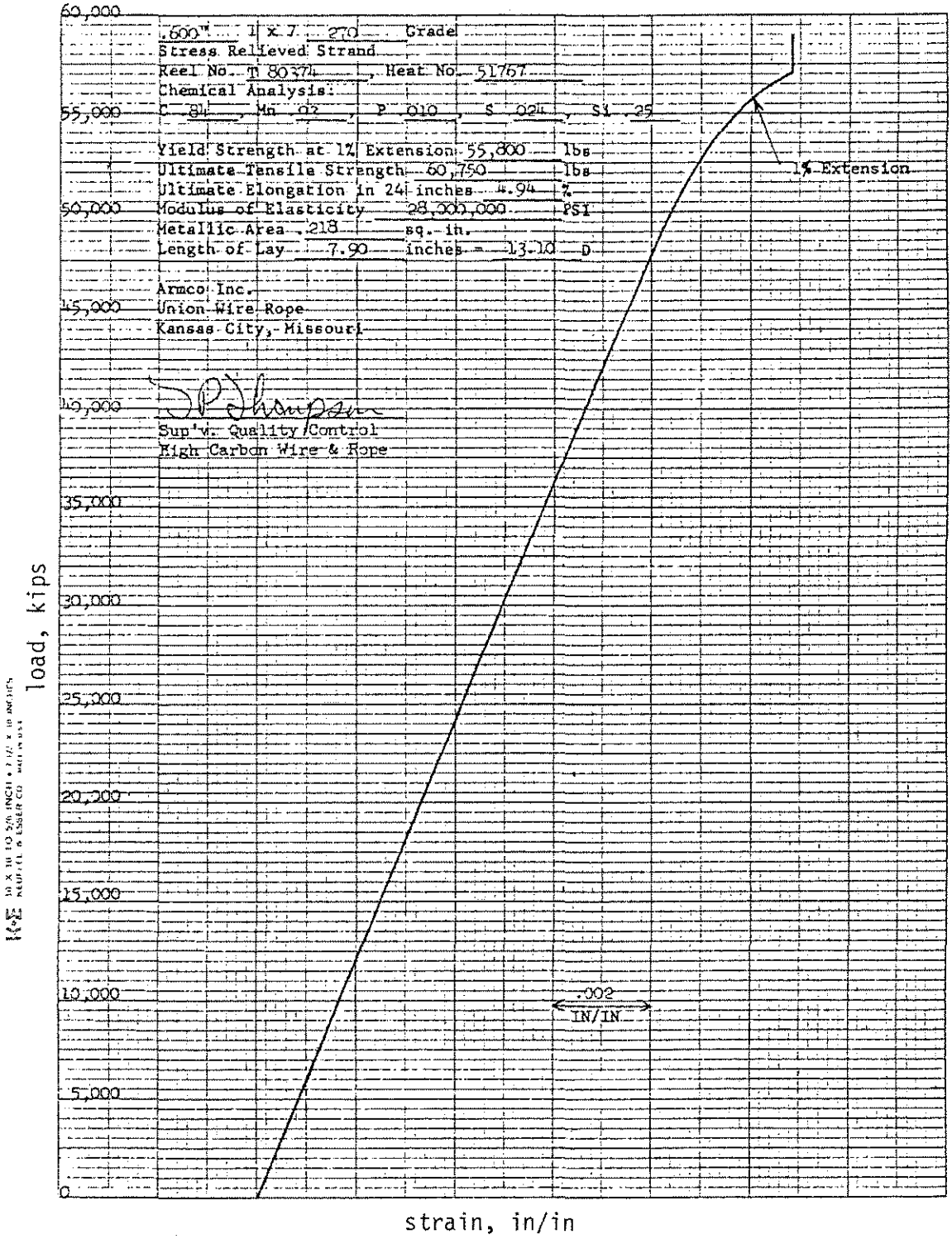

Figure 2.5 Load-strain curve, 0.6 inch Diameter Strand.

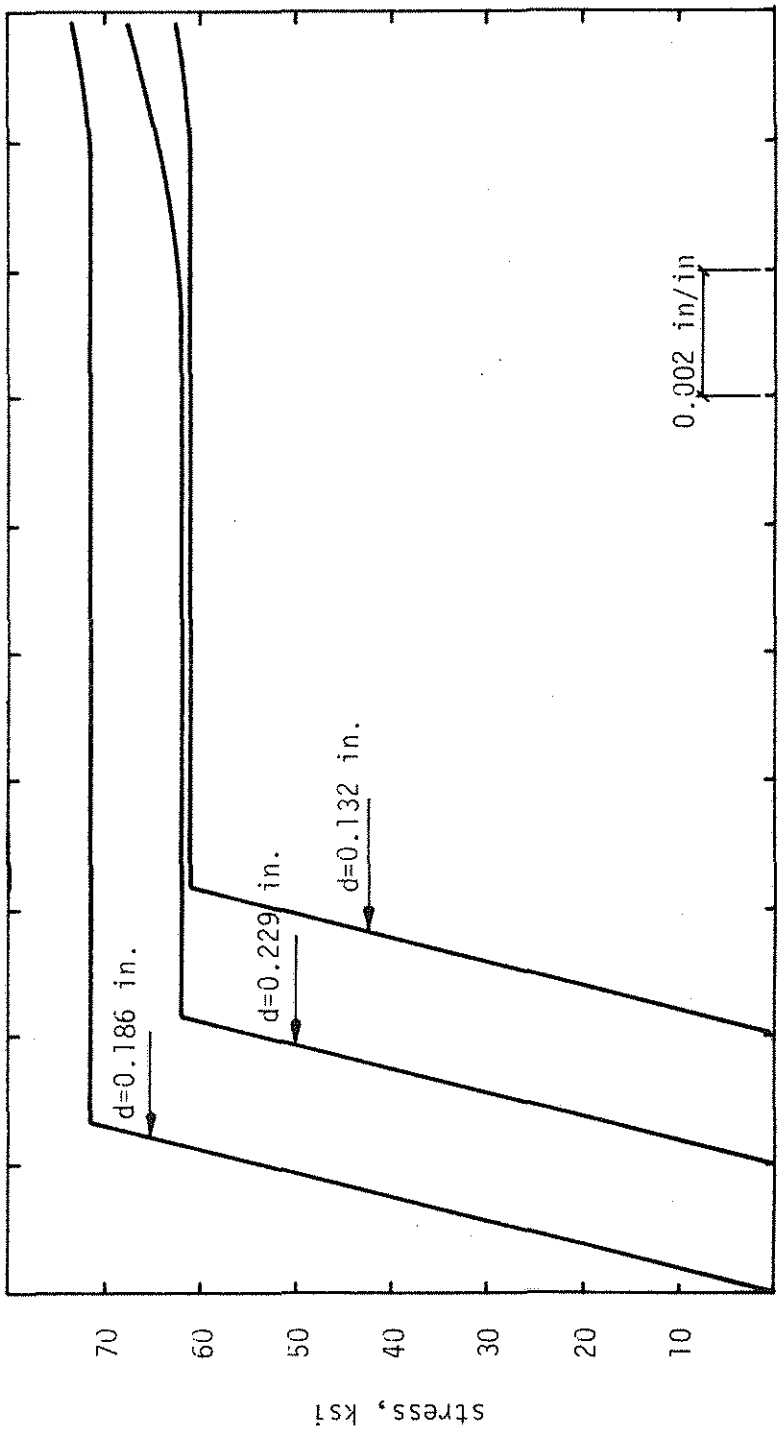

Figure 2.6 Stress-Strain Curves for Smooth Wire.

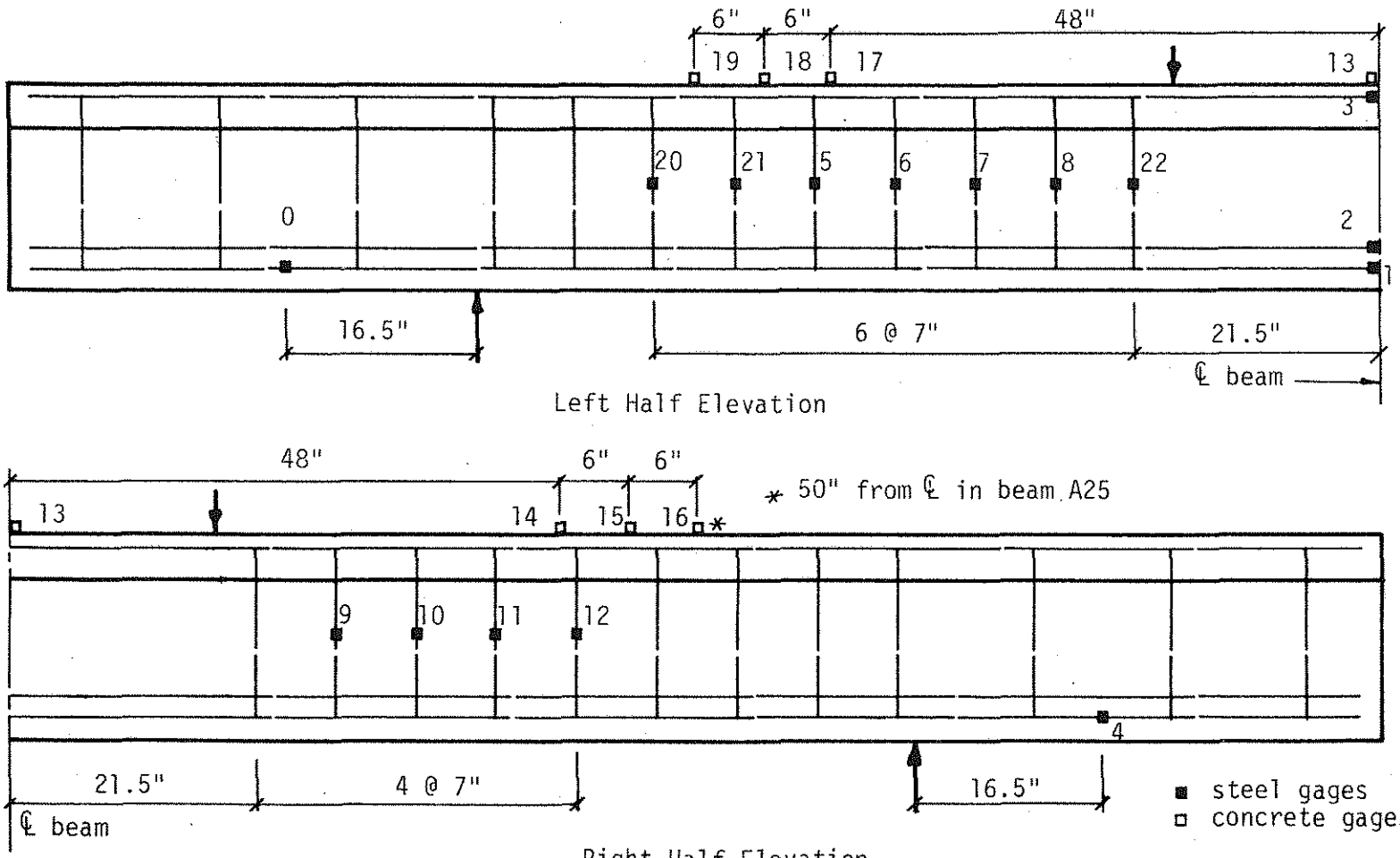

Figure 2.7 Strain Gage Locations

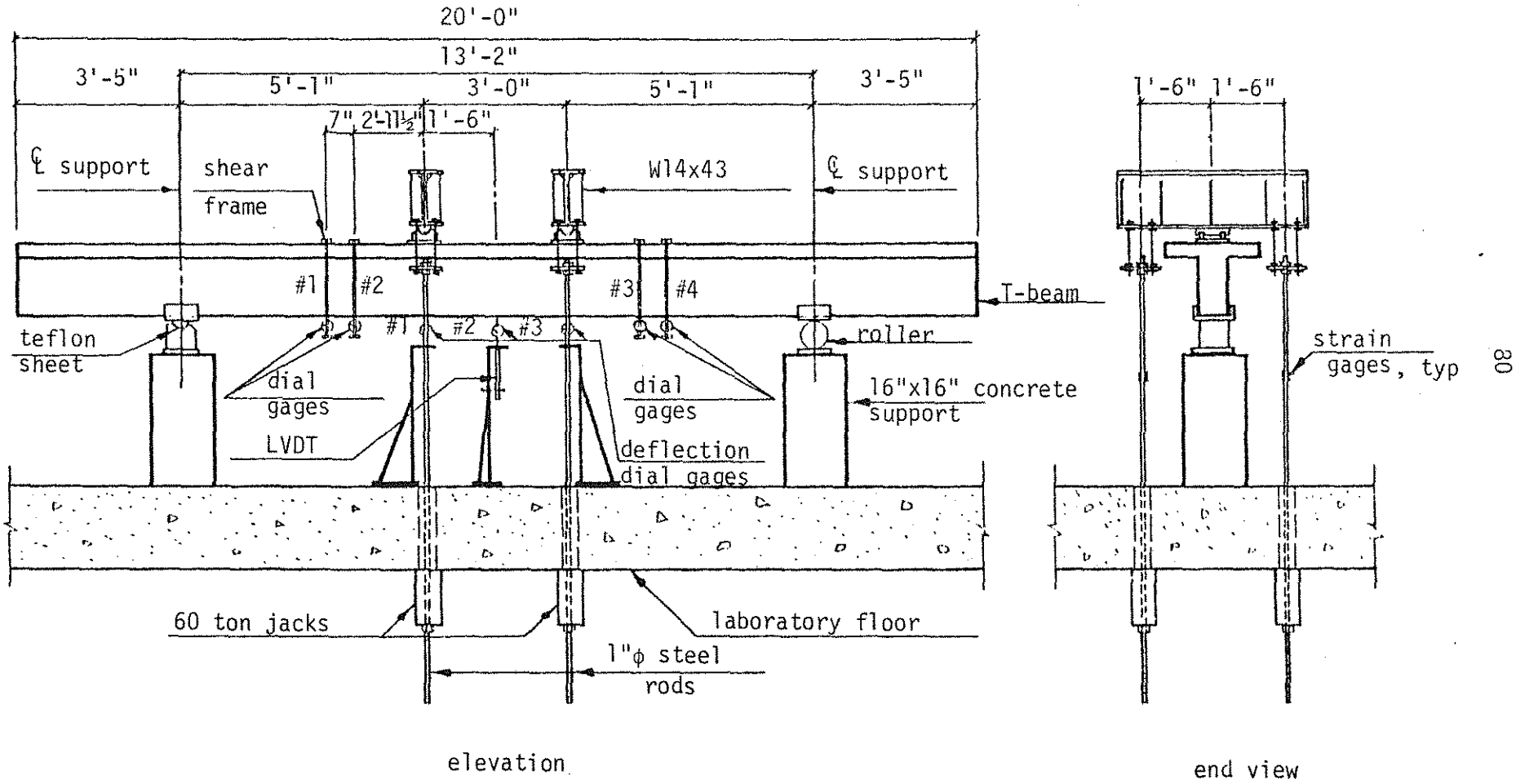

Figure 2.8 Loading System.

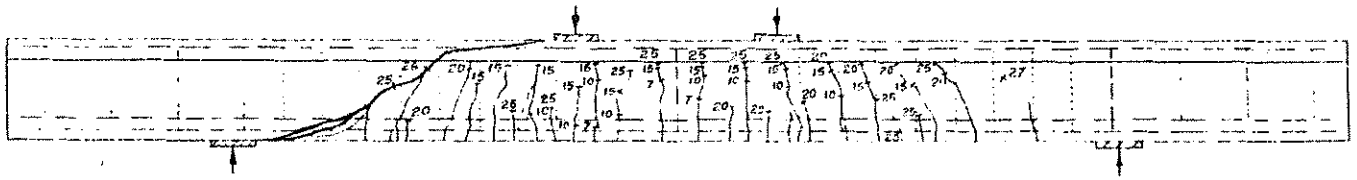

Beam A00 (ρ_w = 0.656%, $\rho_v f_{vy}$ = 0.0 psi)

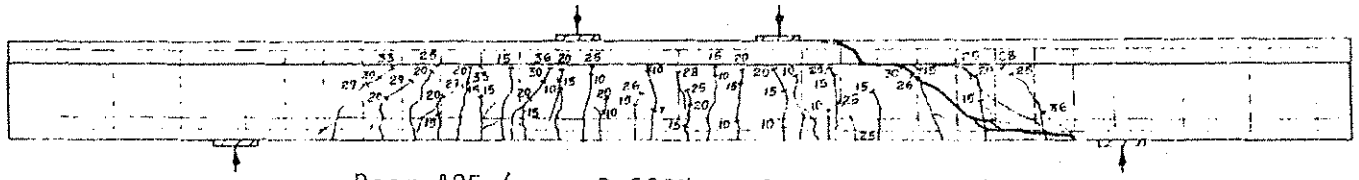

Beam A25 (ρ_w = 0.663%, $\rho_v f_{vy}$ = 31.8 psi)

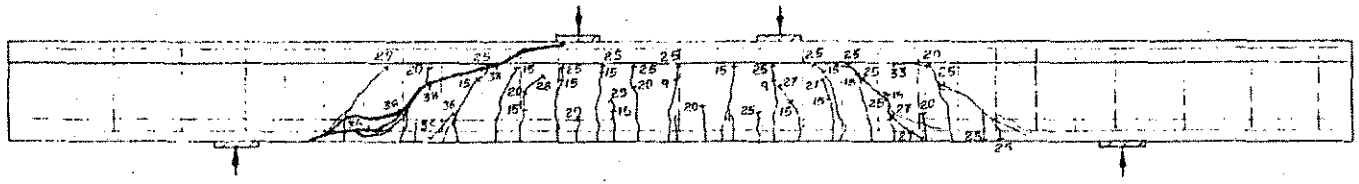

Beam A25a (ρ_w = 0.668%, $\rho_v f_{vy}$ = 31.8 psi)

Figure 2.9 Crack Patterns for Beams A00, A25, and A25a.

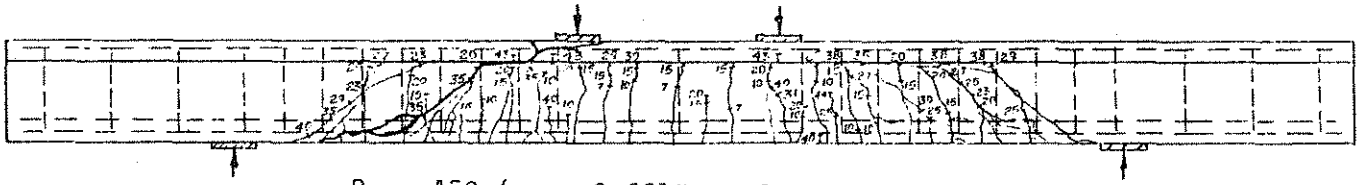

Beam A50 (ρ_w = 0.661%, $\rho_v f_{vy}$ = 73.9 psi)

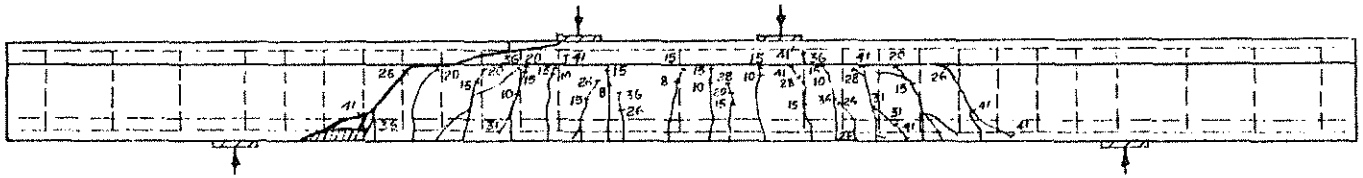

Beam A50a (ρ_w = 0.658%, $\rho_v f_{vy}$ = 75.0 psi)

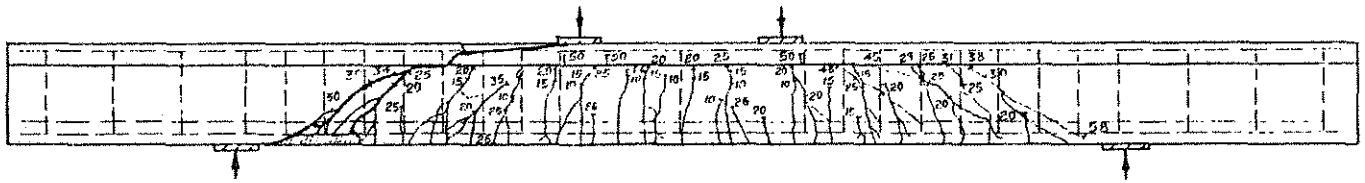

Beam A75 (ρ_w = 0.655%, $\rho_v f_{vy}$ = 97.1 psi)

Figure 2.10 Crack Patterns for Beams A50, A50a, and A75.

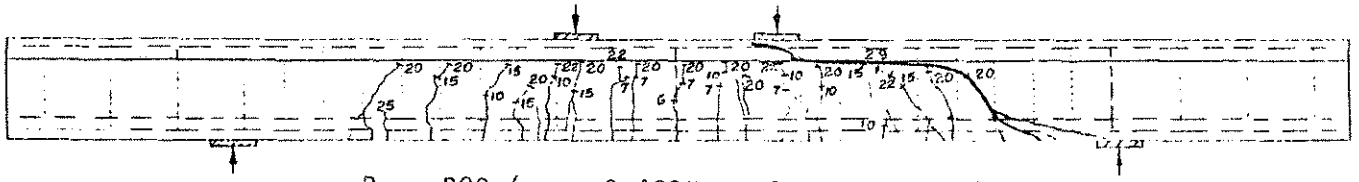

Beam B00 (ρ_w = 0.488%, $\rho_v f_{vy}$ = 0.0 psi)

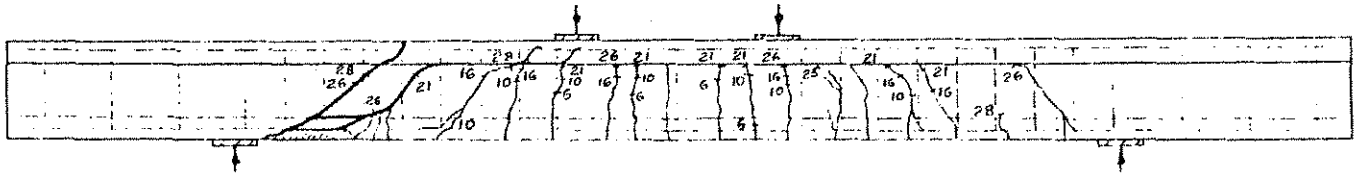

Beam B25 (ρ_w = 0.494%, $\rho_v f_{vy}$ = 32.4 psi)

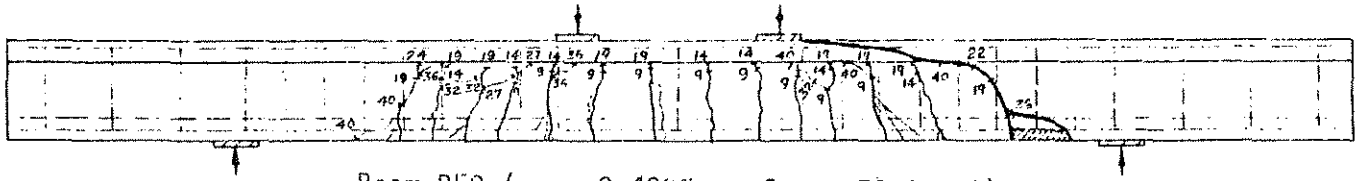

Beam B50 (ρ_w = 0.498%, $\rho_v f_{vy}$ = 76.2 psi)

Figure 2.11 Crack Pattern for Beams B00, B25, and B50.

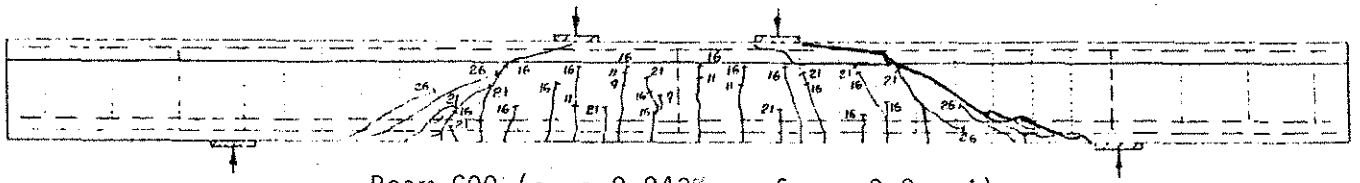

Beam C00 (ρ_w = 0.943%, $\rho_v f_{vy}$ = 0.0 psi)

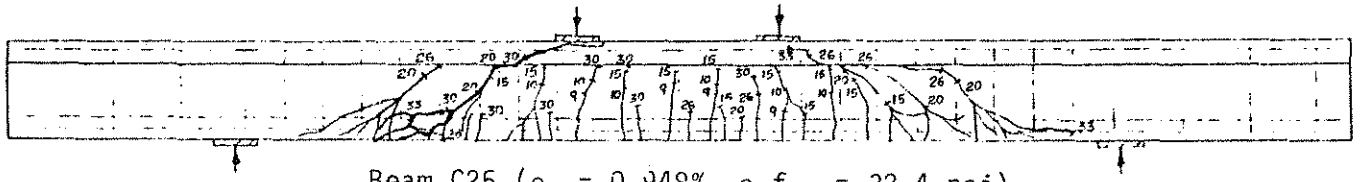

Beam C25 (ρ_w = 0.948%, $\rho_v f_{vy}$ = 32.4 psi)

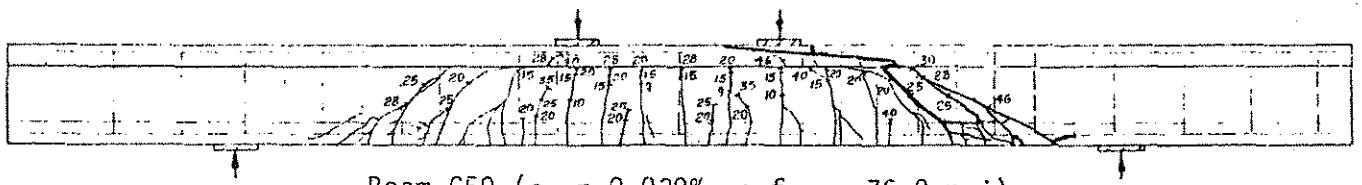

Beam C50 (ρ_w = 0.939%, $\rho_v f_{vy}$ = 76.2 psi)

Figure 2.12 Crack Patterns for Beams C00, C25, and C50.

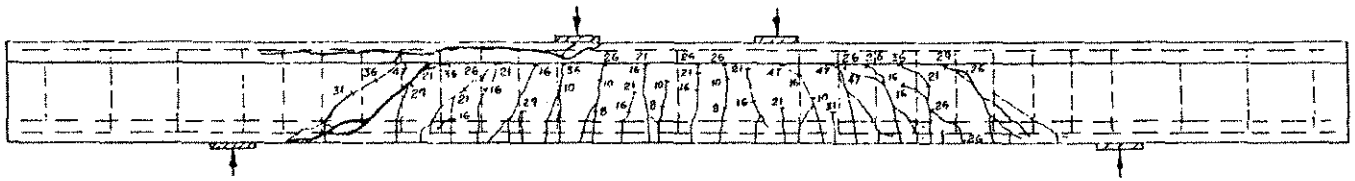

Beam C75 (ρ_w = 0.933%, $\rho_v f_{vy}$ = 103.0 psi)

Figure 2.13 Crack Pattern for Beam C75.

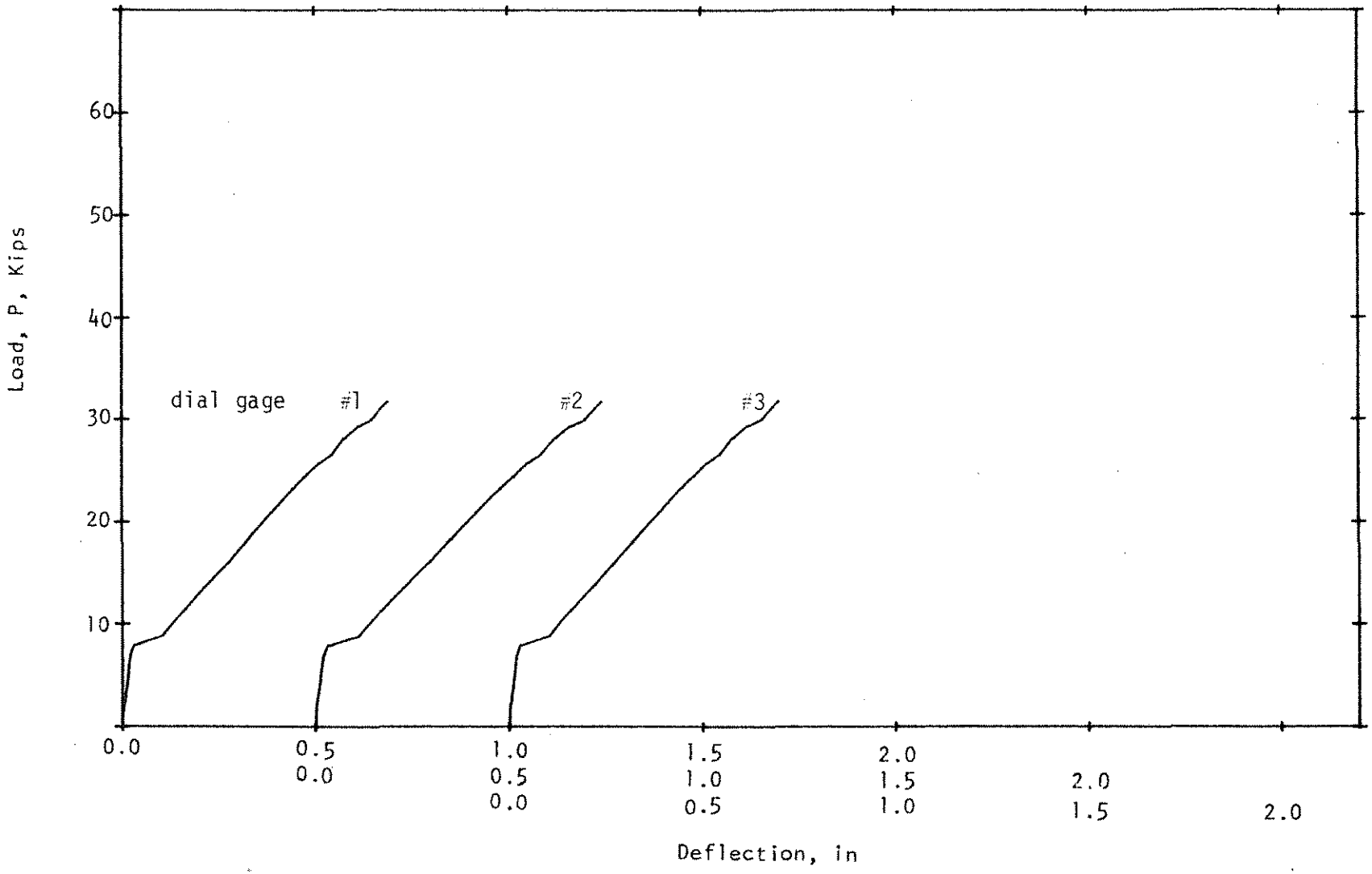

Figure 2.14 Load-Deflection Curves, Beam #2 (ρ_w = 0.693%, $\rho_v f_{vy}$ = 0.0 psi).

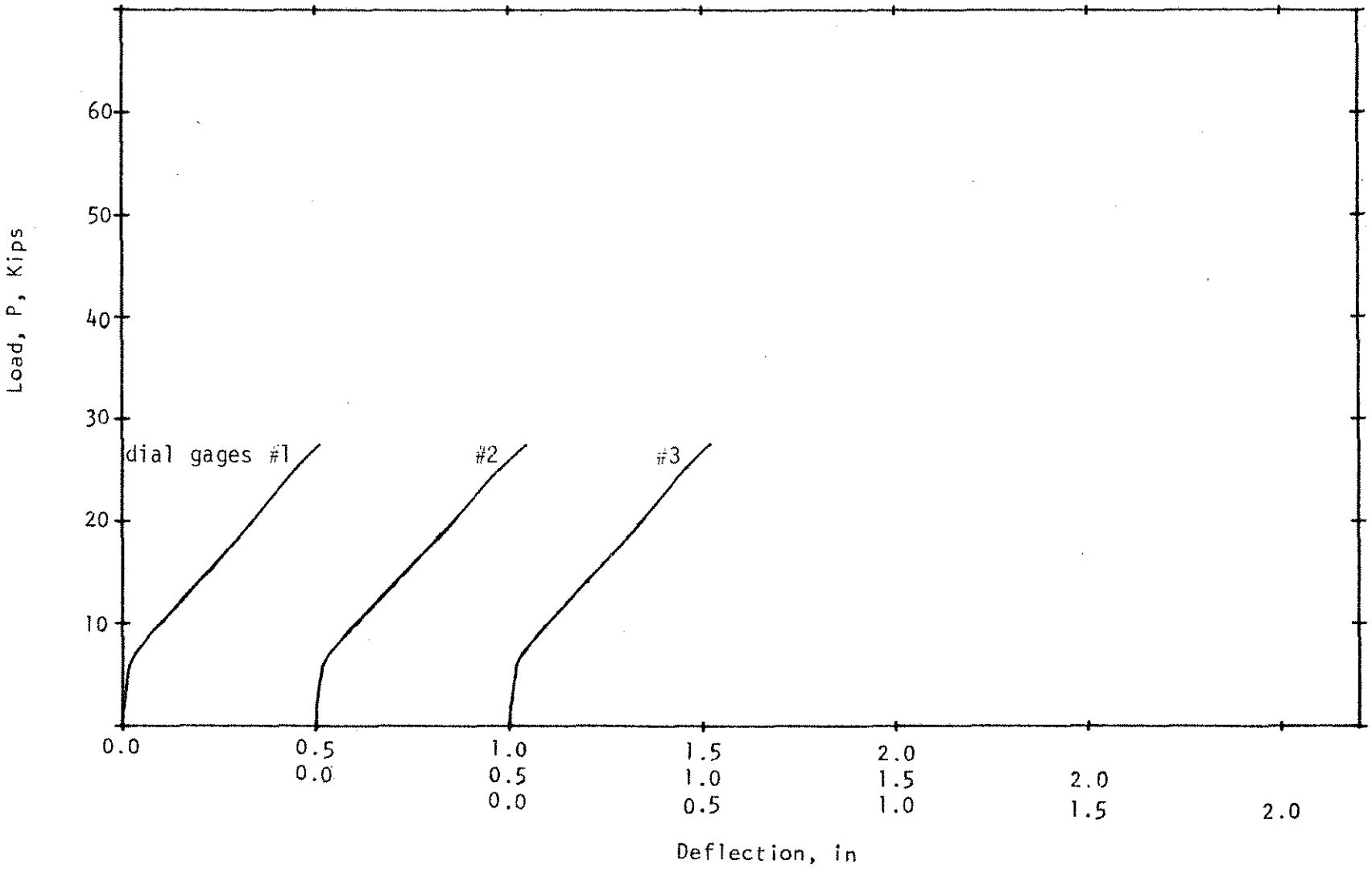

Figure 2.15 Load-Deflection Curves, Beam A00 (ρ_w = 0.656%, $\rho_v f_{vy}$ = 0.0 psi).

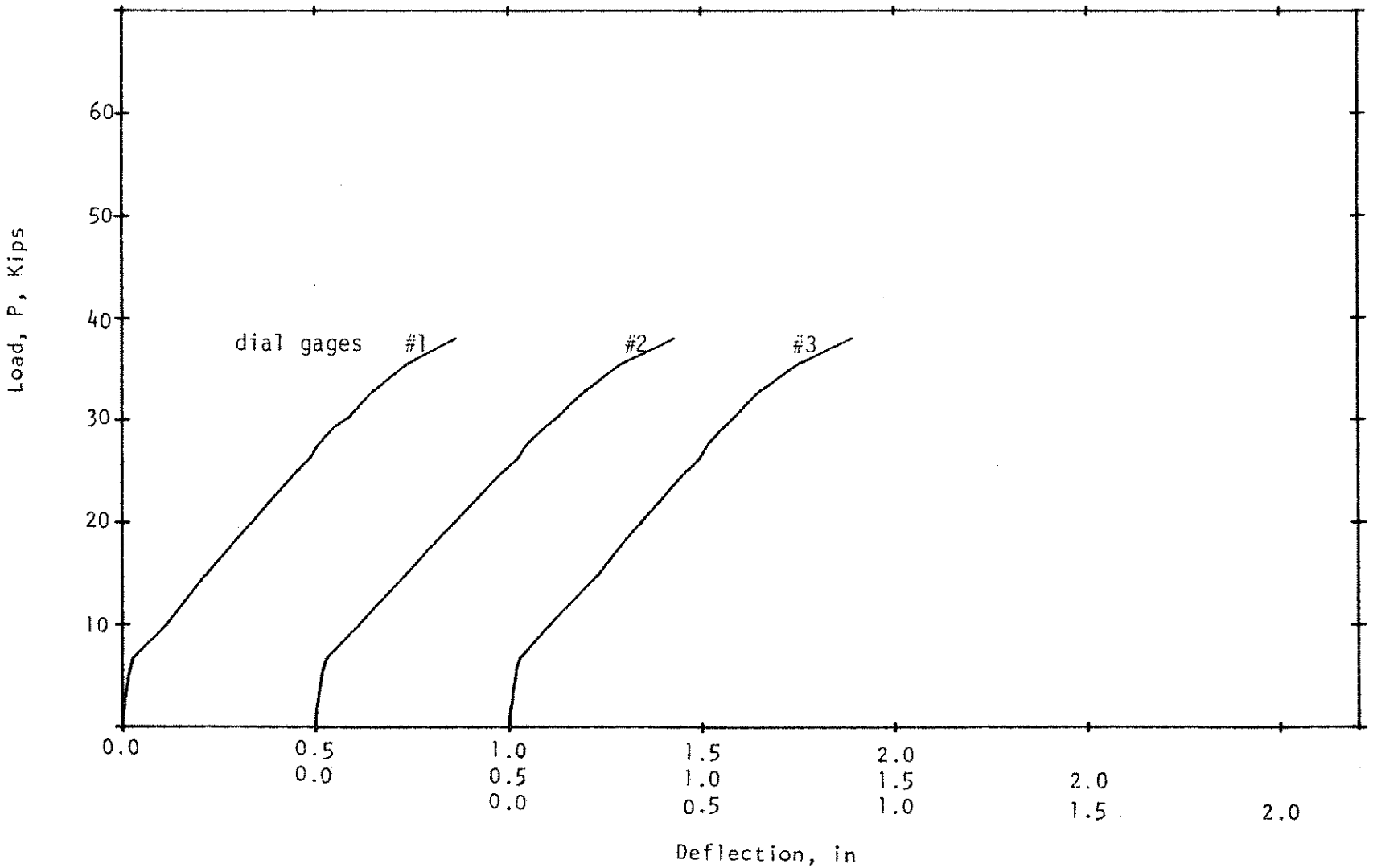

Figure 2.16 Load-Deflection Curves, Beam A25 (ρ_w = 0.663%, $\rho_v f_{vy}$ = 31.8% psi).

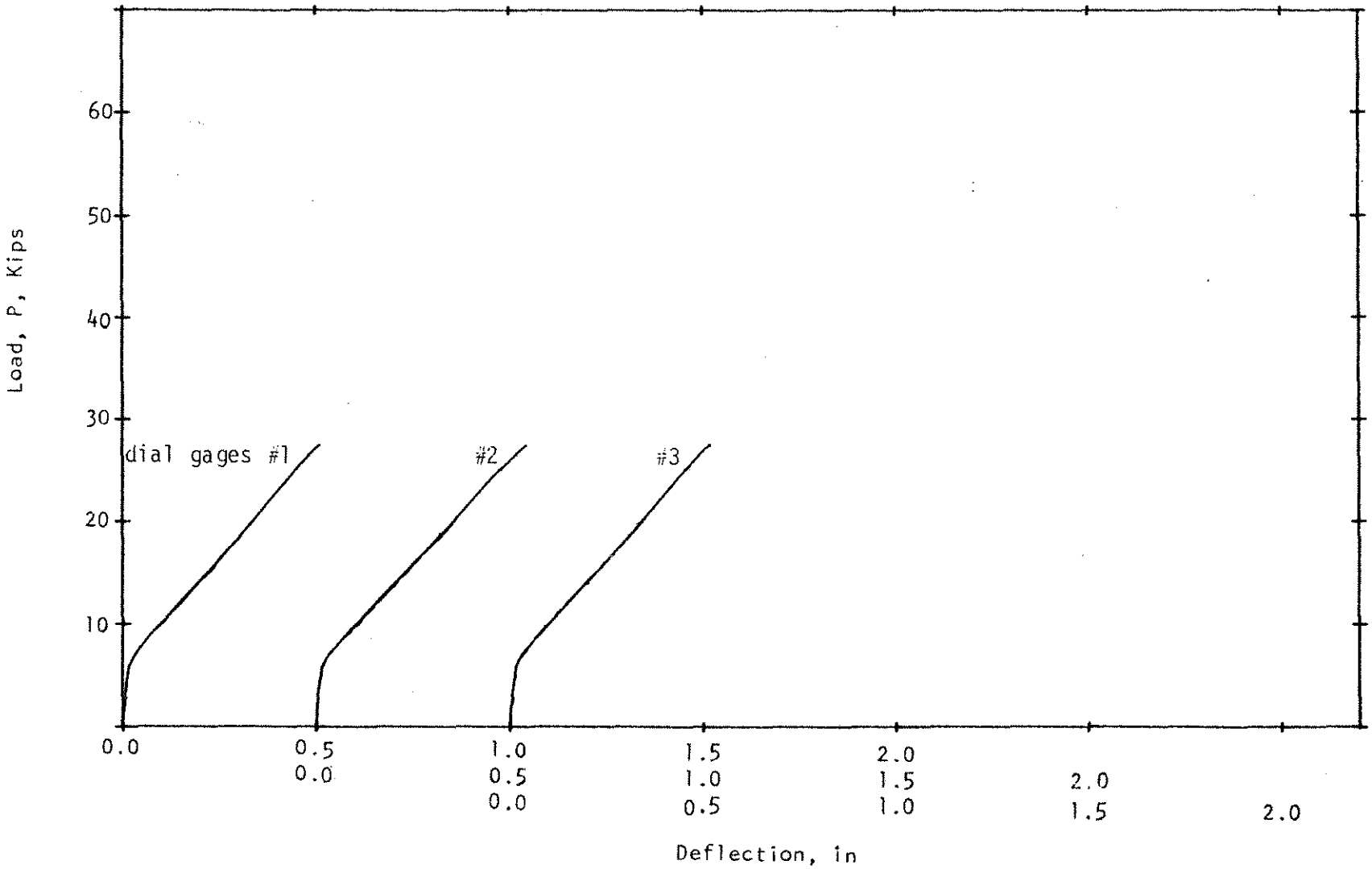

Figure 2.15 Load-Deflection Curves, Beam A00 (ρ_w = 0.656%, $\rho_v f_{vy}$ = 0.0 psi).

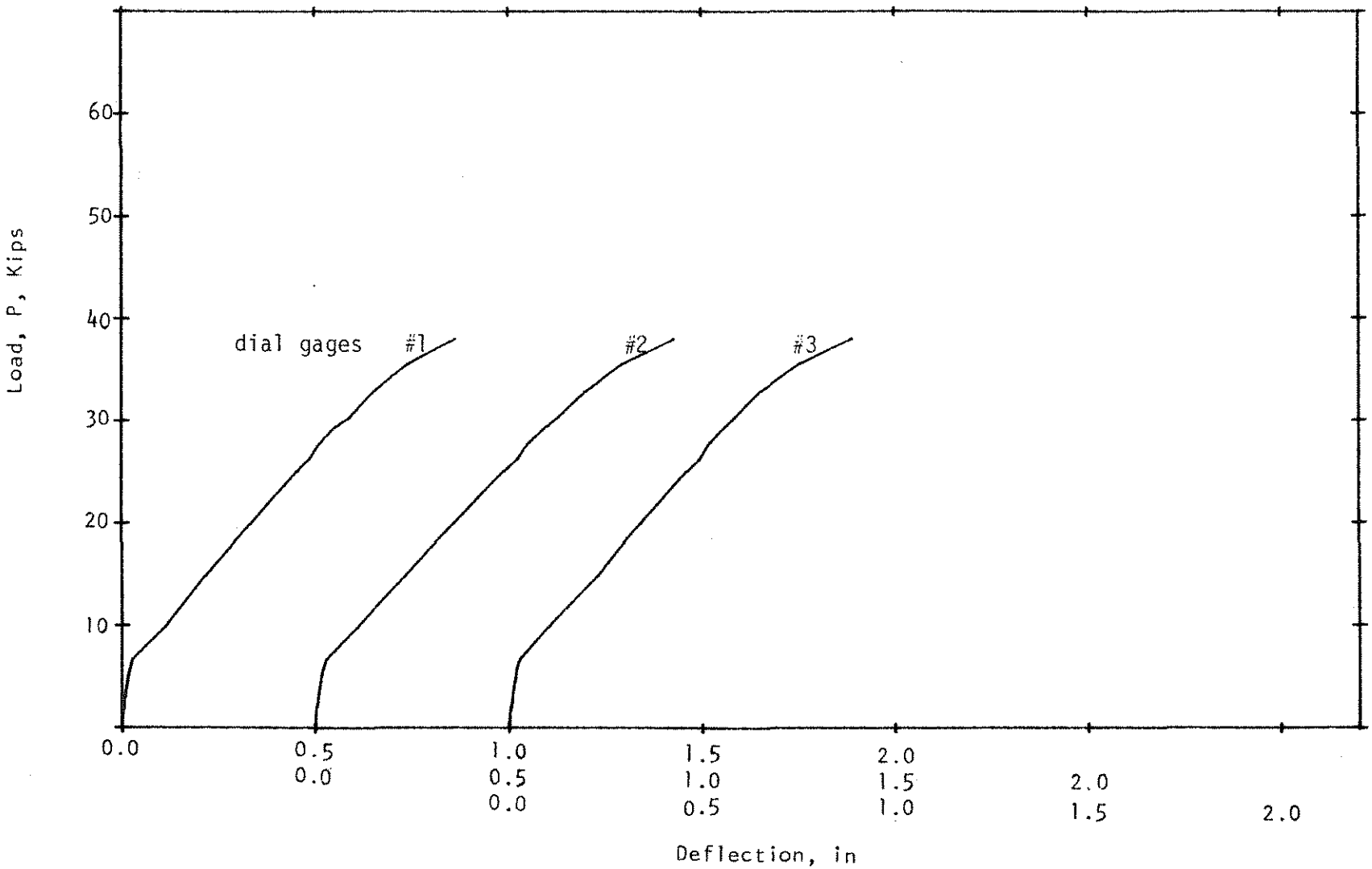

Figure 2.16 Load-Deflection Curves, Beam A25 (ρ_w = 0.663%, $\rho_v f_{vy}$ = 31.8% psi).

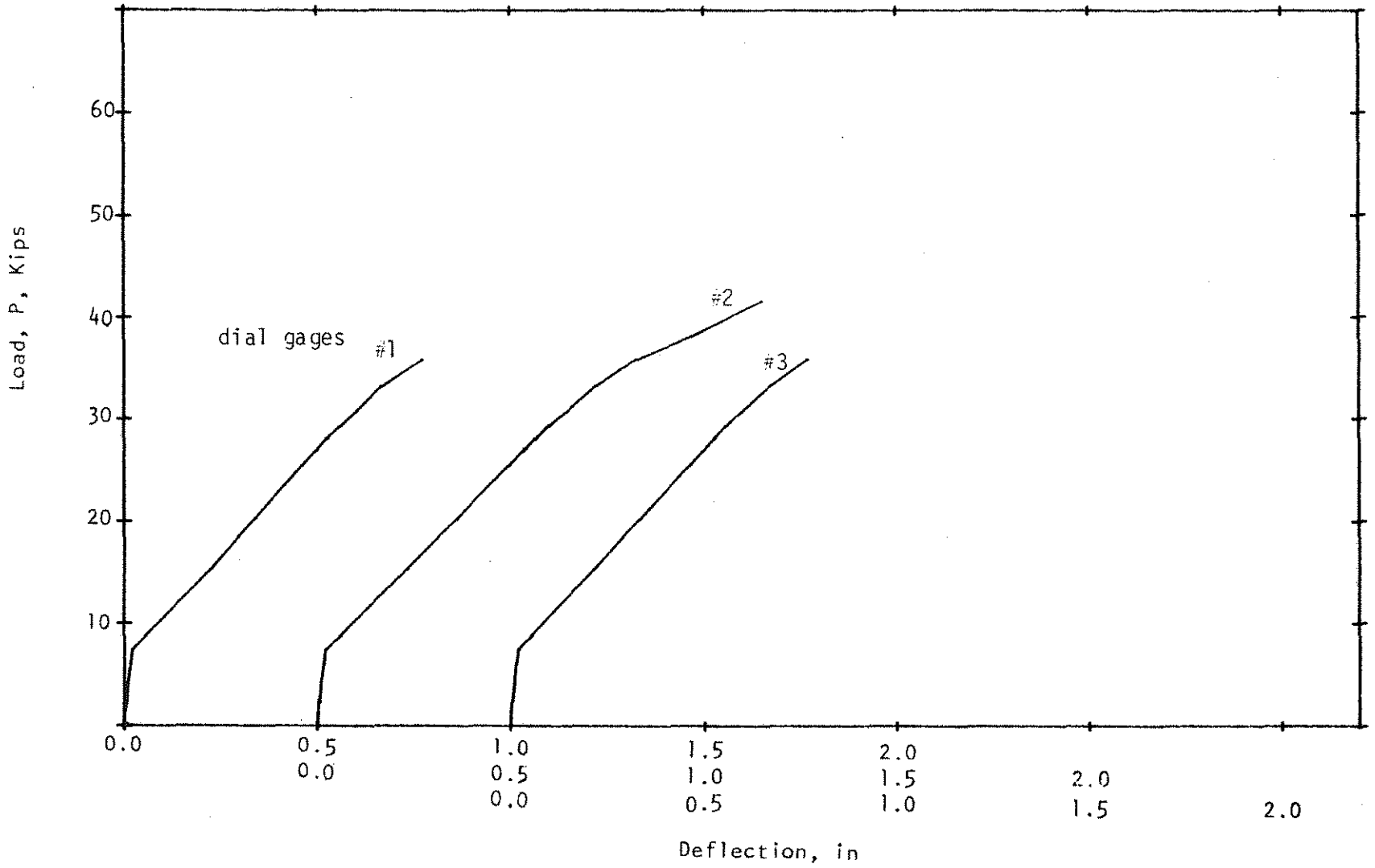

Figure 2.17 Load-Deflection Curves, Beam A25a (ρ_w = 0.668%, $\rho_v f_{vy}$ = 31.8 psi)

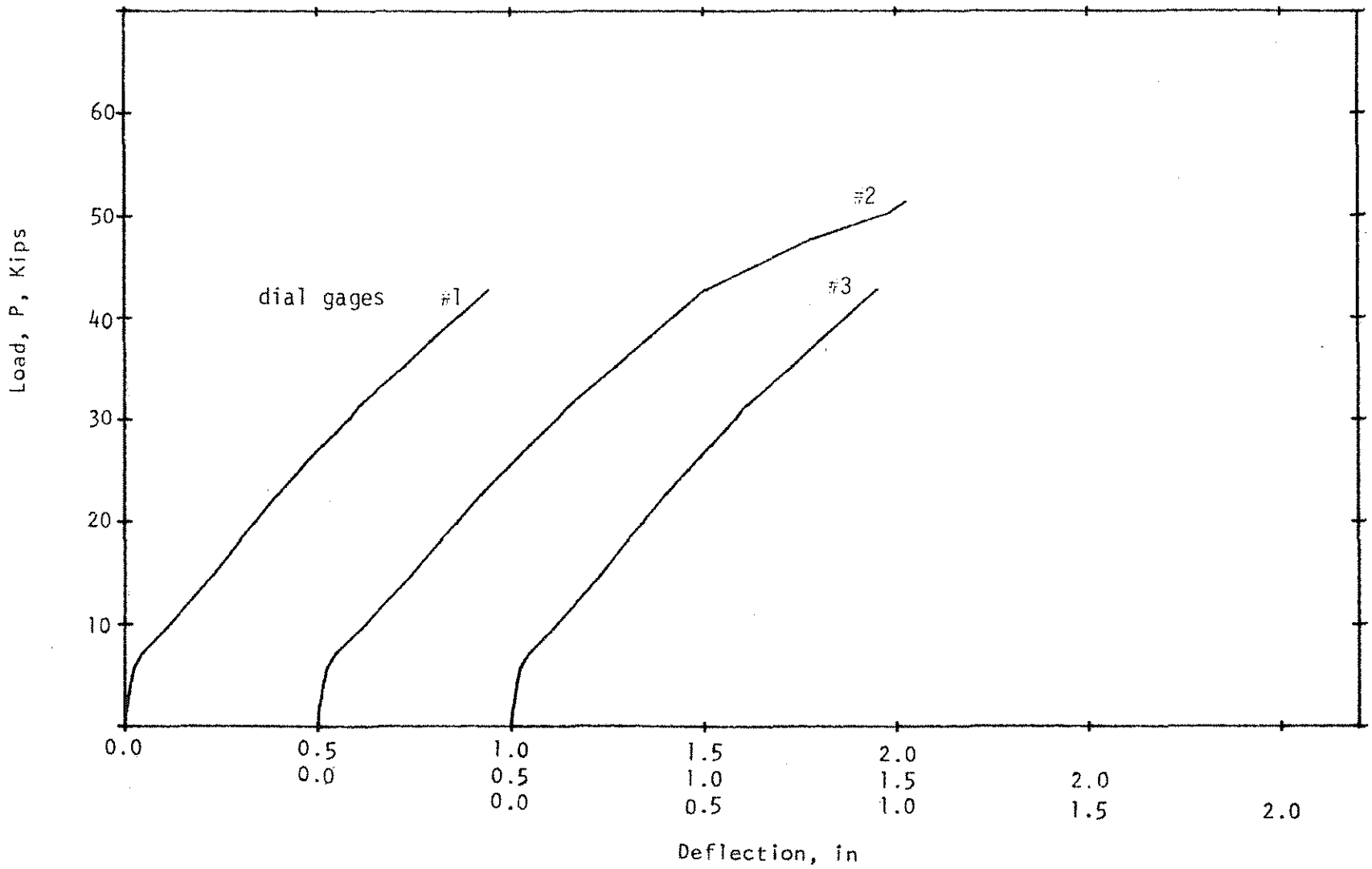

Figure 2.18 Load-Deflection Curves, Beam A50 (ρ_w = 0.661%, $\rho_v f_{vy}$ = 73.9 psi)

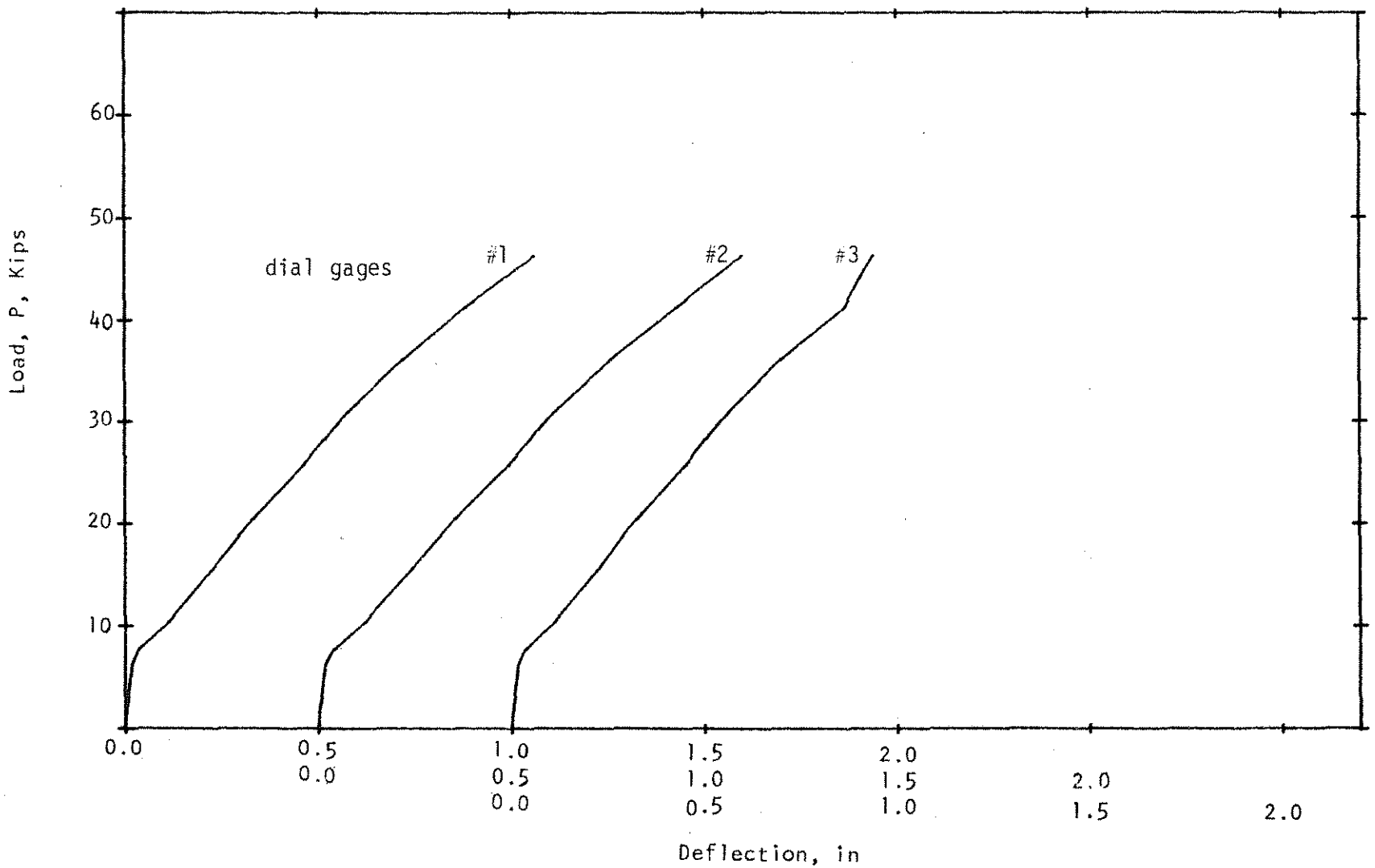

Figure 2.19 Load-Deflection Curves, Beam A50a (ρ_w = 0.658%, $\rho_v f_{vy}$ = 75.0 psi)

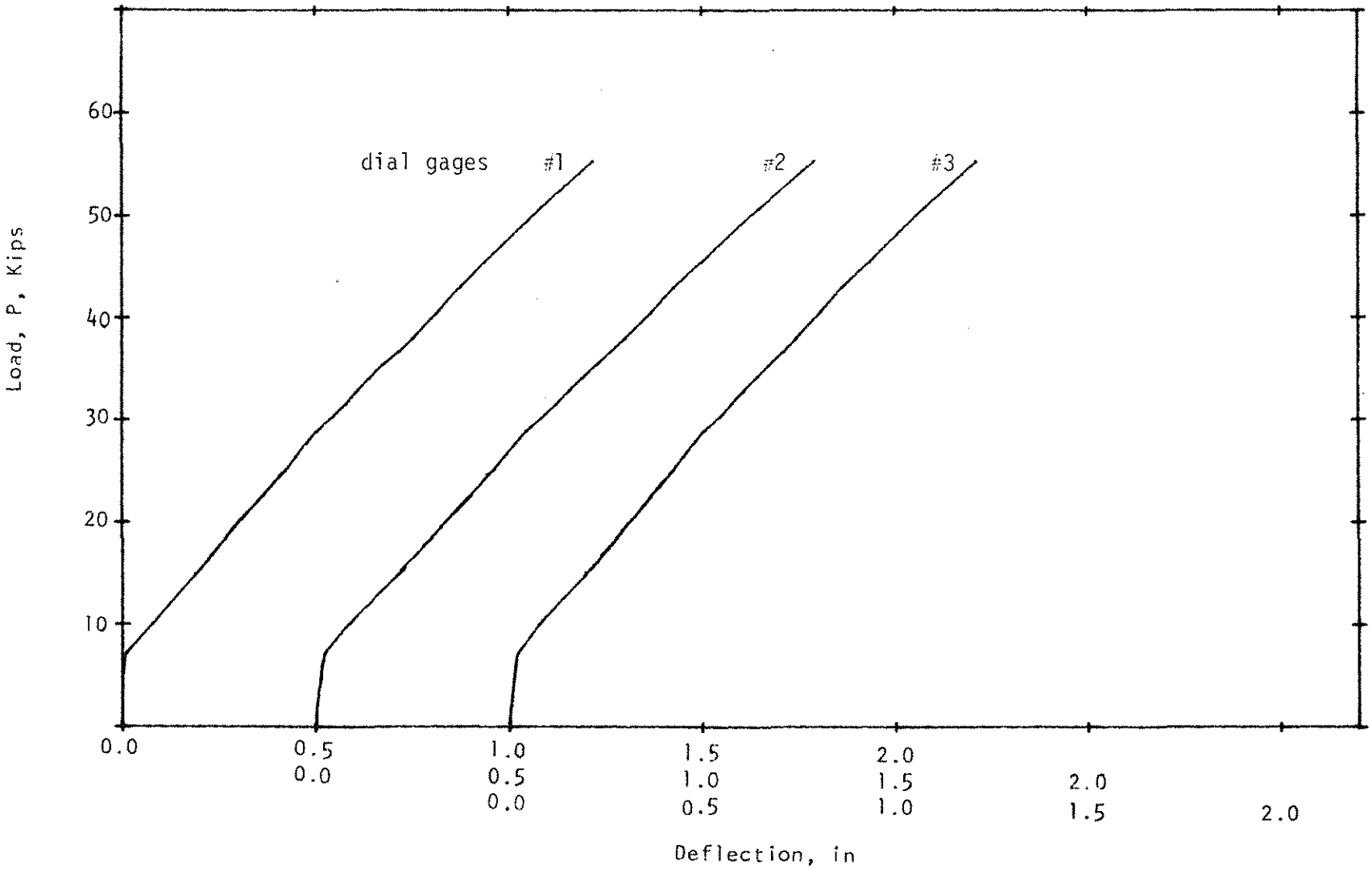

Figure 2.20 Load-Deflection Curves, Beam A75 (ρ_w = 0.655%, $\rho_v f_{vy}$ = 97.1 psi).

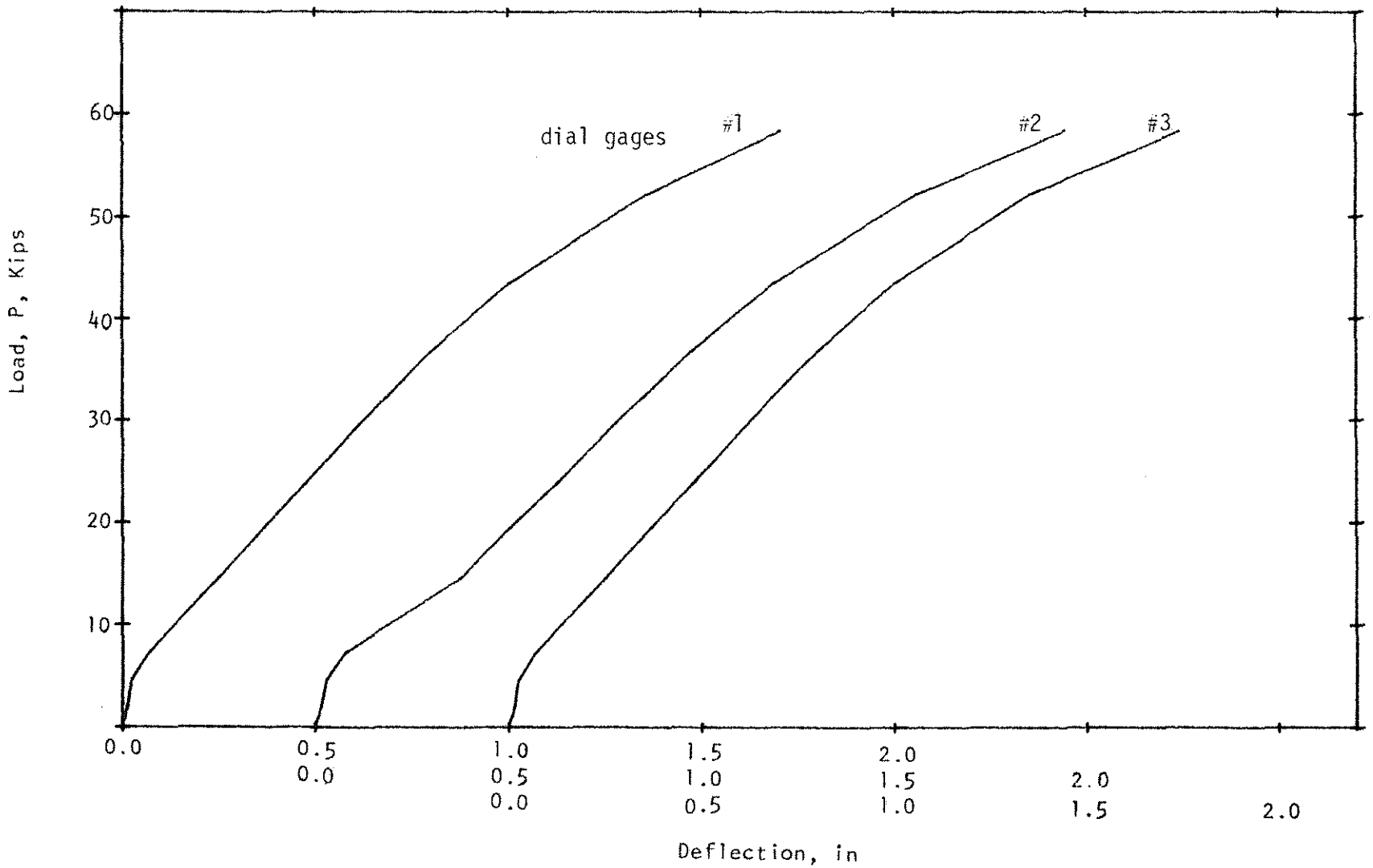

Figure 2.21 Load-Deflection Curves, Beam #1 (ρ_w = 0.699%, $\rho_v f_{vy}$ = 110.2 psi).

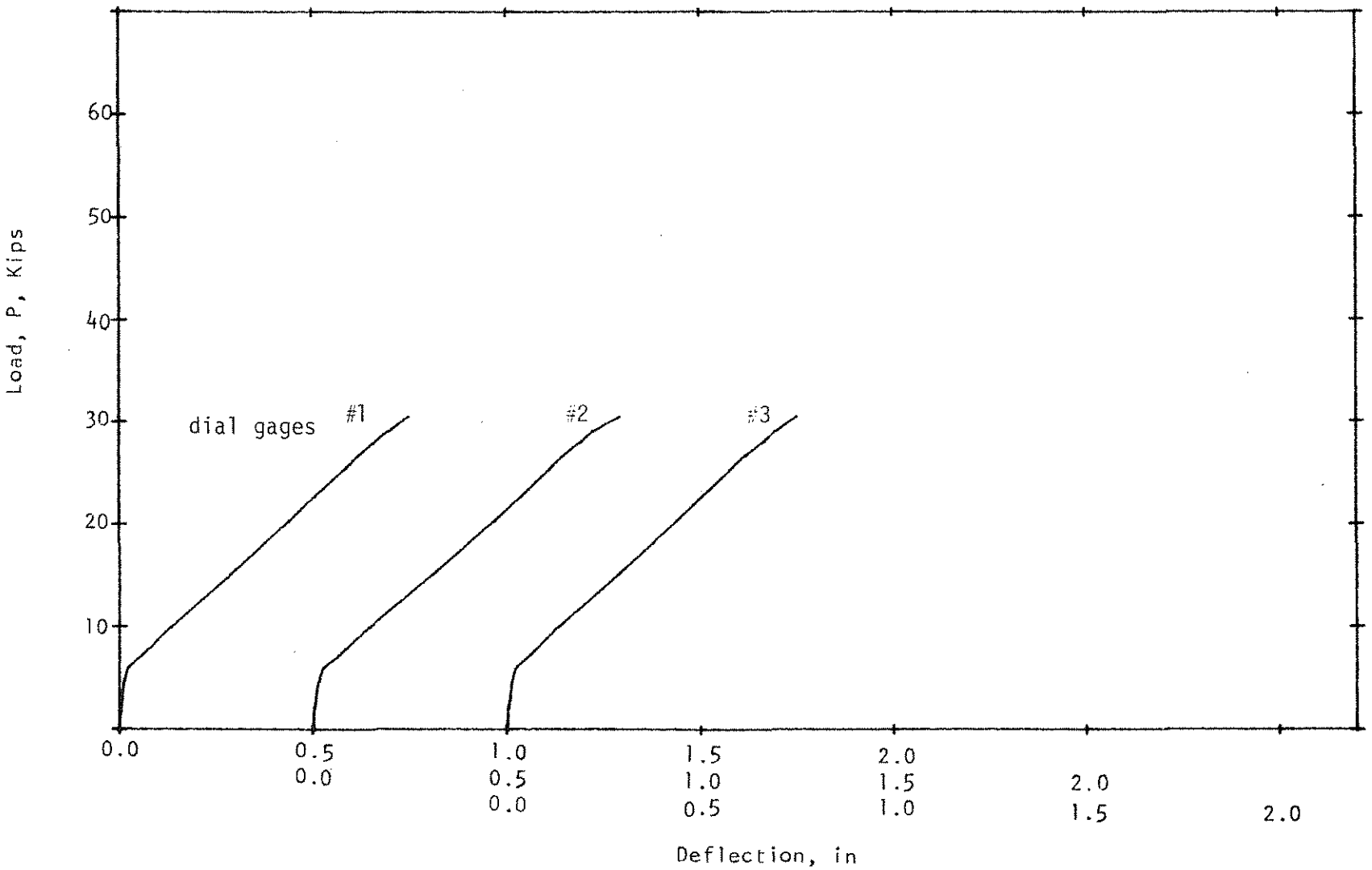

Figure 2.22 Load-Deflection Curves, Beam B00 (ρ_w = 0.488%, $\rho_v f_{vy}$ = 0.0 psi).

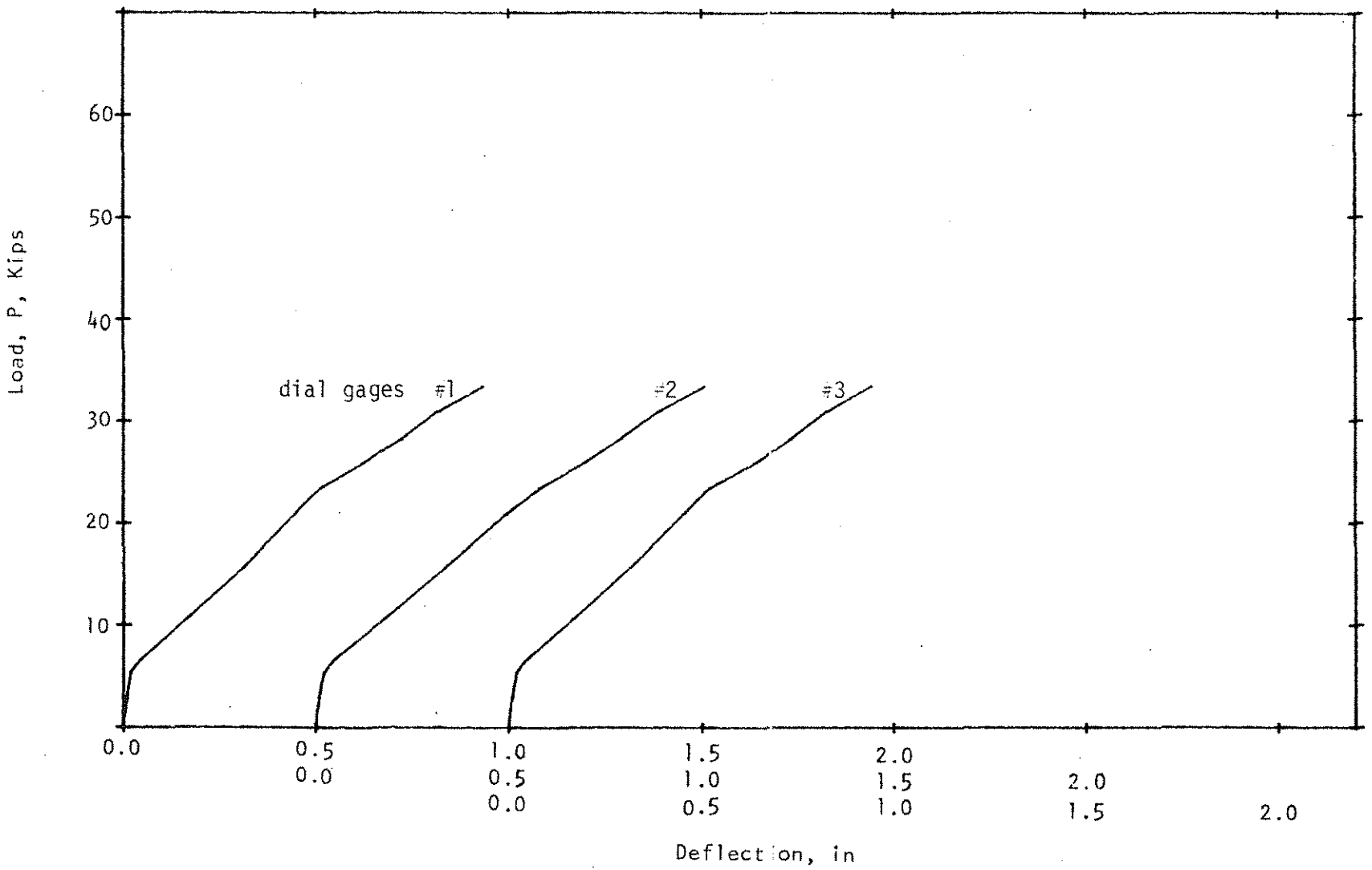

Figure 2.23 Load-Deflection Curves, Beam B25 (ρ_w = 0.494%, $\rho_v f_{vy}$ = 32.4 psi).

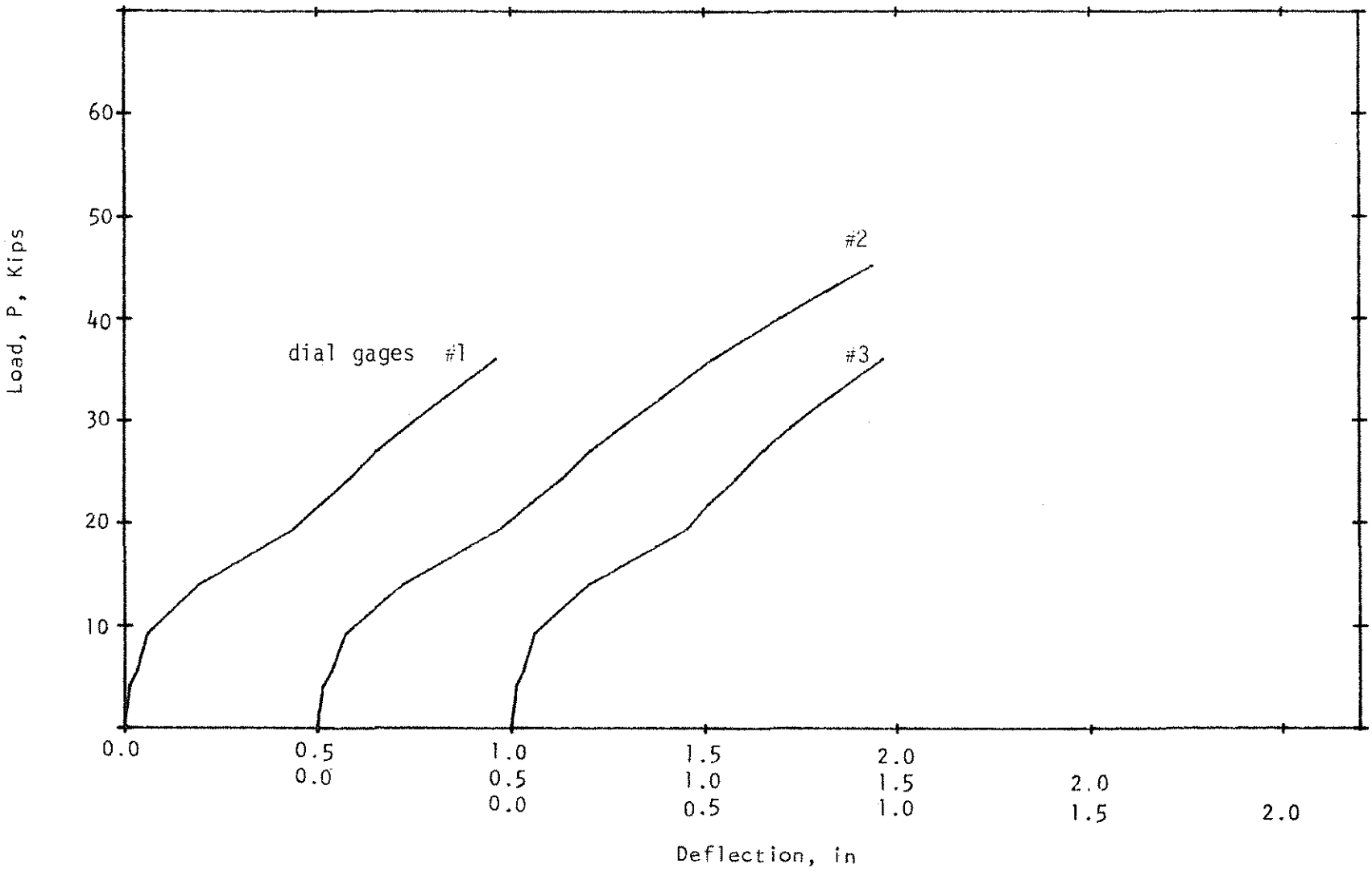

Figure 2.24 Load-Deflection Curves, Beam B50 (ρ_w = 0.498%, $\rho_v f_{vy}$ = 76.2 psi).

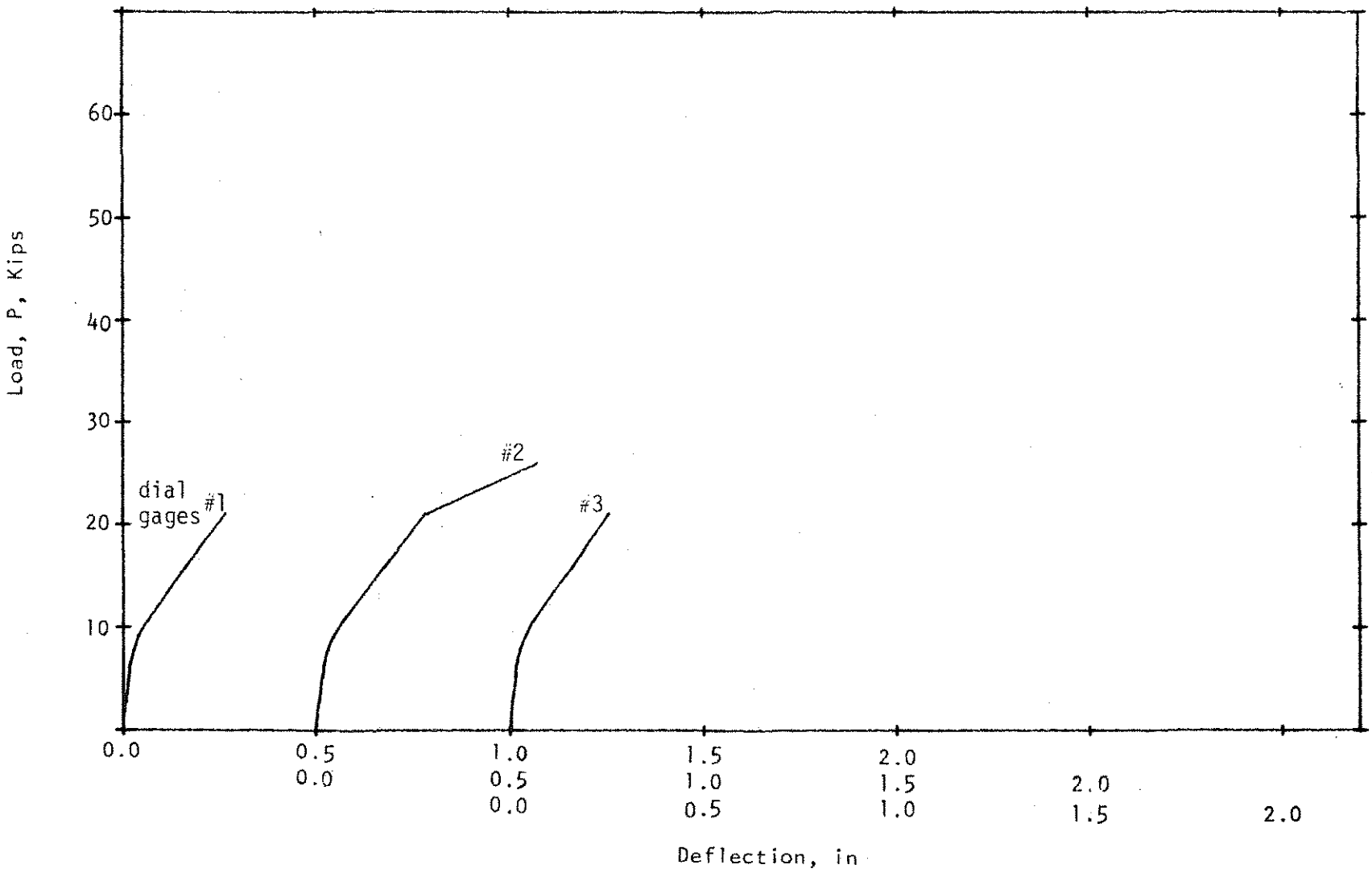

Figure 2.25 Load-Deflection Curves, Beam C00 (ρ_w = 0.943%, $\rho_v f_{vy}$ = 0.0 psi).

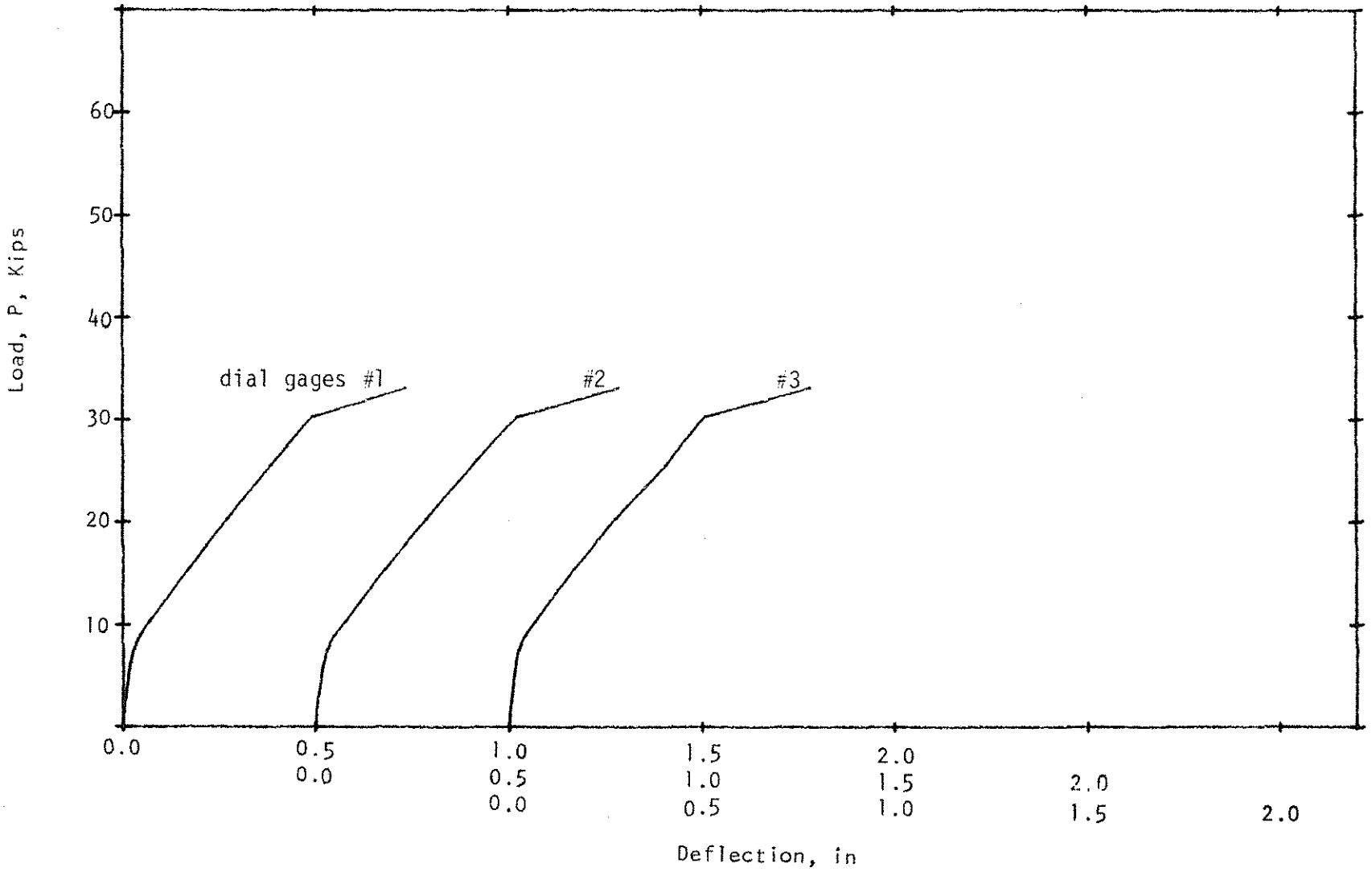

Figure 2.26 Load-Deflection Curves, Beam C25 (ρ_w = 0.948%, $\rho_v f_{vy}$ = 32.4 psi).

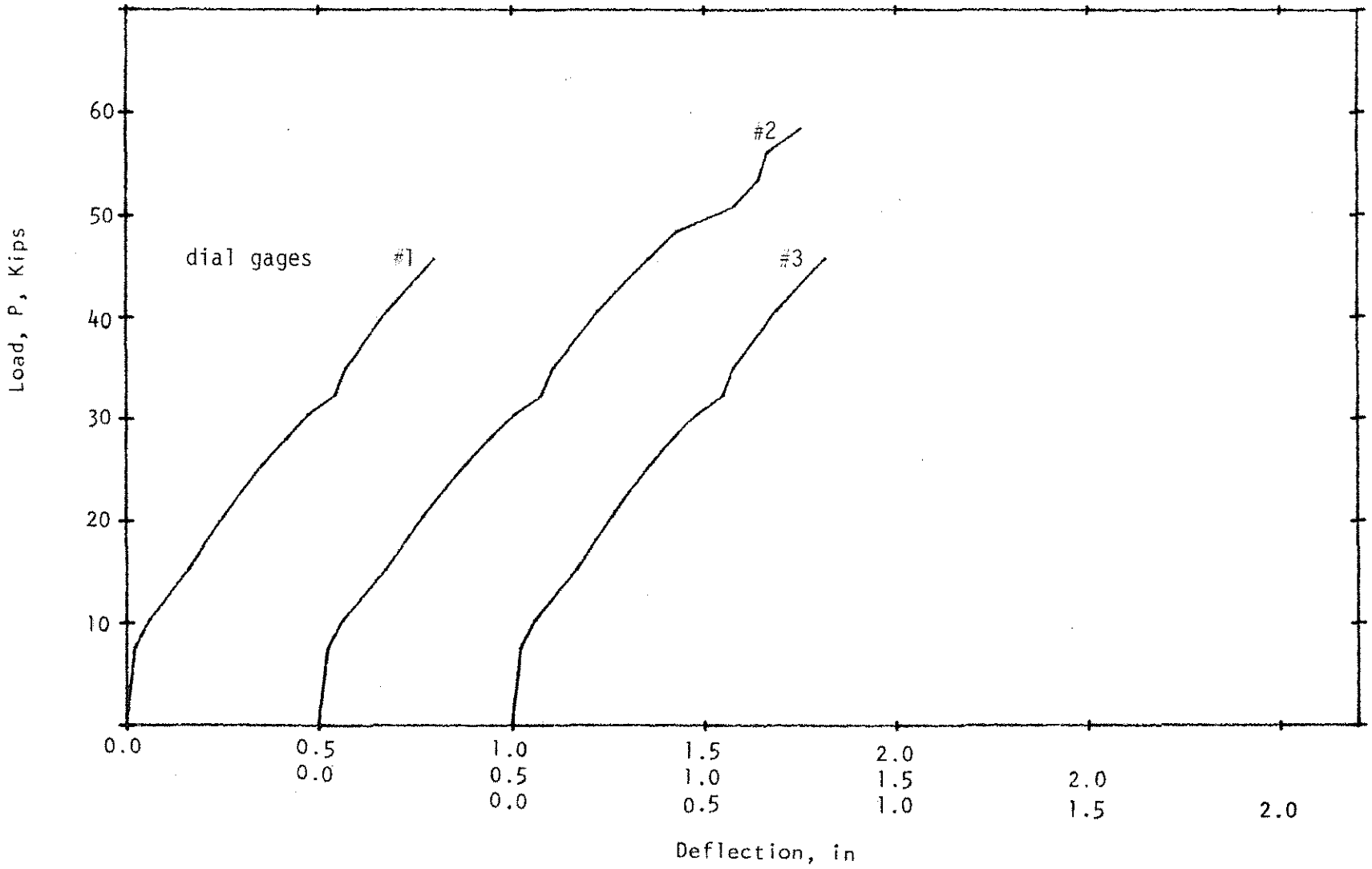

Figure 2.27 Load-Deflection Curves, Beam C50 (ρ_w = 0.948%, $\rho_v f_{vy}$ = 76.2 psi).

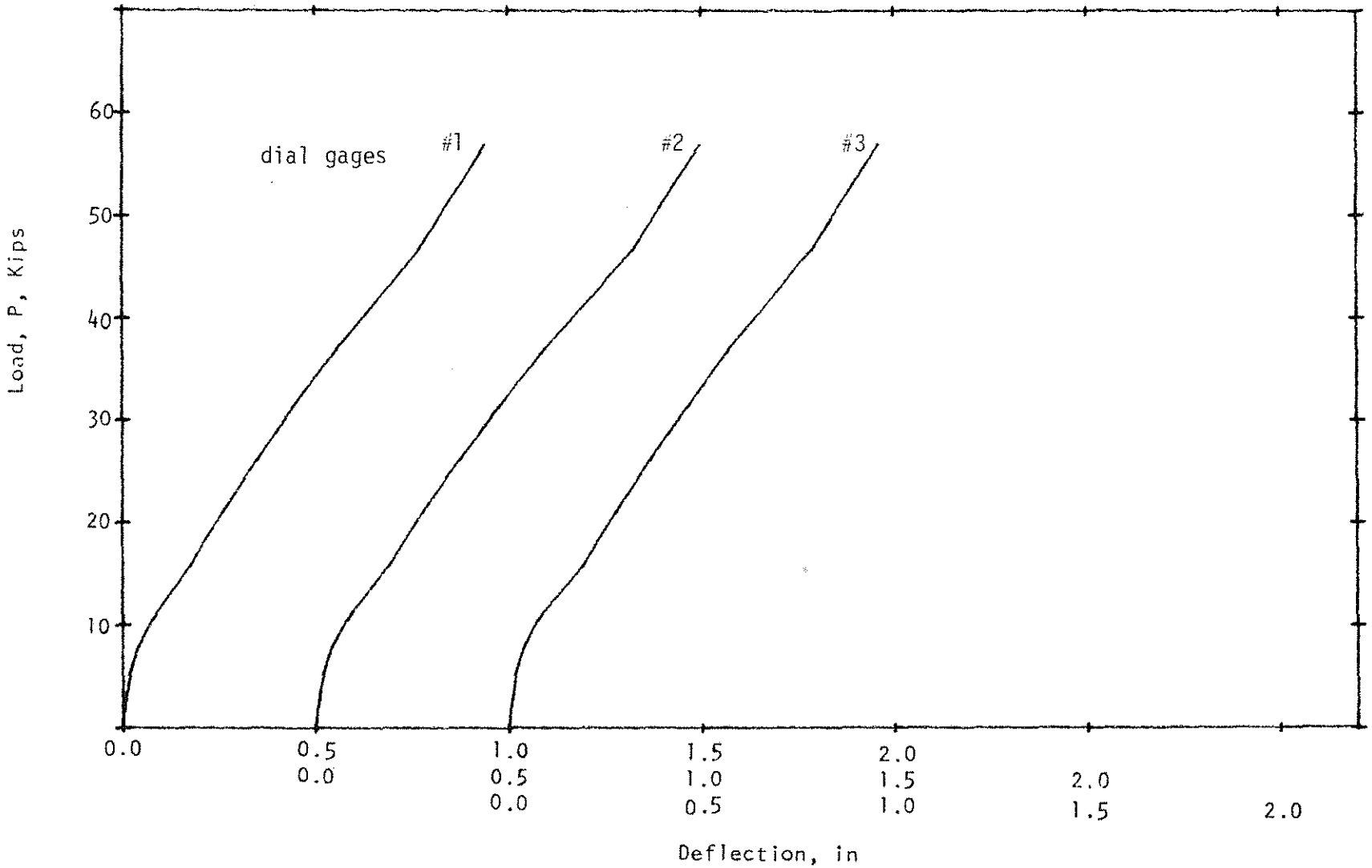

Figure 2.28 Load-Deflection Curves, Beam C75 (ρ_w = 0.933%, $\rho_v f_{vy}$ = 103.0 psi).

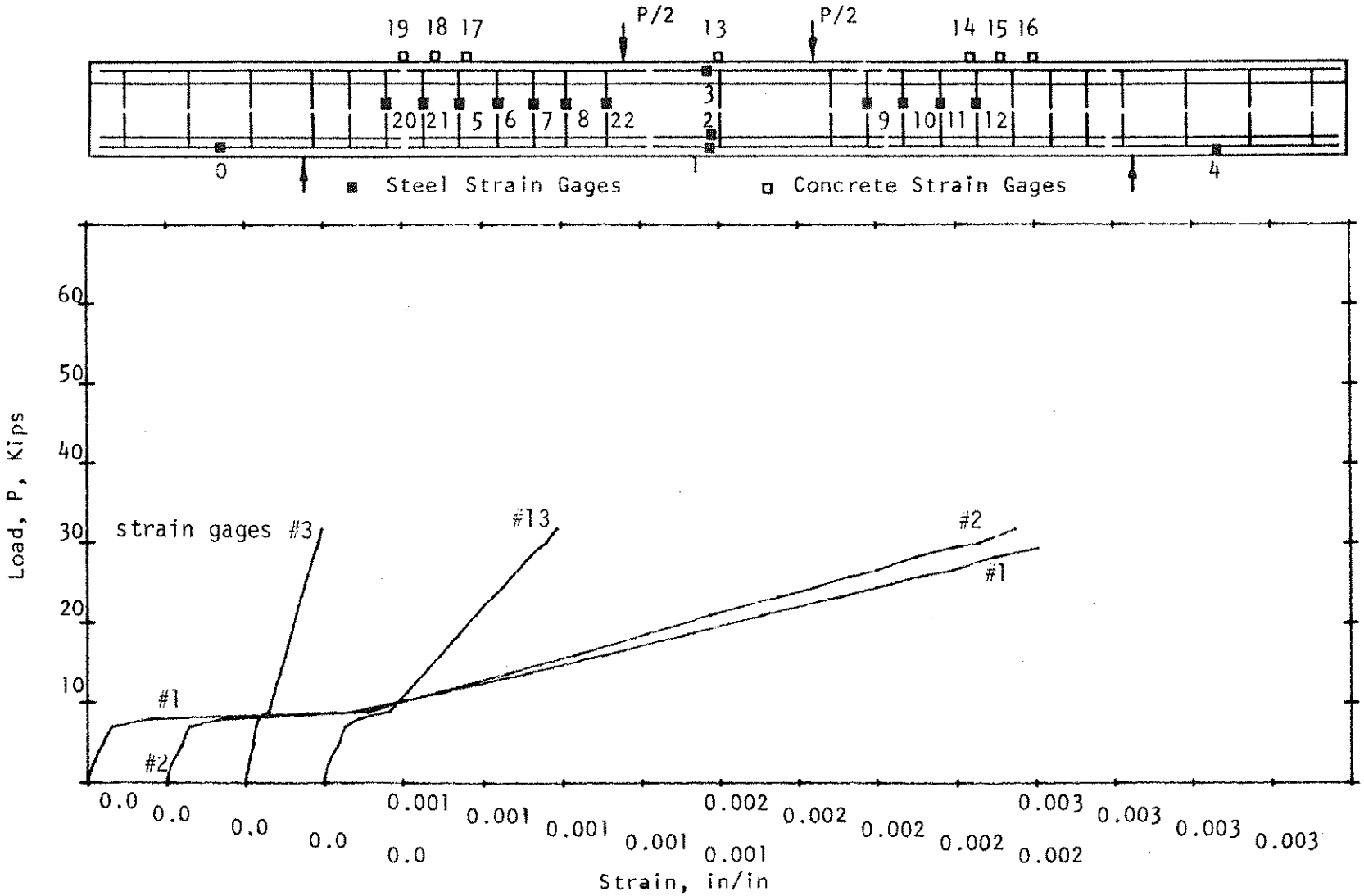

Figure 2.29 Load-Strain Curves, Beam #2 (ρ_w = 0.693%, $\rho_v f_{vy}$ = 0.0 psi).

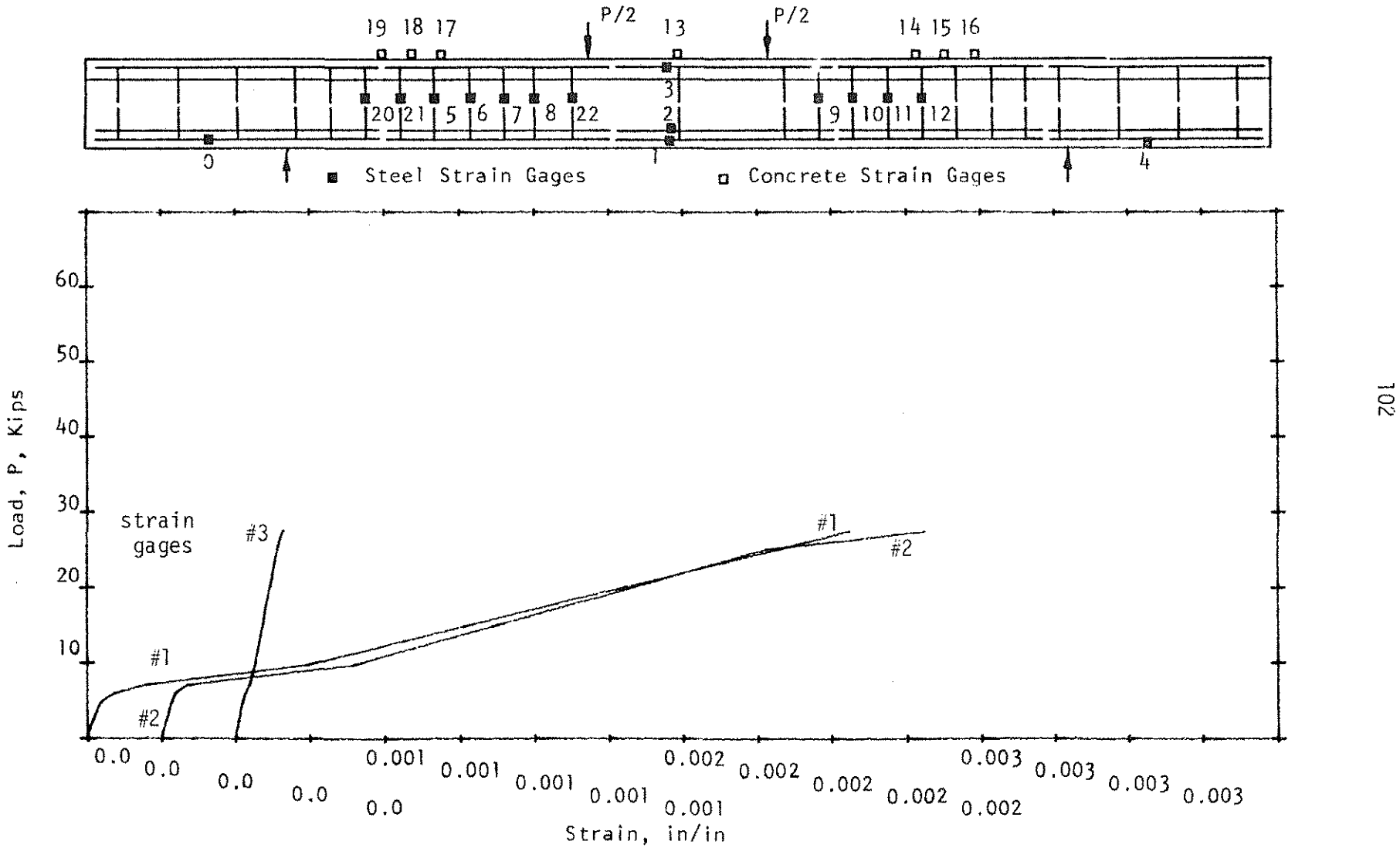

Figure 2.30 Load-Strain Curves, Beam A00 (ρ_w = 0.656%, $\rho_v f_{vy}$ = 0.0 psi).

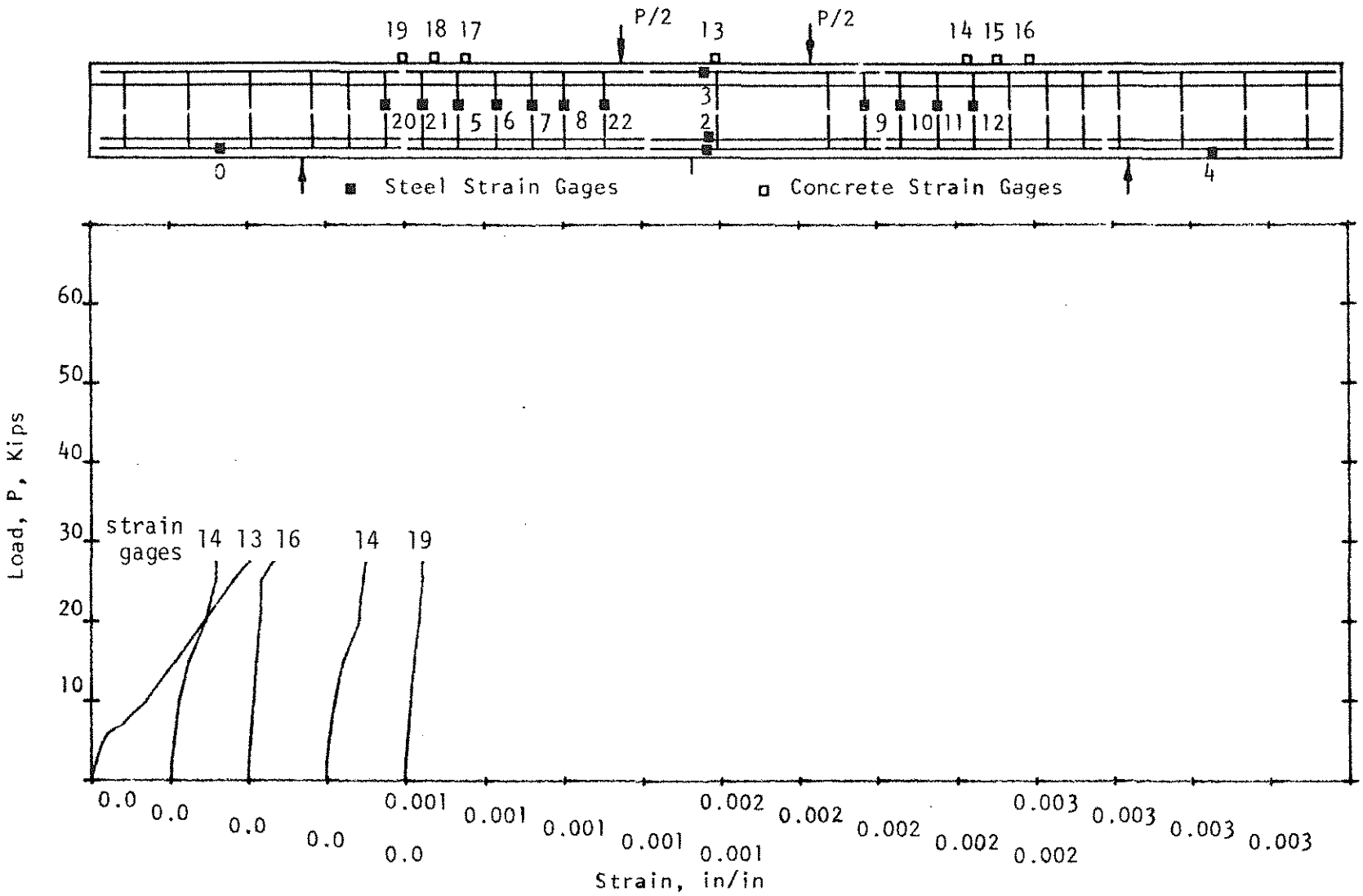

Figure 2.31 Load-Strain Curves, Beam A00 (ρ_w = 0.656%, $\rho_v f_{vy}$ = 0.0 psi).

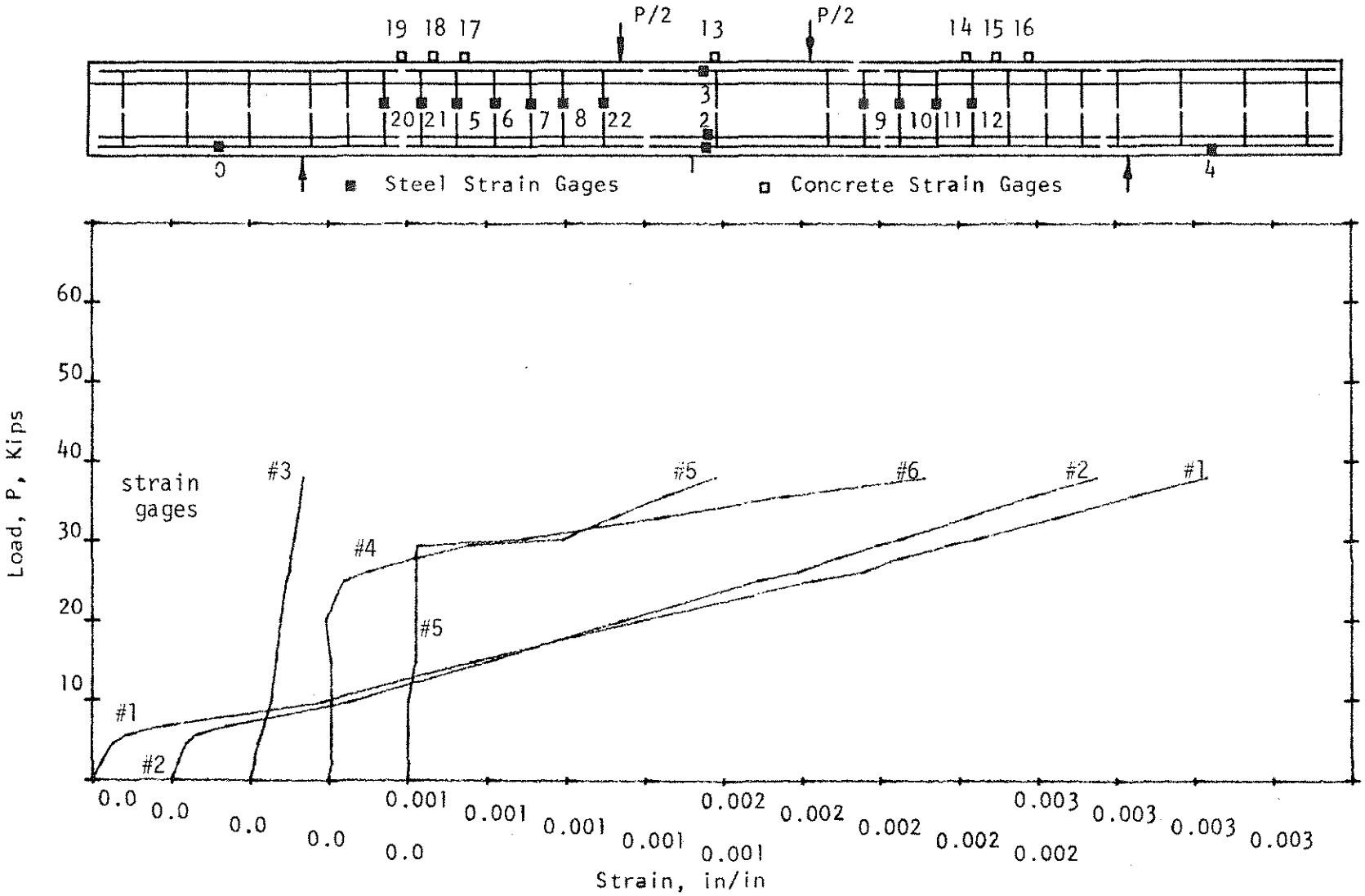

Figure 2.32 Load-Strain Curves, Beam A25 (ρ_w = 0.663%, $\rho_v f_{vy}$ = 31.8 psi).

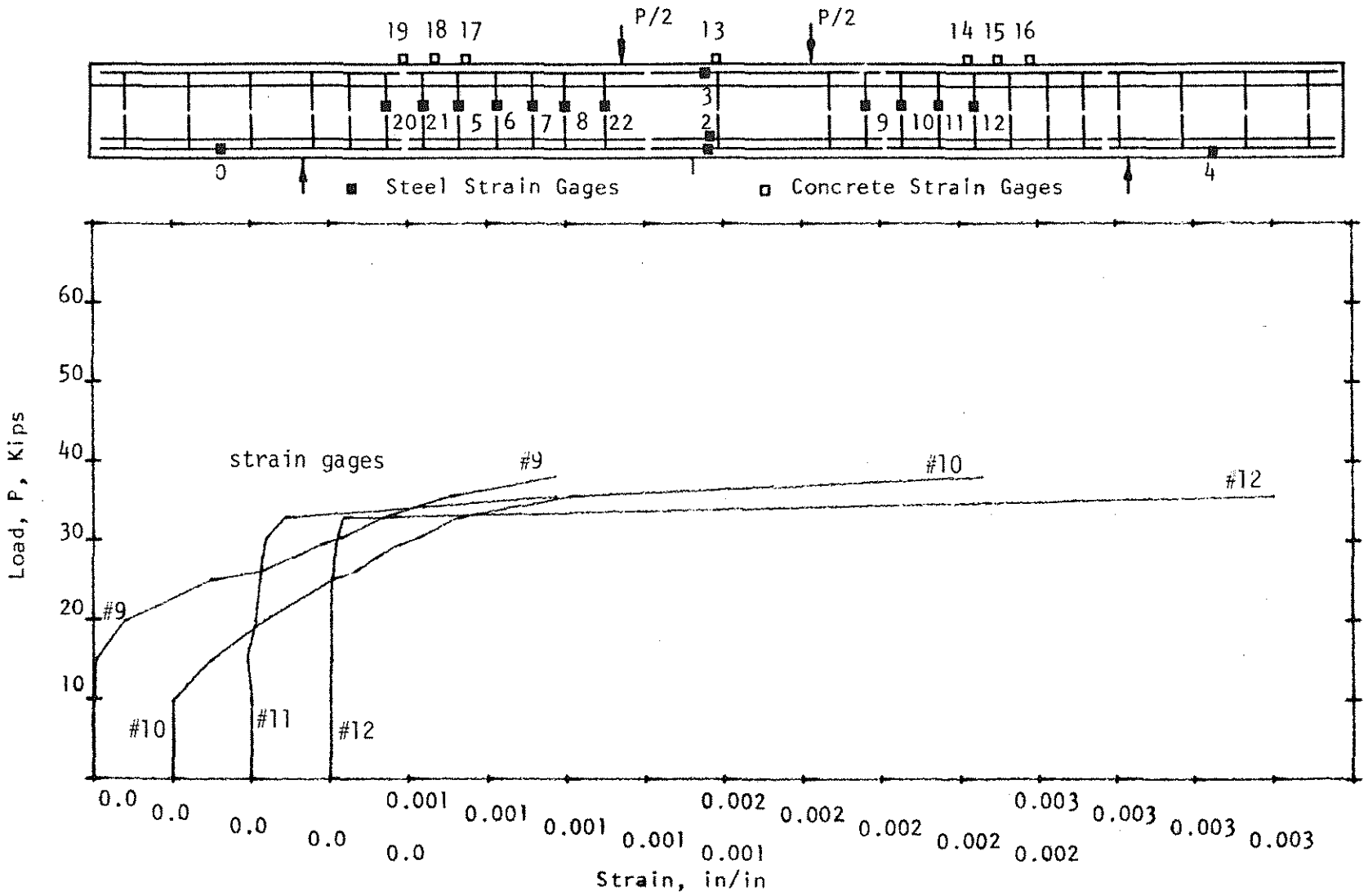

Figure 2.33 Load-Strain Curves, Beam A25 (ρ_w = 0.663%, $\rho_v f_{vy}$ = 31.8 psi).

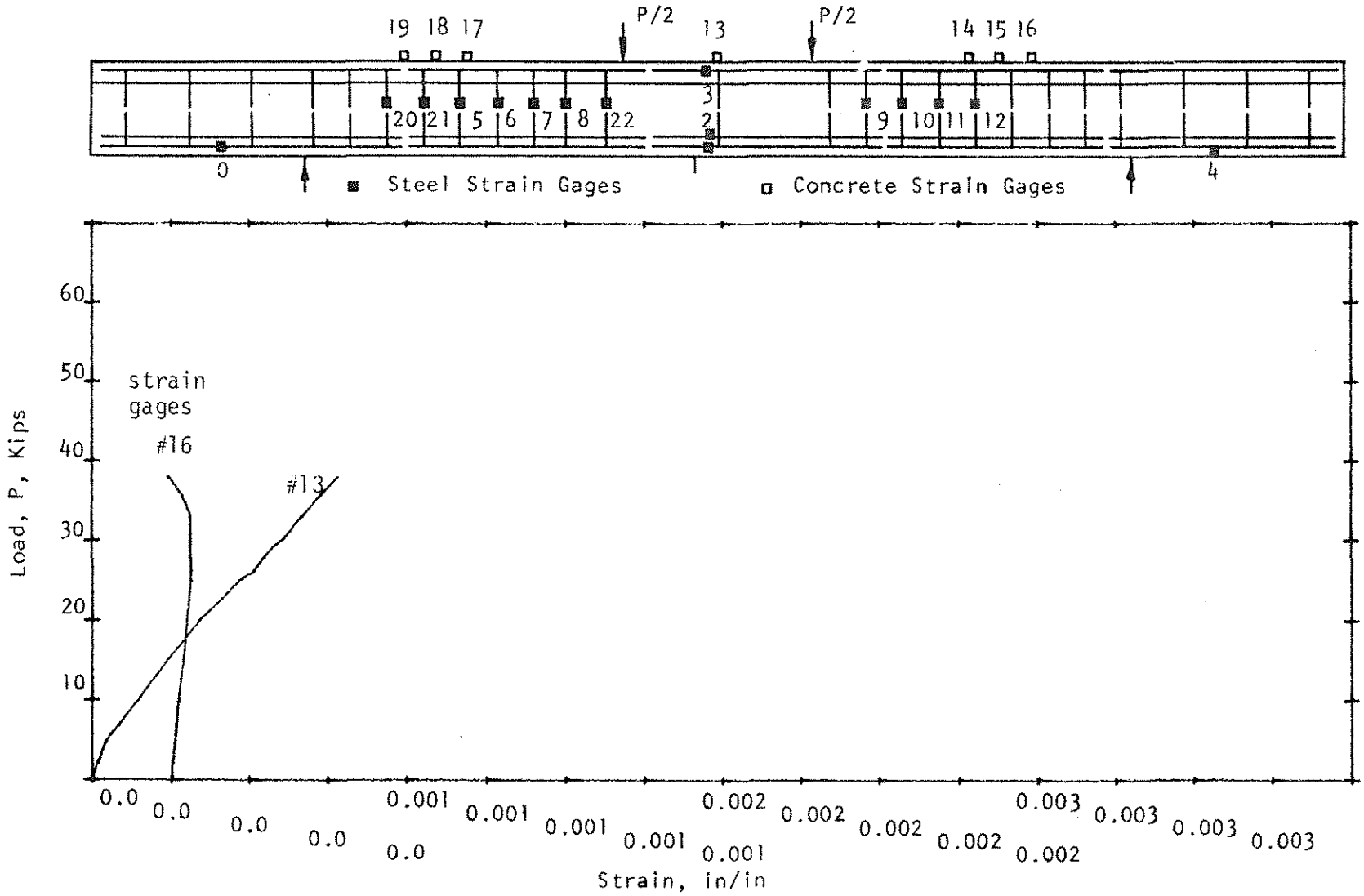

Figure 2.34 Load-Strain Curves, Beam A25 (ρ_w=0.663%, $\rho_v f_{vy}$ = 31.8 psi).

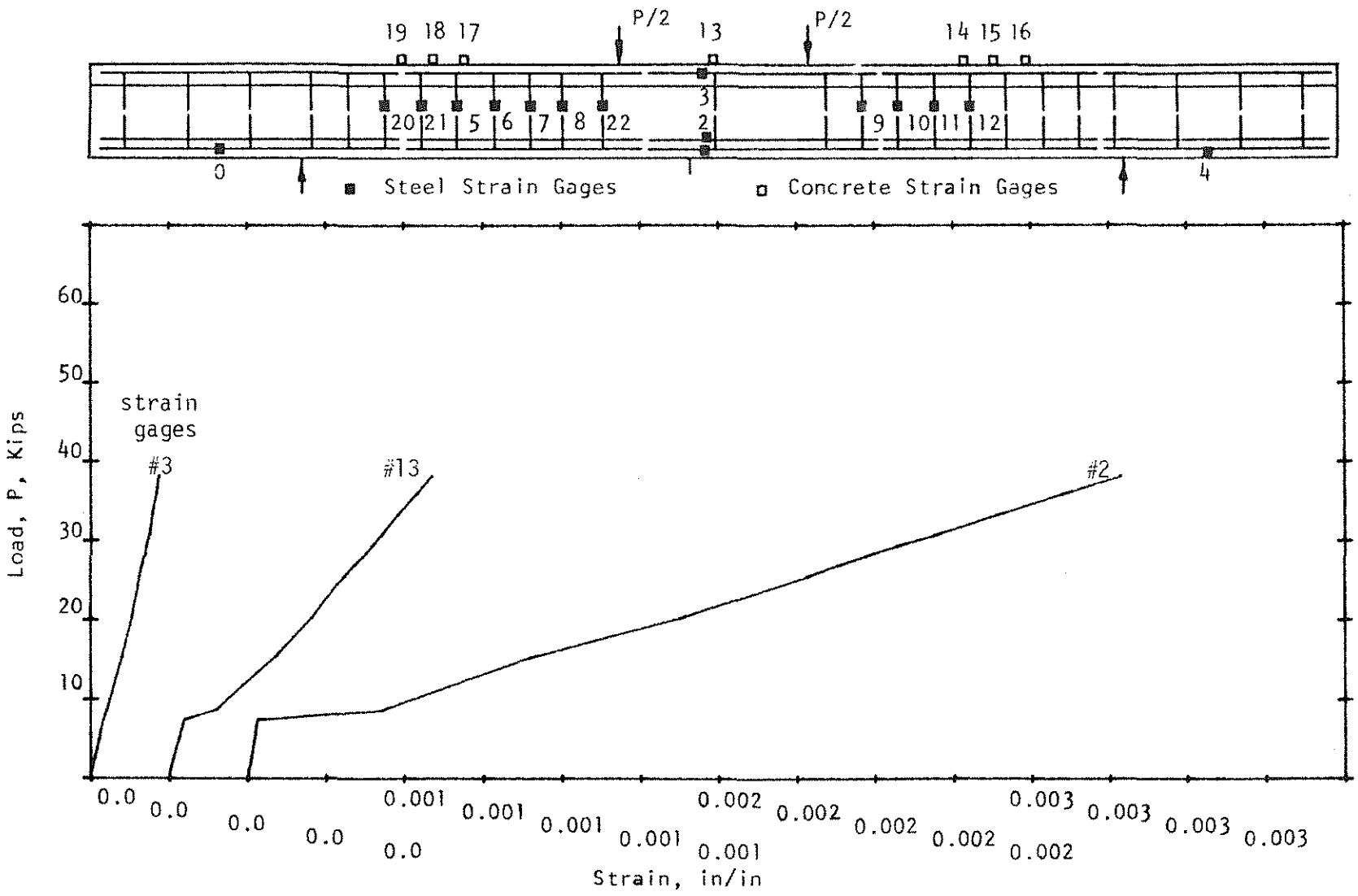

Figure 2.35 Load-Strain Curves, Beam A25a (ρ_w = 0.668%, $\rho_v f_{vy}$ = 31.8 psi).

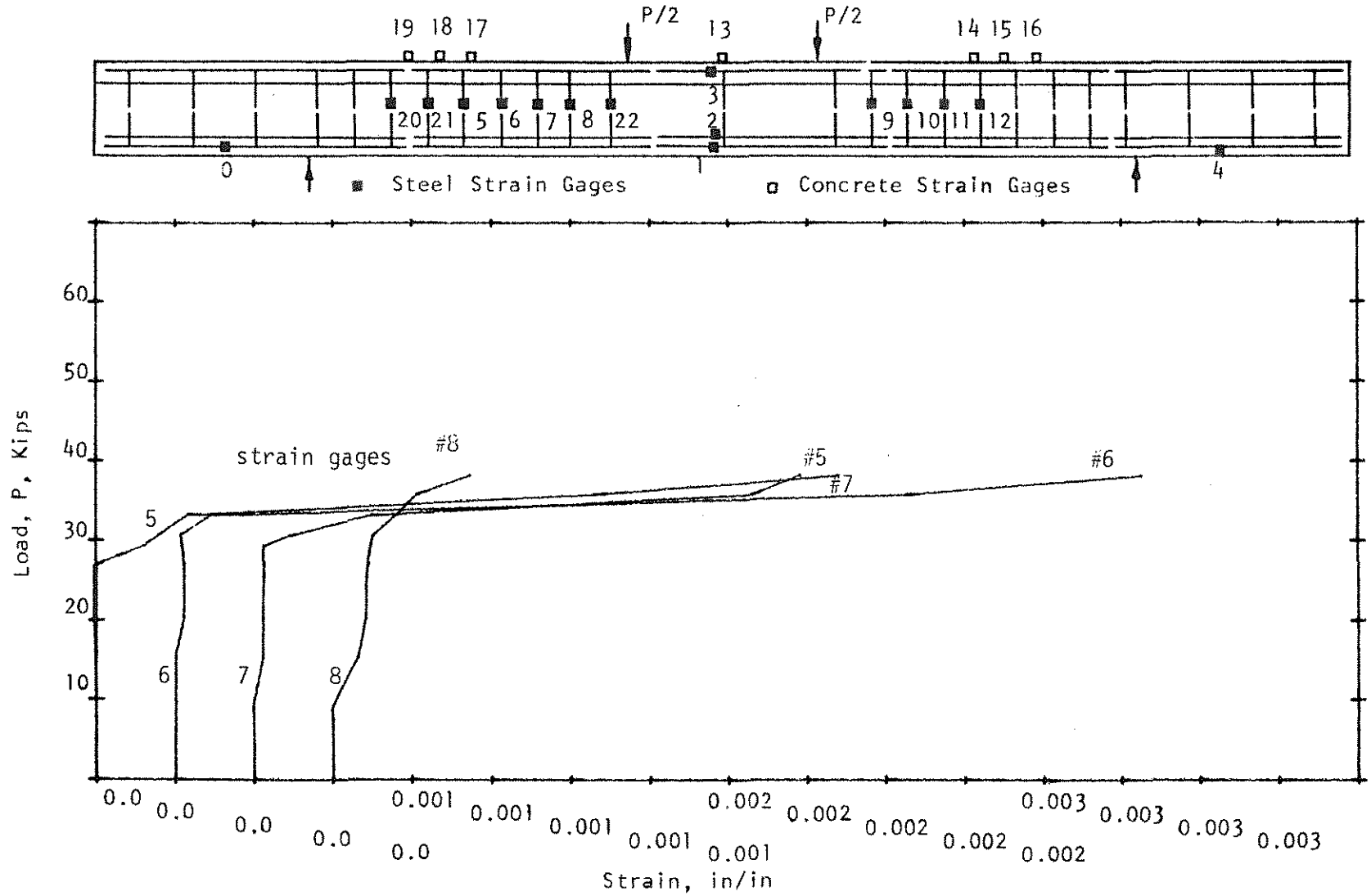

Figure 2.36 Load-Strain Curves, Beam A25a (ρ_w = 0.668%, $\rho_v f_{vy}$ = 31.8 psi).

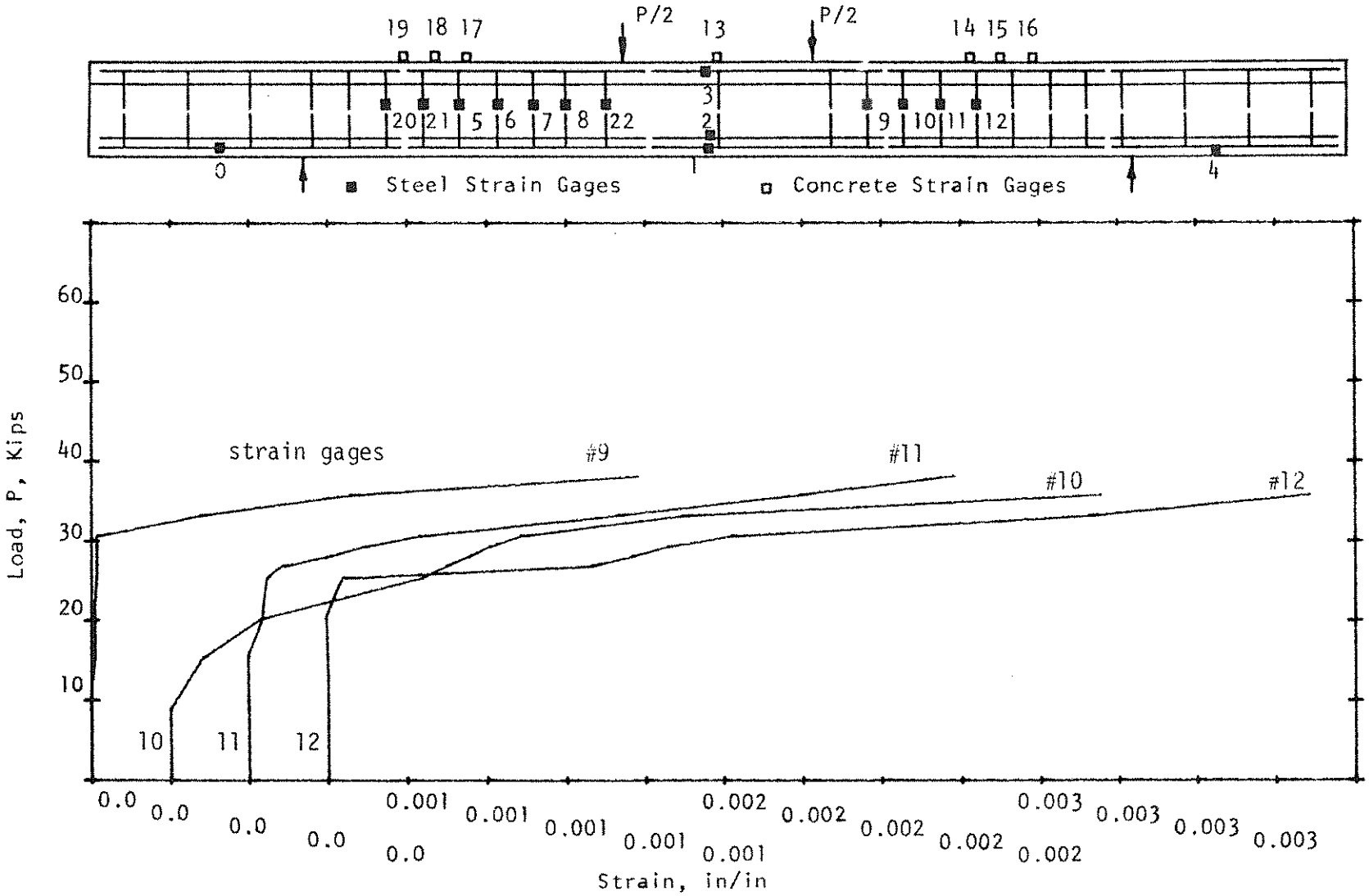

Figure 2.37 Load-Strain Curves, Beam A25a (ρ_w = 0.668%, $\rho_v f_{vy}$ = 31.8 psi).

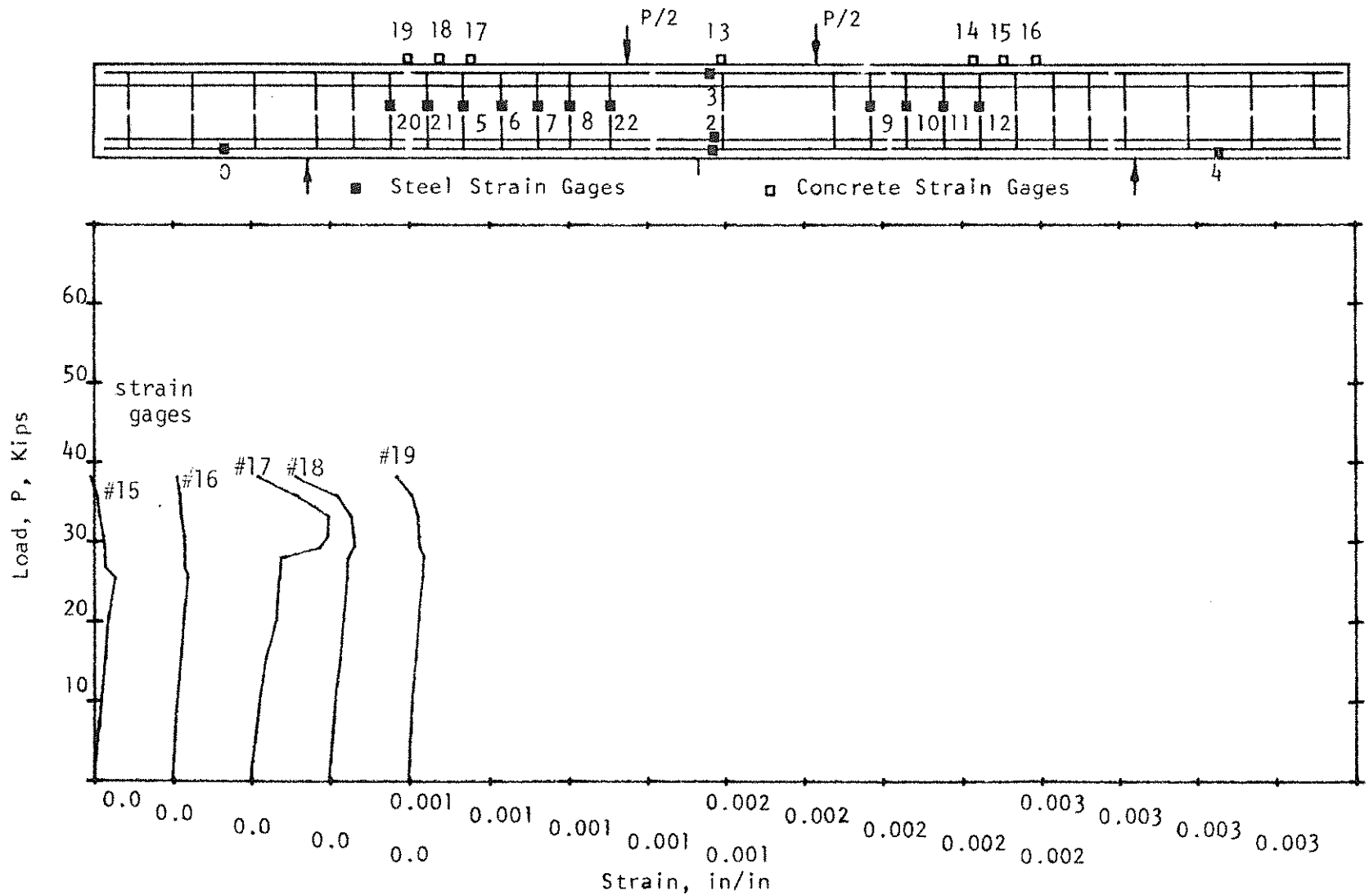

Figure 2.38 Load-Strain Curves, Beam A2Ɔa (ρ_w = 0.668%, $\rho_v f_{vy}$ = 31.8 psi).

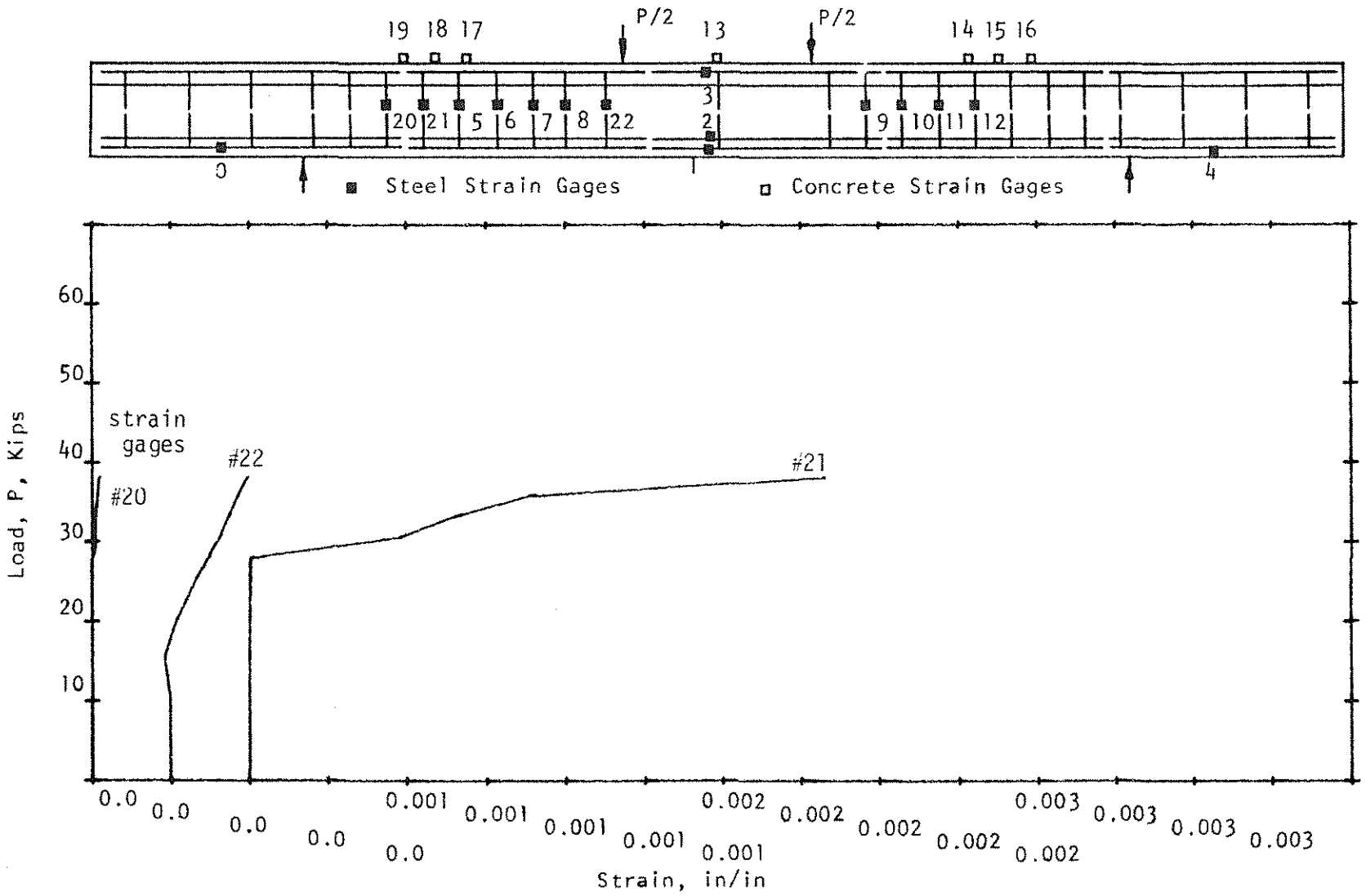

Figure 2.39 Load-Strain Curves, Beam A25a (ρ_w = 0.668%, $\rho_v f_{vy}$ = 31.8 psi).

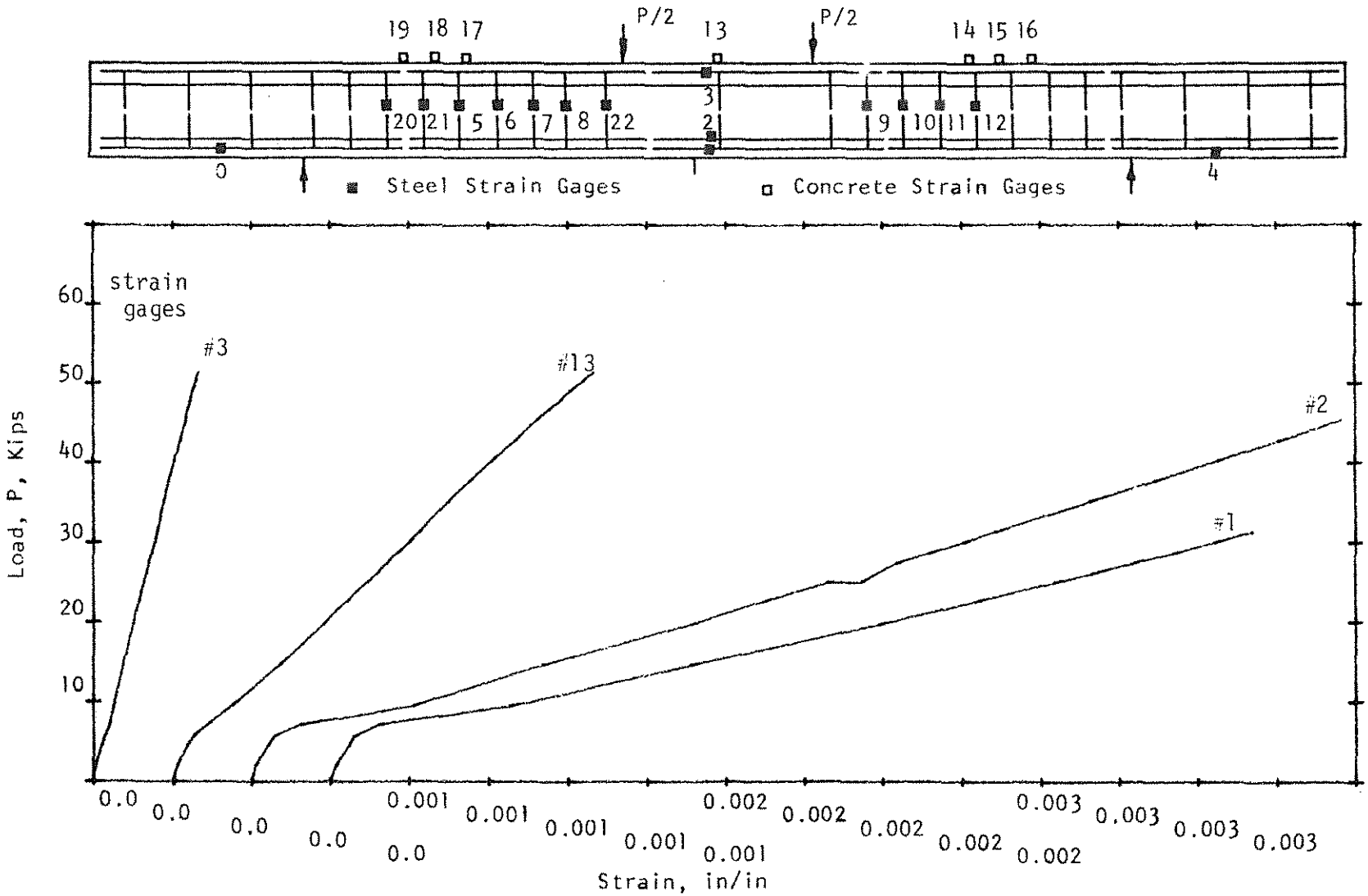

Figure 2.40 Load-Strain Curves, Beam A50 (ρ_w = 0.661%, $\rho_v f_{vy}$ = 73.9 psi).

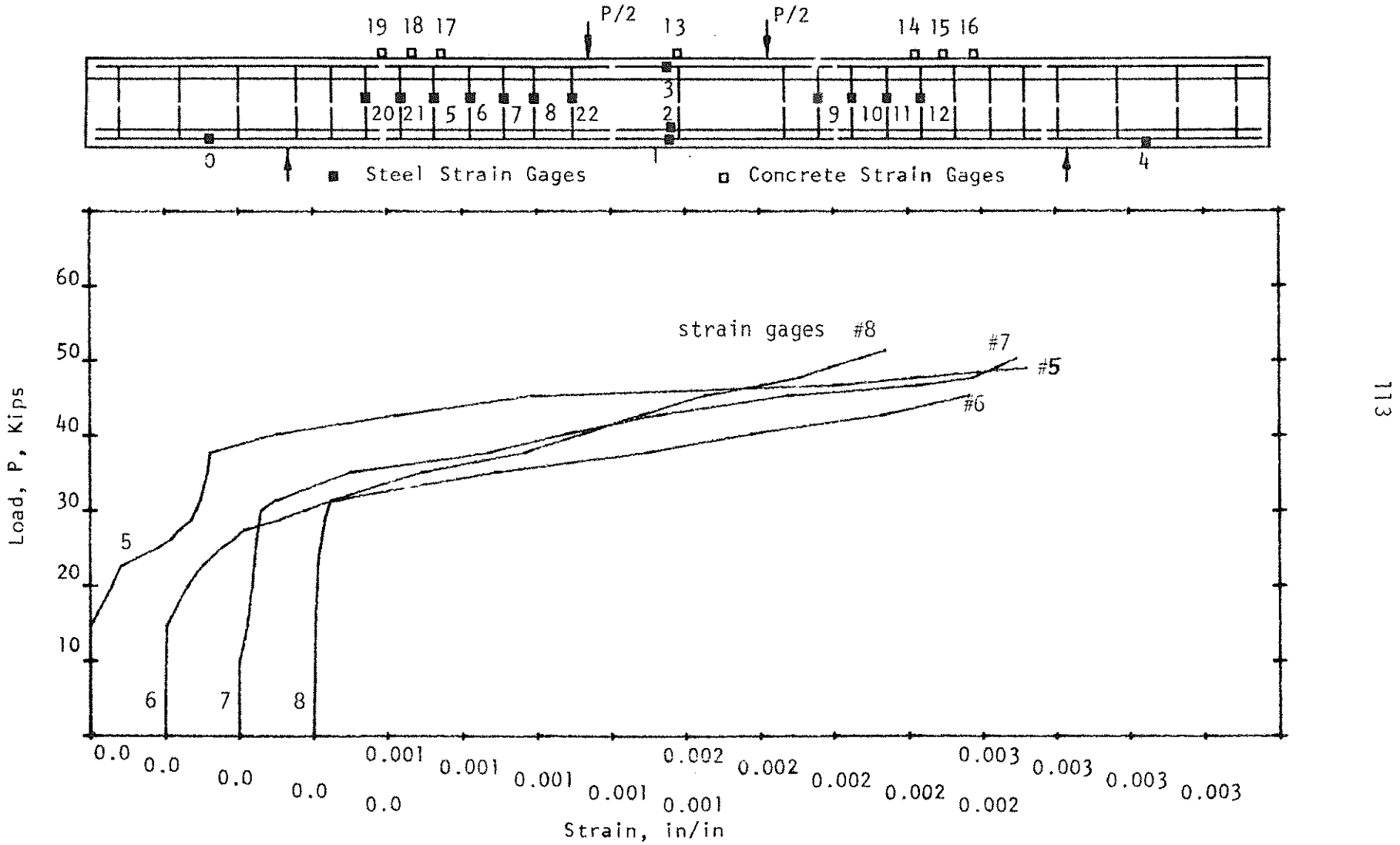

Figure 2.41 Load-Strain Curves, Beam A50 (ρ_w = 0.661%, $\rho_v f_{vy}$ = 73.9 psi).

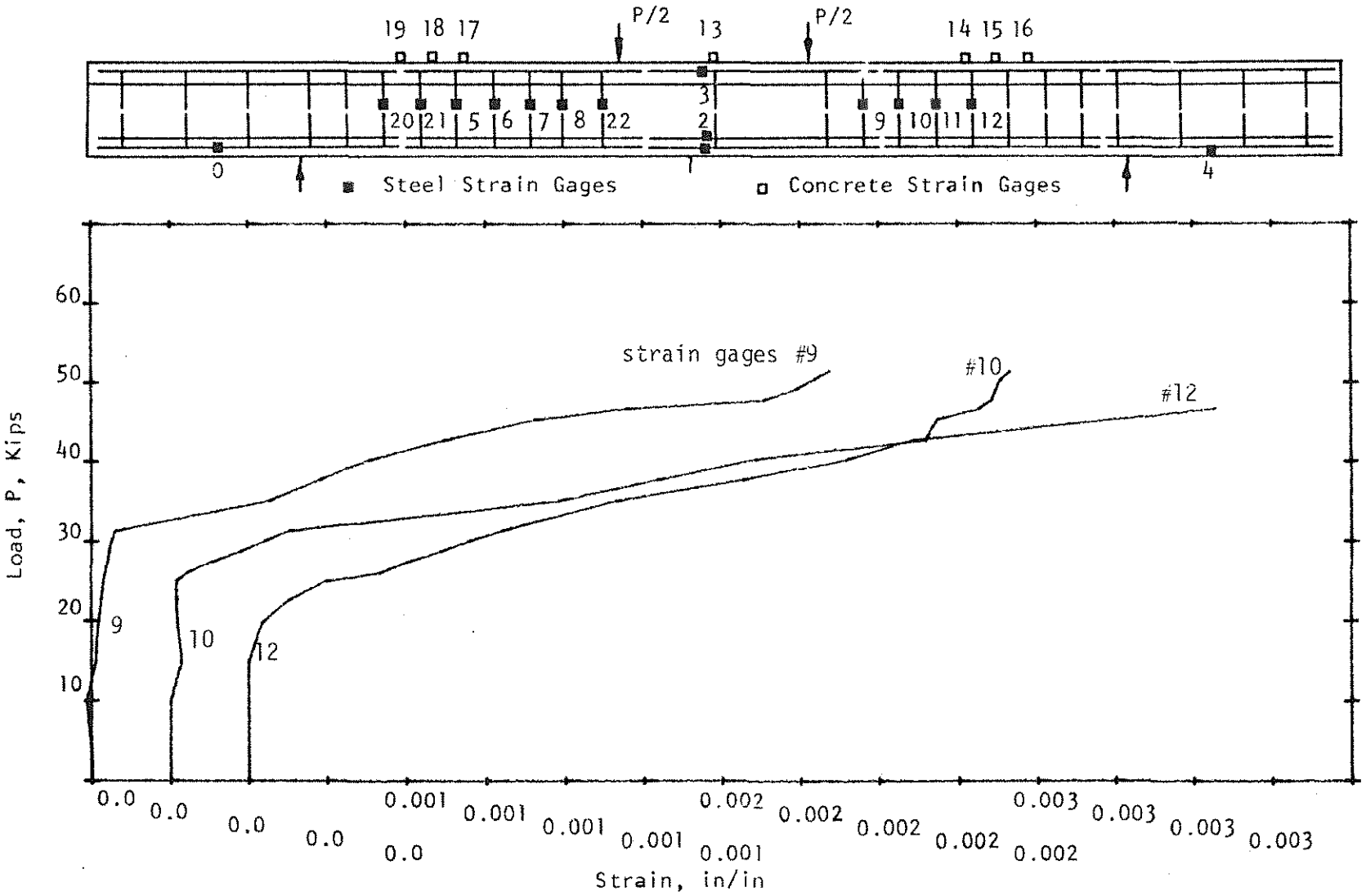

Figure 2.42 Load-Strain Curves, Beam A50 (ρ_w = 0.661%, $\rho_v f_{vy}$ = 73.9 psi).

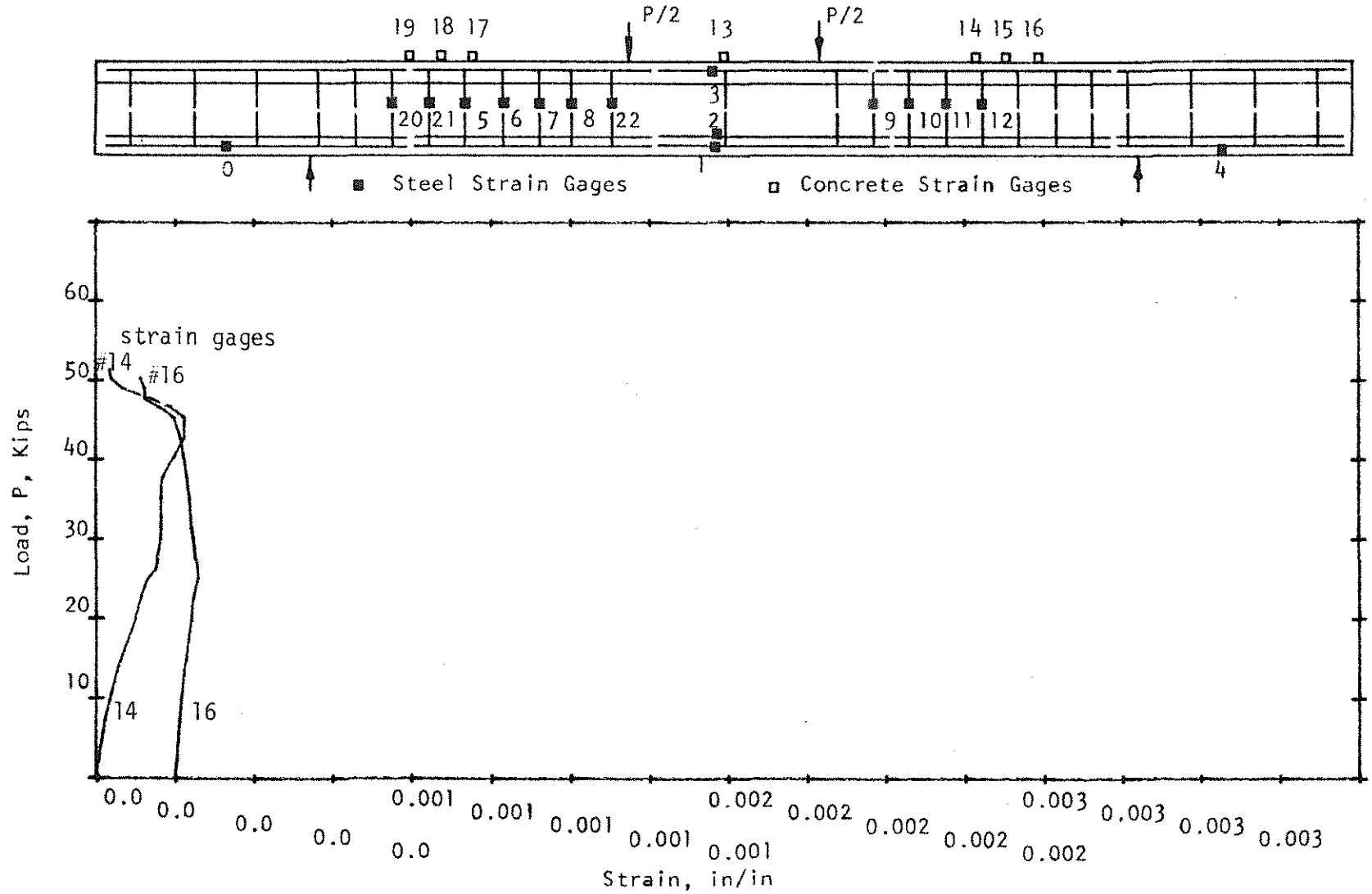

Figure 2.43 Load-Strain Curves, Beam A50 (ρ_w = 0.661%, $\rho_v f_{vy}$ = 73.9 psi).

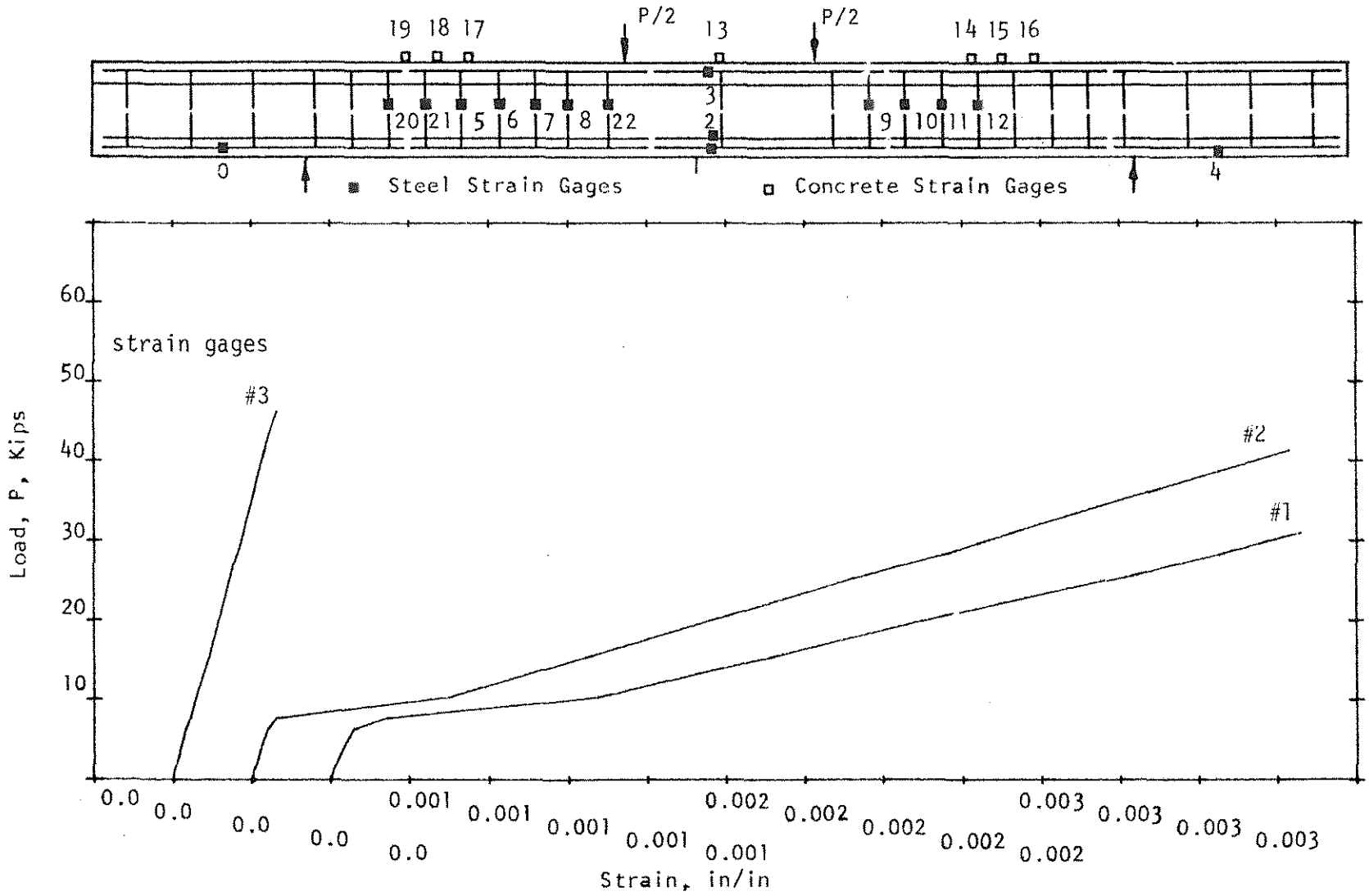

Figure 2.44 Load-Strain Curves, Beam A50a (ρ_w = 0.658%, $\rho_v f_{vy}$ = 75.0 psi).

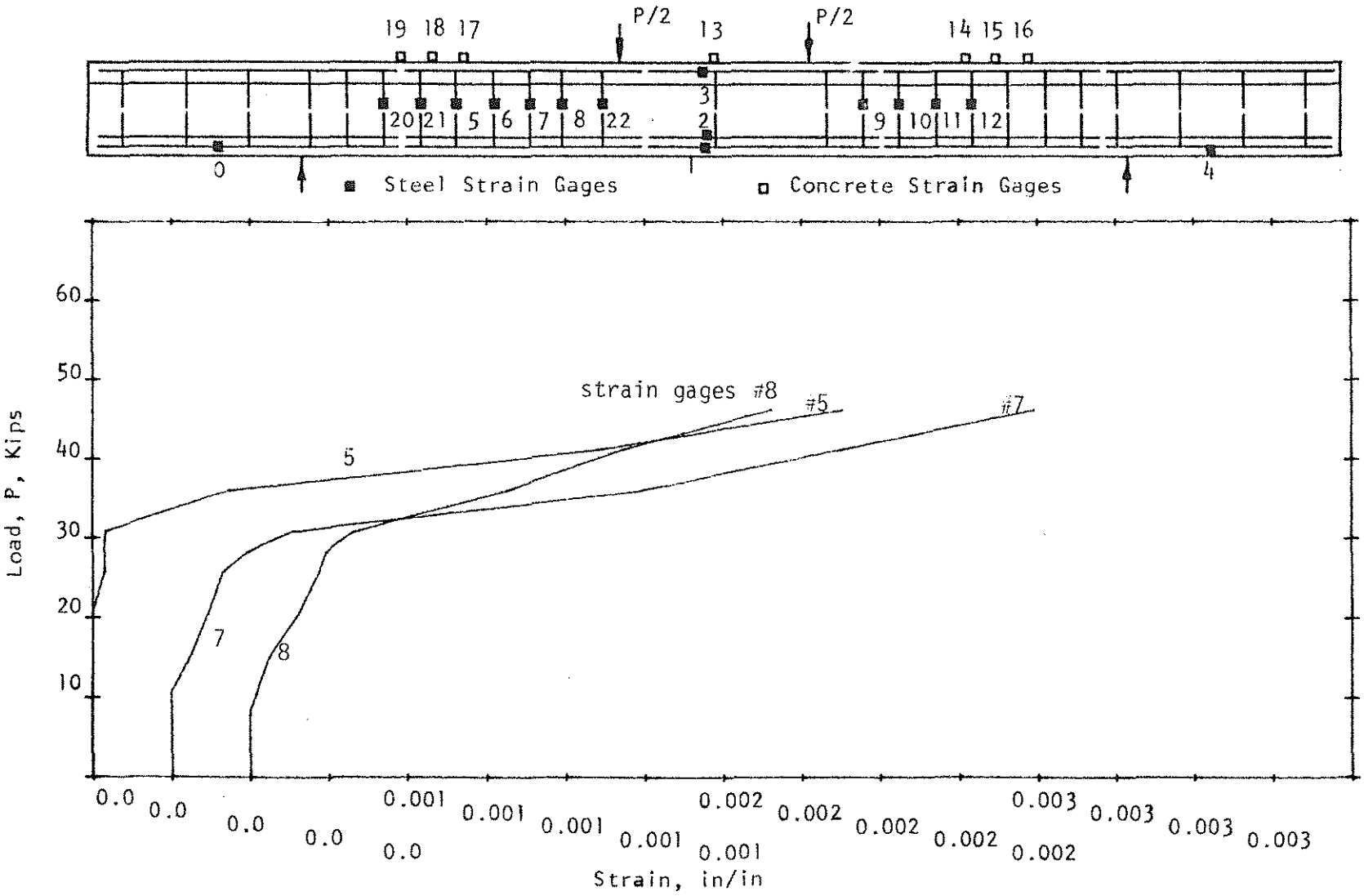

Figure 2.45 Load-Strain Curves, Beam A30a (ρ_w = 0.658%, $\rho_v f_{vy}$ = 97.1 psi).

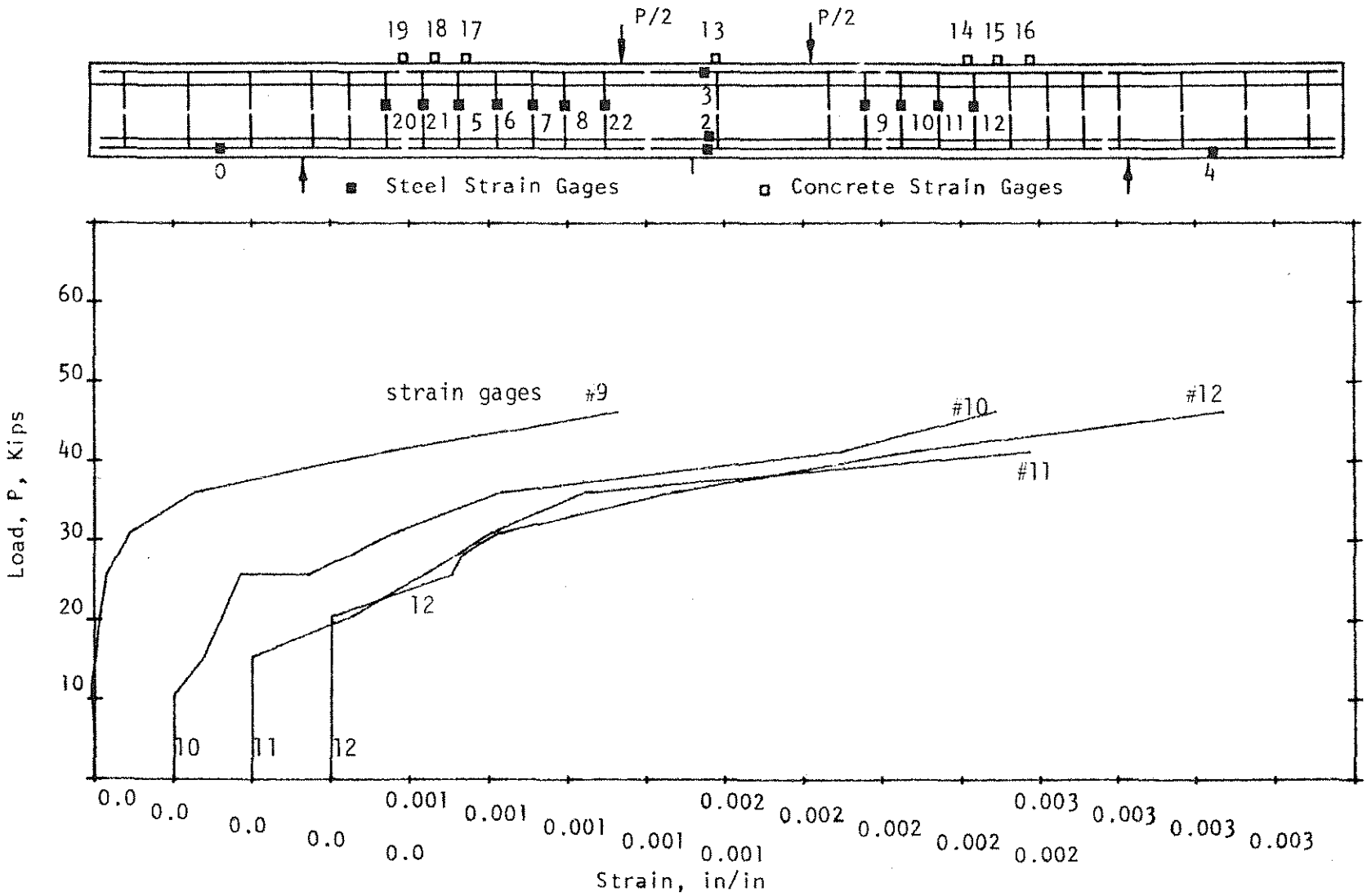

Figure 2.46 Load-Strain Curves, Beam A50a (ρ_w = 0.658%, $\rho_v f_{vy}$ = 75.0 psi).

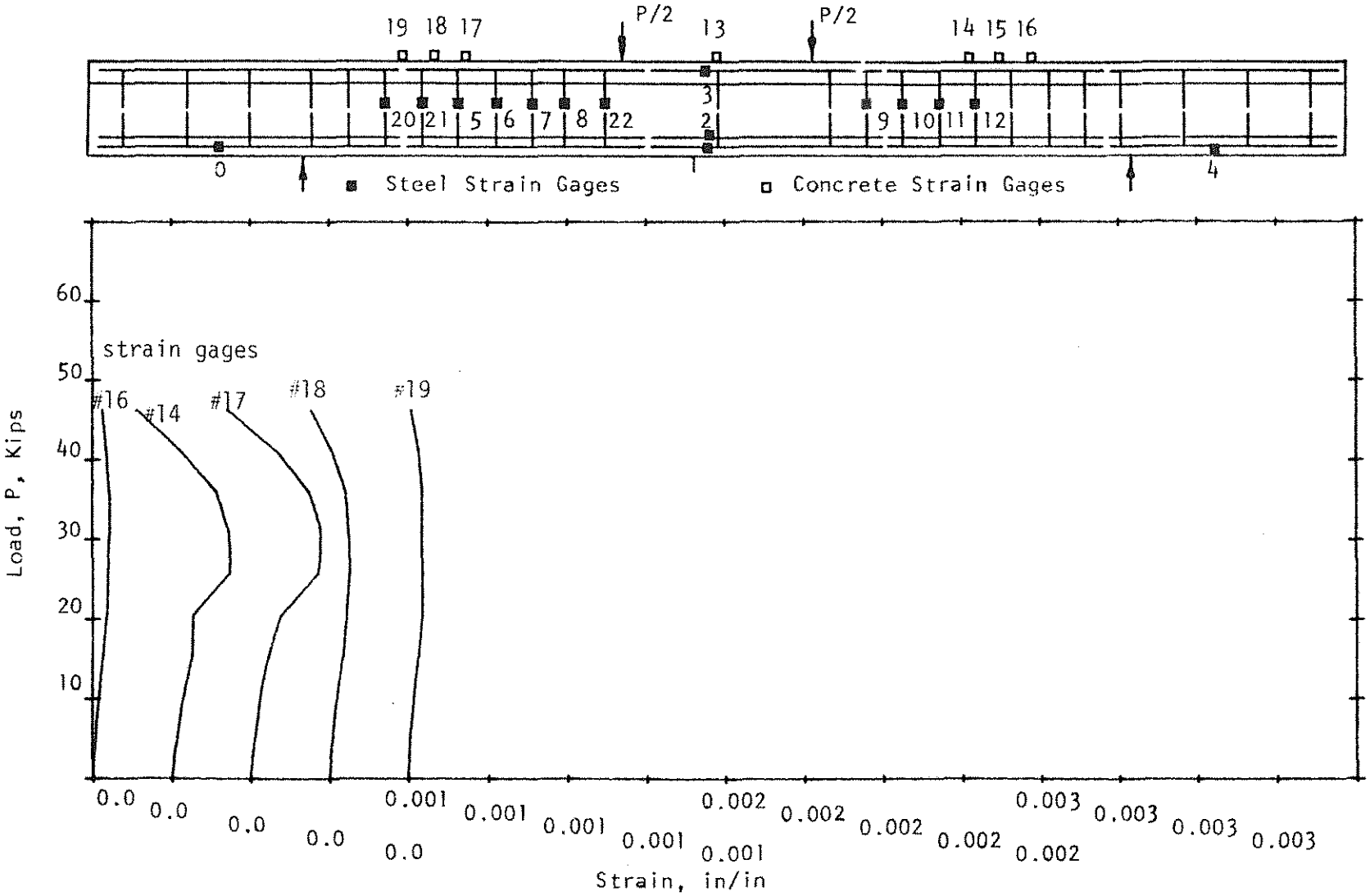

Figure 2.47 Load-Strain Curves, Beam A50a (ρ_w = 0.658%, $\rho_v f_{vy}$ = 75.0 psi).

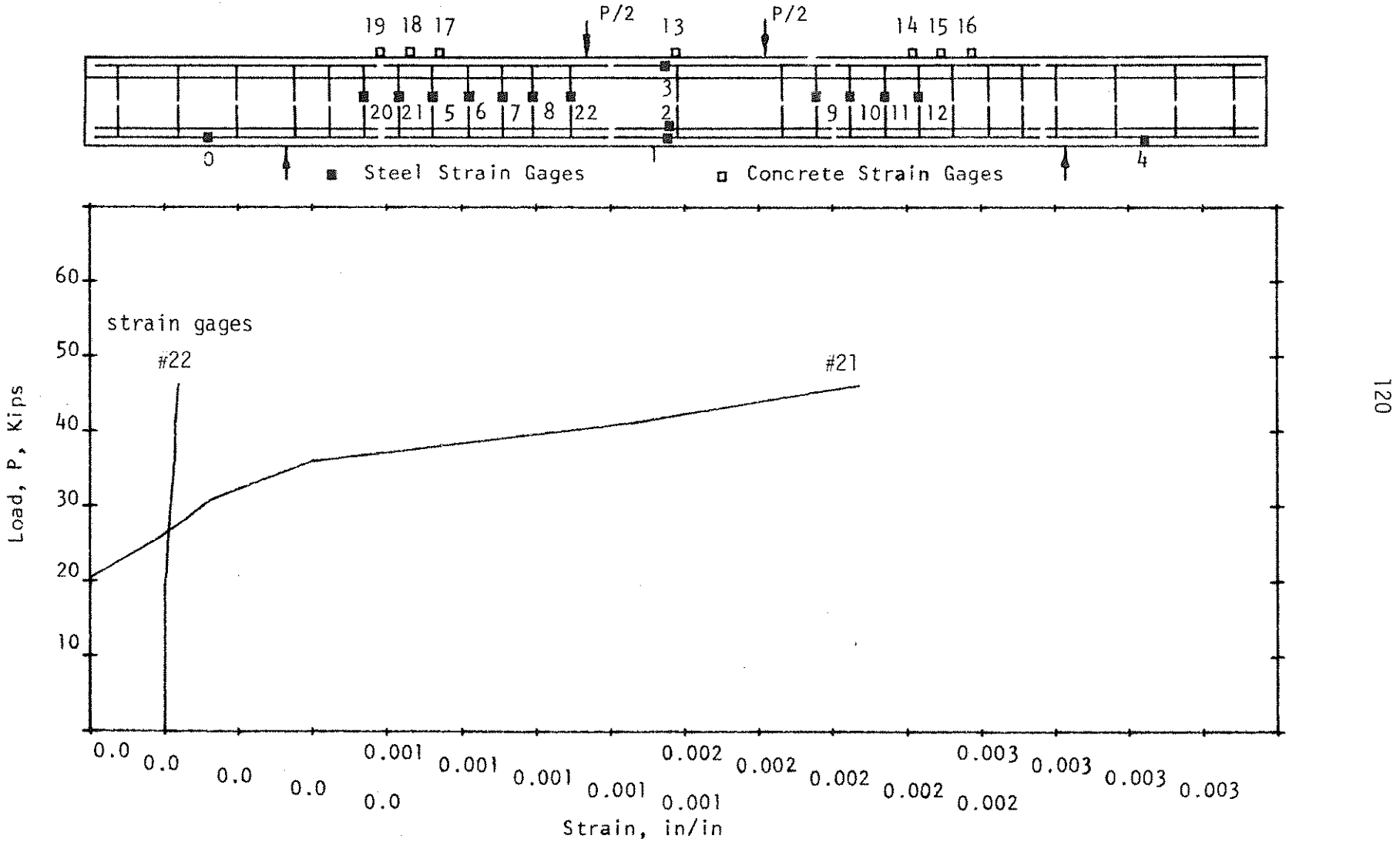

Figure 2.48 Load-Strain Curves, Beam A50a (ρ_w = 0.658%, $\rho_v f_{vy}$ = 75.0 psi).

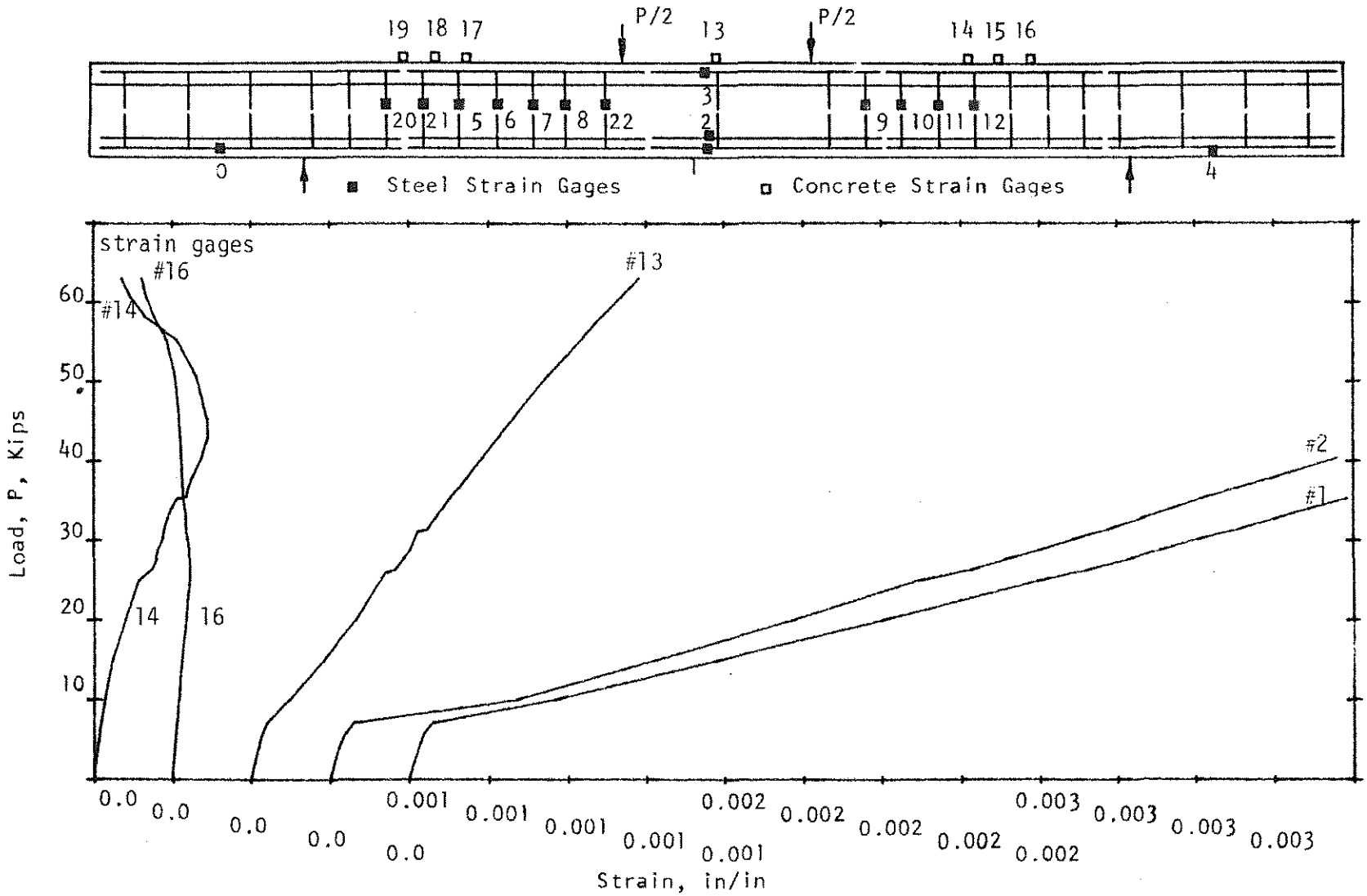

Figure 2.49 Load-Strain Curves, Beam A75 (ρ_w = 0.655%, $\rho_v f_{vy}$ = 97.1 psi).

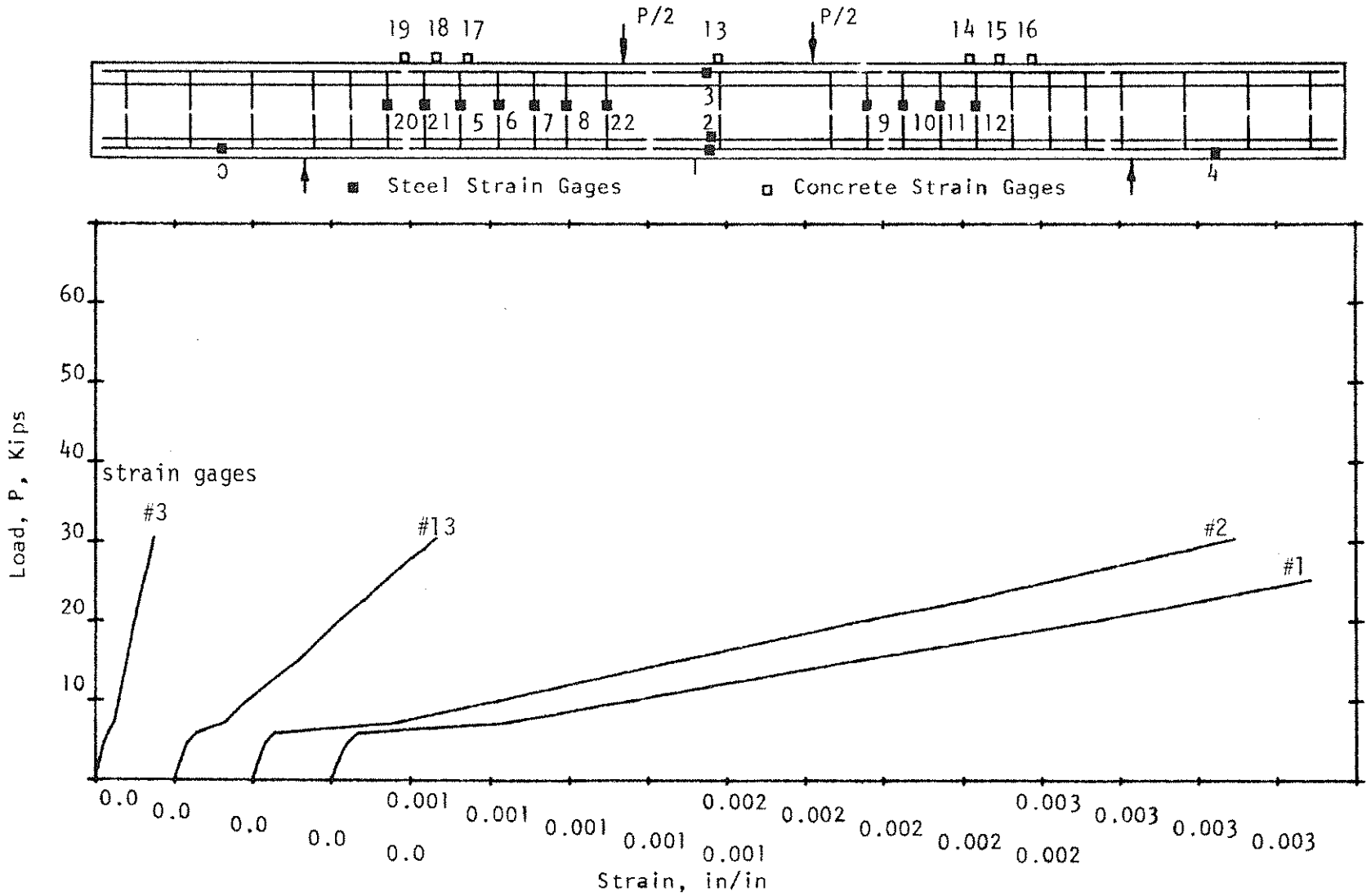

Figure 2.54 Load-Strain Curves, Beam B00 (ρ_w = 0.488%, $\rho_v f_{vy}$ = 0.0 psi).

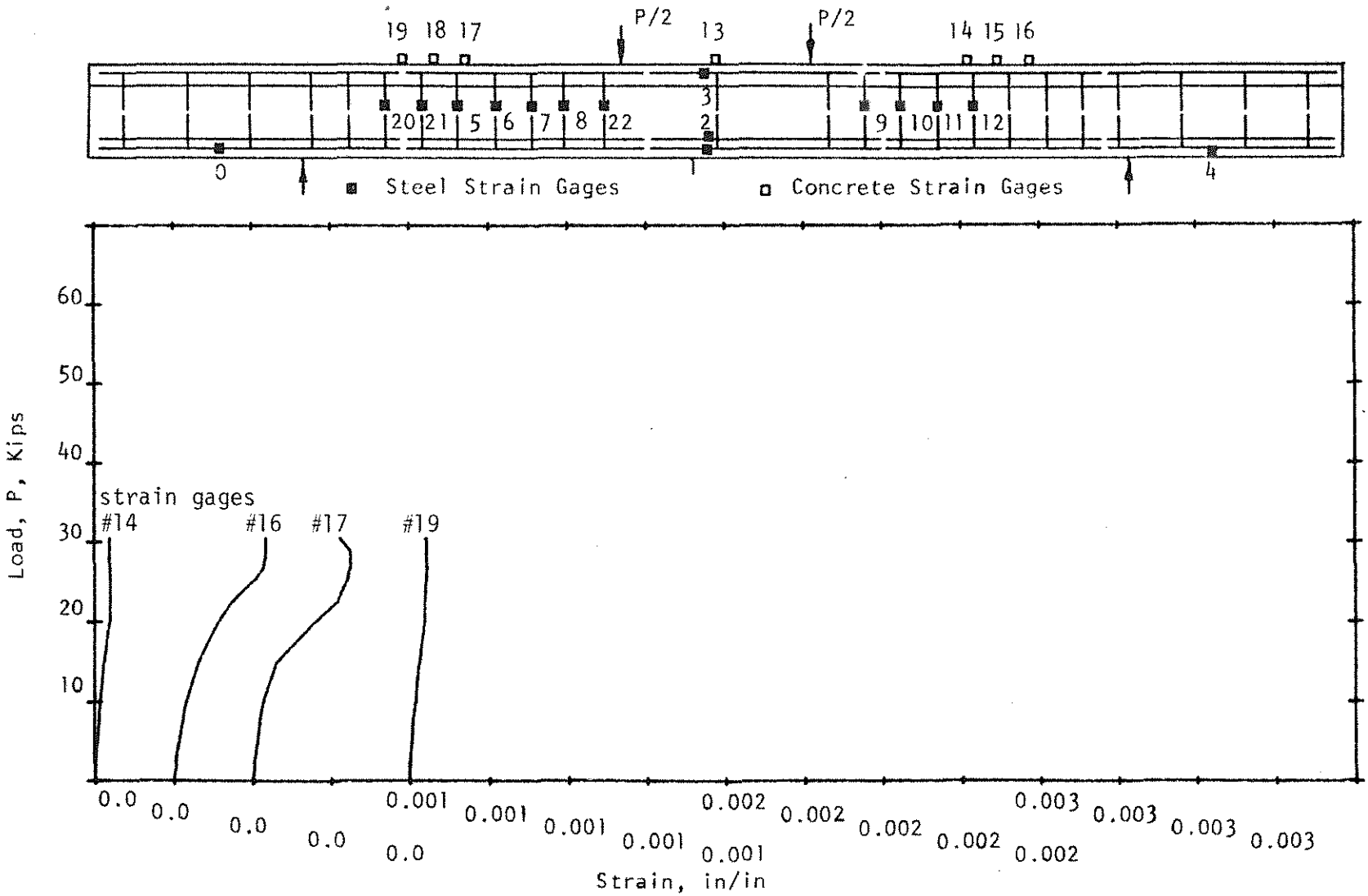

Figure 2.55 Load-Strain Curves, Beam B00 (ρ_w = 0.488%, $\rho_v f_{vy}$ = 0.0 psi).

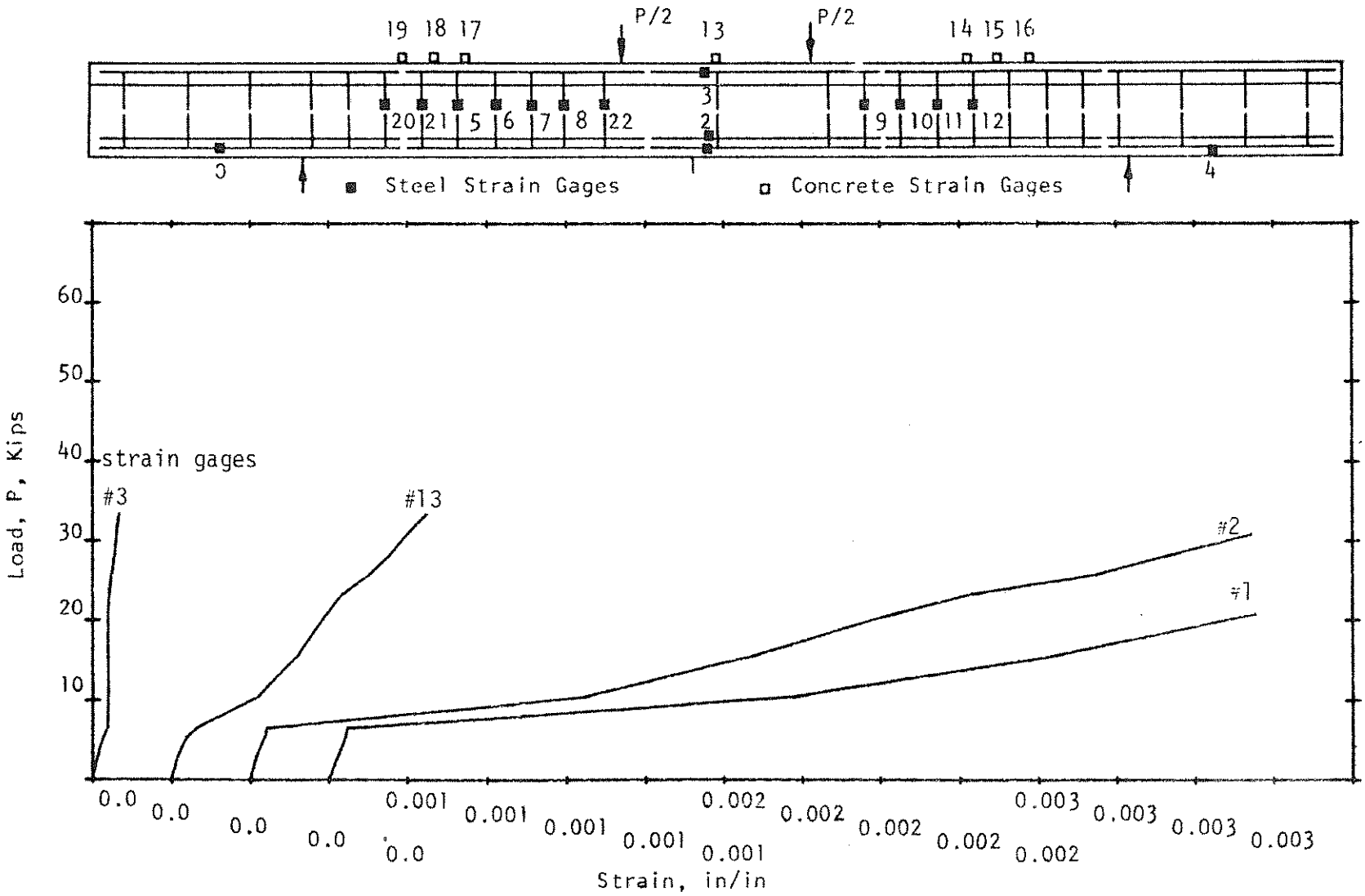

Figure 2.56 Load-Strain Curves, Beam B25 (ρ_w = 0.494%, $\rho_v f_{vy}$ = 32.4 psi).

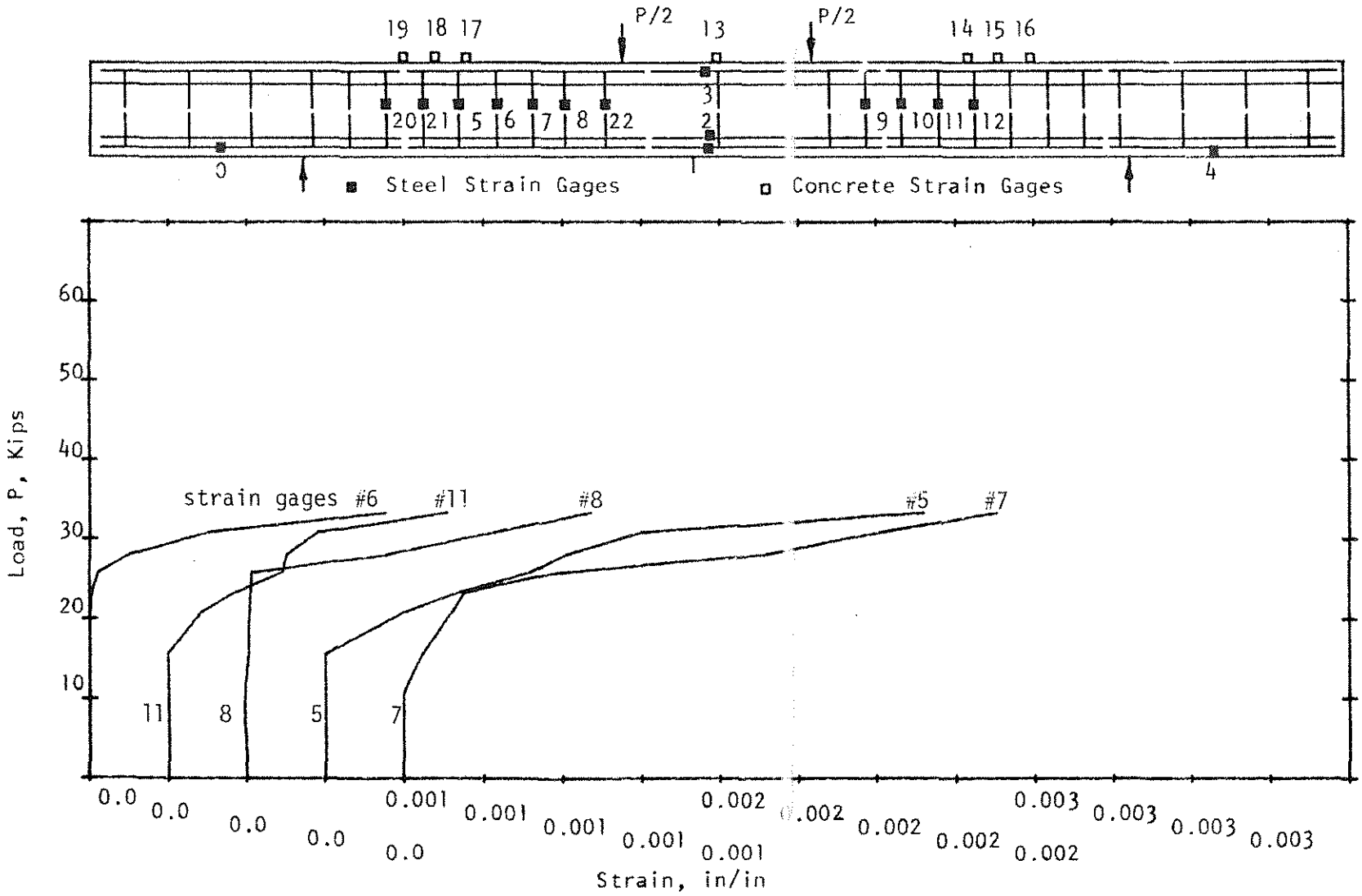

Figure 2.57 Load-Strain Curves, Beam B25 (ρ_w = 0.494%, $\rho_v f_{vy}$ = 32.4 psi).

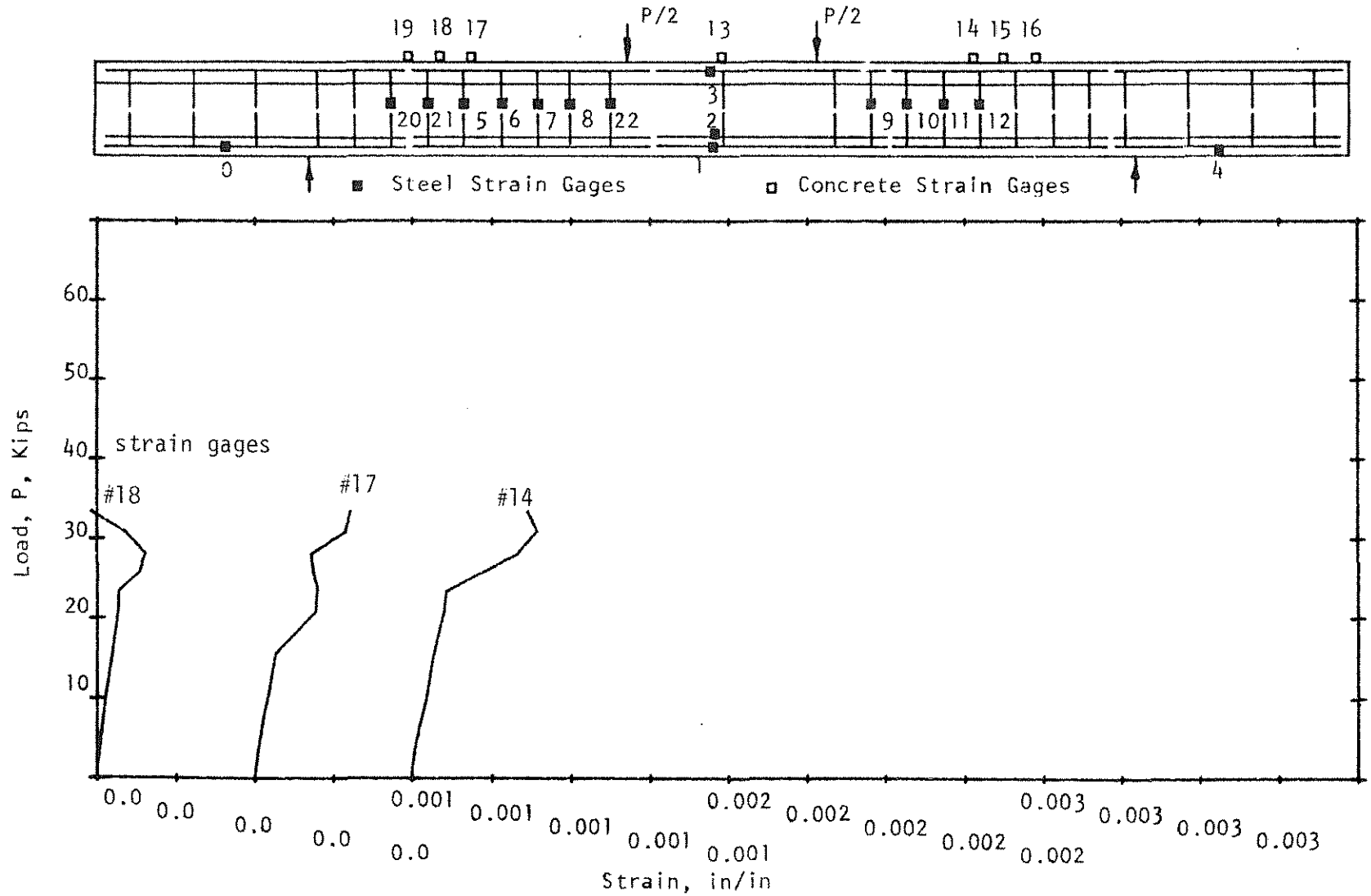

Figure 2.58 Load-Strain Curves, Beam B25 (ρ_w = 0.494%, $\rho_v f_{vy}$ = 32.4 psi).

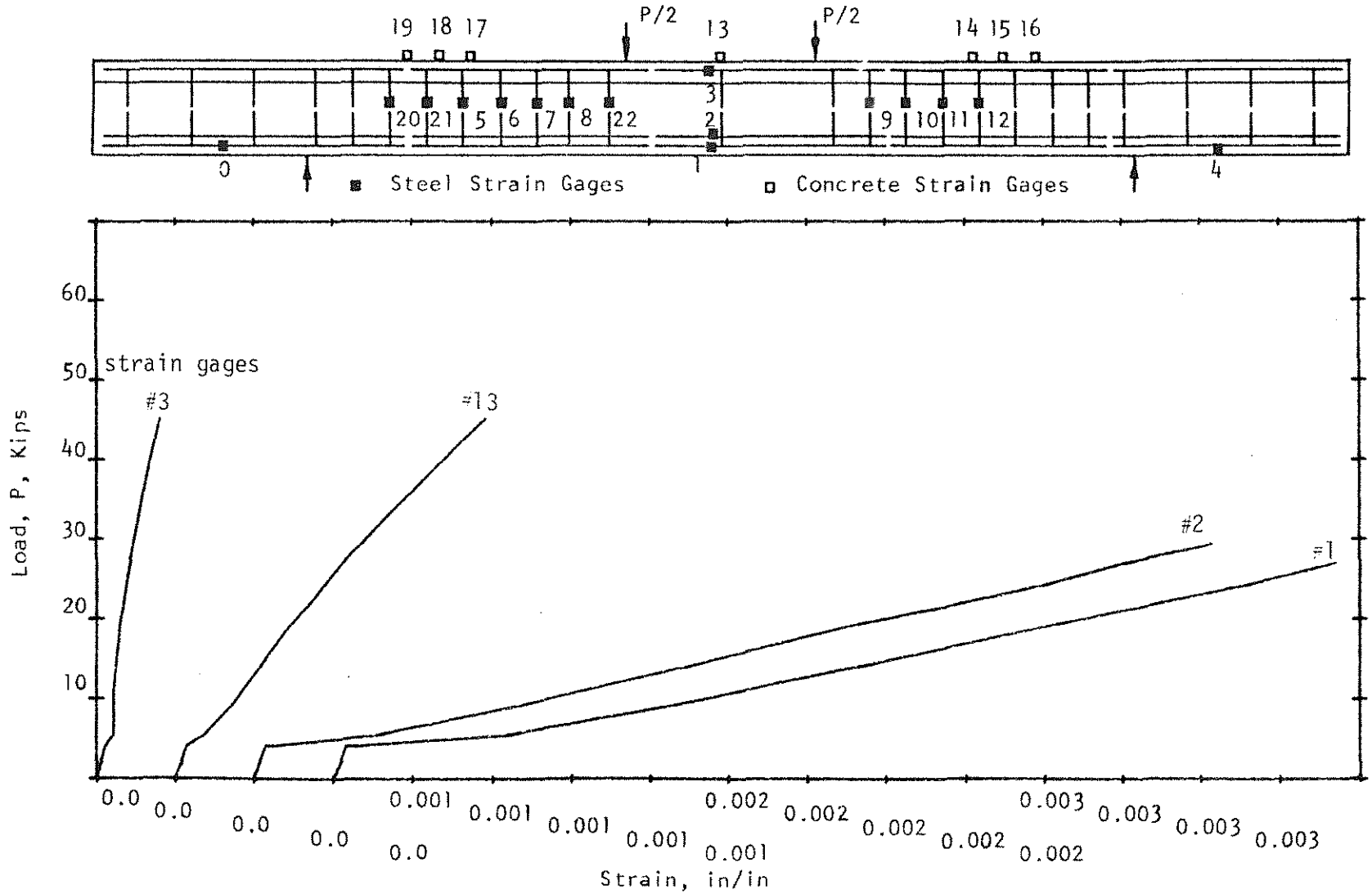

Figure 2.59 Load-Strain Curves, Beam B50 (ρ_w = 0.498%, $\rho_v f_{vy}$ = 76.2 psi).

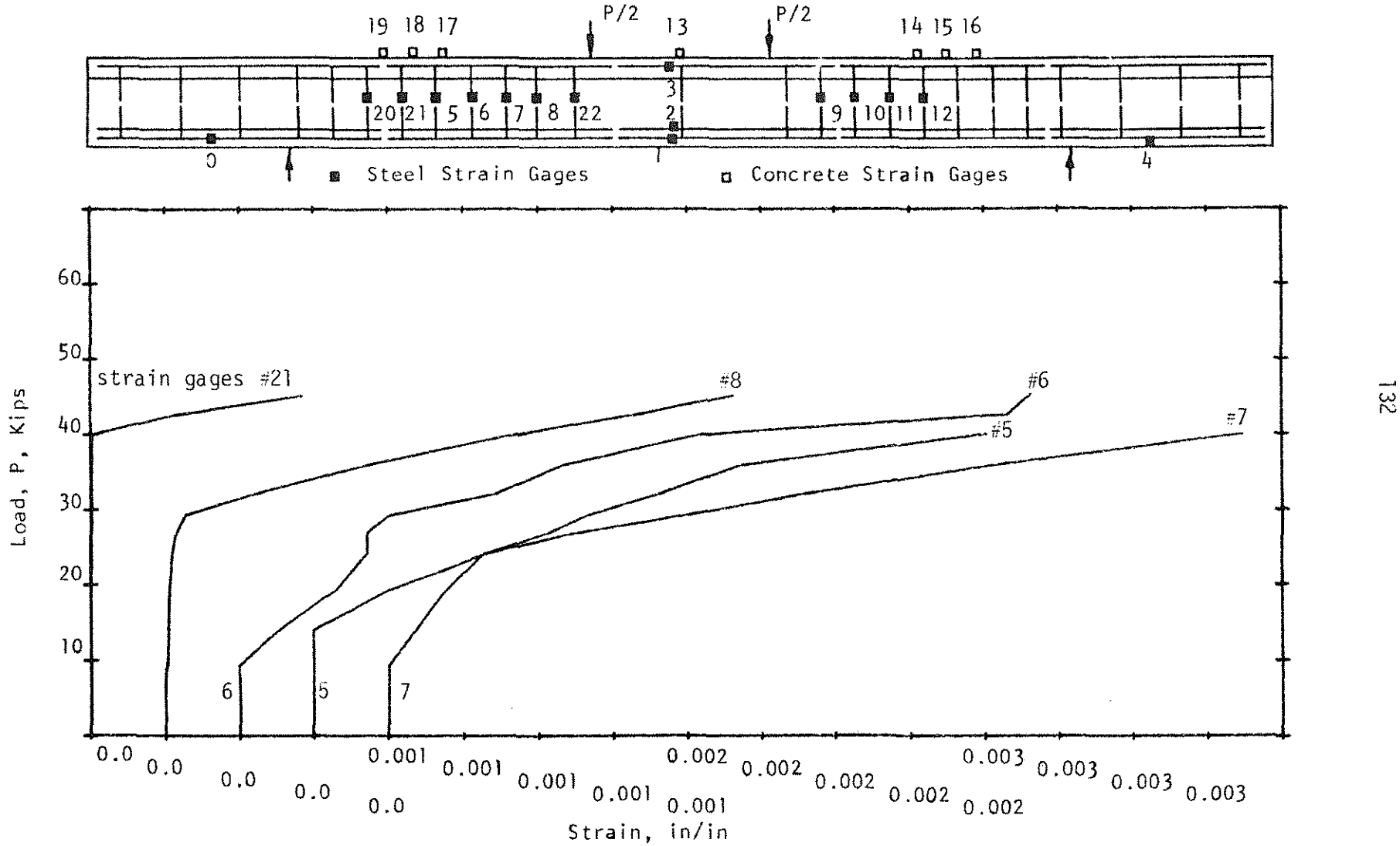

Figure 2.60 Load-Strain Curves, Beam B50 (ρ_w = 0.498%, $\rho_v f_{vy}$ = 76.2 psi).

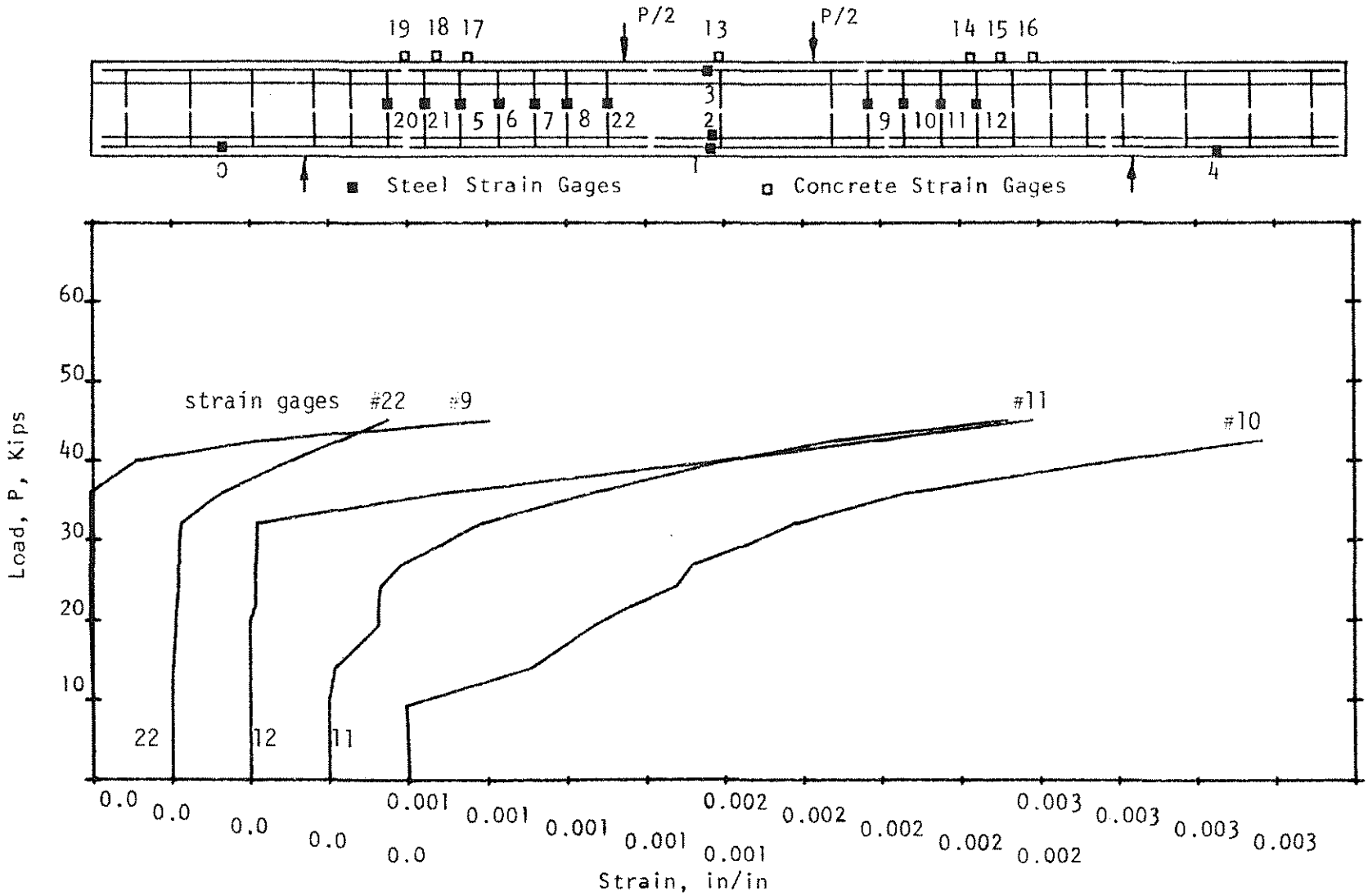

Figure 2.61 Load-Strain Curves, Beam B50 (ρ_w = 0.498%, $\rho_v f_{vy}$ = 76.2 psi).

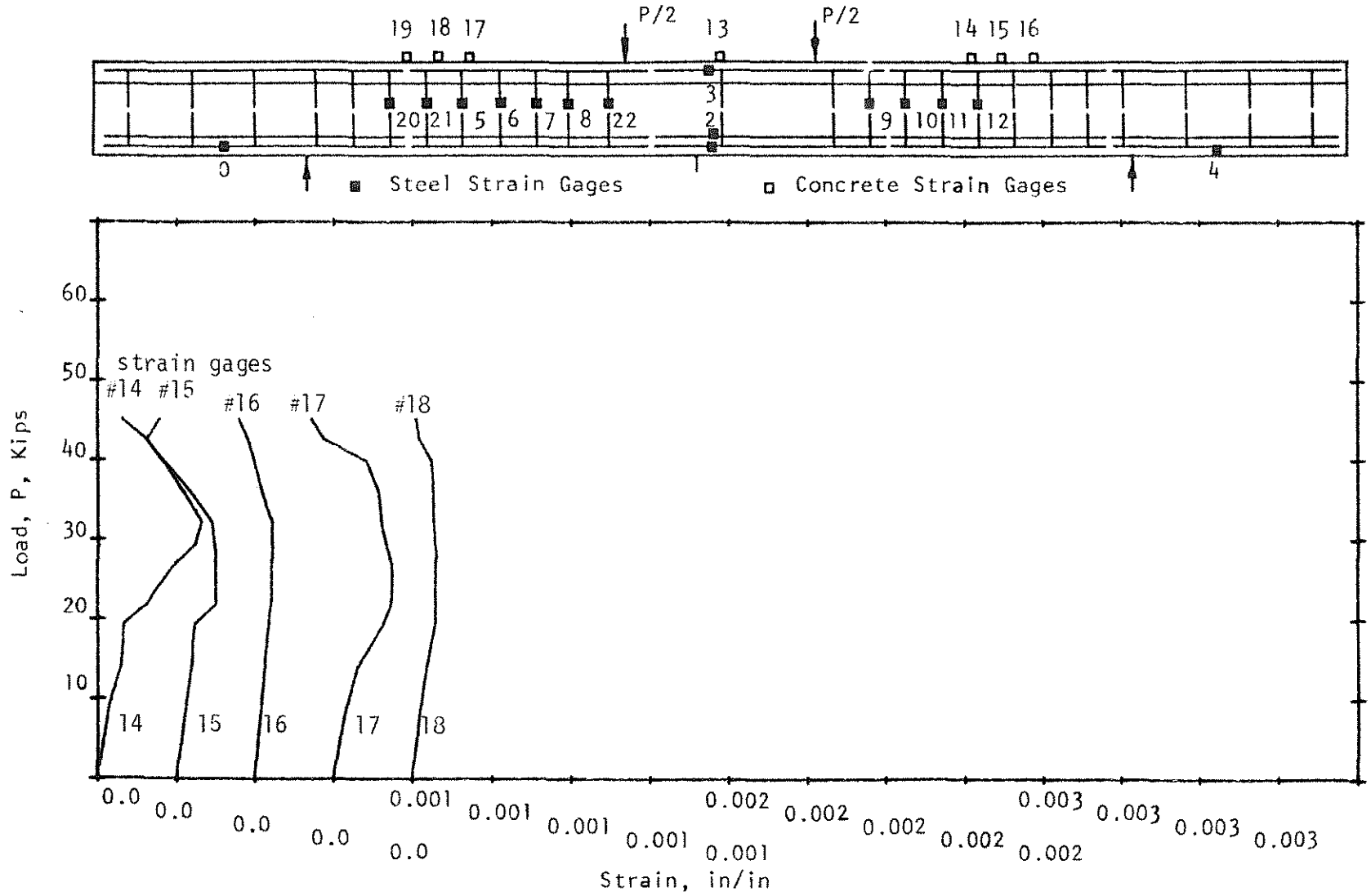

Figure 2.62 Load-Strain Curves, Beam B50 (ρ_w = 0.498%, $\rho_v f_{vy}$ = 76.2 psi).

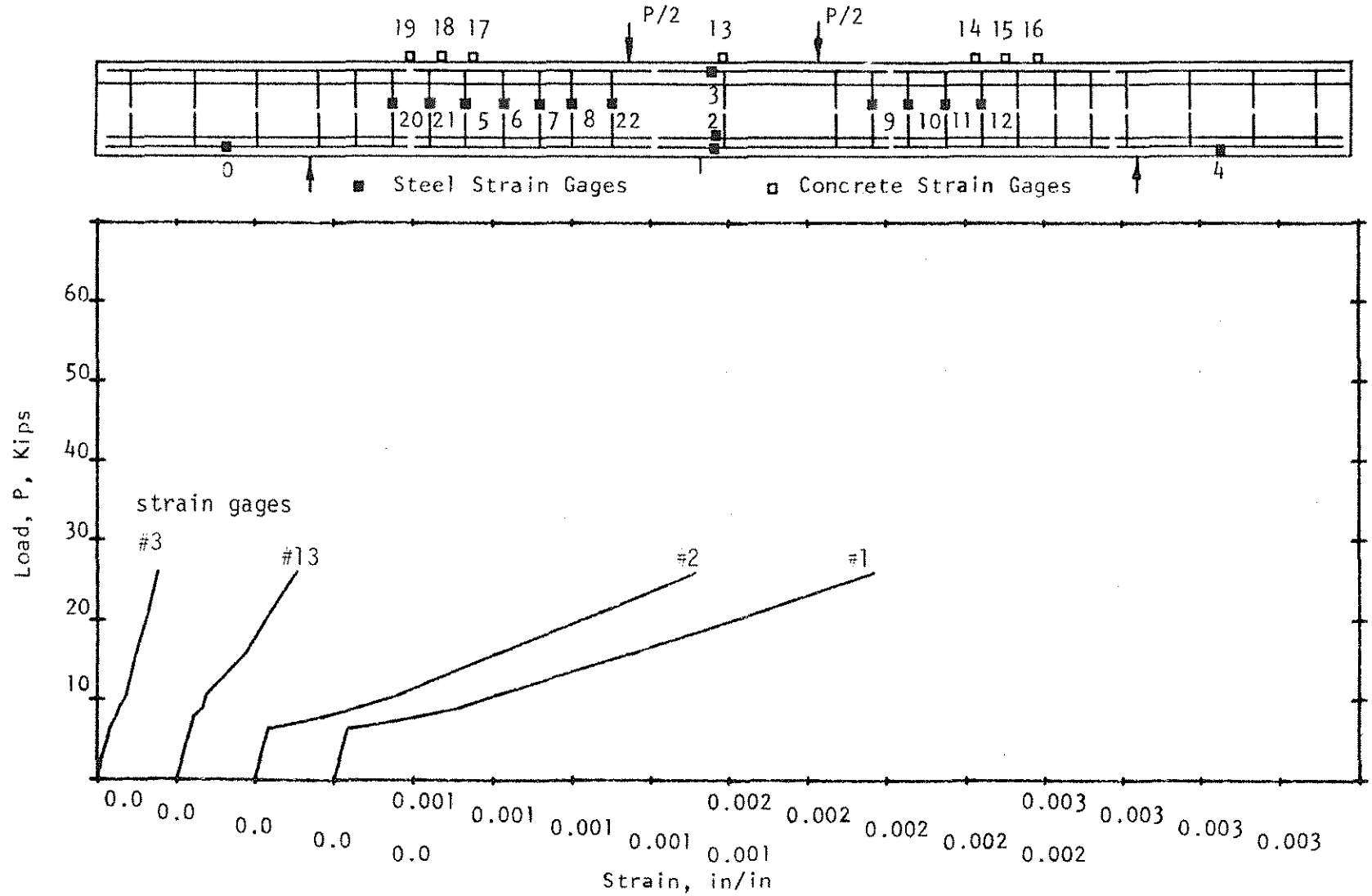

Figure 2.63 Load-Strain Curves, Beam C00 (ρ_w = 0.943%, $\rho_v f_{vy}$ = 0.0 psi)

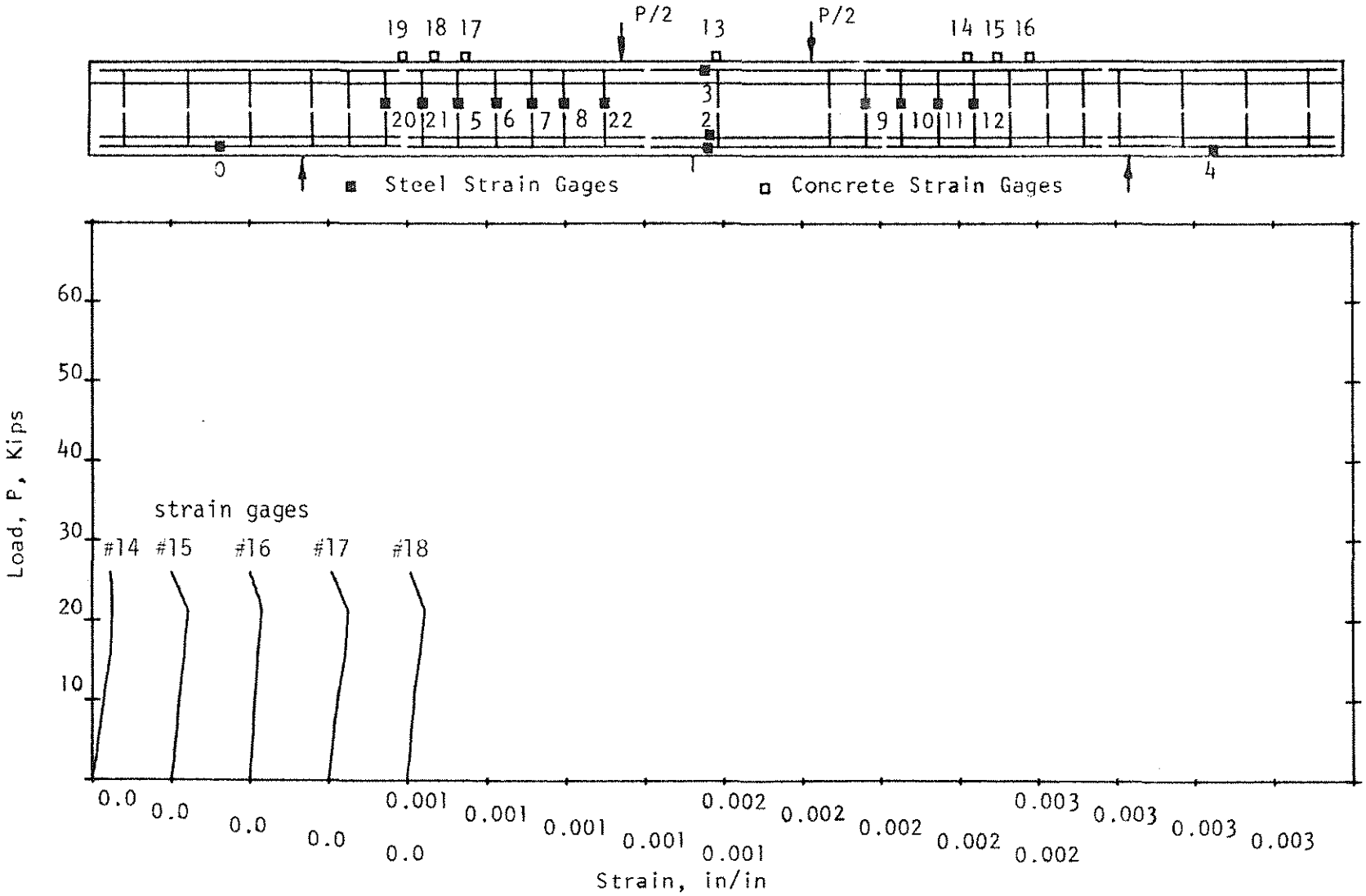

Figure 2.64 Load-Strain Curves, Beam C00 (ρ_w = 0.943%, $\rho_v f_{vy}$ = 0.0 psi).

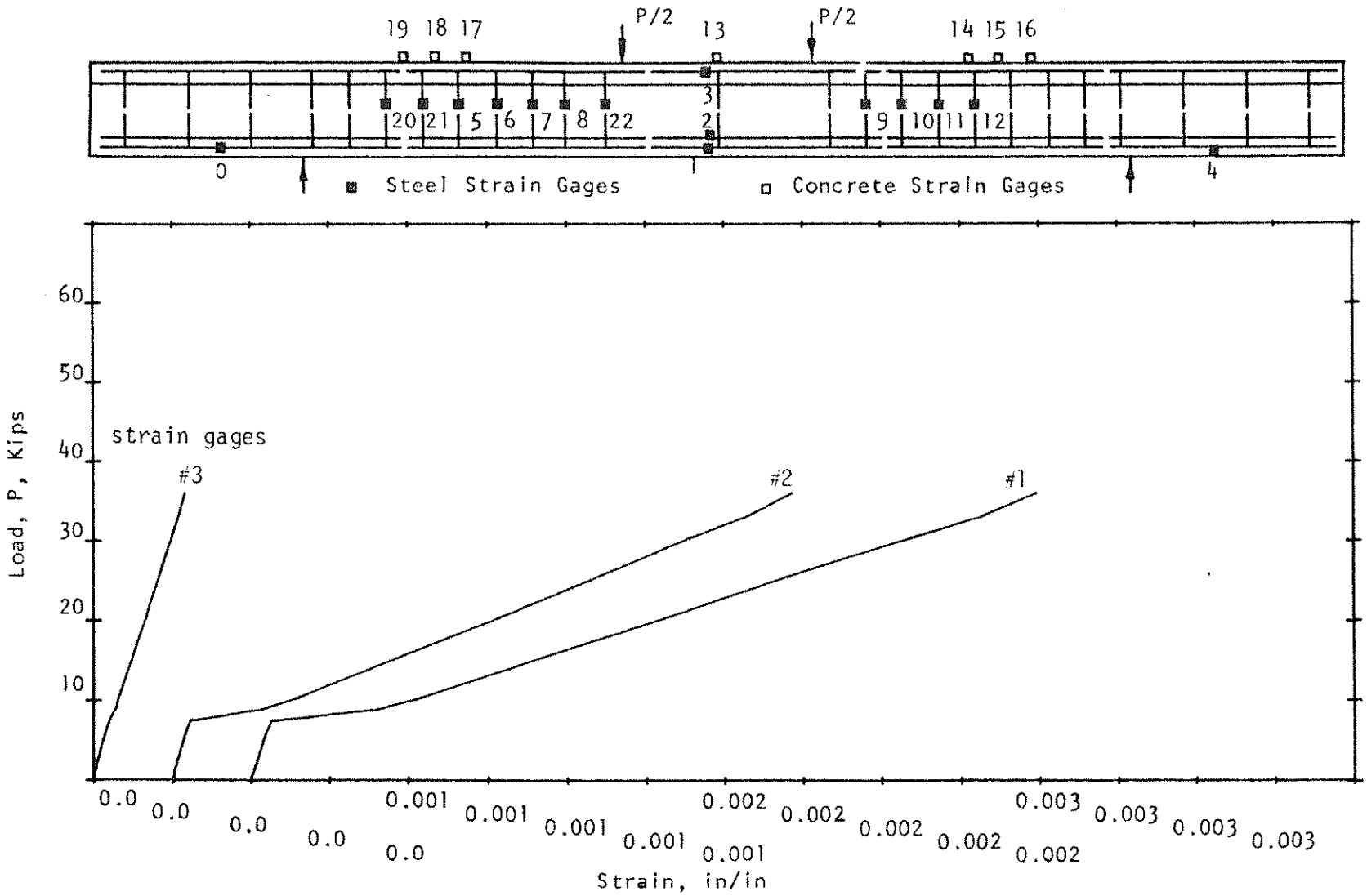

Figure 2.65 Load-Strain Curves, Beam C25 (ρ_w = 0.948%, $\rho_v f_{vy}$ = 32.4 psi).

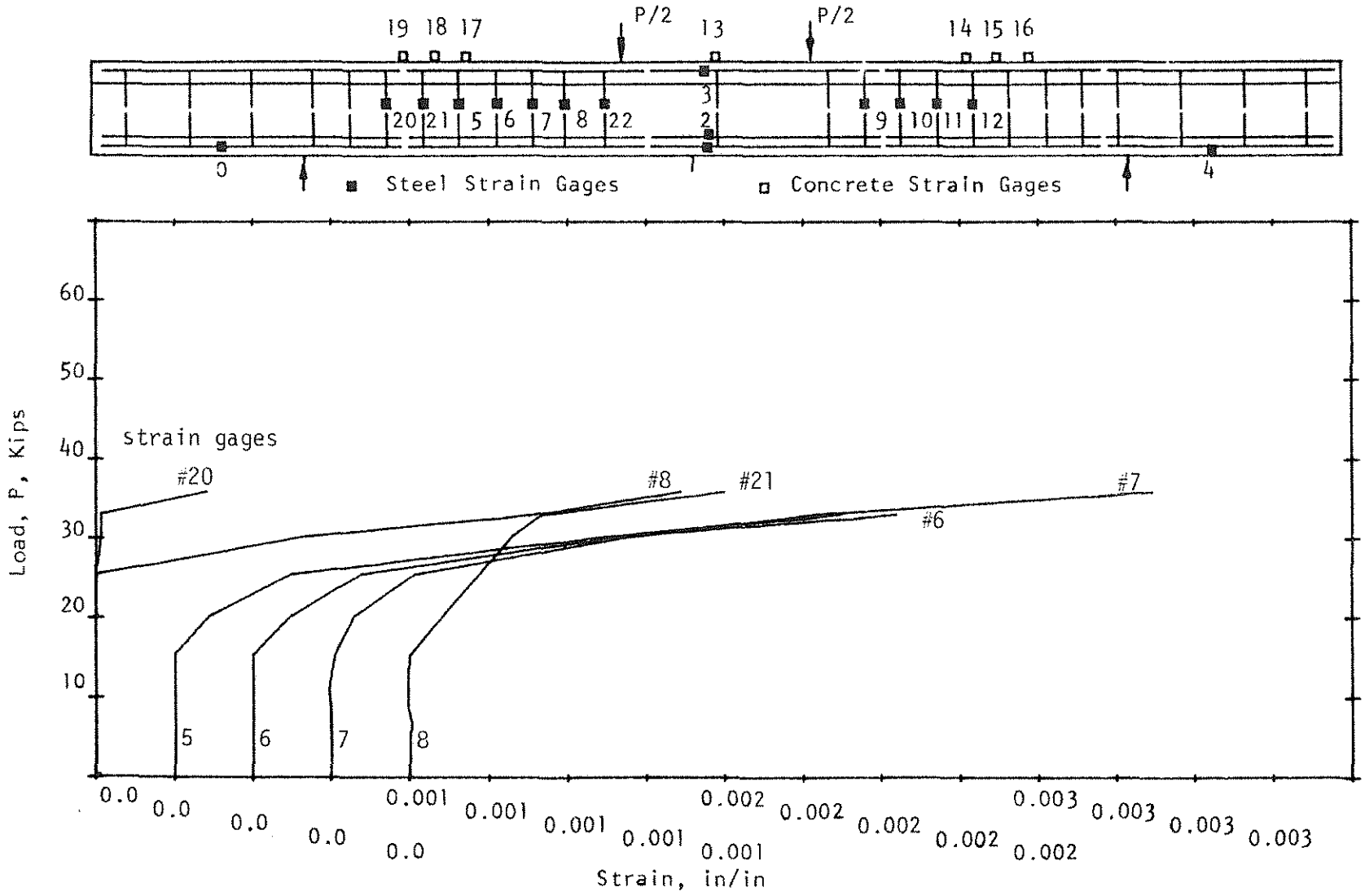

Figure 2.66 Load-Strain Curves, Beam C25 (ρ_w = 0.948%, $\rho_v f_{vy}$ = 32.4 psi).

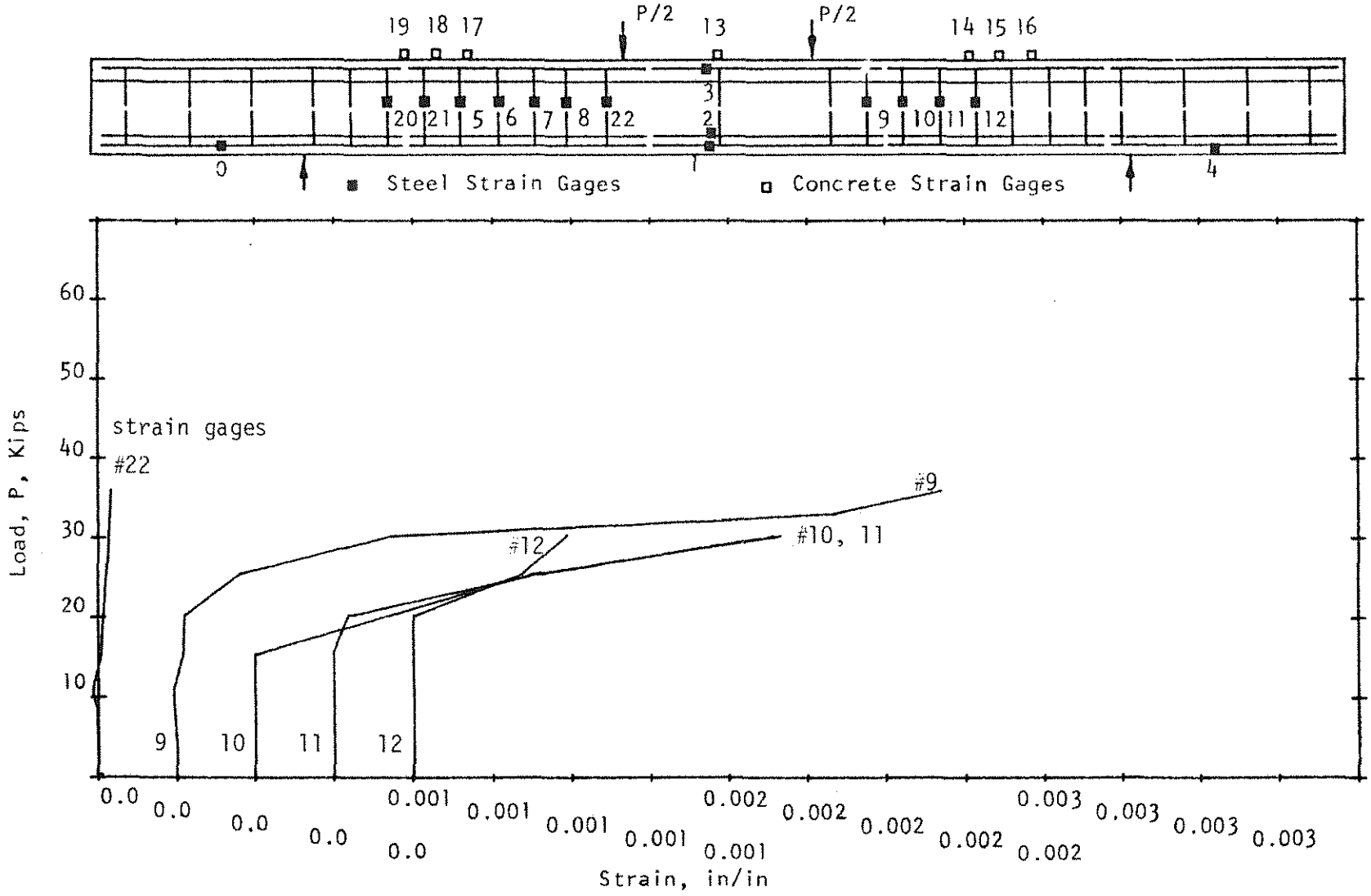

Figure 2.67 Load-Strain Curves, Beam C25 (ρ_w = 0.948%, $\rho_v f_{vy}$ = 32.4 psi).

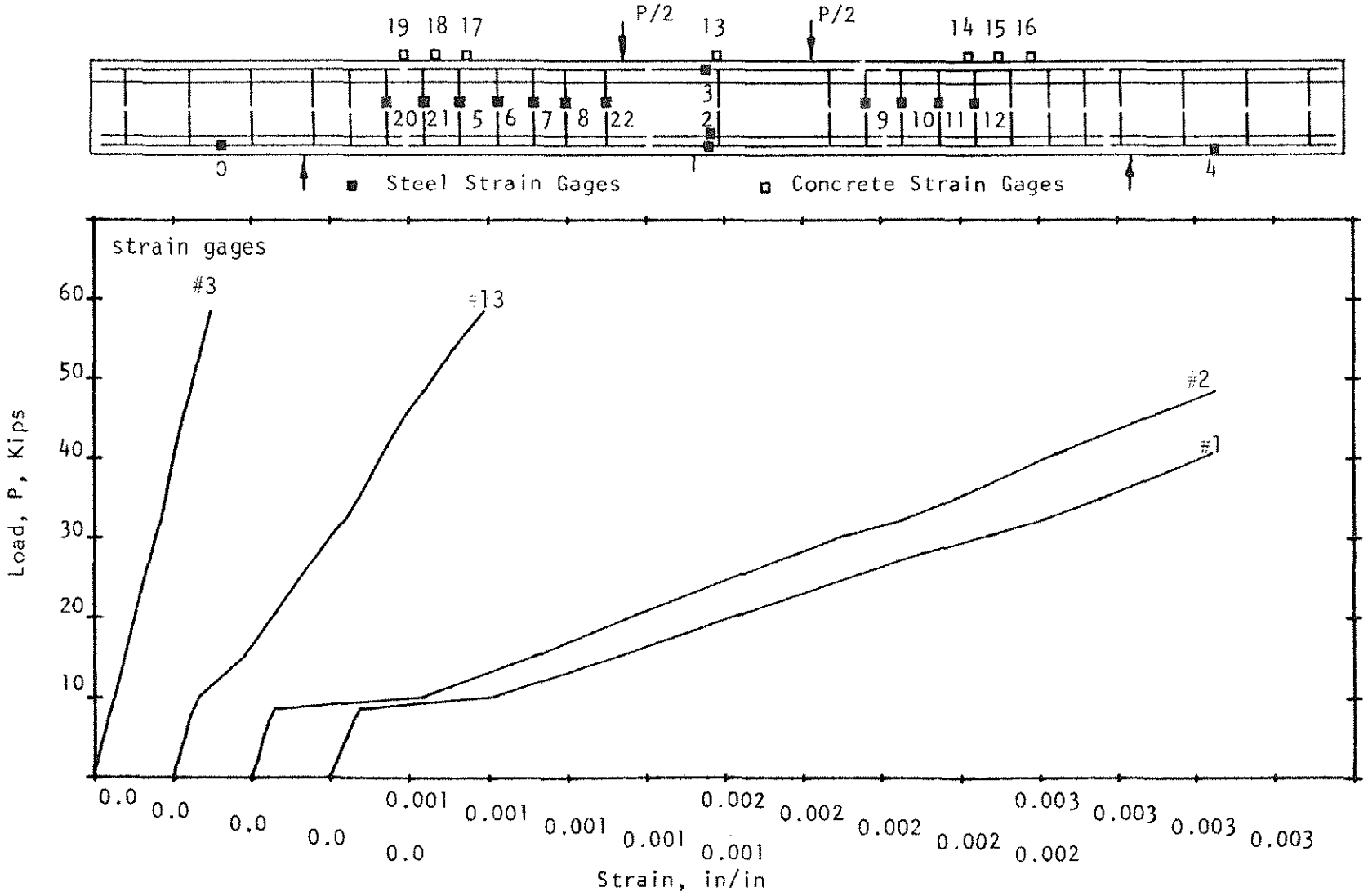

Figure 2.68 Load-Strain Curves, Beam C50 (ρ_w = 0.939%, $\rho_v f_{vy}$ = 76.2 psi).

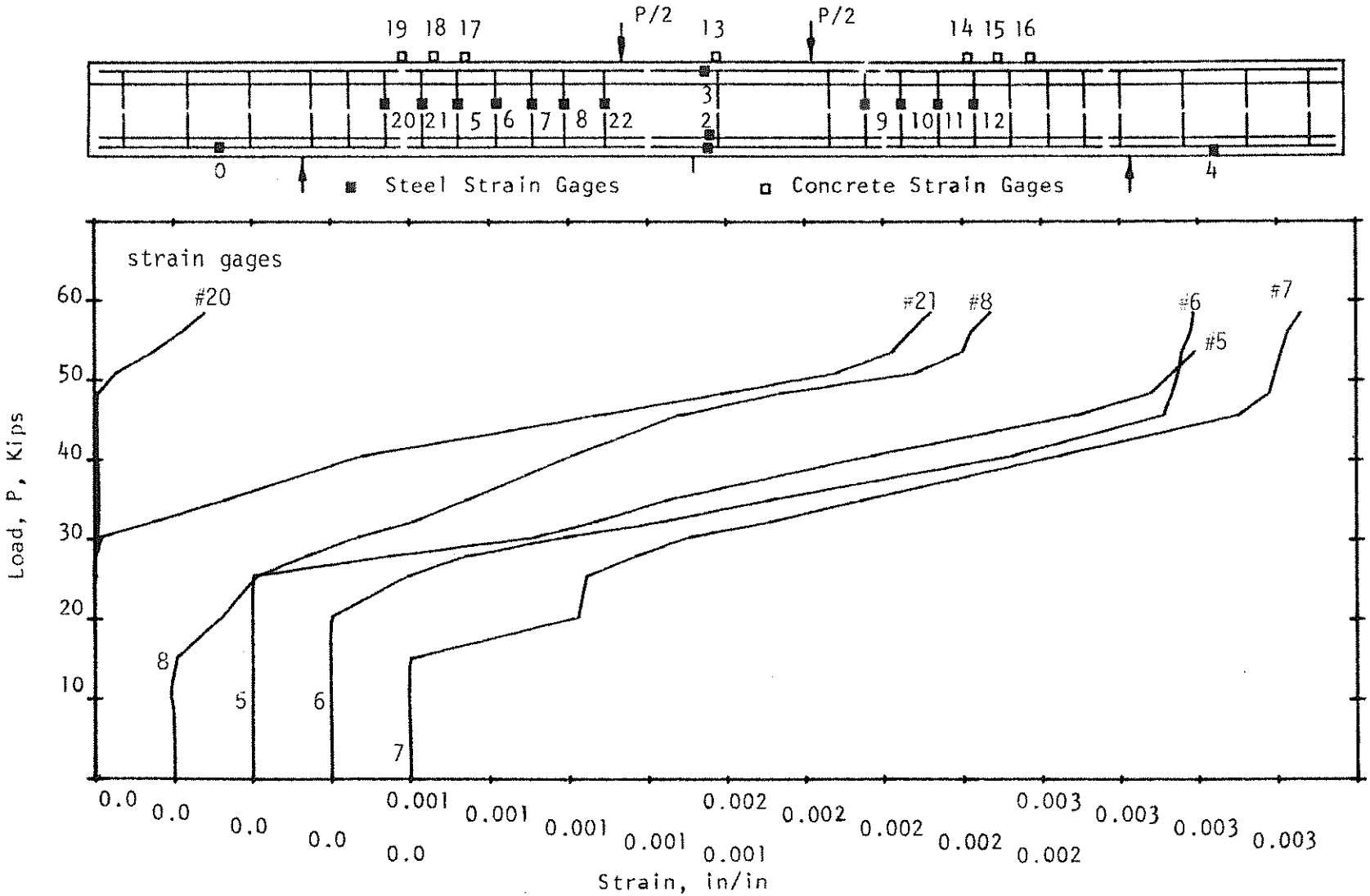

Figure 2.69 Load-Strain Curves, Beam C50 (ρ_w = 0.939%, $\rho_v f_{vy}$ = 76.2 psi).

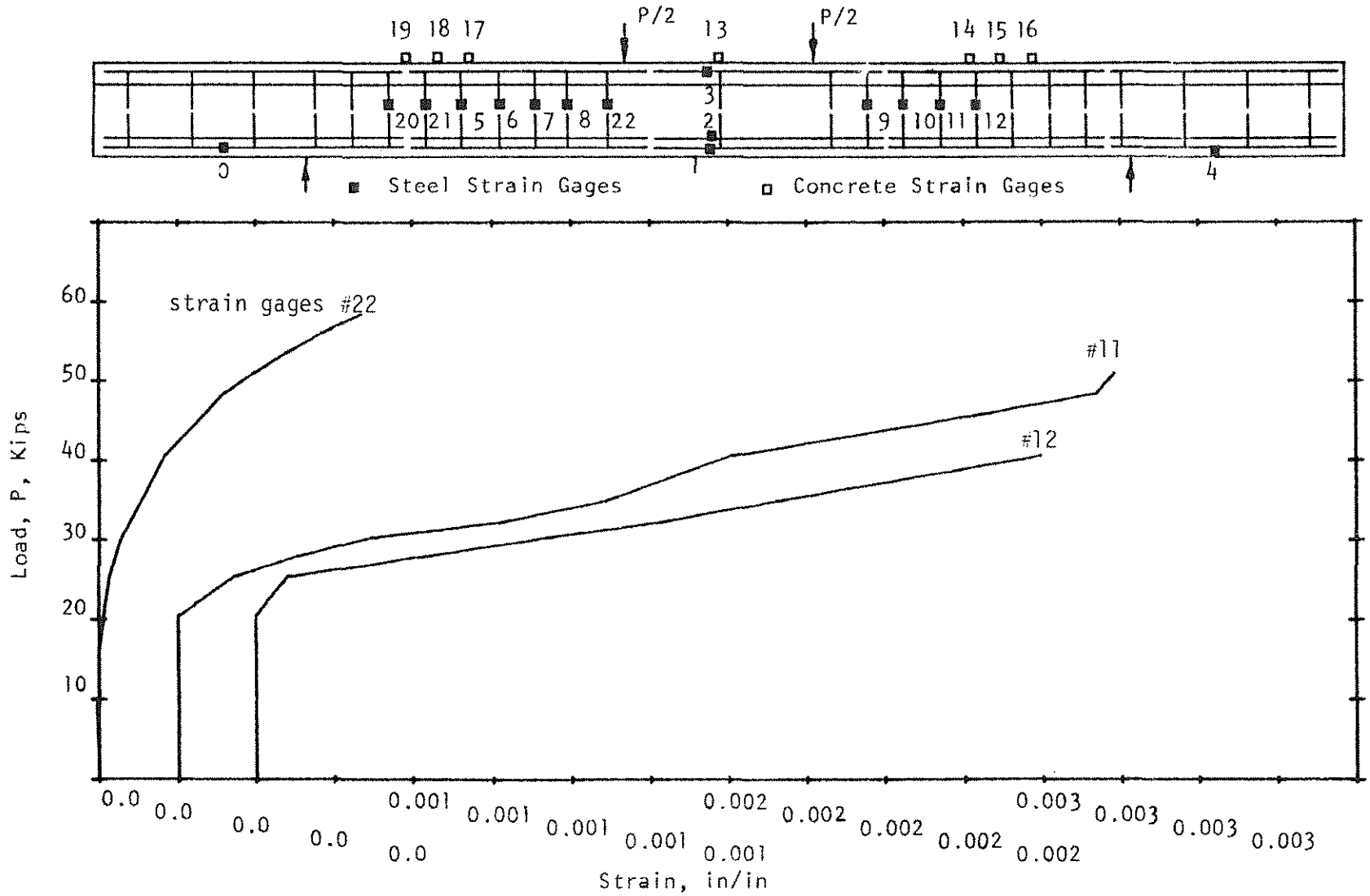

Figure 2.70 Load-Strain Curves, Beam C50 (ρ_w = 0.939%, $\rho_v f_{vy}$ = 76.2 psi).

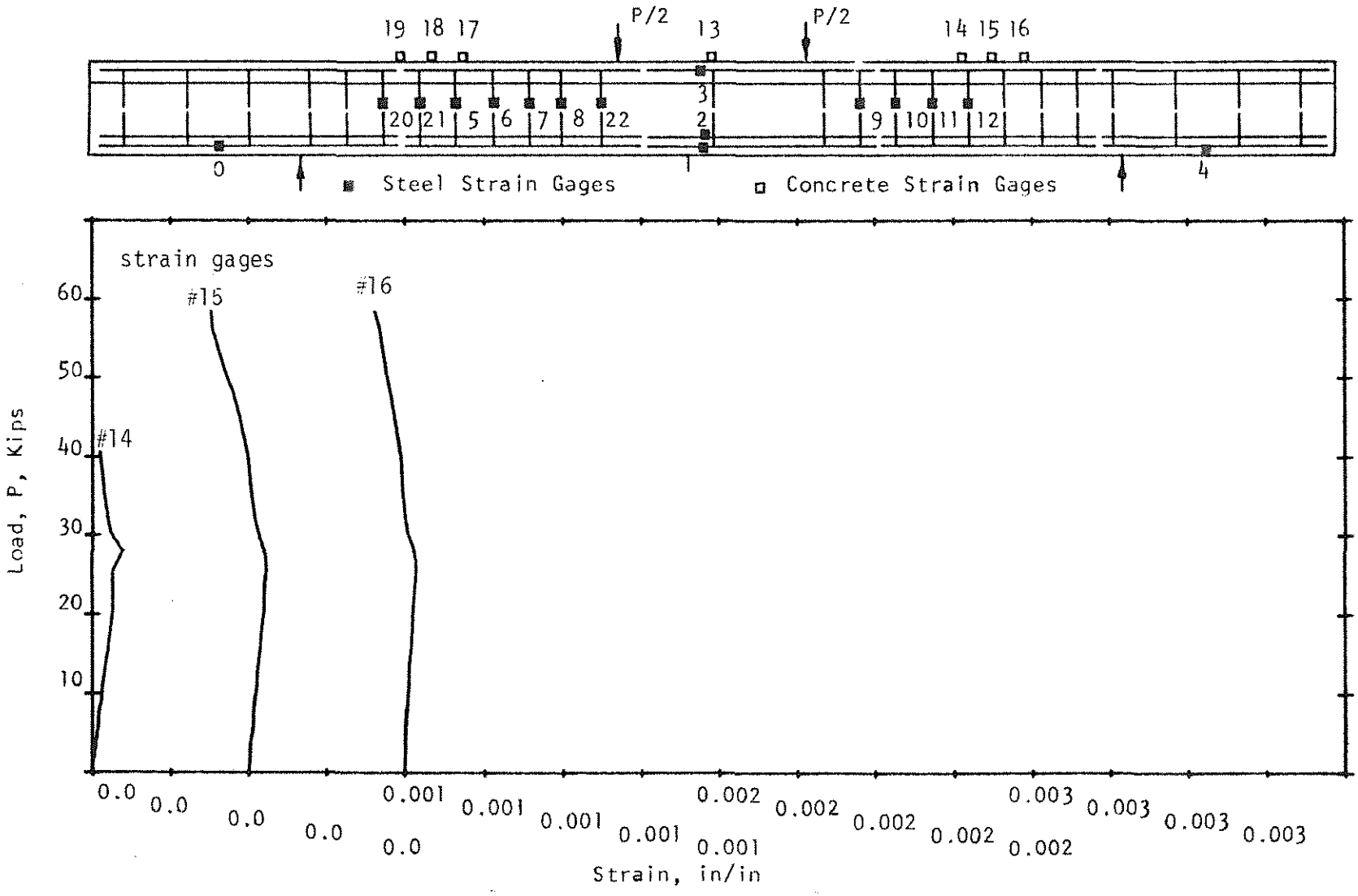

Figure 2.71 Load-Strain Curves, Beam C50 (ρ_w = 0.939%, $\rho_v f_{vy}$ = 76.2 psi).

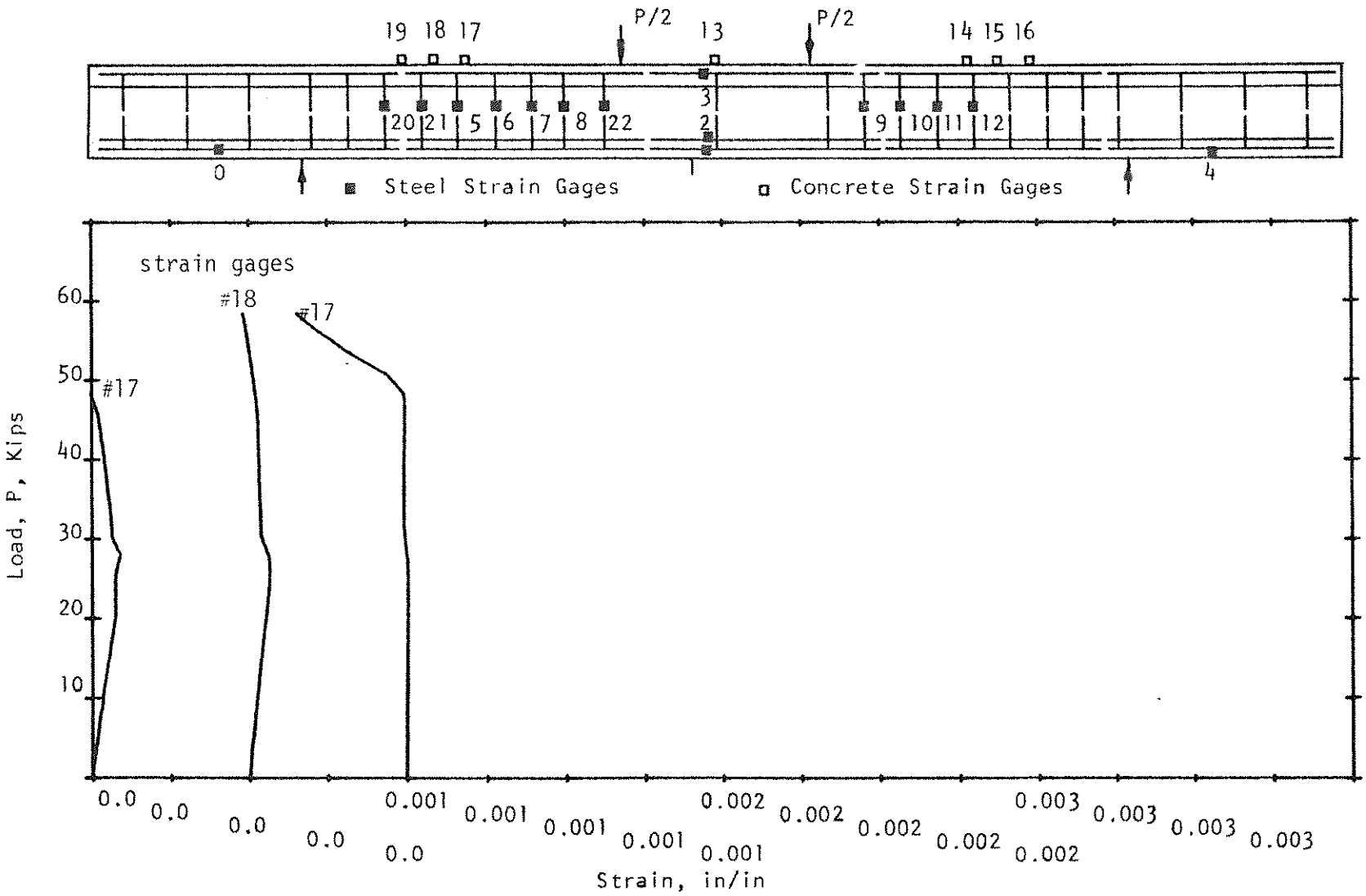

Figure 2.72 Load-Strain Curves, Beam C50 (ρ_w = 0.939%, $\rho_v f_{vy}$ = 76.2 psi).

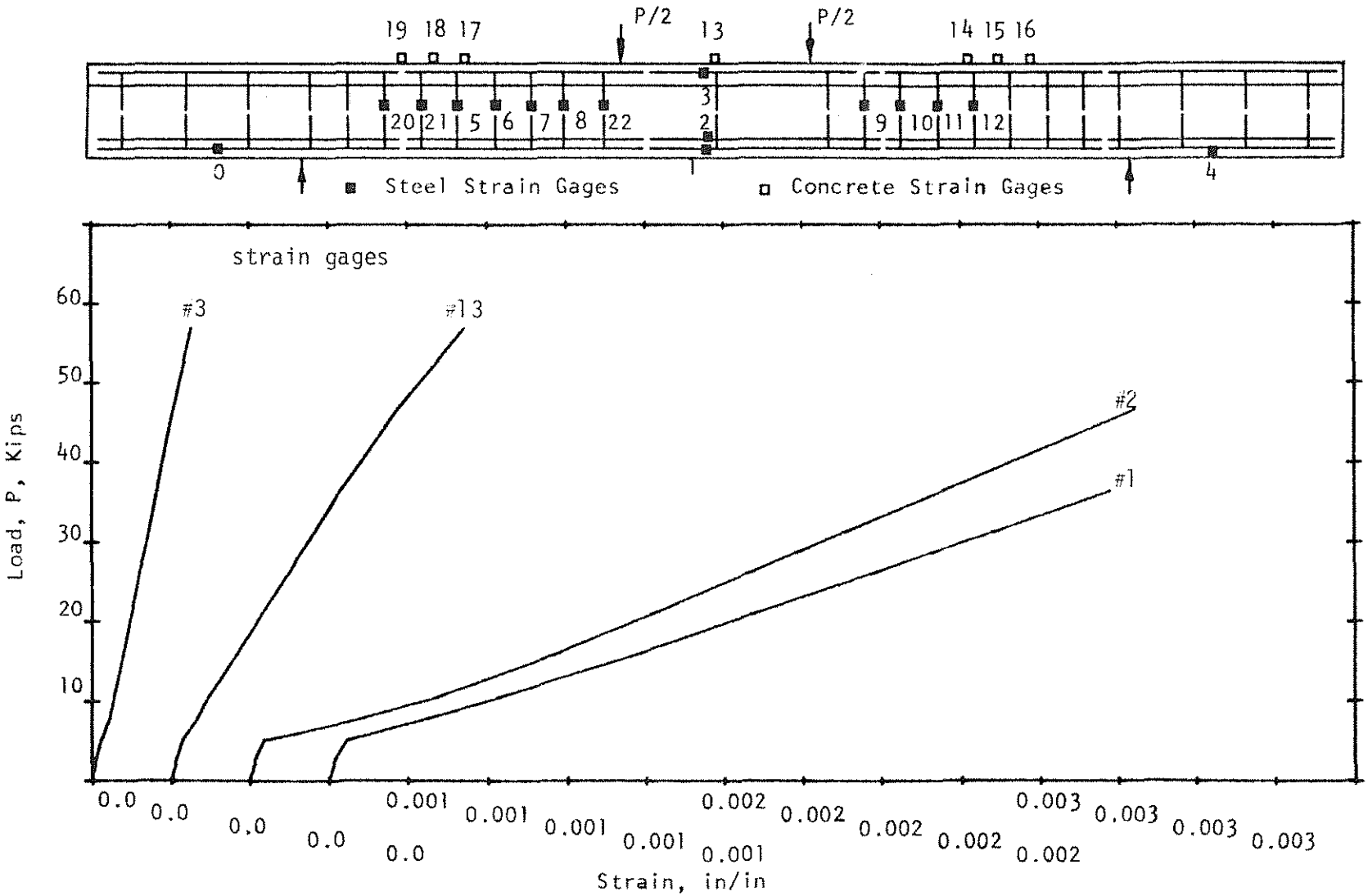

Figure 2.73 Load-Strain Curves, Beam C75 (ρ_w = 0.933%, $\rho_v f_{vy}$ = 103.0 psi).

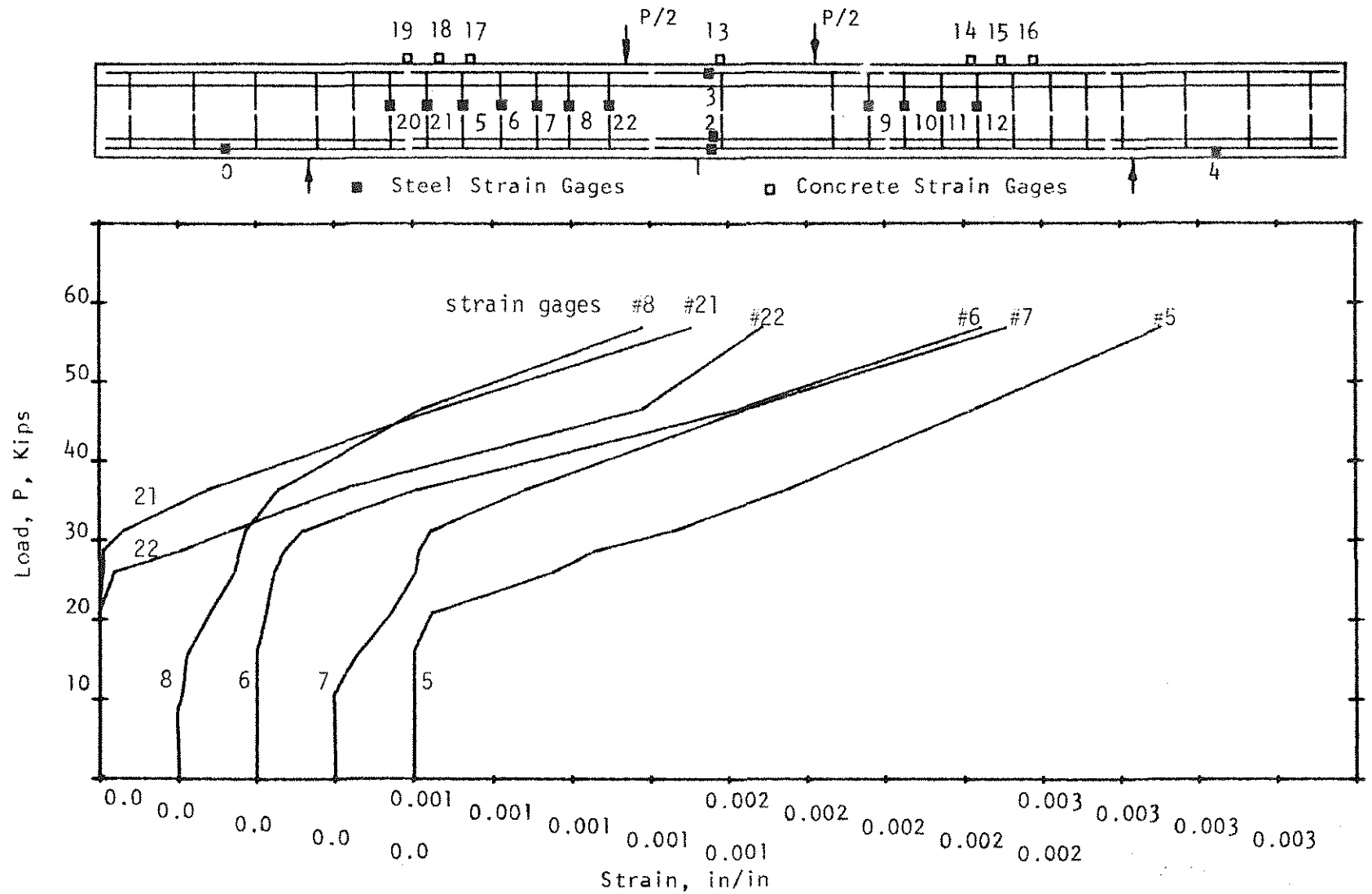

Figure 2.74 Load-Strain Curves, Beam C75 (ρ_w = 0.933%, $\rho_v f_{vy}$ = 103.0 psi).

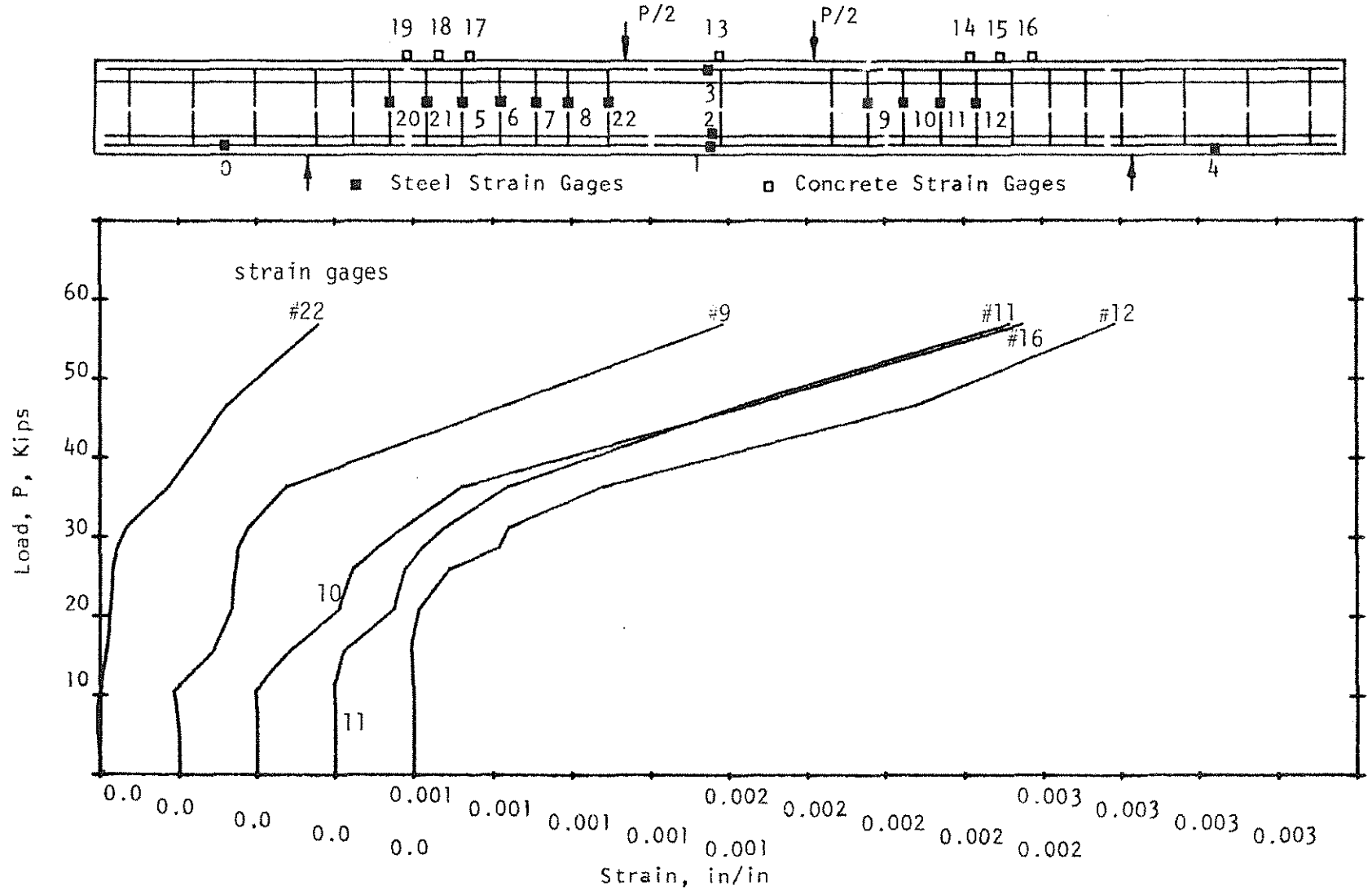

Figure 2.75 Load-Strain Curves, Beam C75 (ρ_w = 0.933%, $\rho_v f_{vy}$ = 103.0 psi).

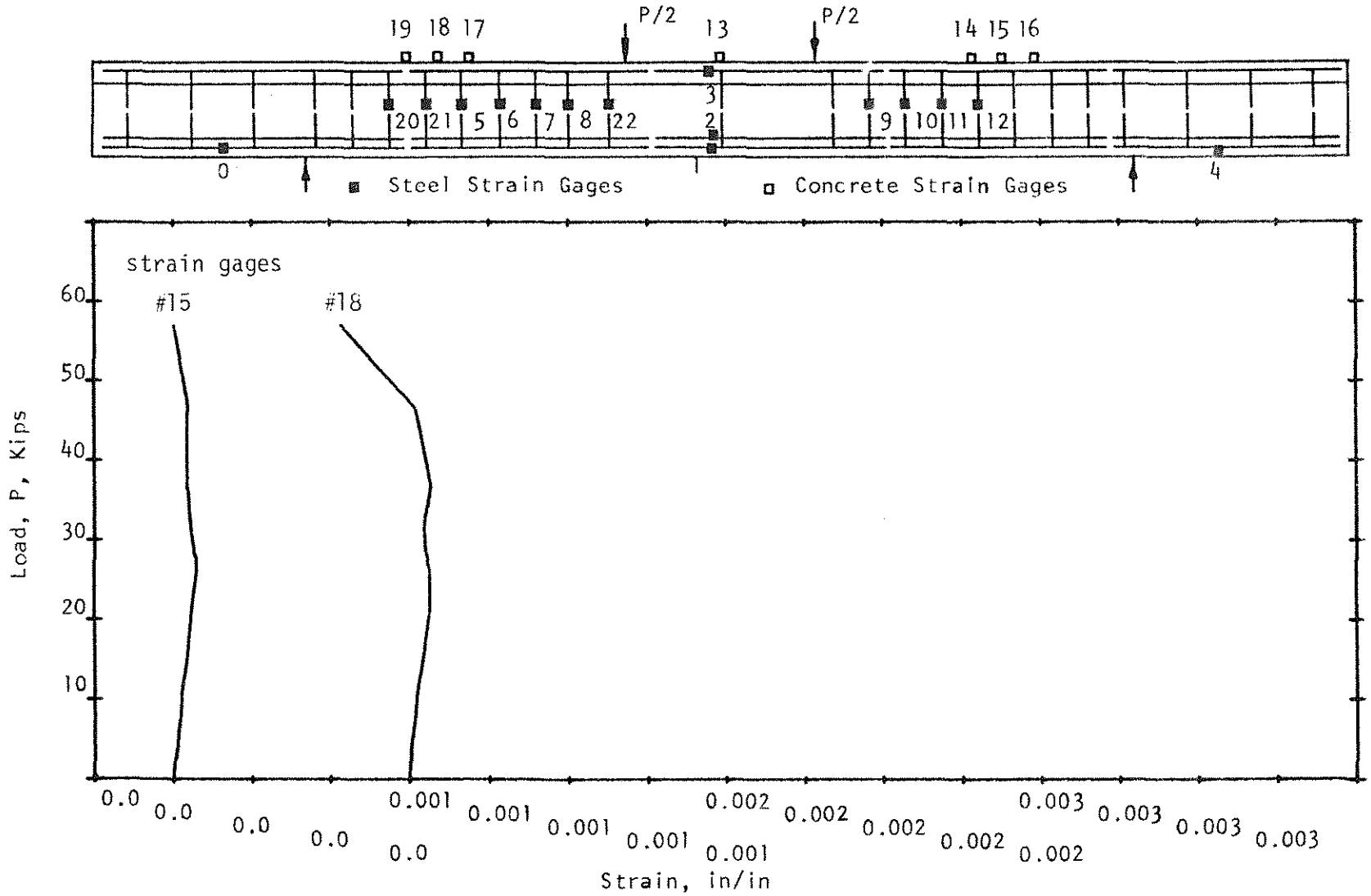

Figure 2.76 Load-Strain Curves, Beam C75 (ρ_w = 0.933%, $\rho_v f_{vy}$ = 103.0 psi).

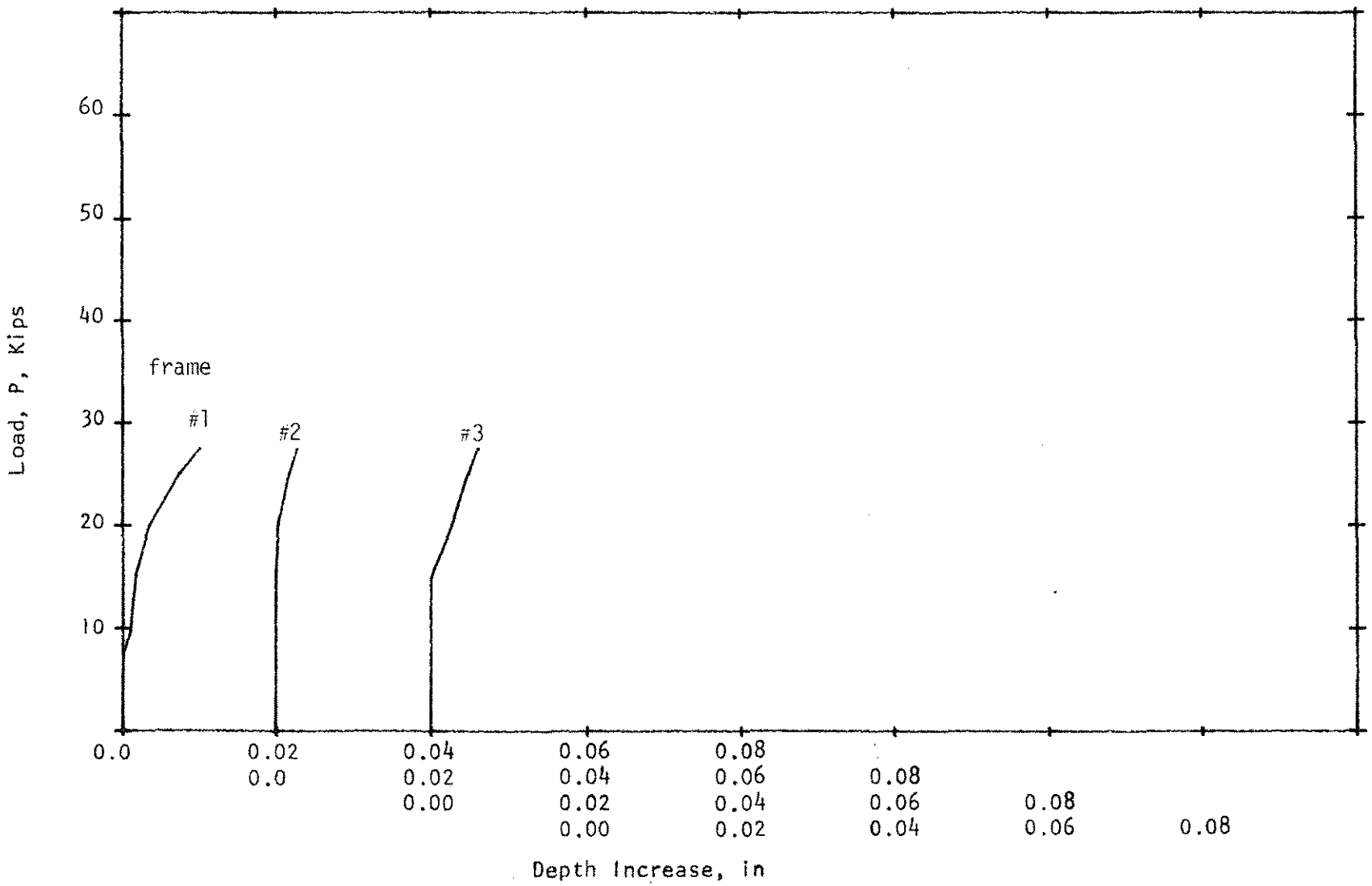

Figure 2.77 Load-Depth Increase Curves, Beam A00 (ρ_w = 0.656%, $\rho_v f_{vy}$ = 0.0 psi).

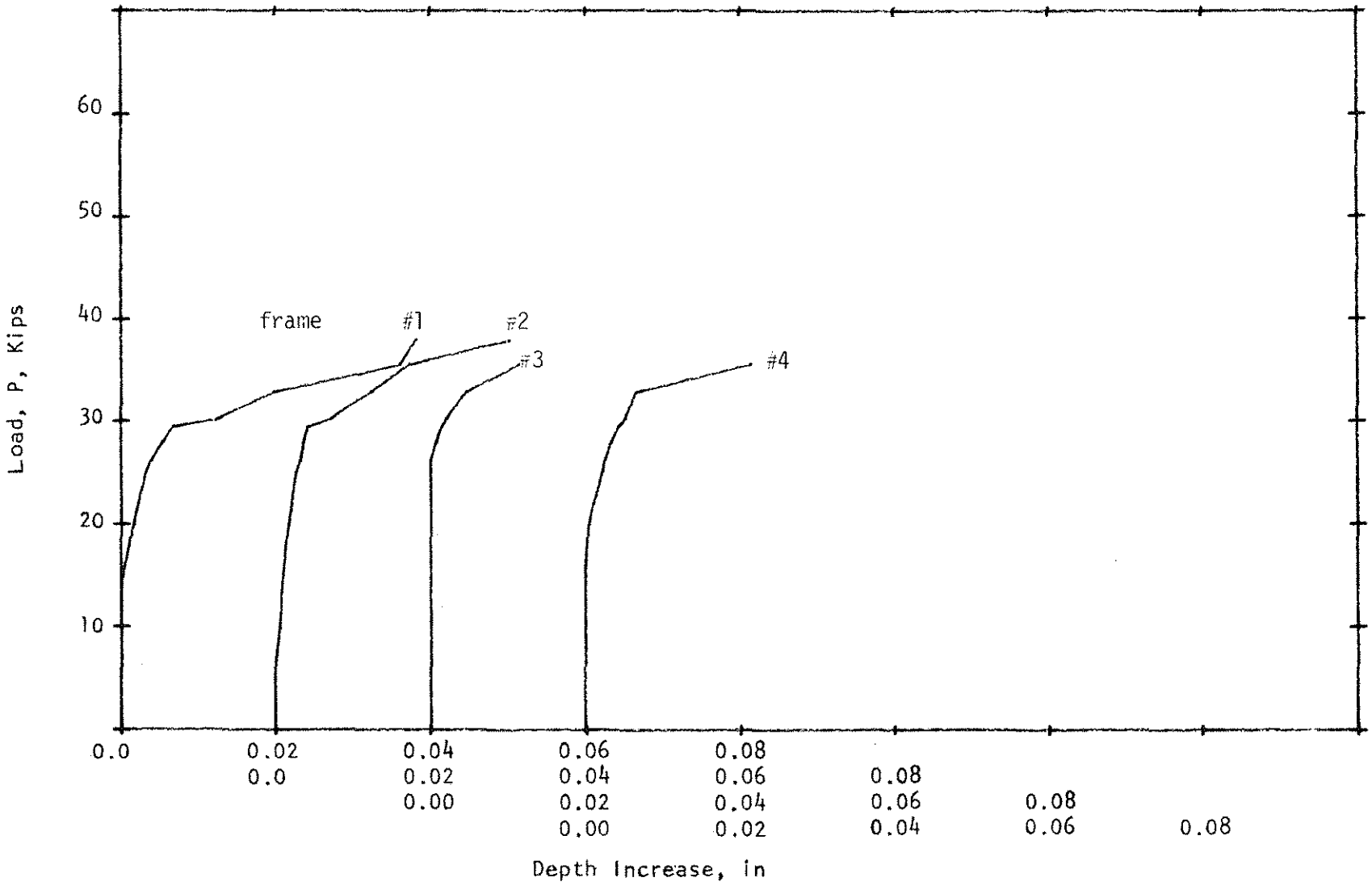

Figure 2.78 Load-Depth Increase Curves, Beam A25 (ρ_w = 0.663%, $\rho_v f_{vy}$ = 31.8 psi).

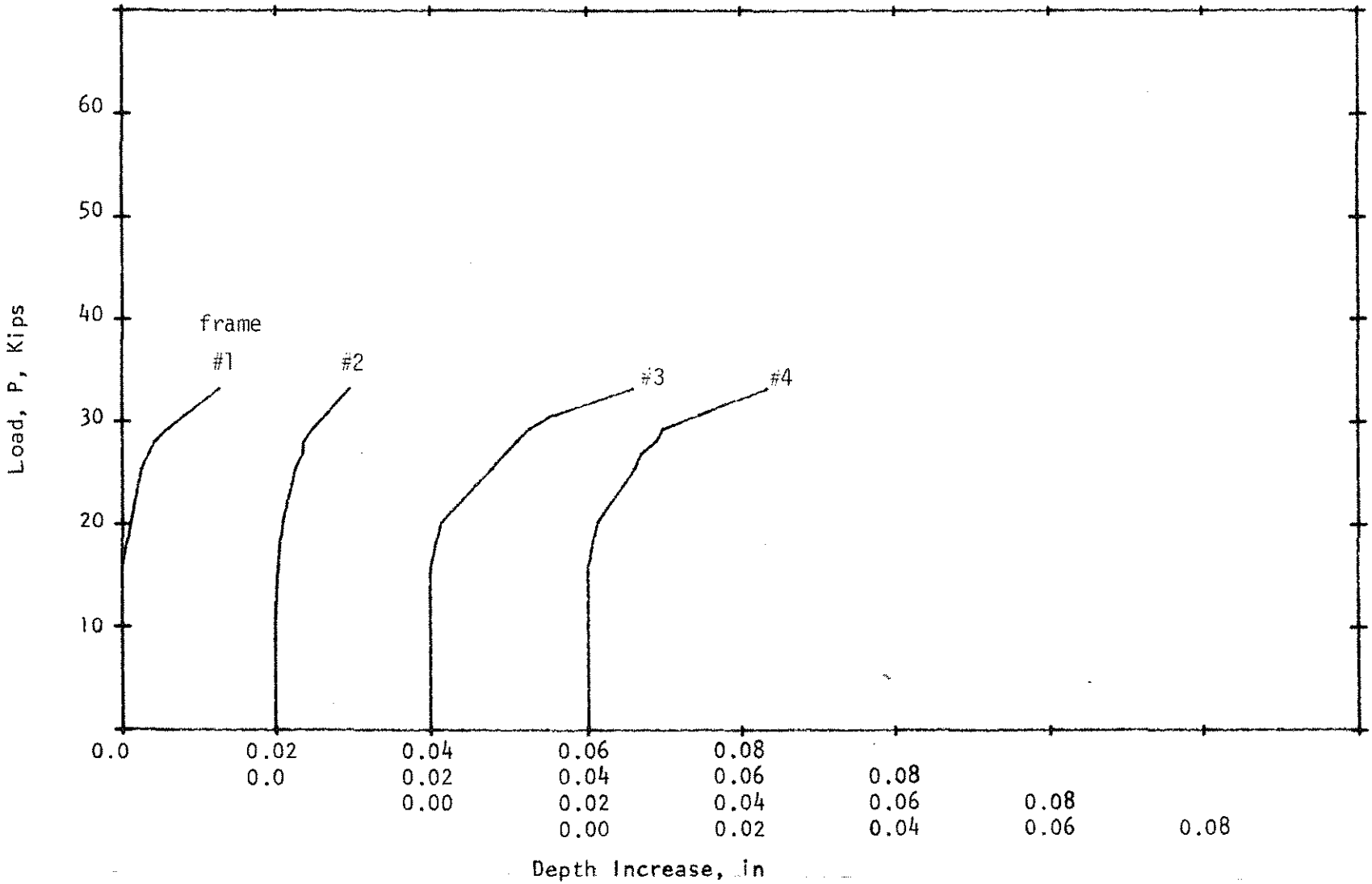

Figure 2.79 Load-Depth Increase Curves, Beam A25a (ρ_w = 0.668%, $\rho_v f_{vy}$ = 31.8 psi).

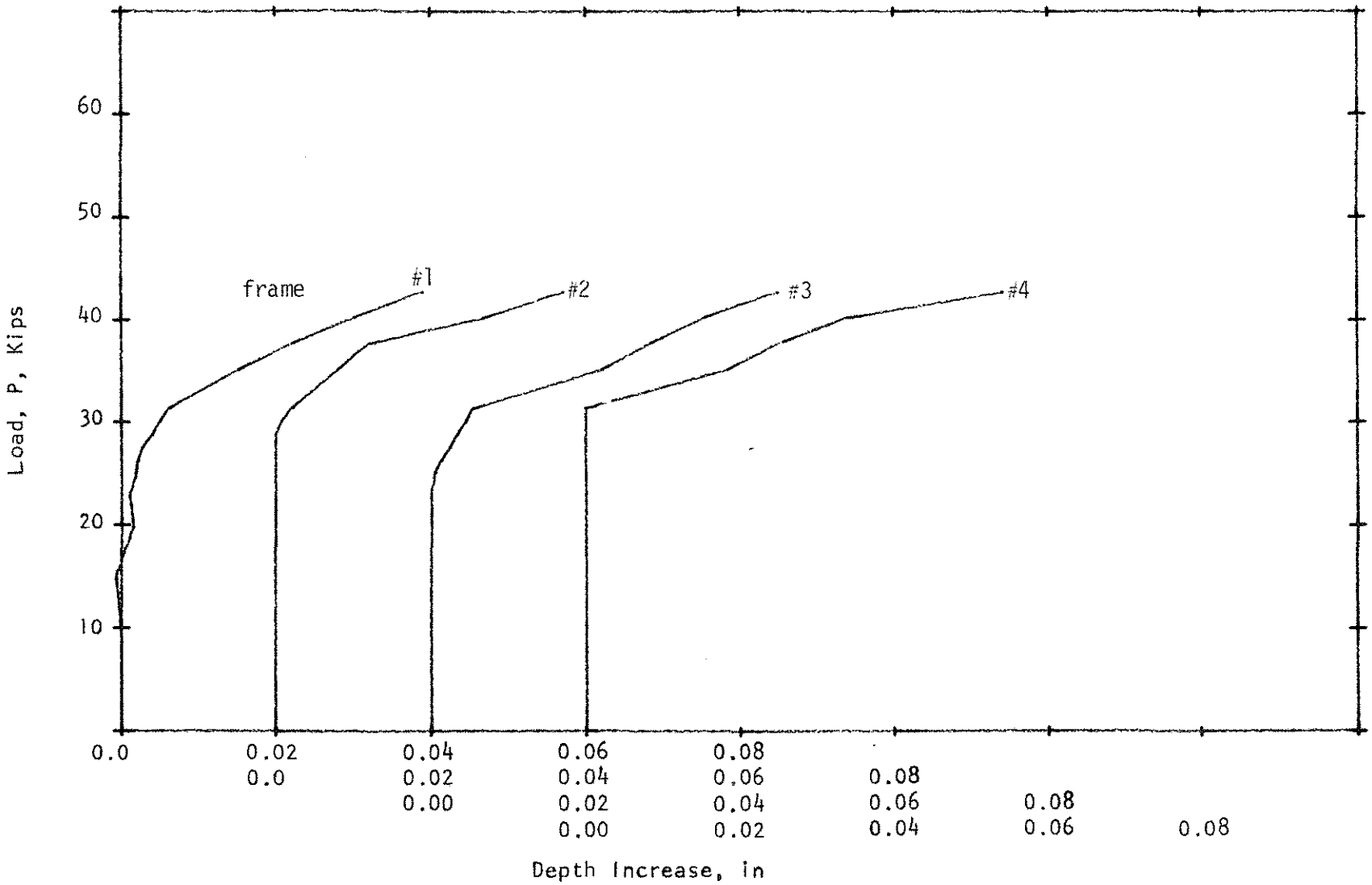

Figure 2.80 Load-Depth Increase Curves, Beam A50 (ρ_w = 0.661%, $\rho_v f_{vy}$ = 73.9 psi).

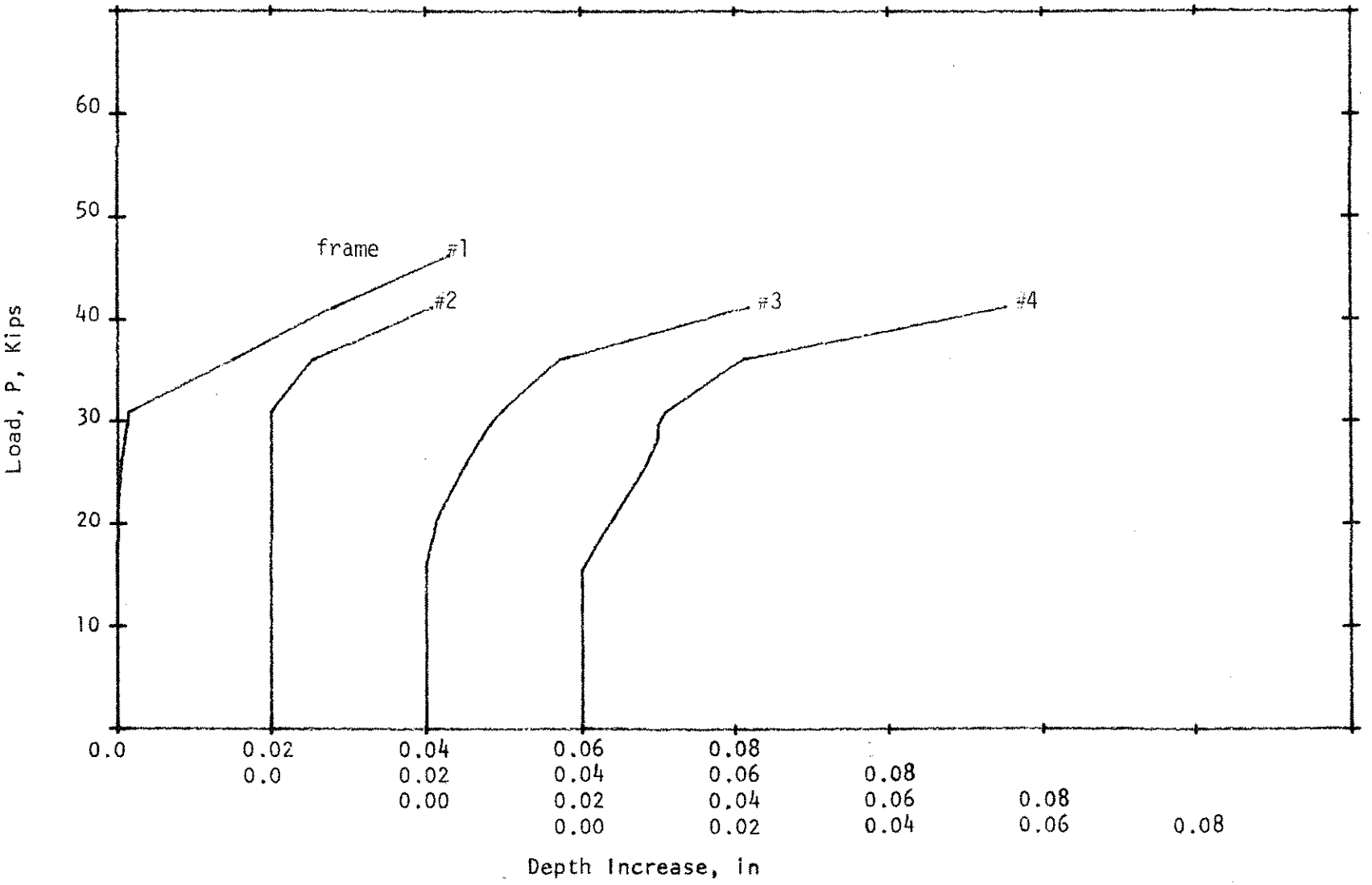

Figure 2.81 Load-Depth Increase Curves, Beam A50a (ρ_w = 0.658%, $\rho_v f_{vy}$ = 75.0 psi).

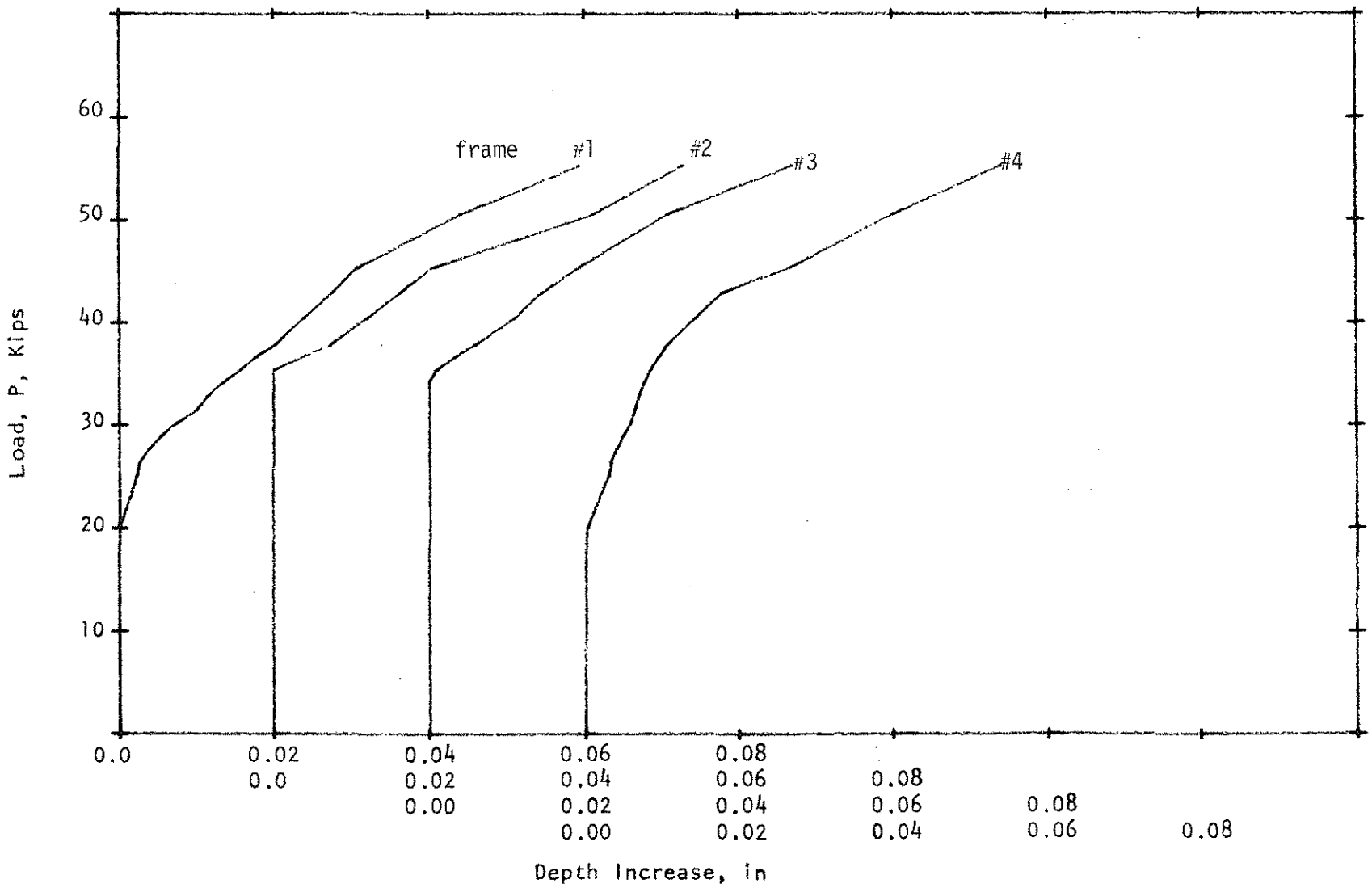

Figure 2.82 Load-Depth Increase Curves, Beam A75 (ρ_w = 0.655%, $\rho_v f_{vy}$ = 97.1 psi).

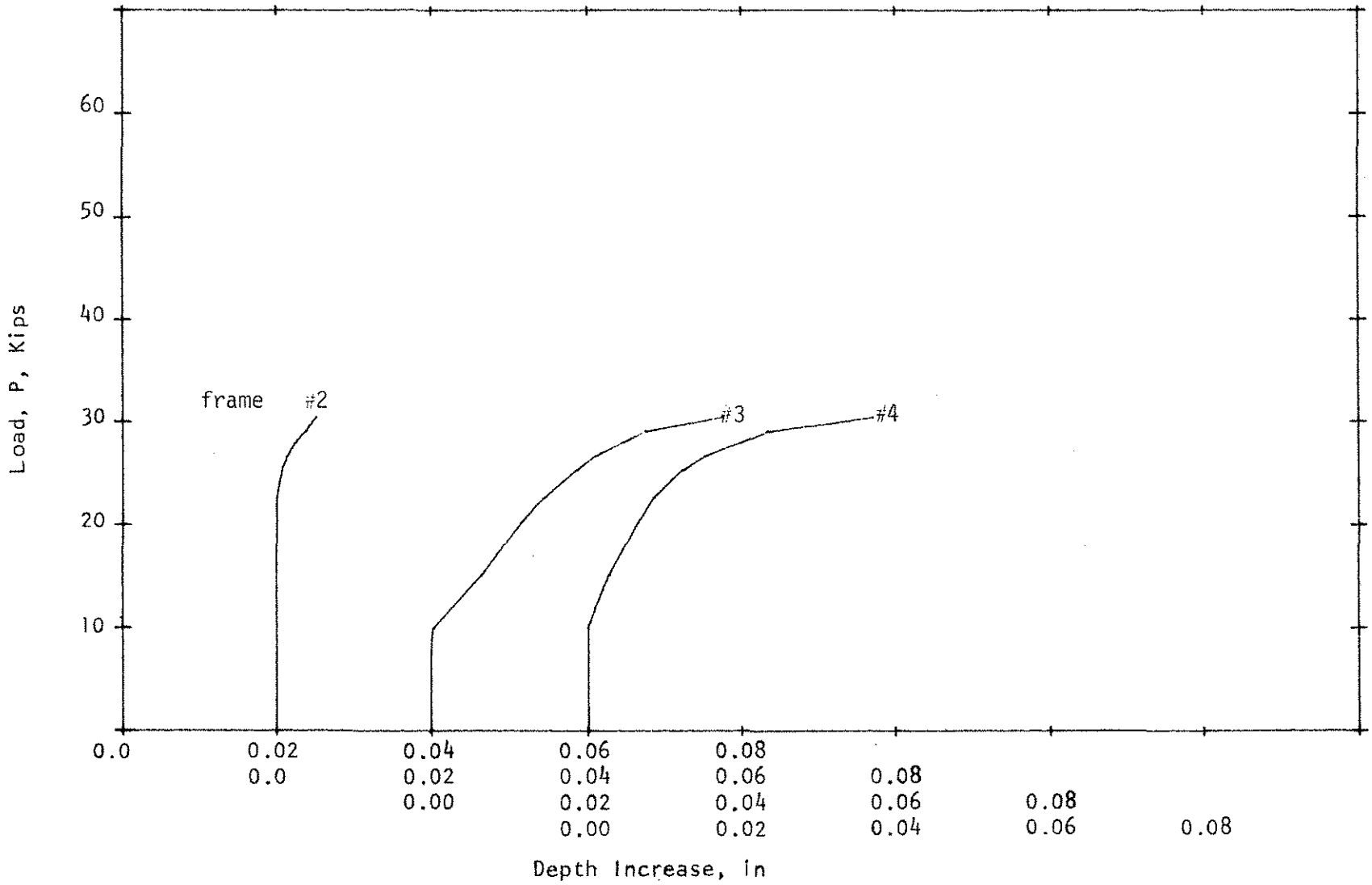

Figure 2.83 Load-Depth Increase Curves, Beam B00 (ρ_w = 0.488%, $\rho_v f_{vy}$ = 0.0 psi).

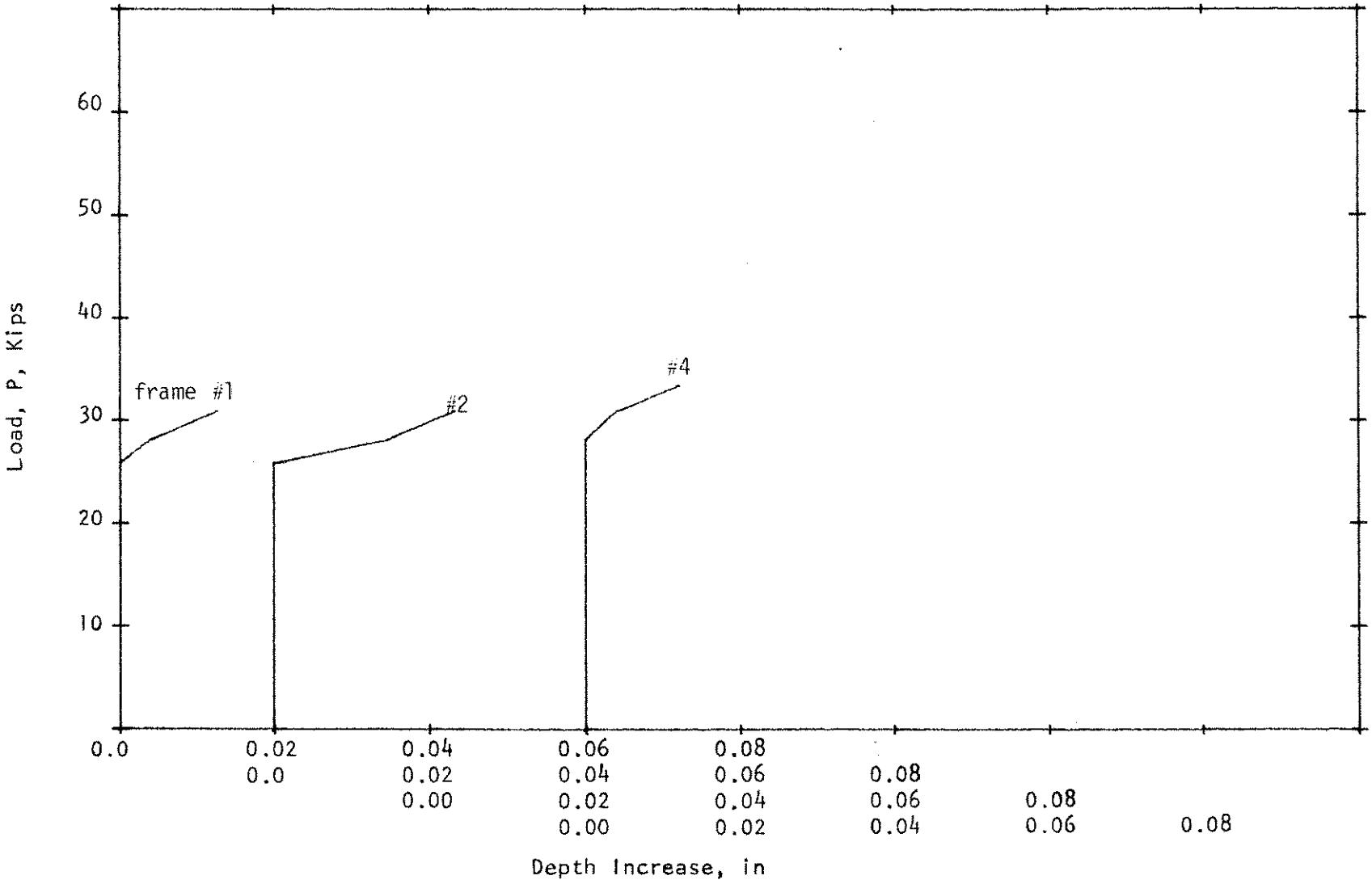

Figure 2.84 Load-Depth Increase Curves, Beam B25 (ρ_w = 0.494%, $\rho_v f_{vy}$ = 32.4 psi).

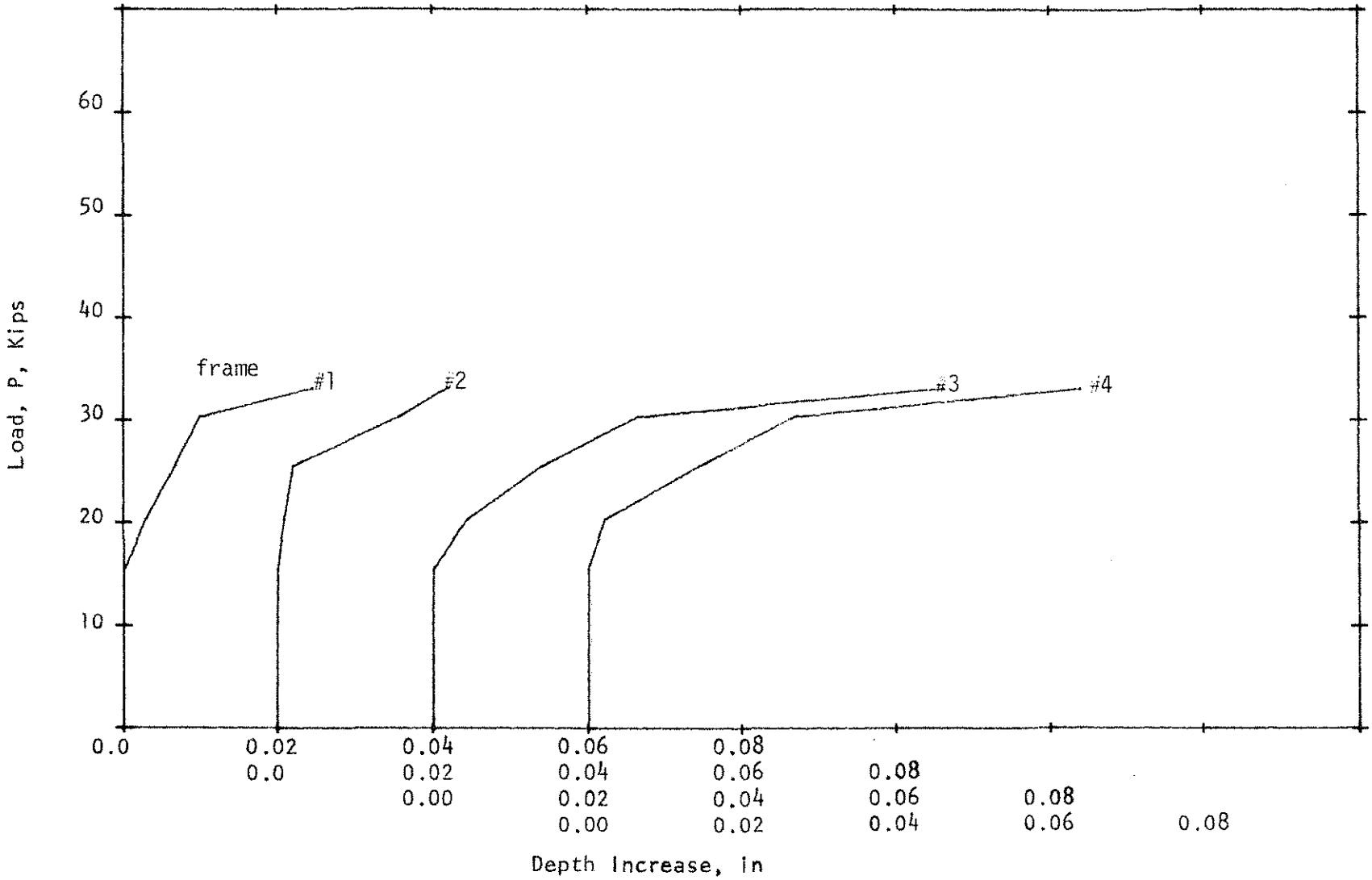

Figure 2.85 Load-Depth Increase Curves, Beam C25 (ρ_w = 0.948%, $\rho_v f_{vy}$ = 32.4 psi).

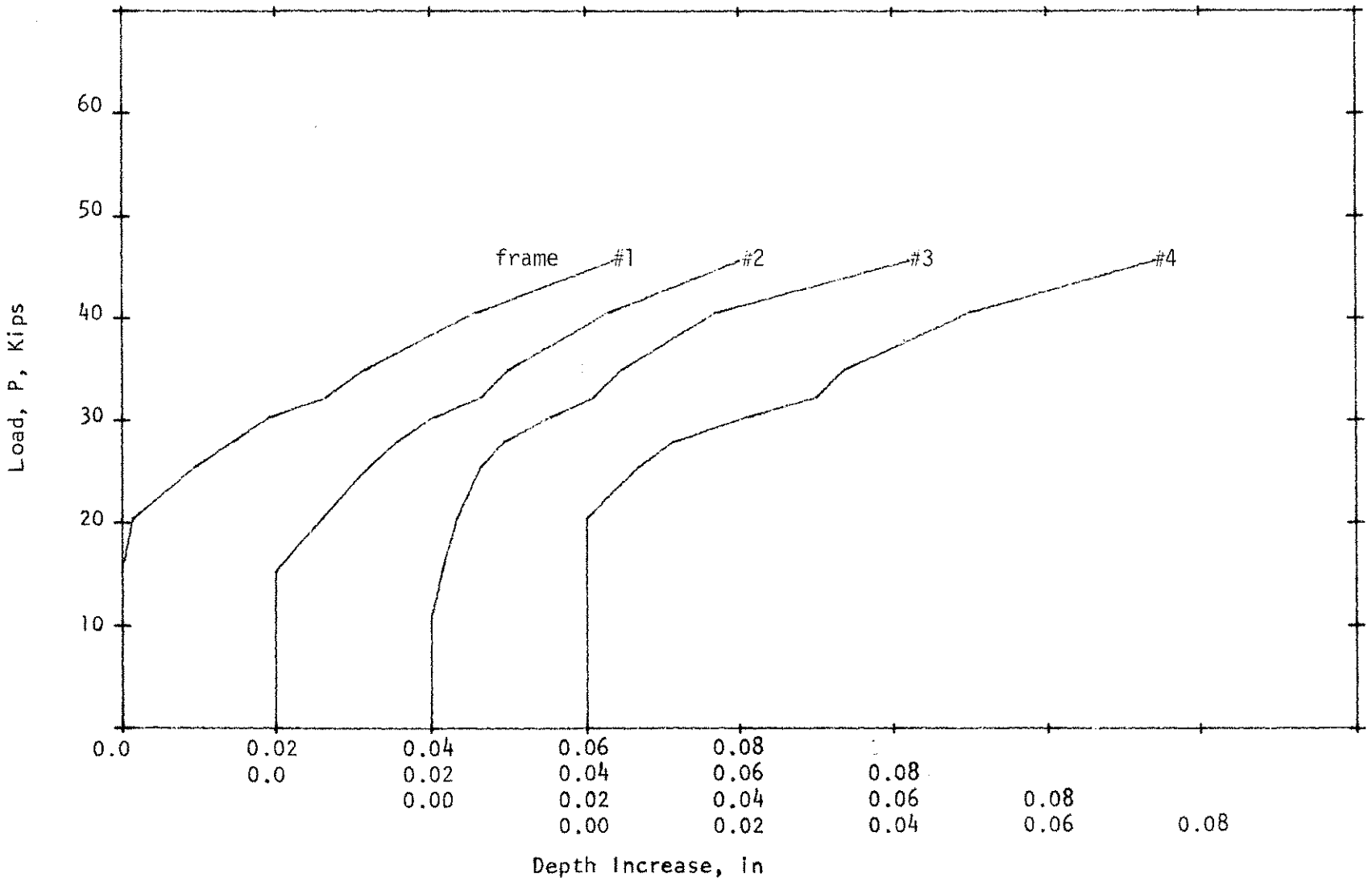

Figure 2.86 Load-Depth Increase Curves, Beam C50 (ρ_w = 0.939%, $\rho_v f_{vy}$ = 76.2 psi).

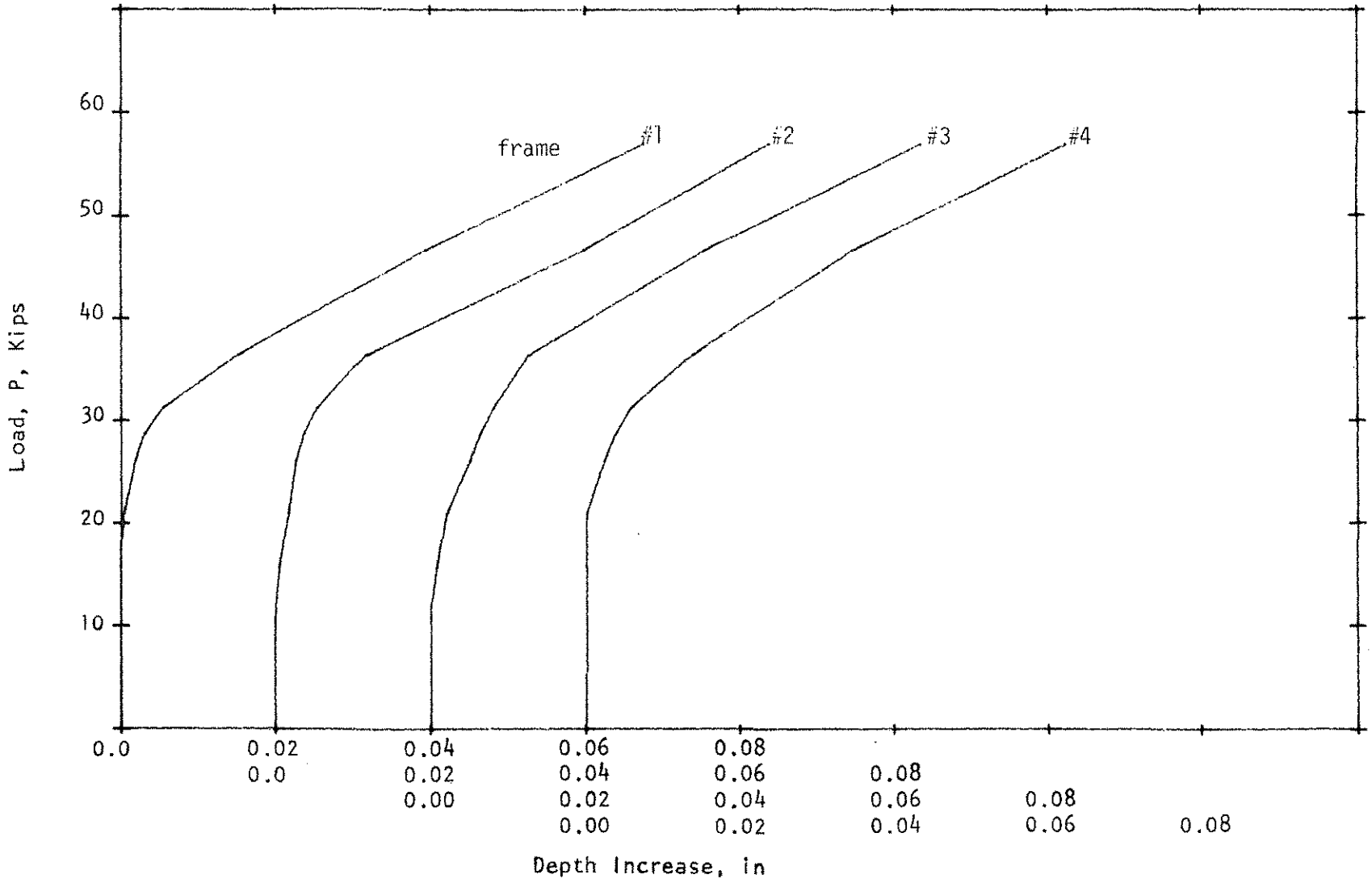

Figure 2.87 Load-Depth Increase Curves, Beam C75 (ρ_w = 0.933%, $\rho_v f_{vy}$ = 103.0 psi).

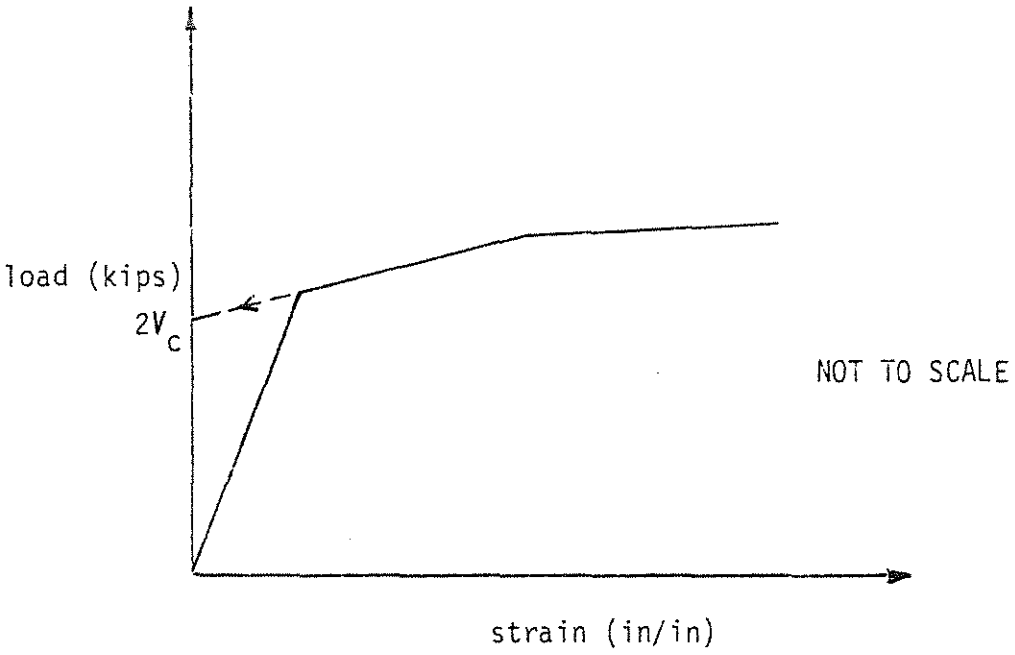

Figure 3.1. Method of Determining Shear Cracking Load from Stirrup Strain and Depth Increase Data (6).

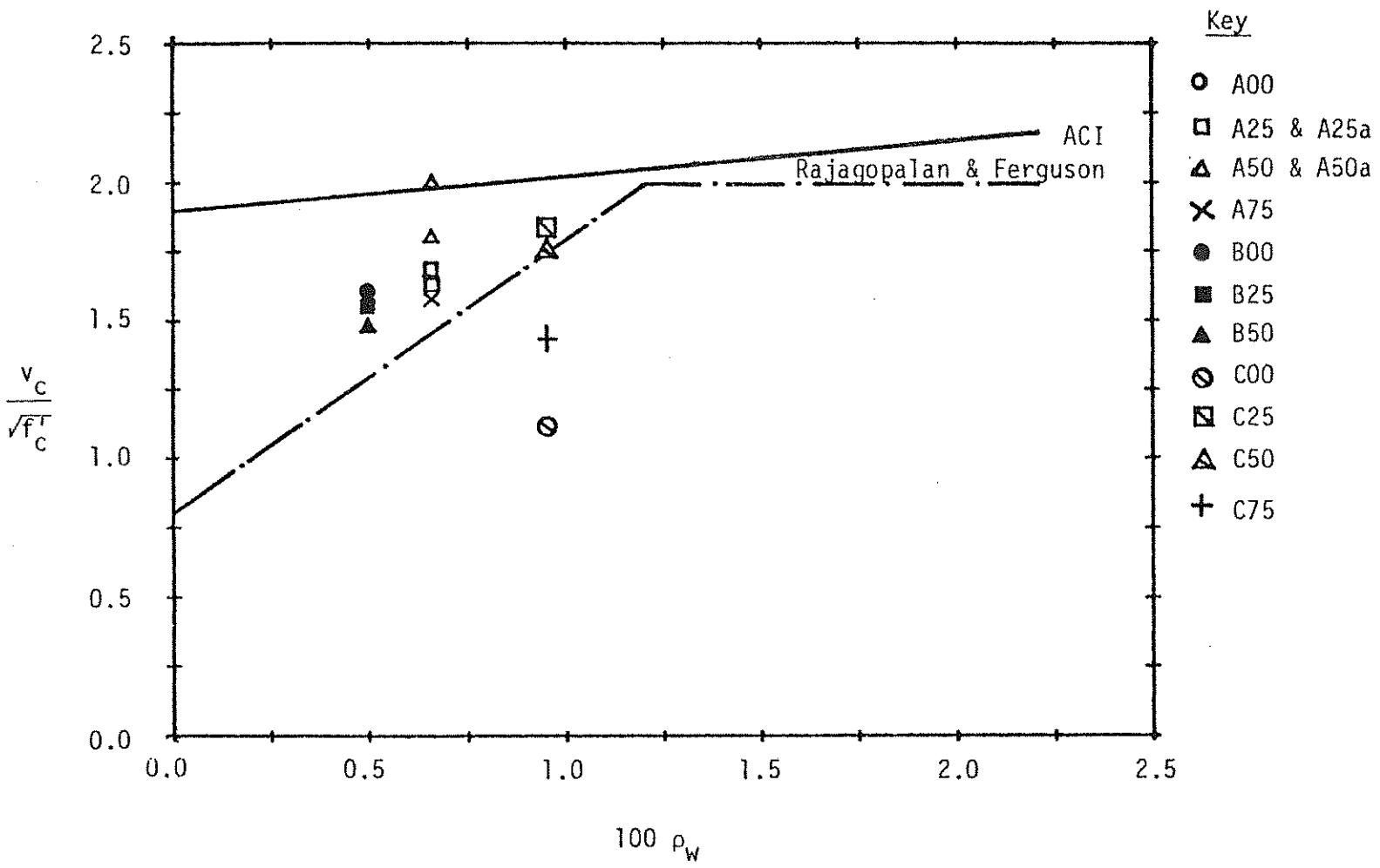

Figure 3.2(a). Stress at Diagonal Tension Cracking, v_c, from Crack Pattern (6).

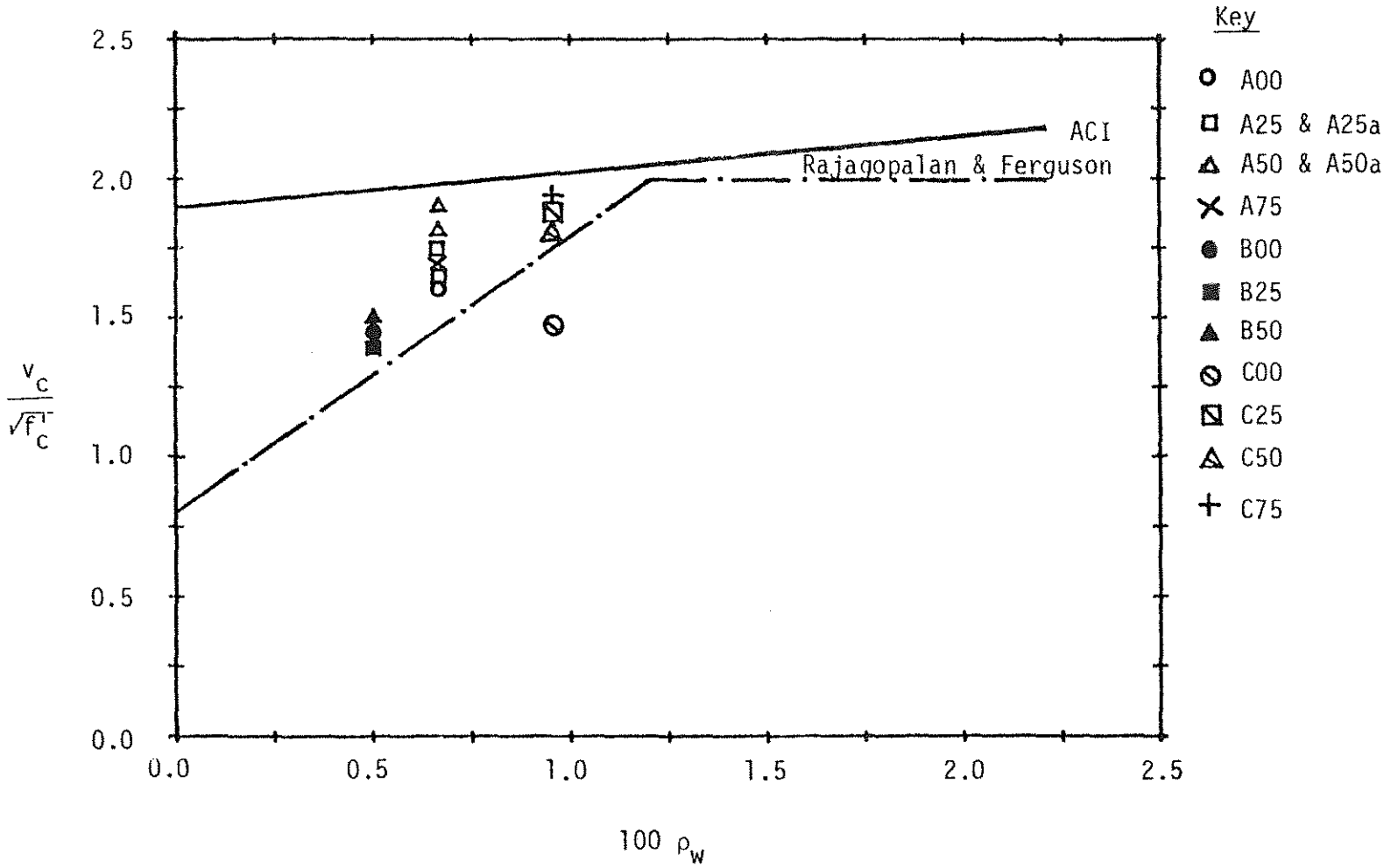

Figure 3.2(b). Stress at Diagonal Tension Cracking, v_c, from Concrete Strain (6).

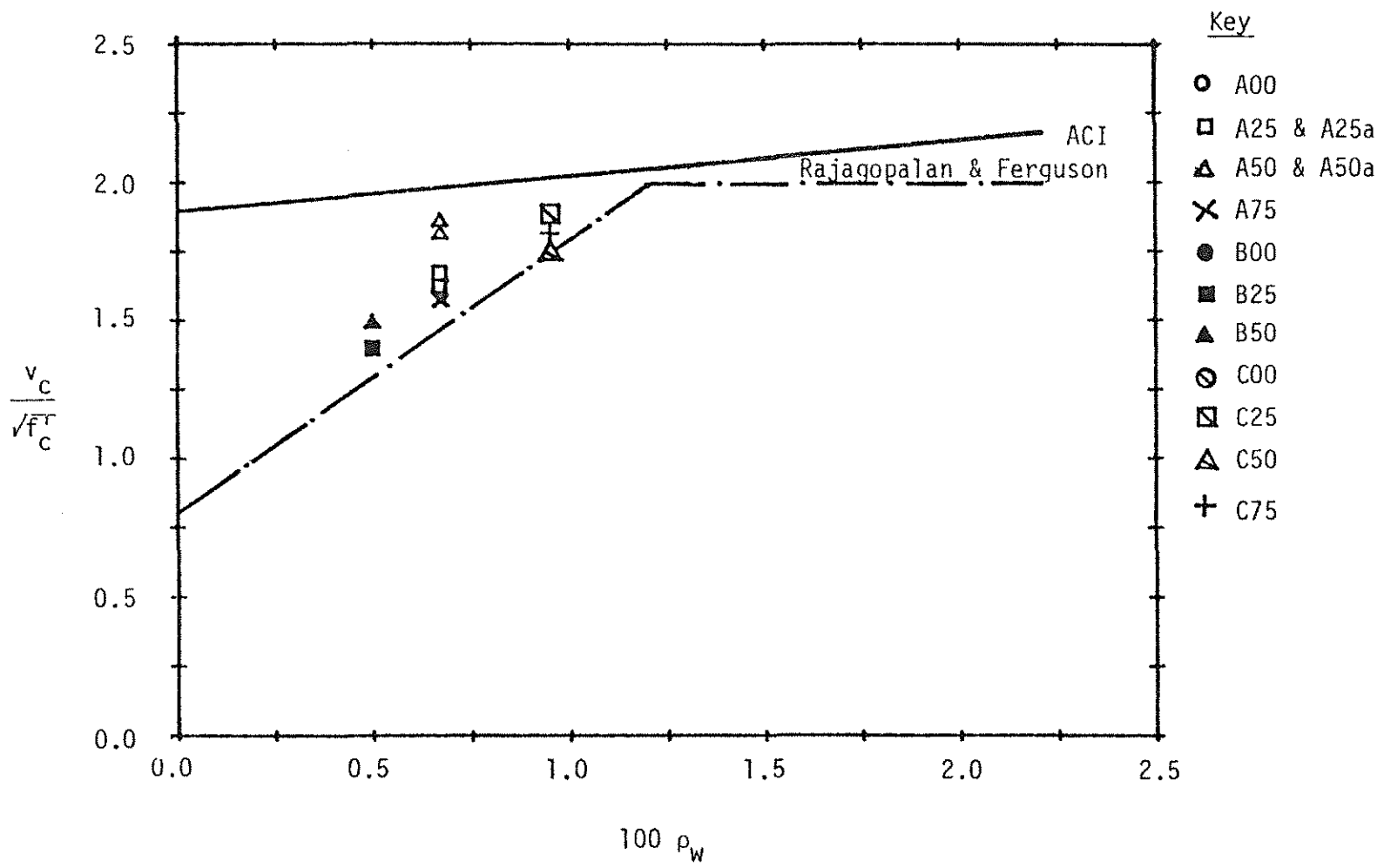

Figure 3.2(c). Stress at Diagonal Tension Cracking, v_c, from Stirrup Strain (6).

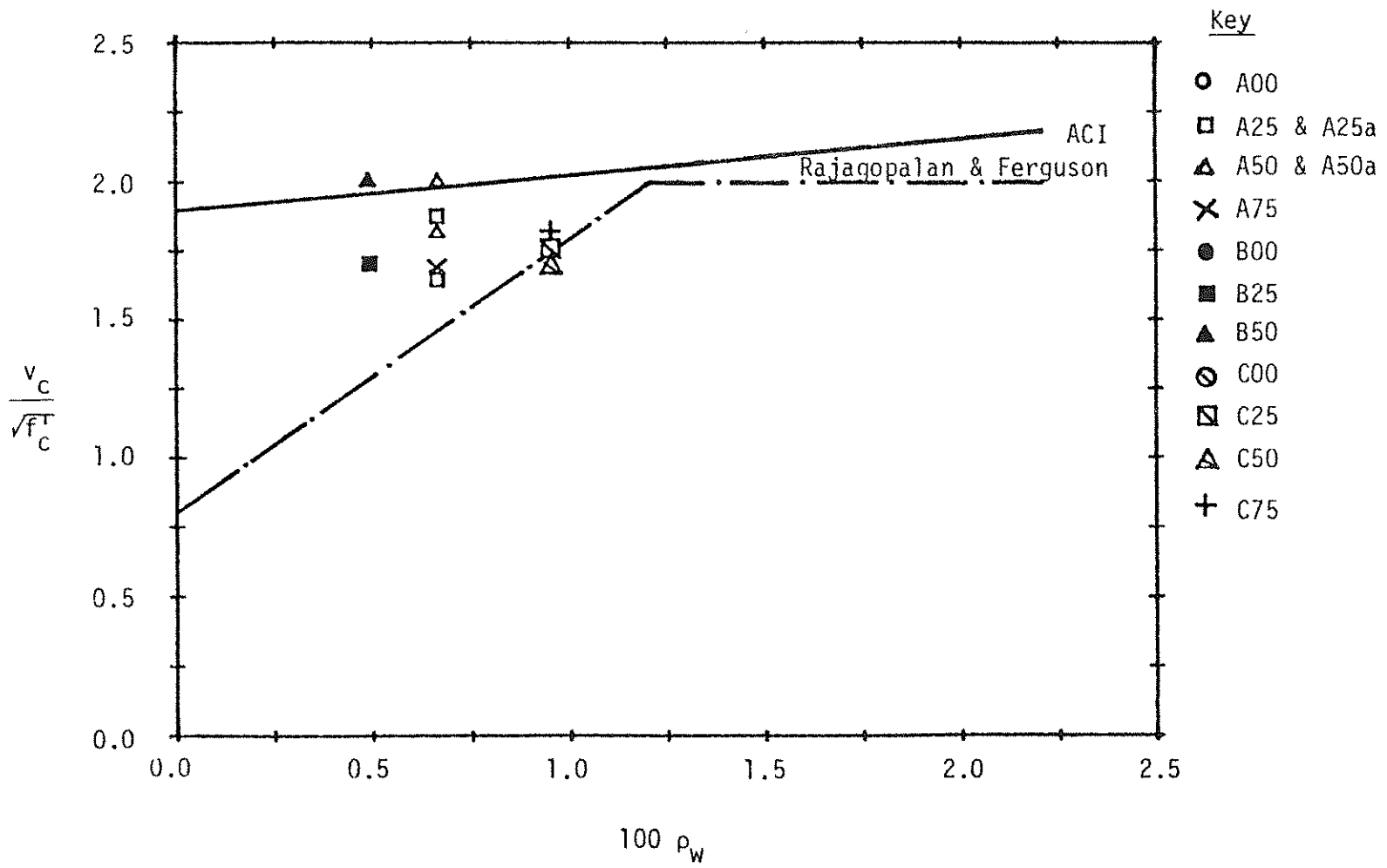

Figure 3.2(d). Stress at Diagonal Tension Cracking, v_c, from Depth Increase (6).

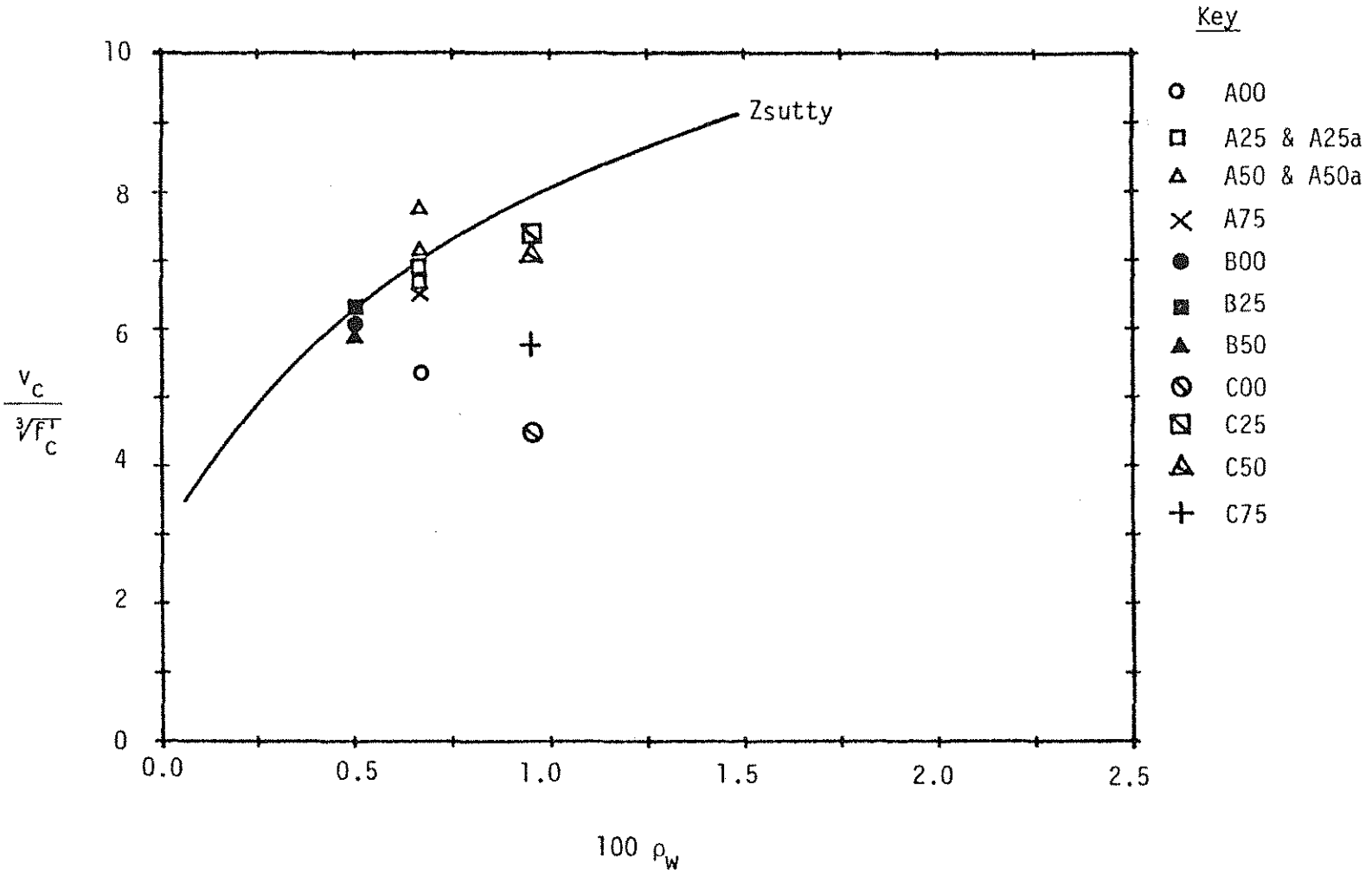

Figure 3.3(a). Stress at Diagonal Tension Cracking, v_c, from Crack Pattern (6).

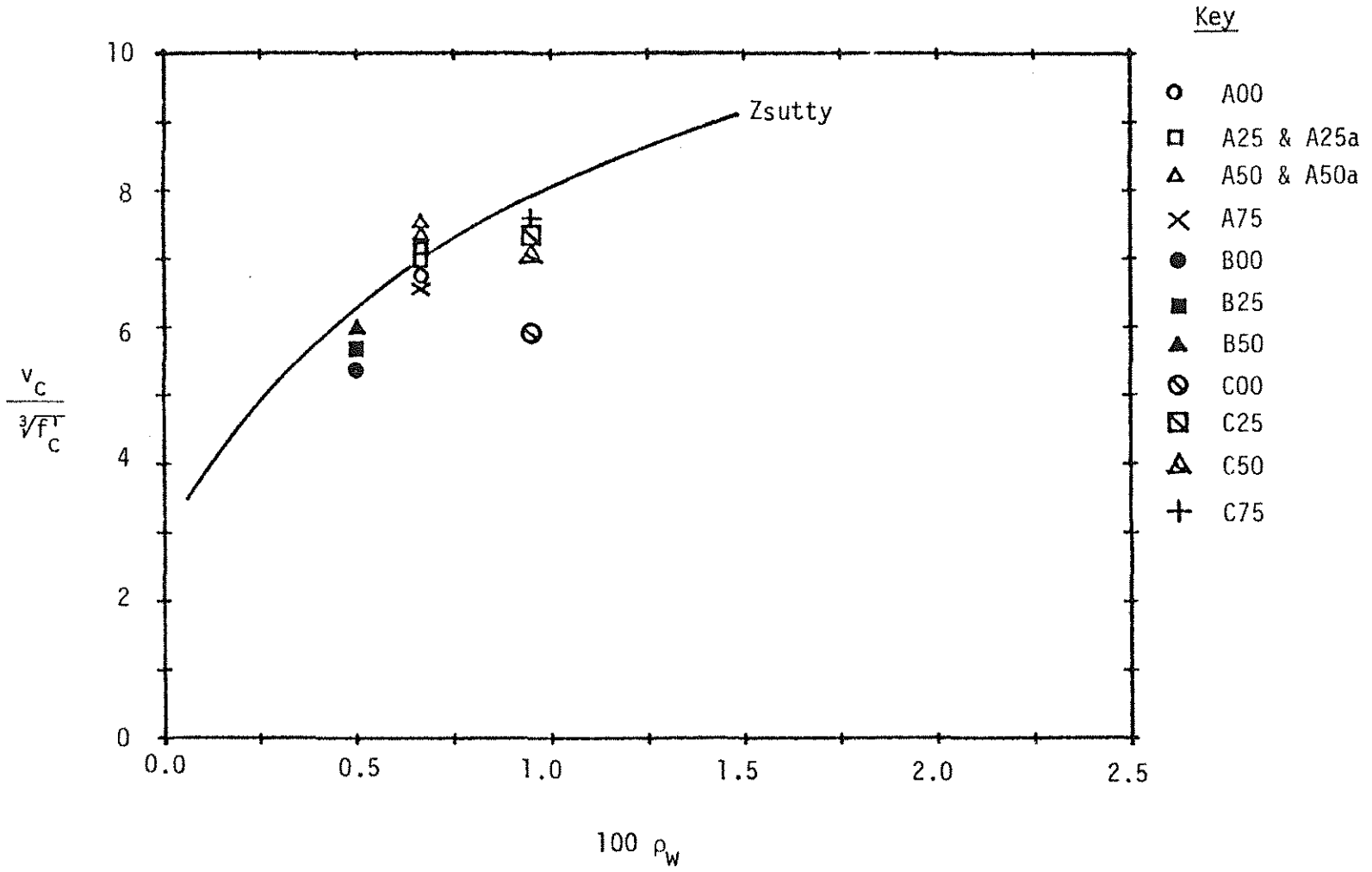

Figure 3.3(b). Stress at Diagonal Tension Cracking, v_c, from Concrete Strain (6).

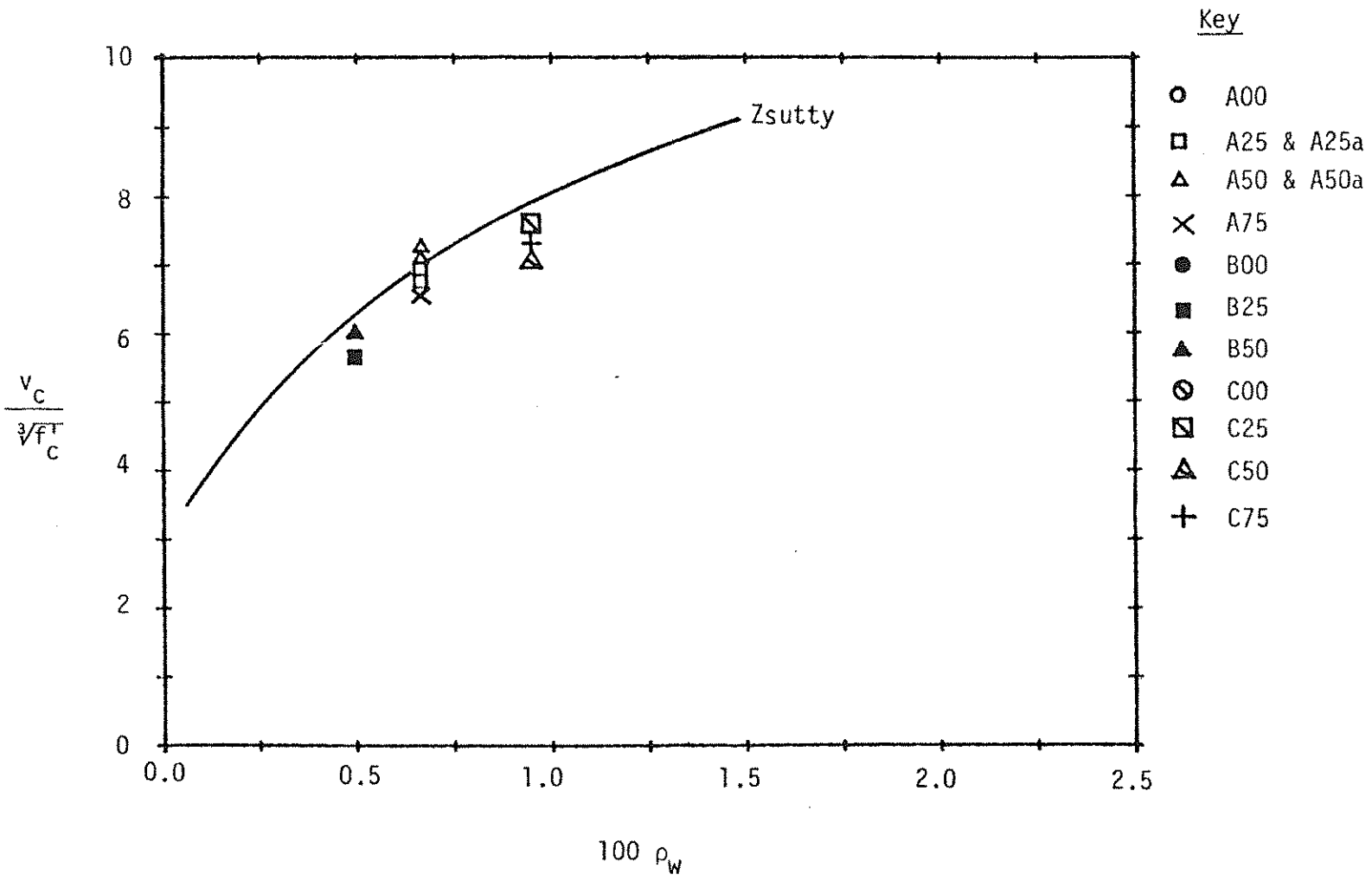

Figure 3.3(c). Stress at Diagonal Tension Cracking, v_c, from Stirrup Strain (6).

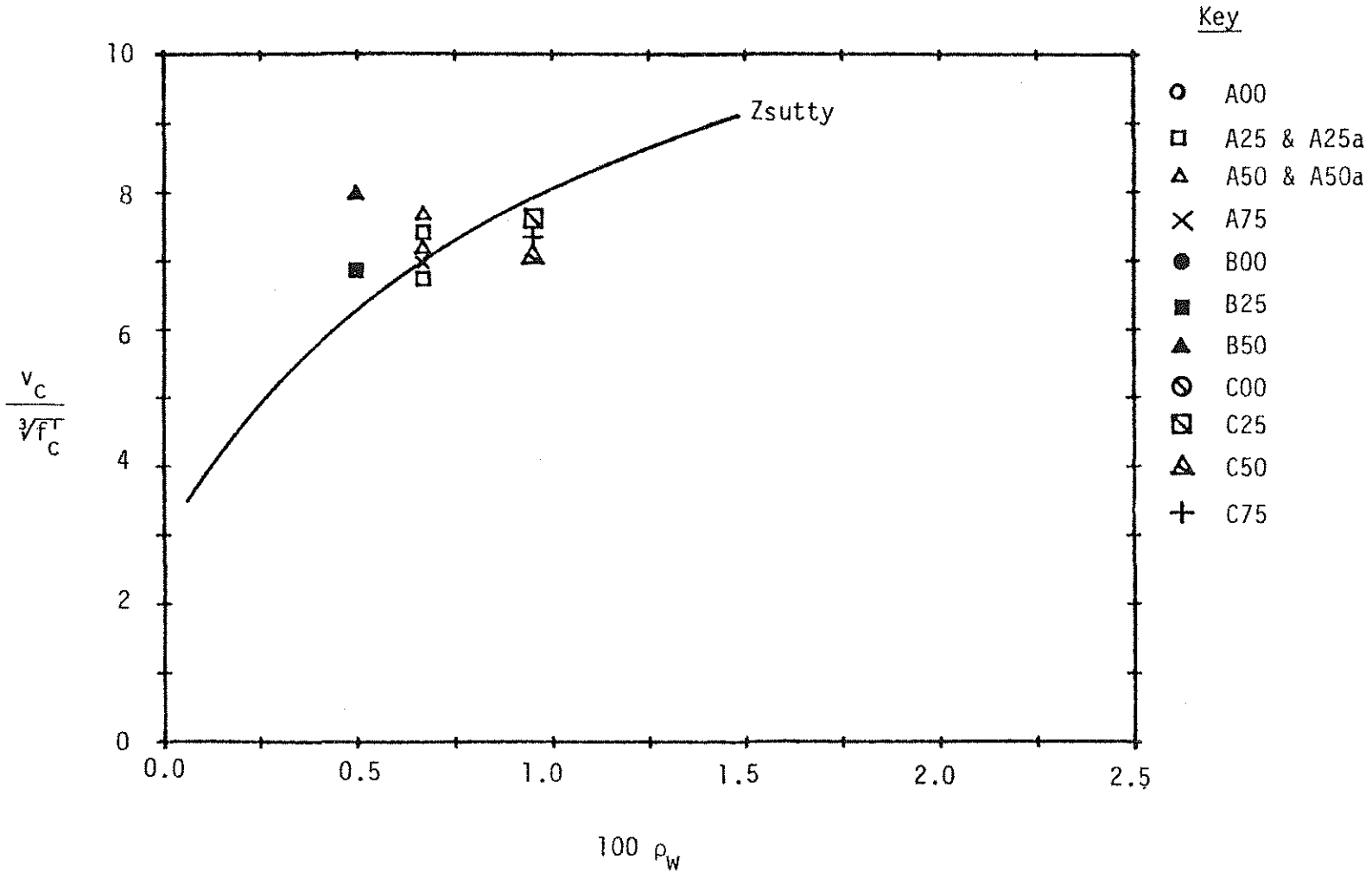

Figure 3.3(d). Stress at Diagonal Tension Cracking, v_c, from Depth Increase (6).

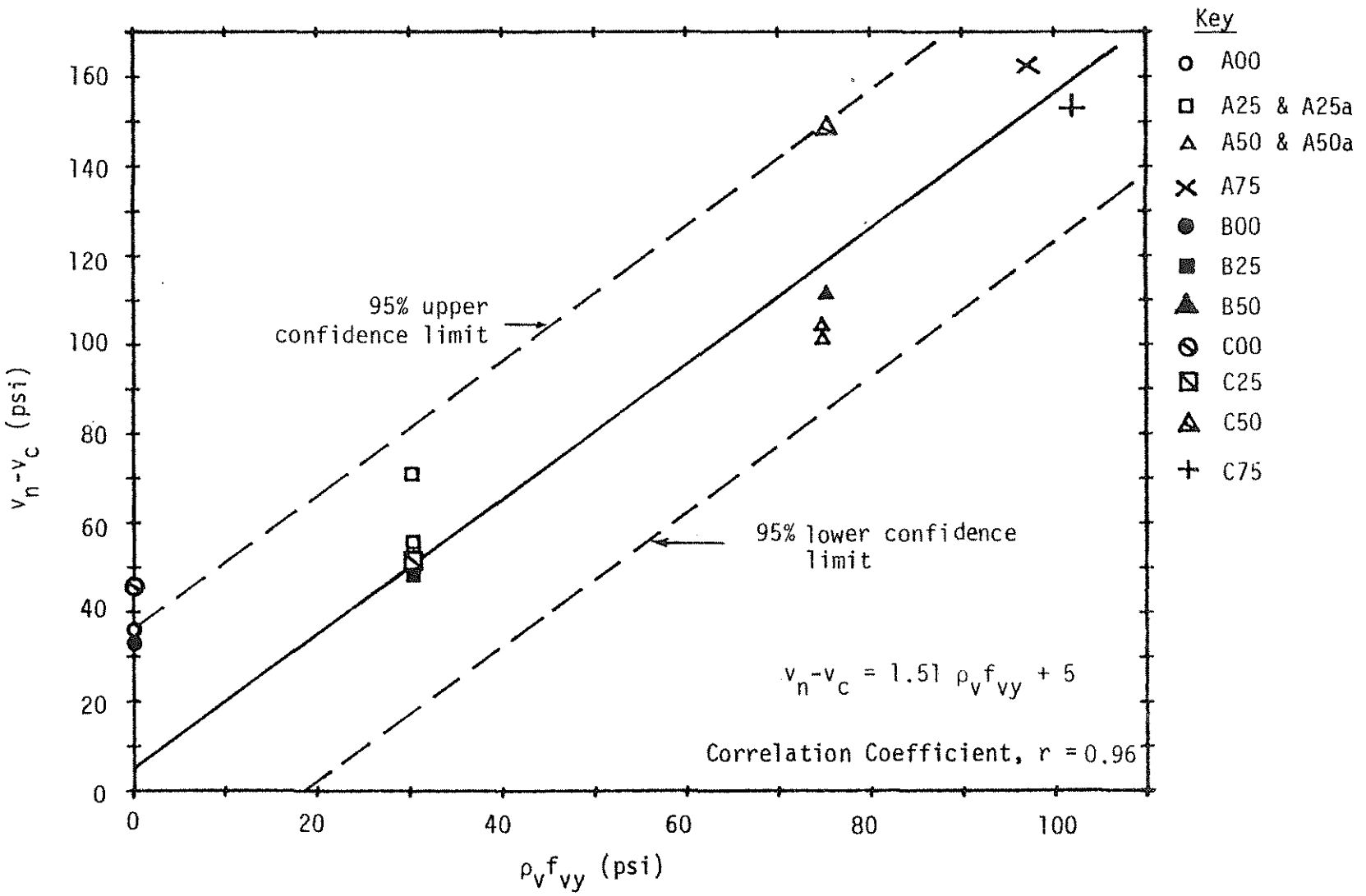

Figure 3.4(a). Effectiveness of Web Reinforcement, $v_n - v_c$, from Crack Patterns (6).

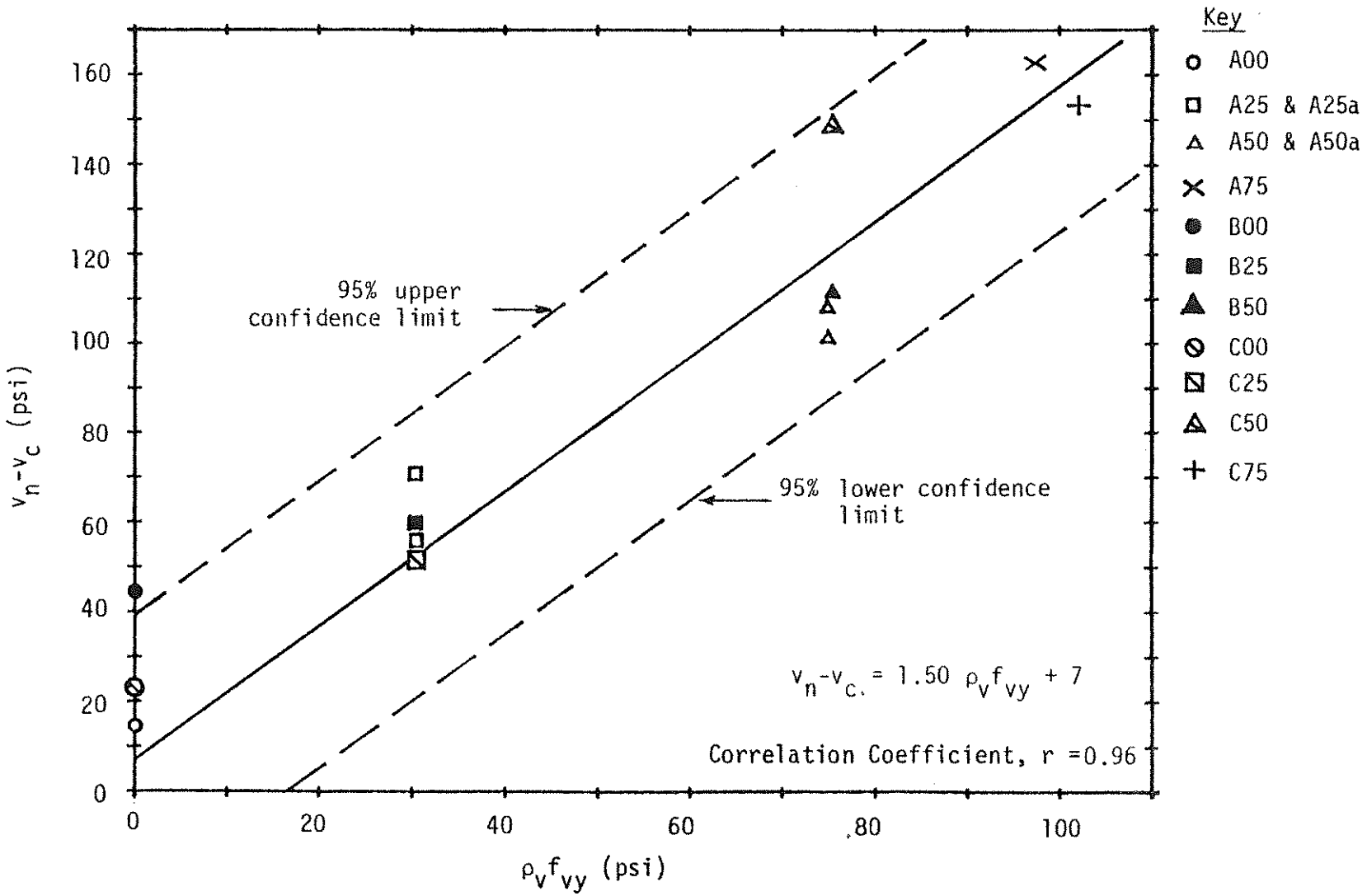

Figure 3.4(b). Effectiveness of Web Reinforcement, $v_n - v_c$, from Concrete Strain [6].

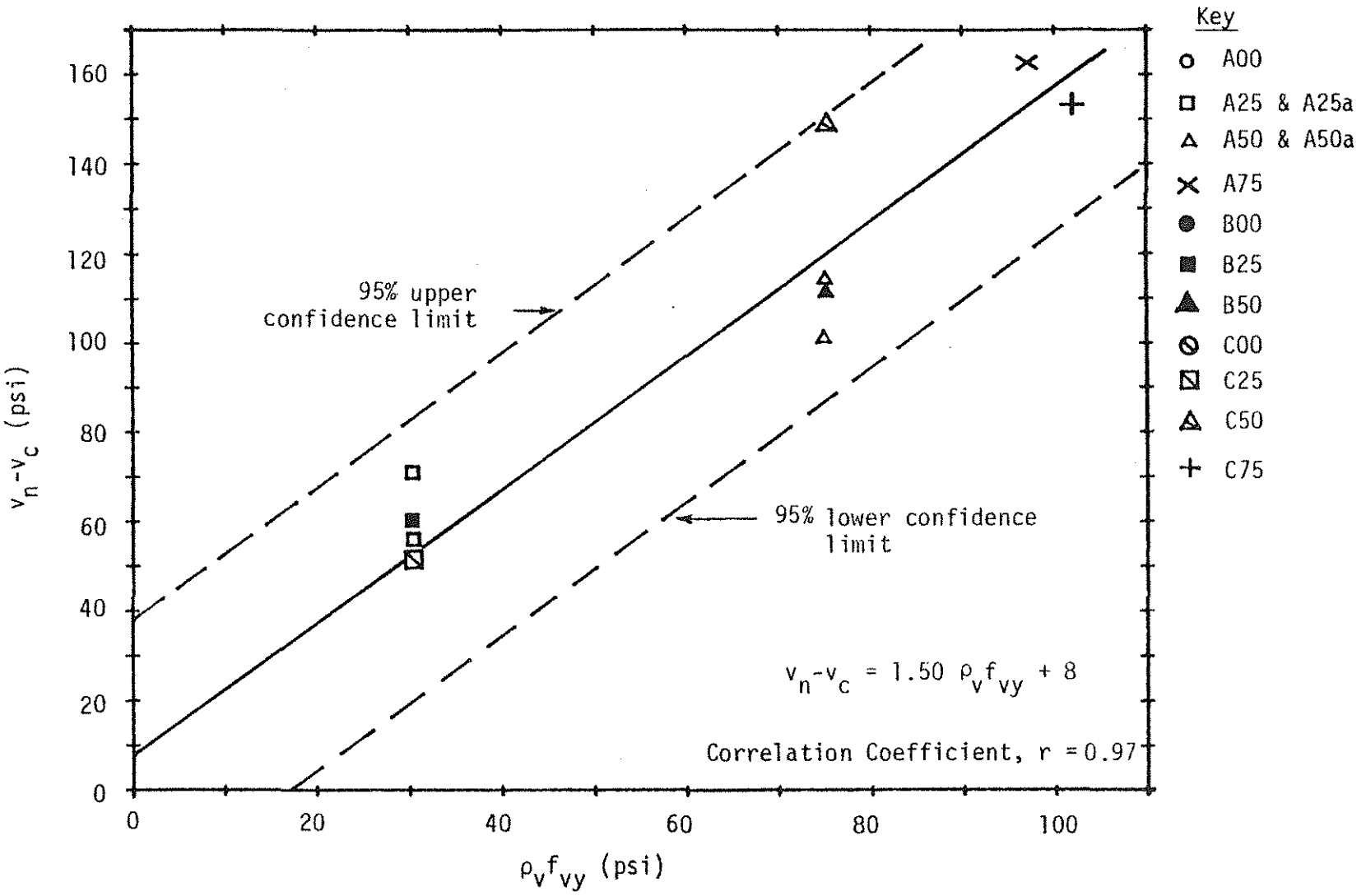

Figure 3.4(c) Effectiveness of Web Reinforcement, $v_n - v_c$, from Stirrup Strain (6).

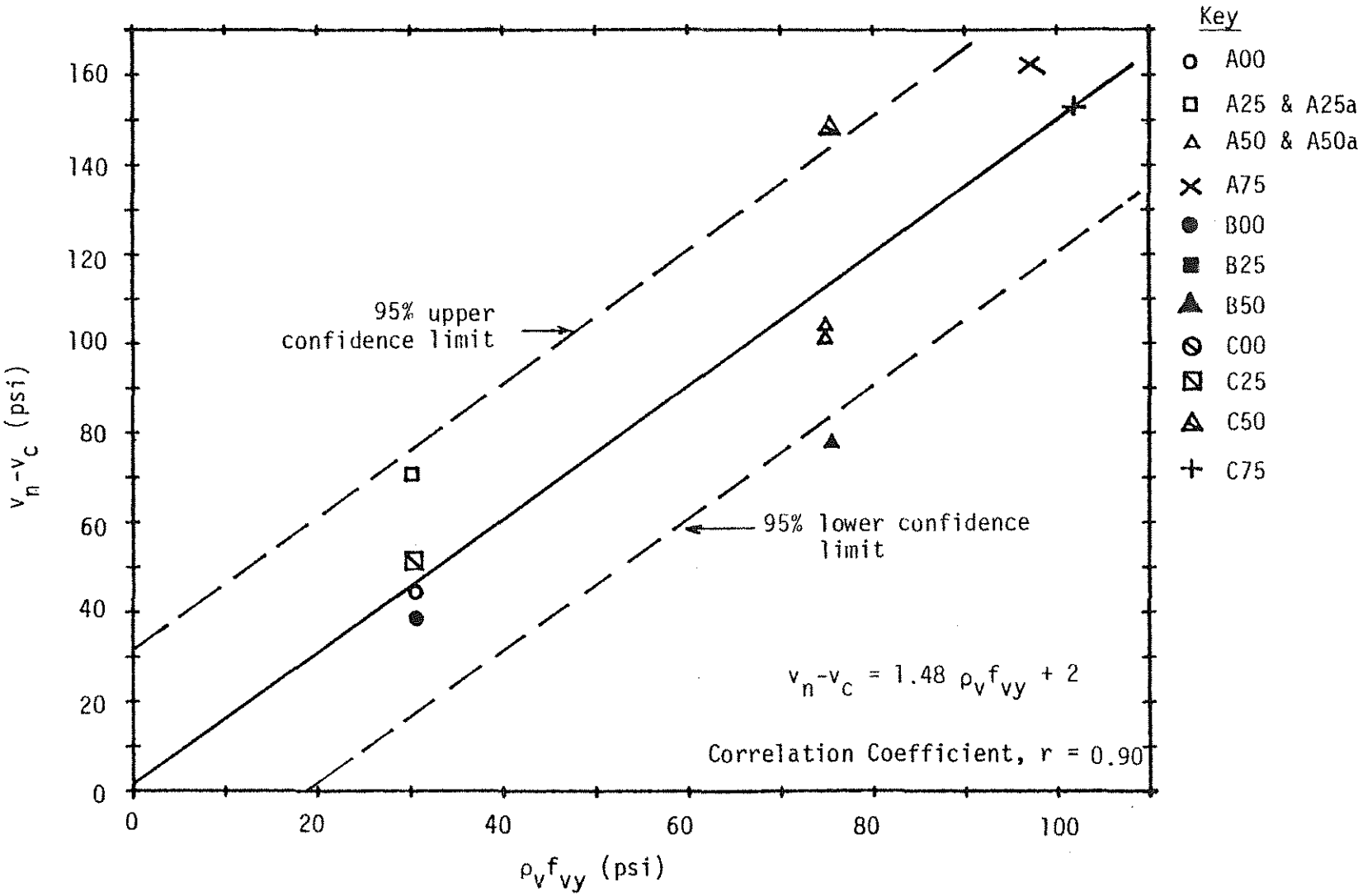

Figure 3.4(d) Effectiveness of Web Reinforcement, $v_n - v_c$, from Depth Increase (6).

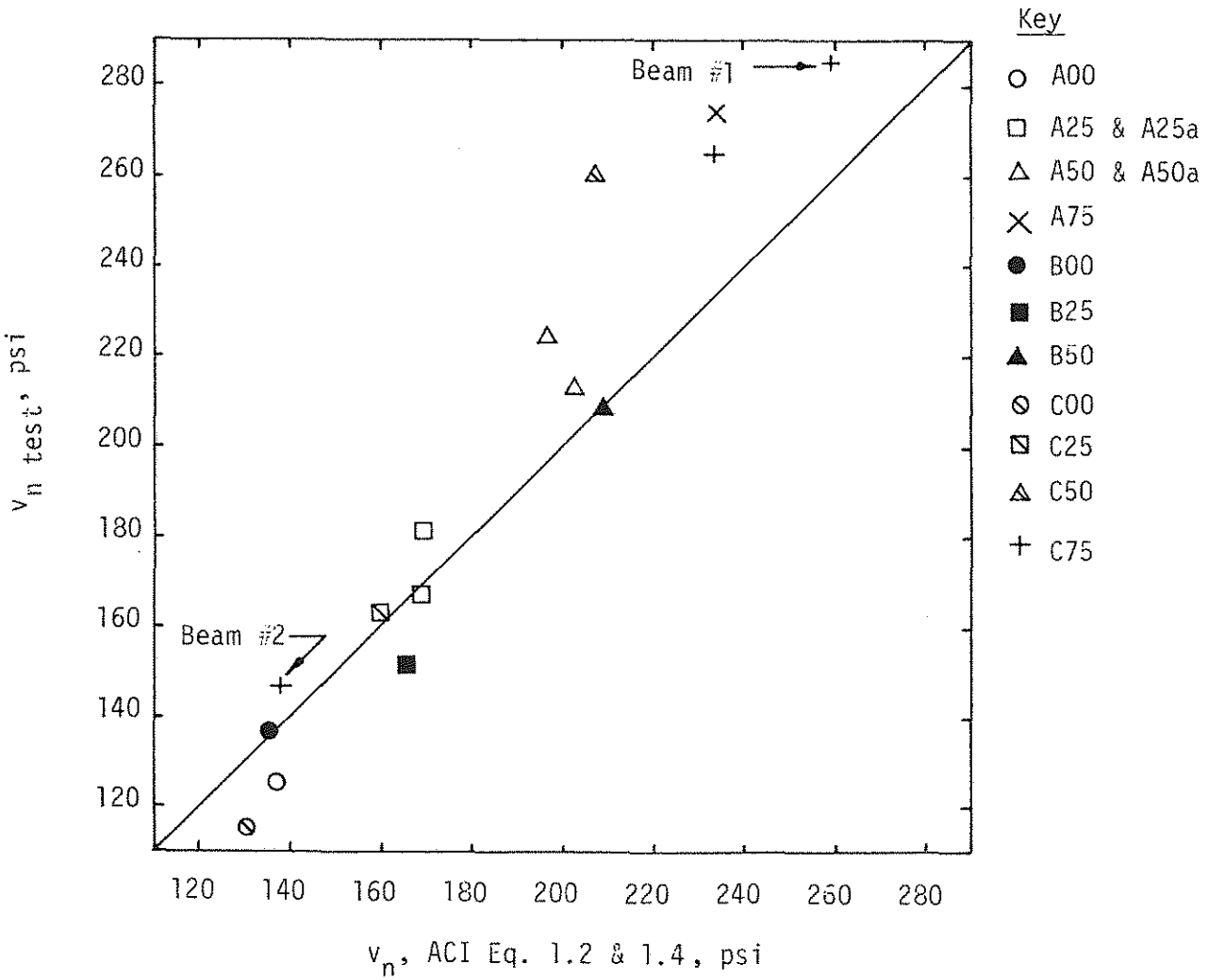

Figure 3.5 Comparison of ACI and Experimental Nominal (ultimate) Shear Stresses.

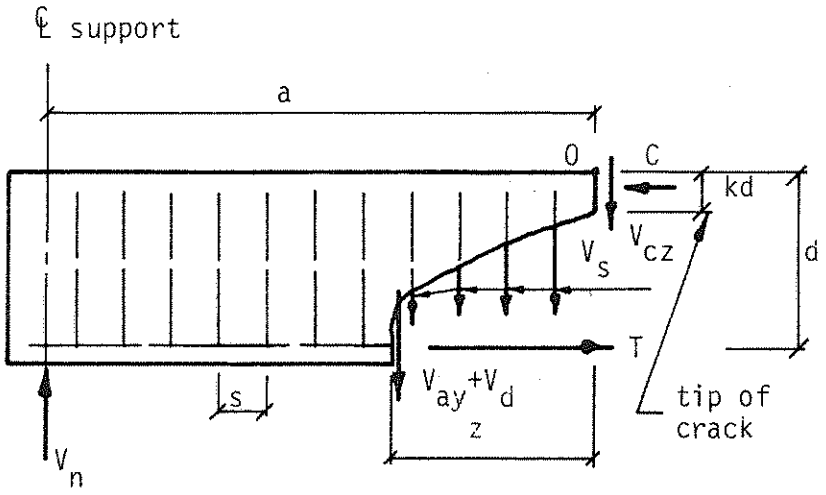

Figure 4.1 Truss Model.

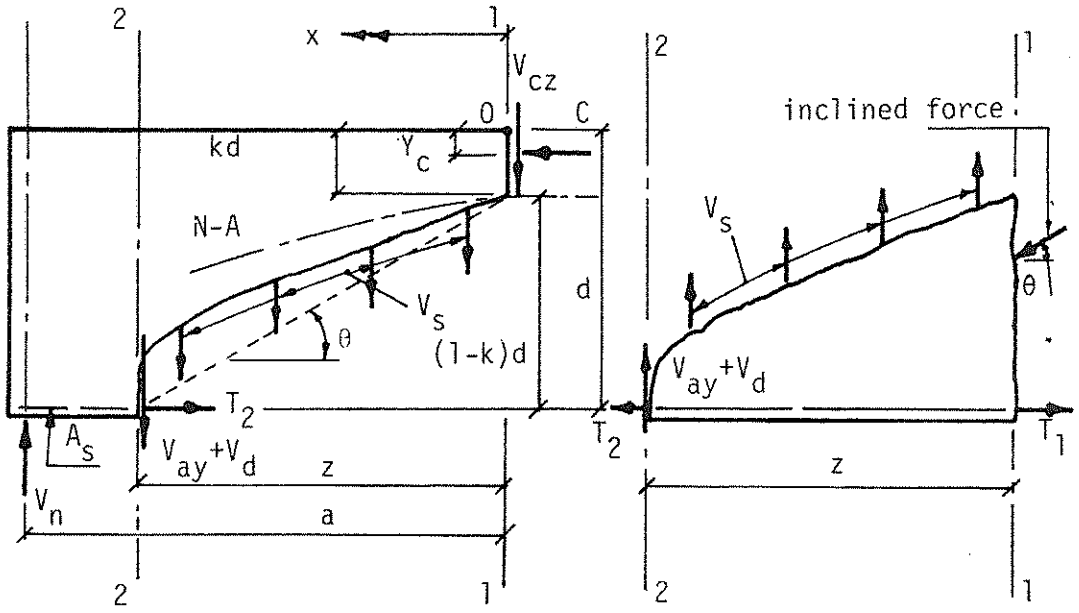

a. Beam Under Bending and Shear

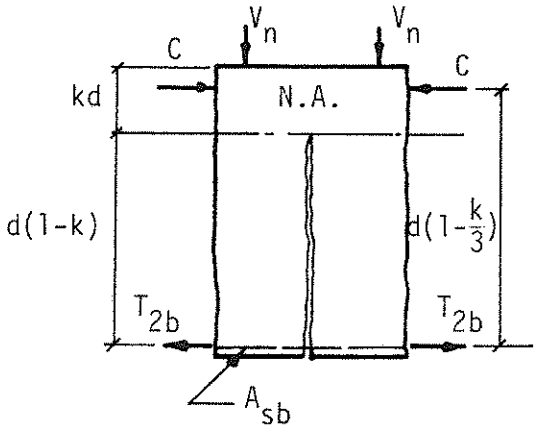

b. Beam Under Pure Bending

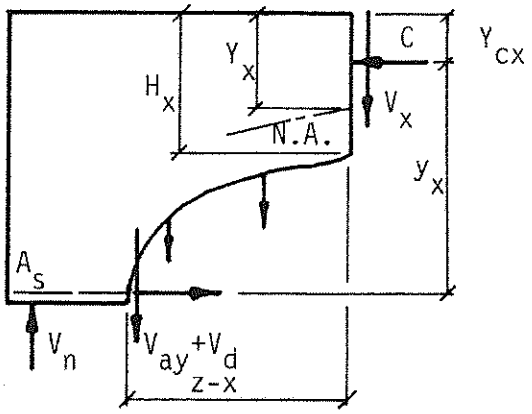

c. Section at x

Figure 4.2 Configuration of Model.

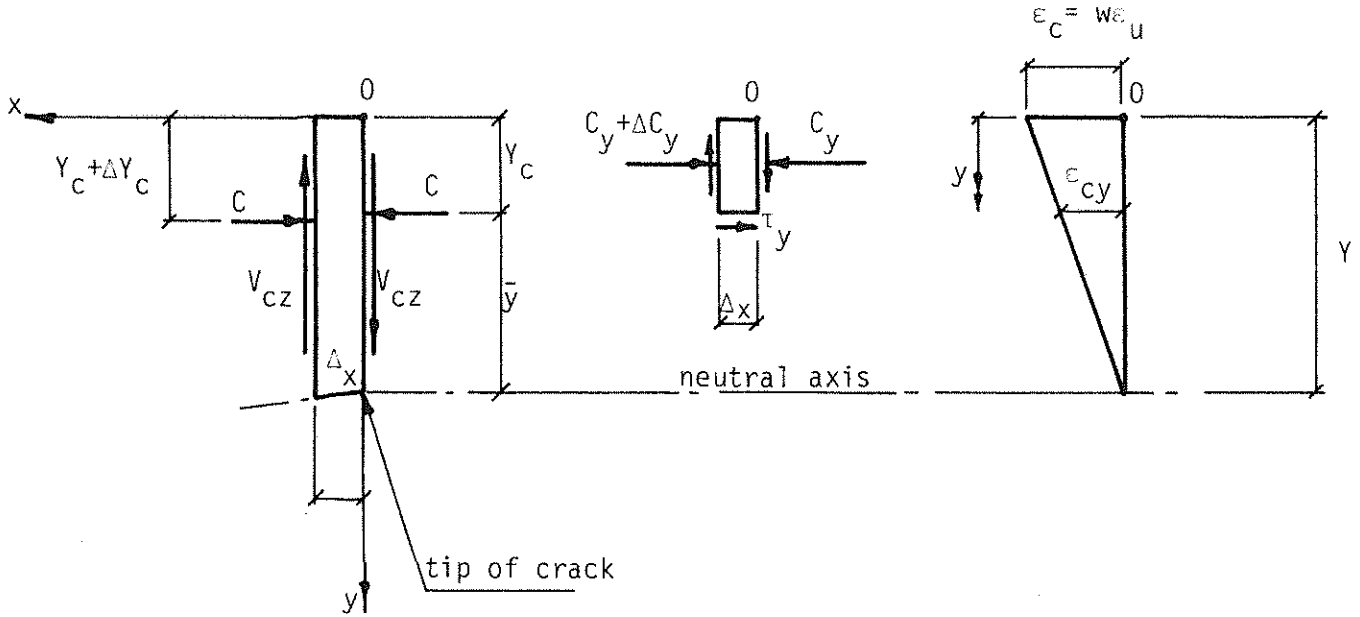

Figure 4.3 Forces and Strains in the Compression Zone.

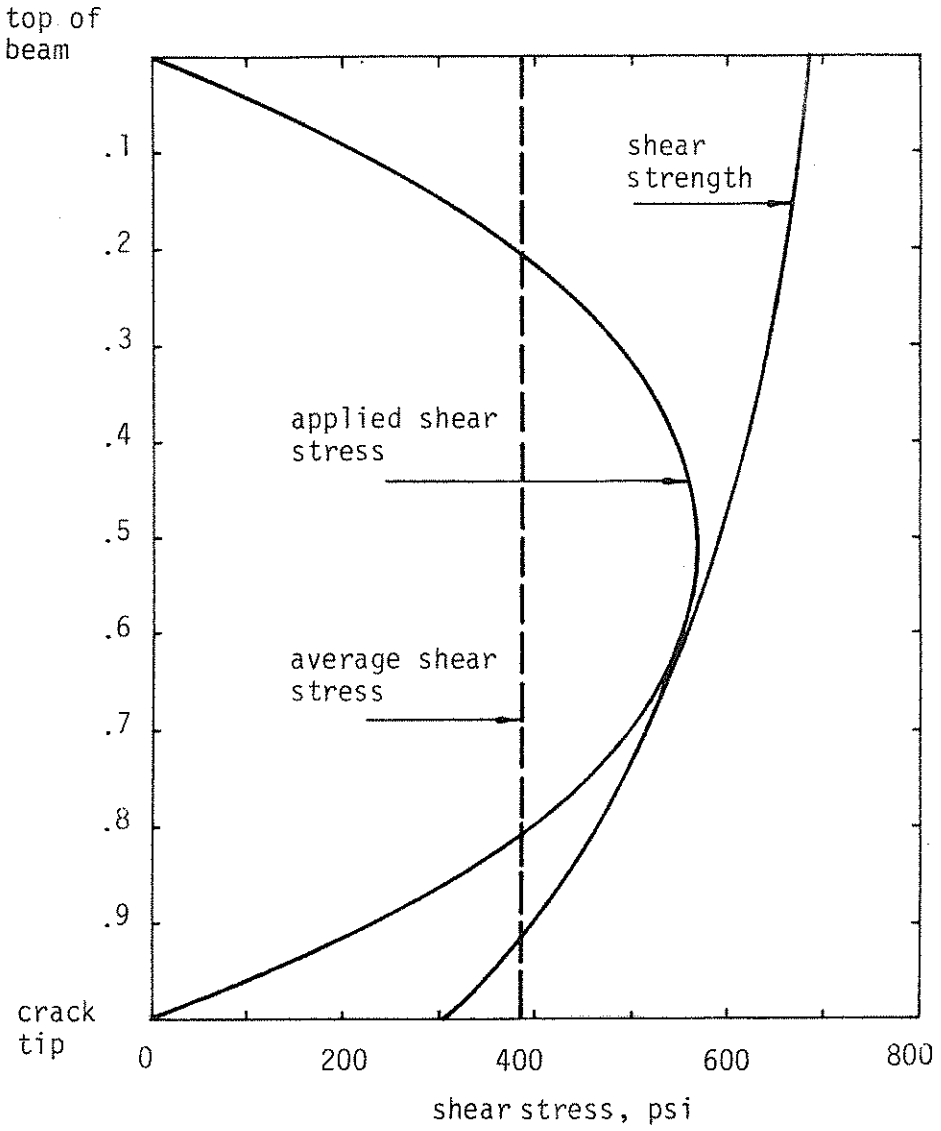

Figure 4.4 Compression Zone Shear Stress Profiles (f'_c = 4000 psi, w = .60).

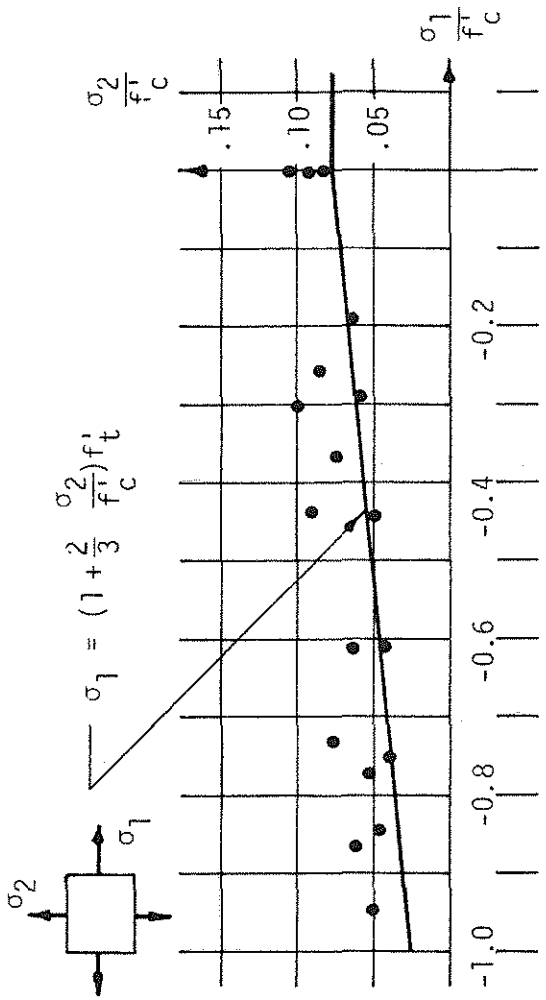

Figure 4.5 Analytical Biaxial Strength Envelope (25,26).

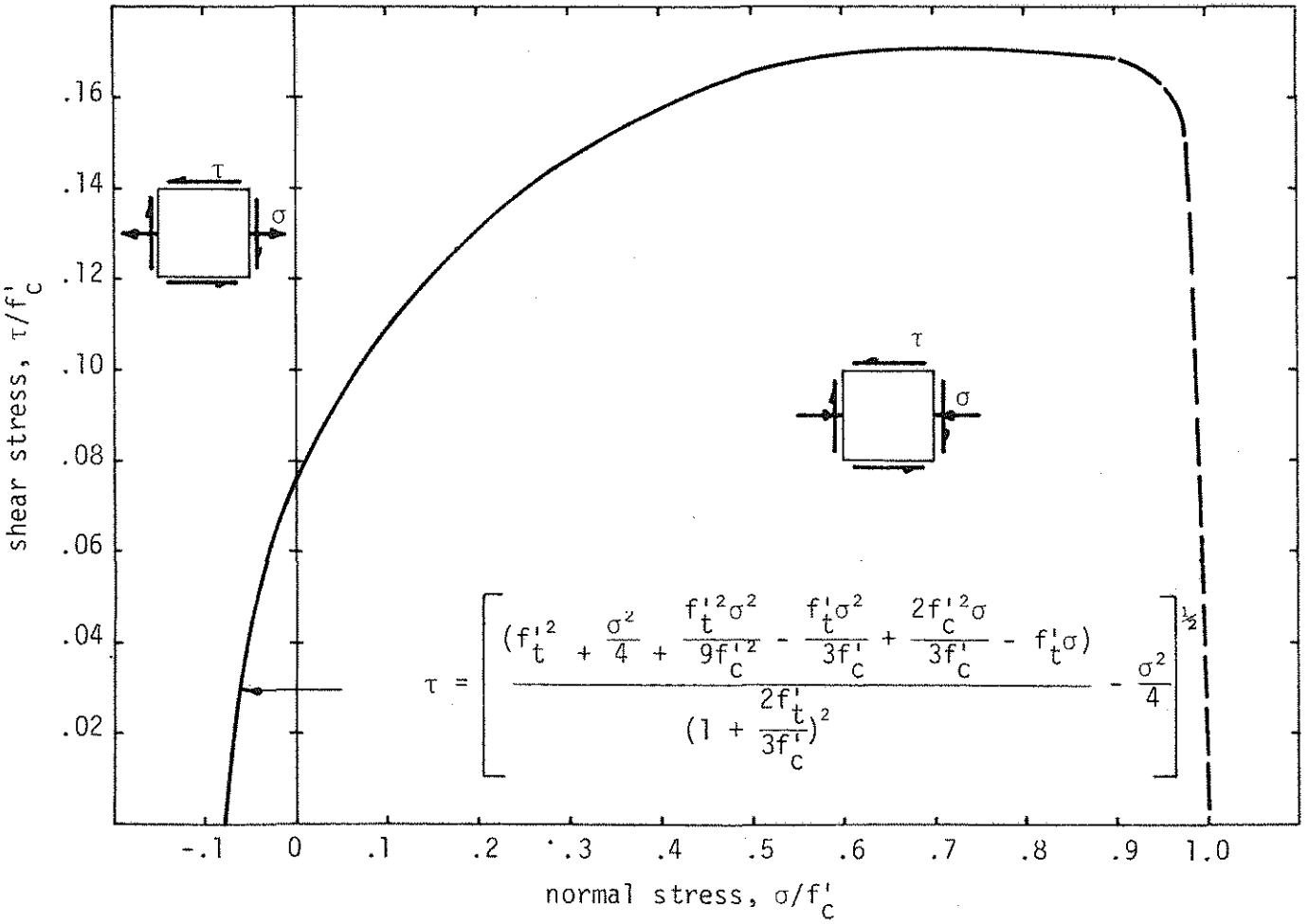

Figure 4.6 Biaxial σ-τ Stress Failure Criterion (f'_c = 4000 psi).

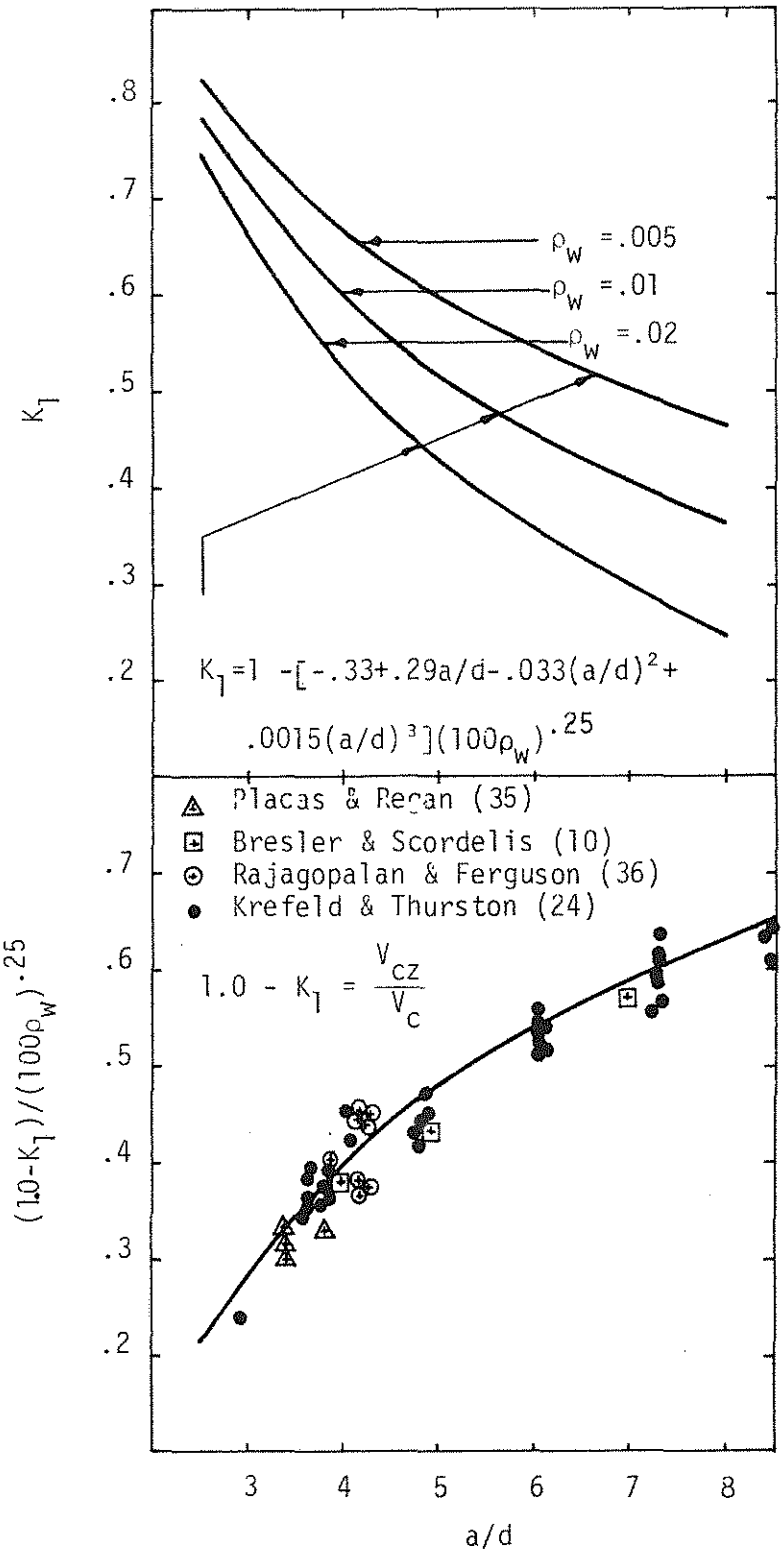

Figure 4.7 Shear Force Distribution Factor versus Shear-Span to Depth Ratios and Percentage of Longitudinal Reinforcement.

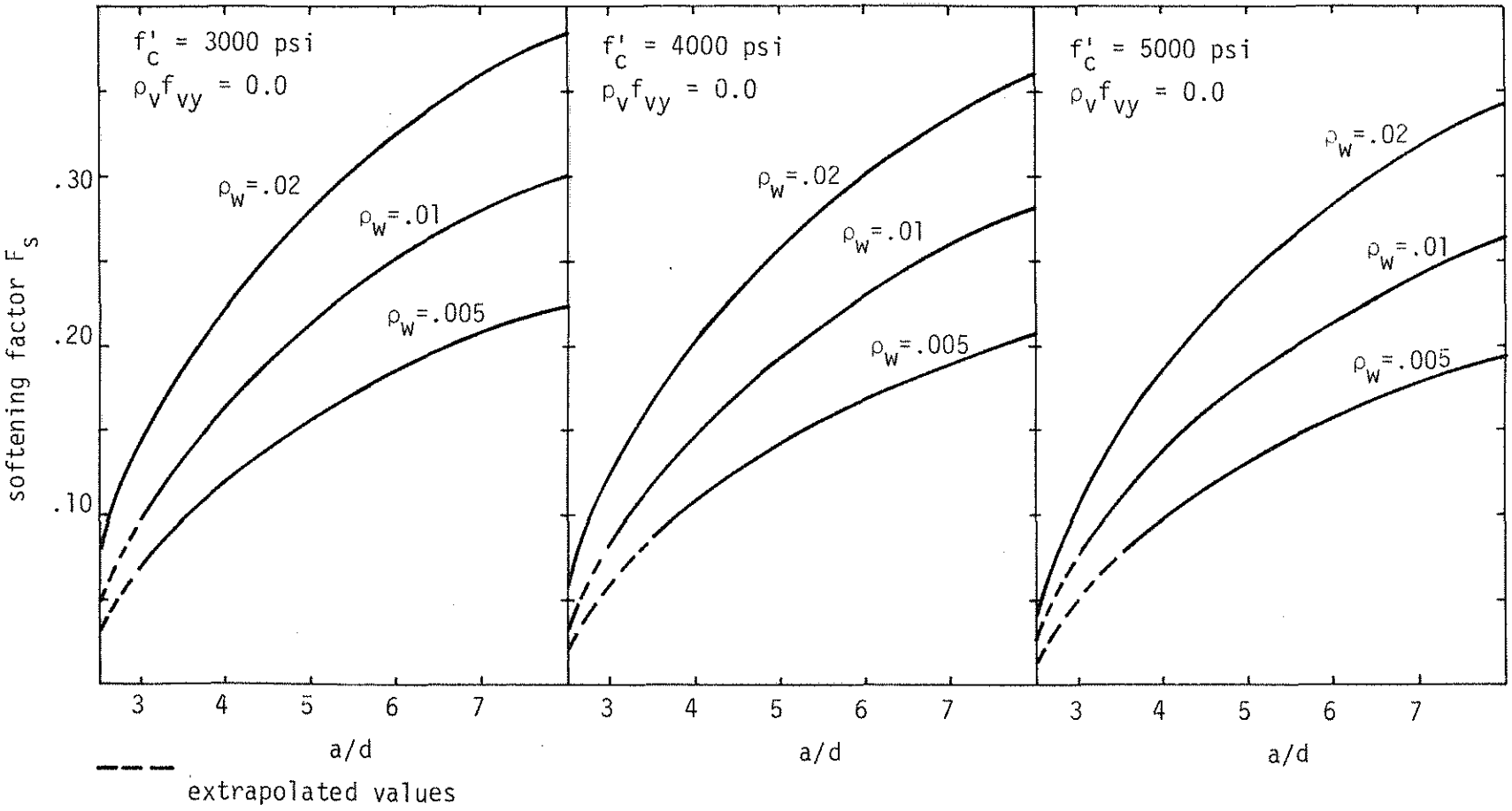

Figure 4.8 Softening Factor Versus Concrete Strength, Shear-Span to Depth Ratio, and Percentage of Longitudinal Reinforcement.

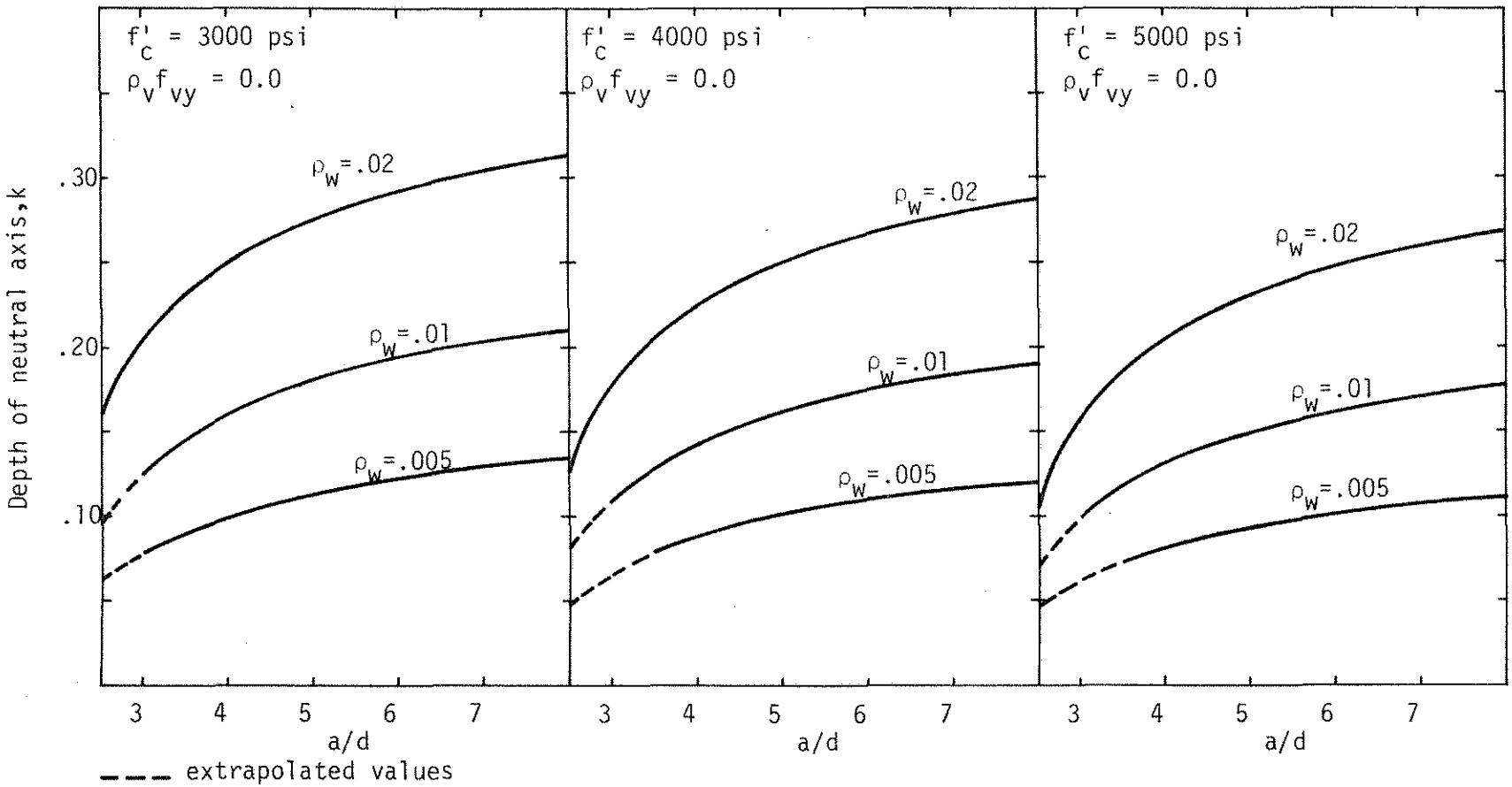

Figure 4.9 Neutral Axis Depth, k , versus Concrete Strength, Shear-Span to Depth Ratio, and Percentage of Longitudinal Reinforcement.

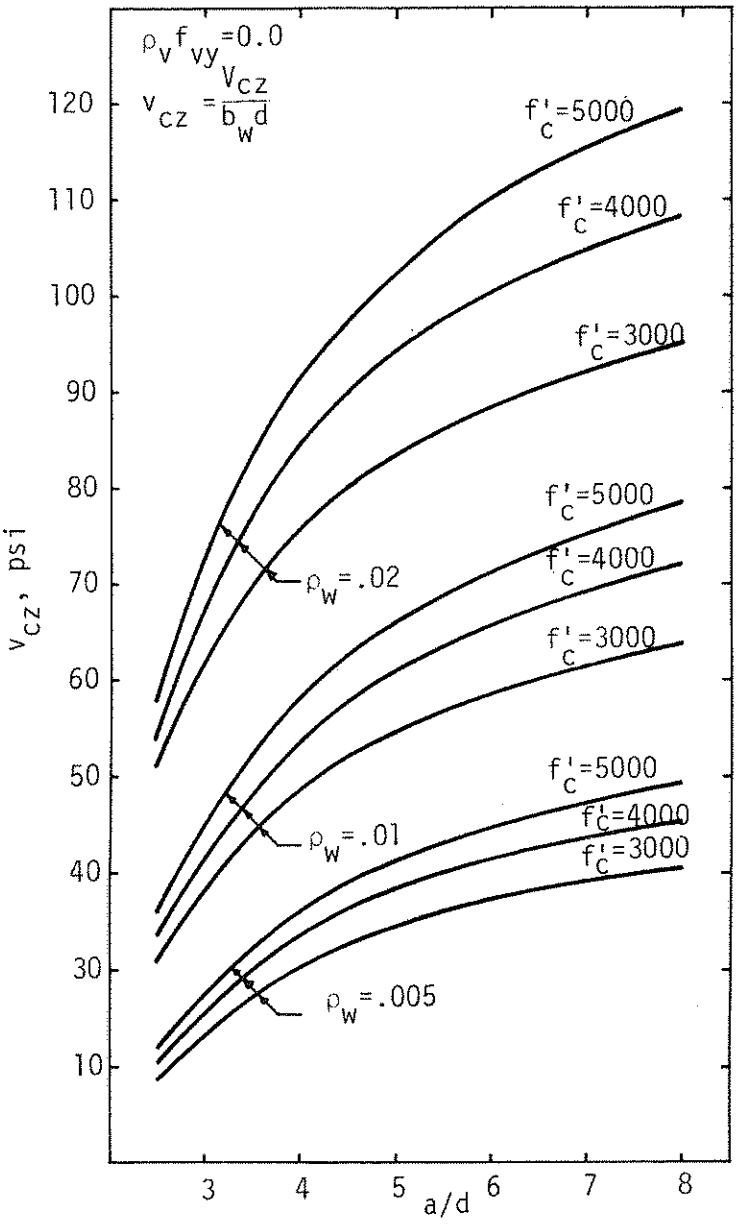

Figure 4.10 Nominal Concrete Compression Zone Shear Strength, v_{cz}, Versus Concrete Strength, Shear-Span to Depth Ratio, and Percentage of Longitudinal Reinforcement.

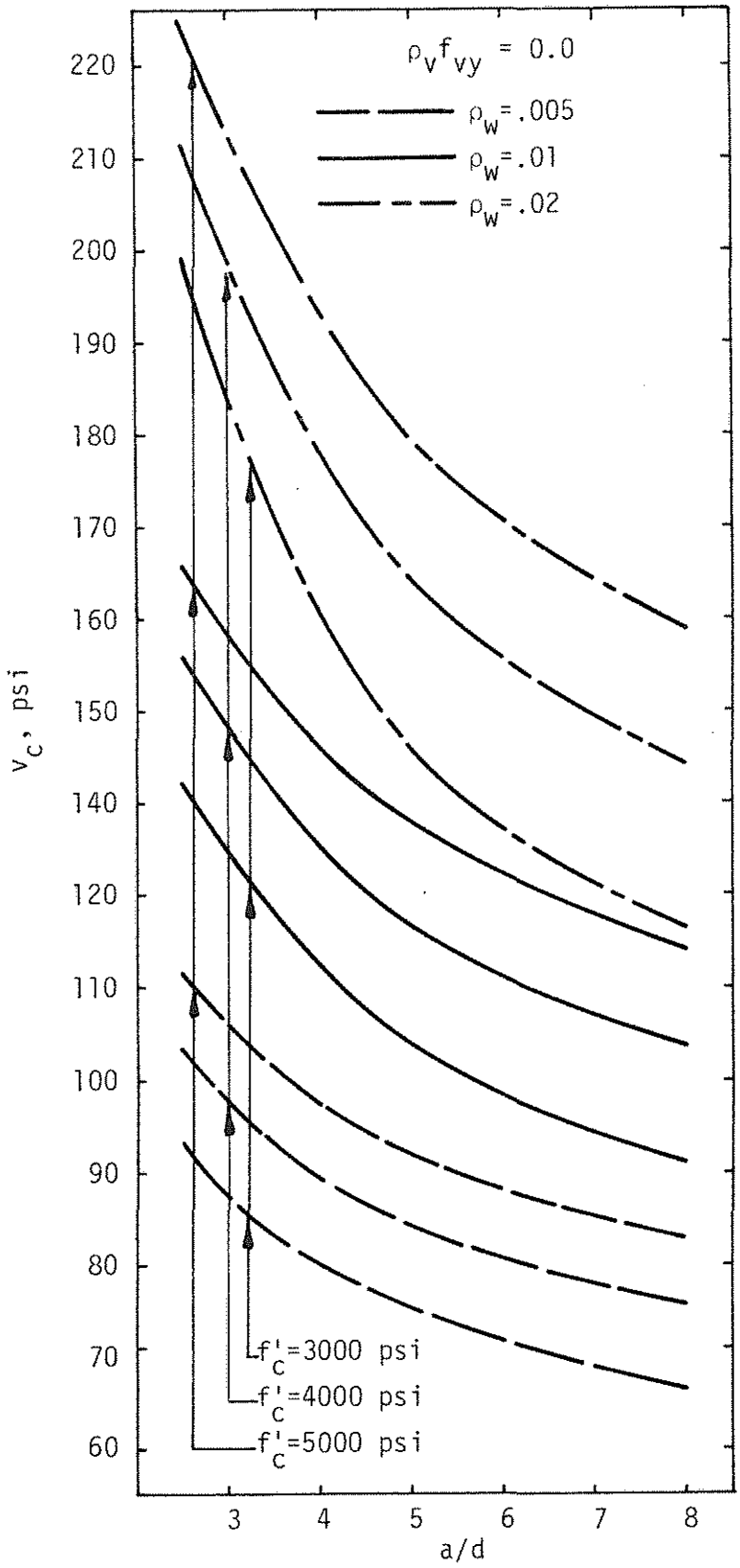

Figure 4.11 Concrete Capacity, v_c, Versus Concrete Strength, Shear-Span to Depth Ratio, and Percentage of Longitudinal Reinforcement.

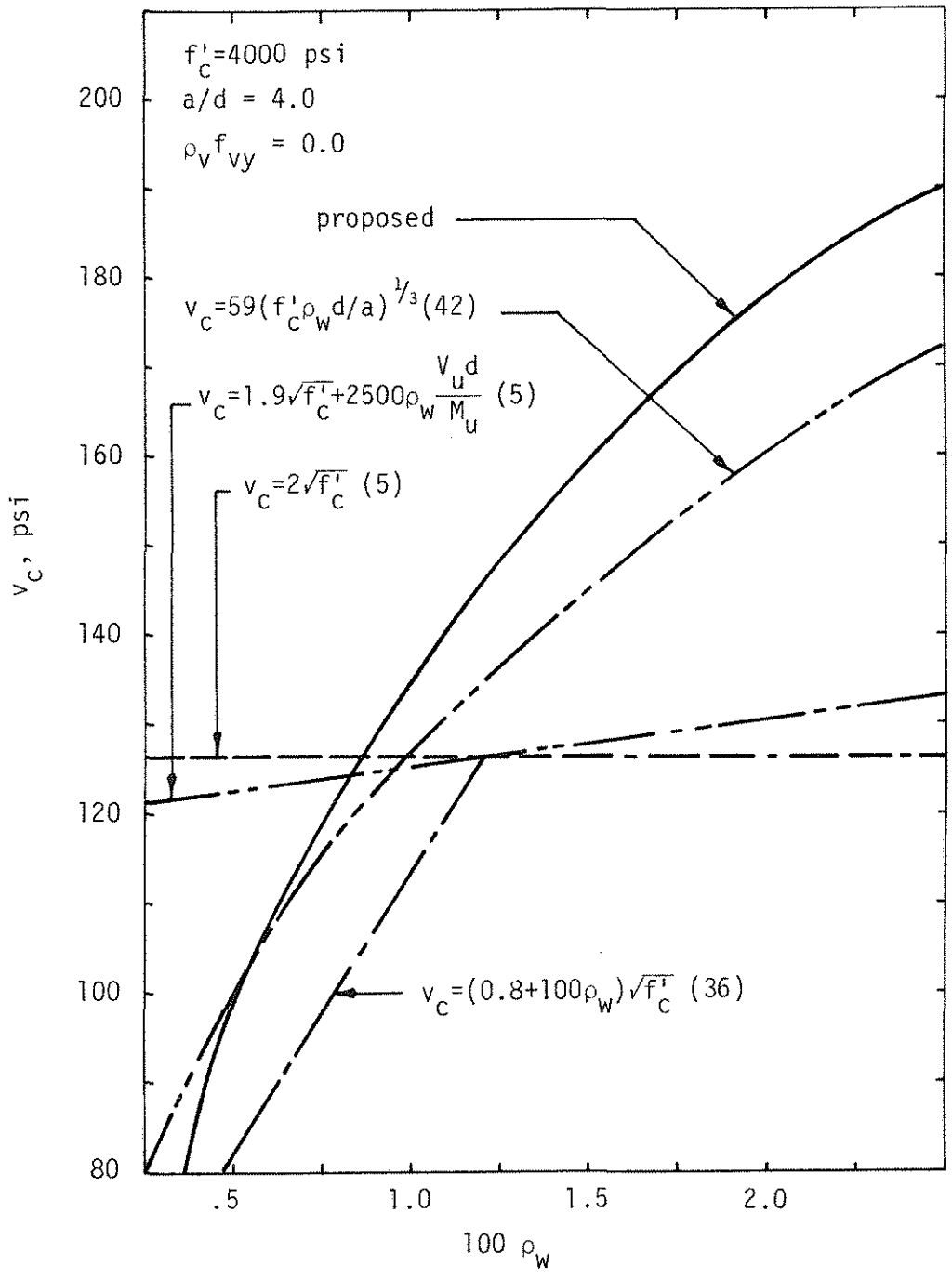

Figure 4.12 Comparison of Predicted Equations for Shear Capacity.

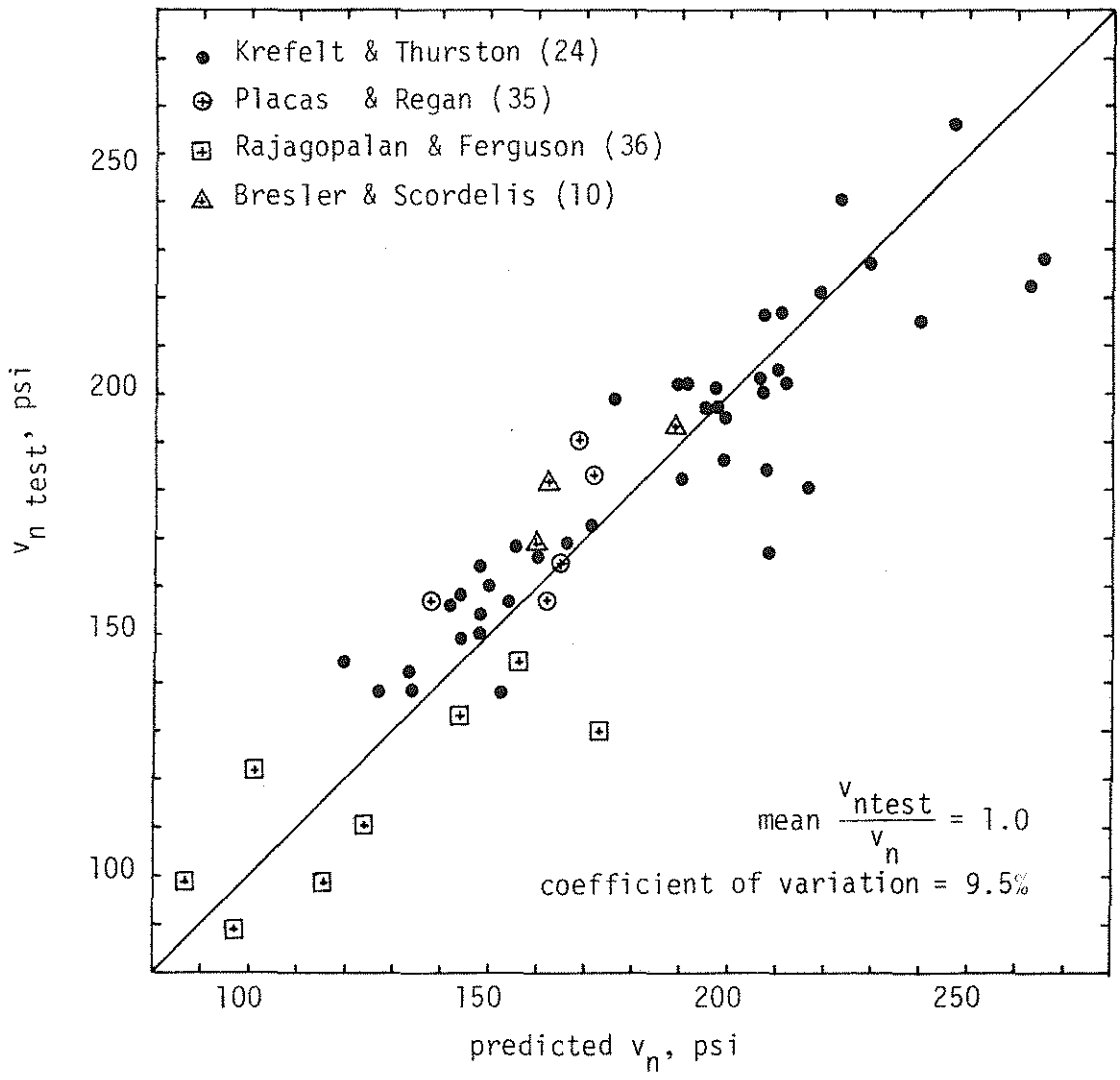

Figure 4.13 Comparison of Predicted with Experimental Shear Strengths for Rectangular Beams without Stirrups Used to Develop the Proposed Model.

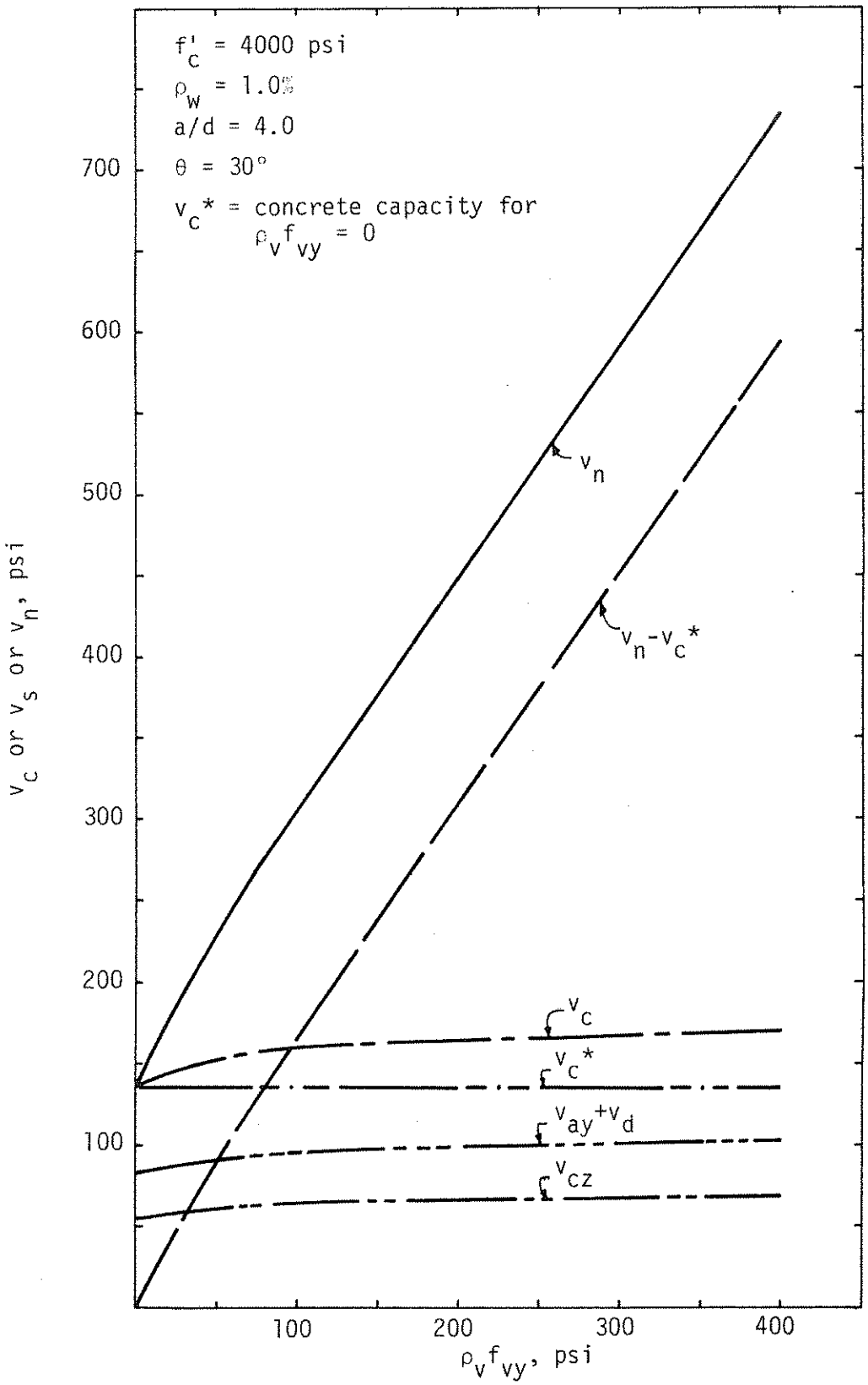

Figure 4.14 Nominal Shear Stress versus Amount of Shear Reinforcing.

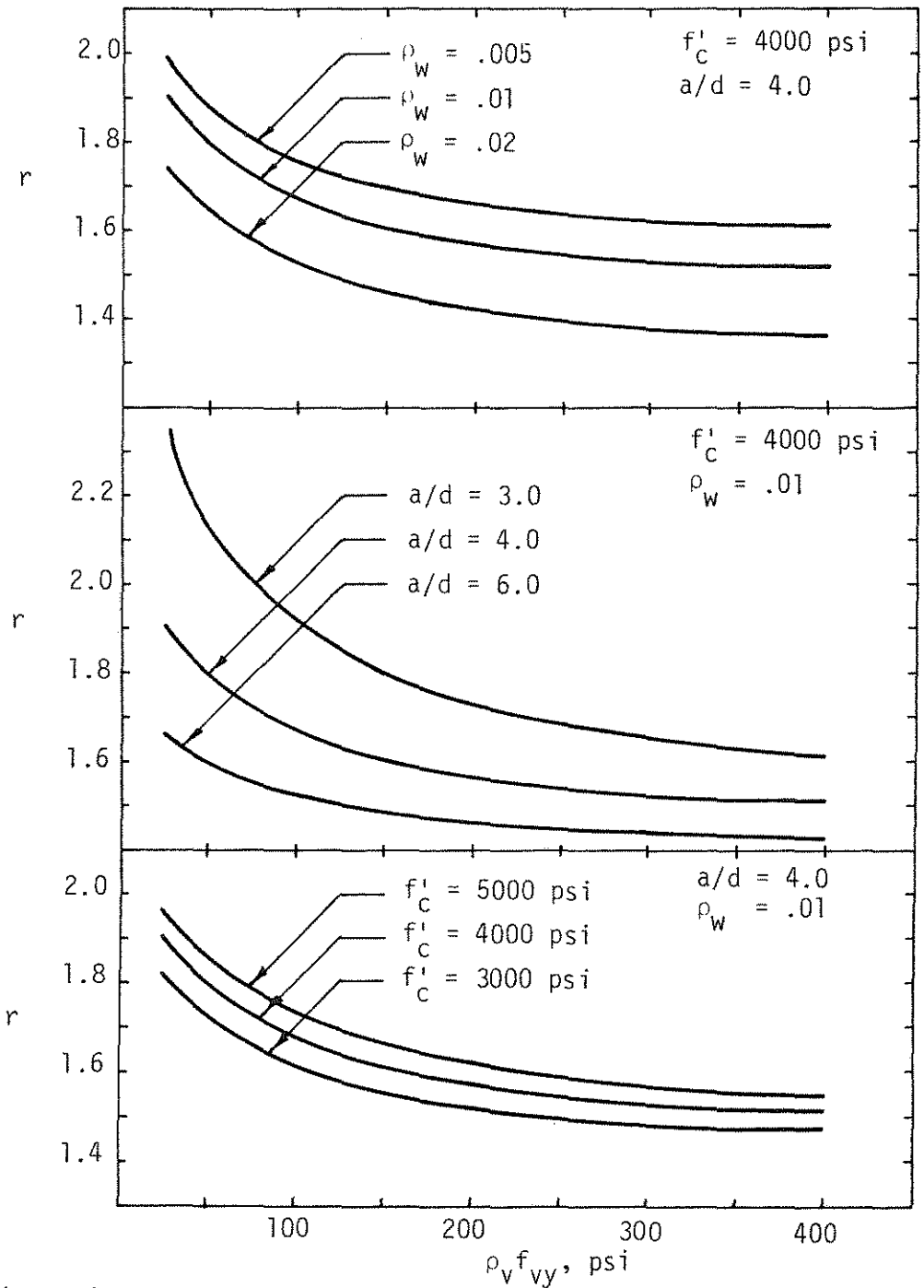

Figure 4.15 Effectiveness Factor of Shear Reinforcement, r, versus Concrete Strength, Shear-Span to Depth Ratio, and Amounts of Flexural and Shear Reinforcement.

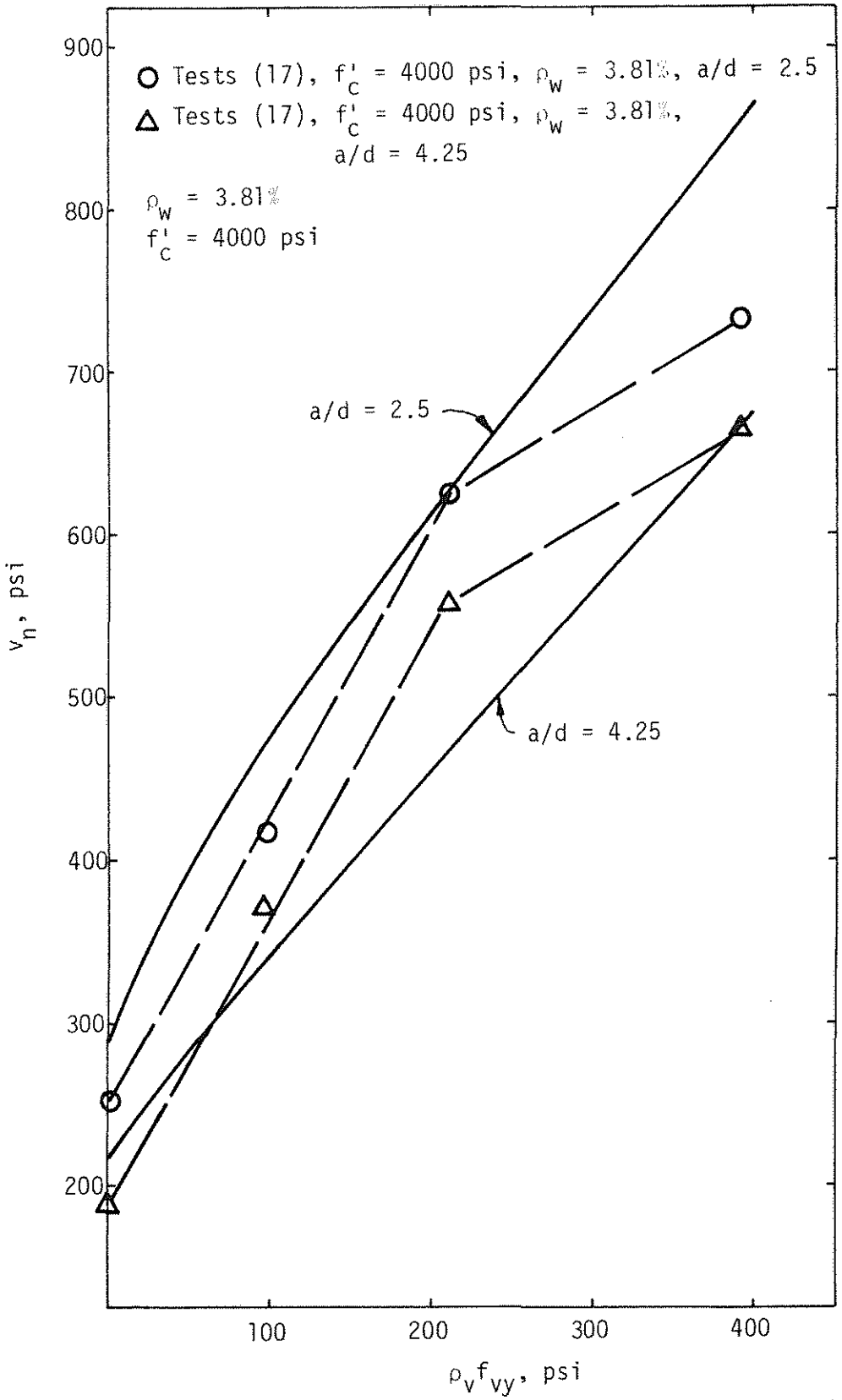

Figure 4.16 Effect of Shear-Span to Depth Ratio on Shear Capacity.

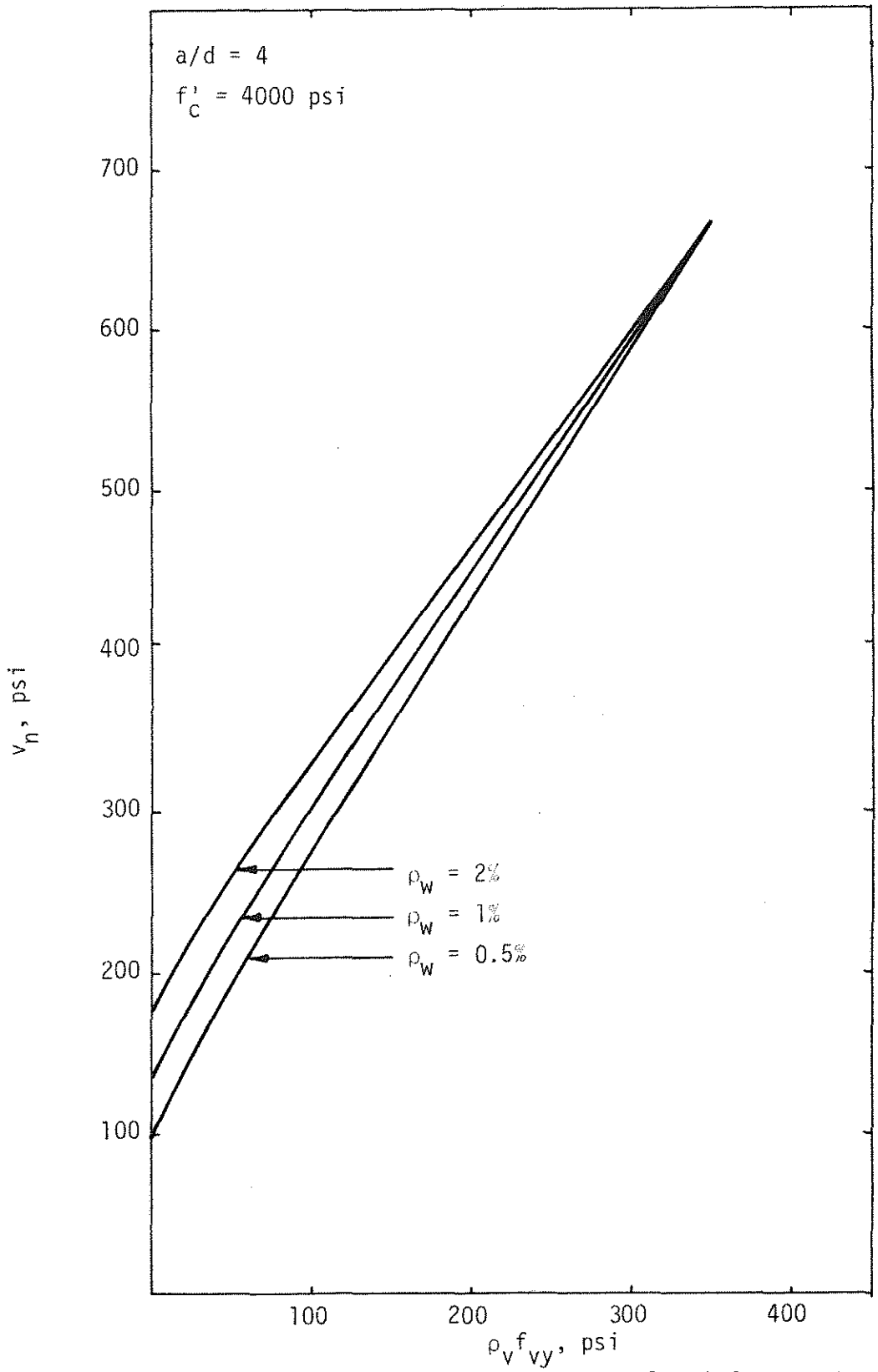

Figure 4.17 Effect of Percentage of Longitudinal Reinforcement on Shear Capacity.

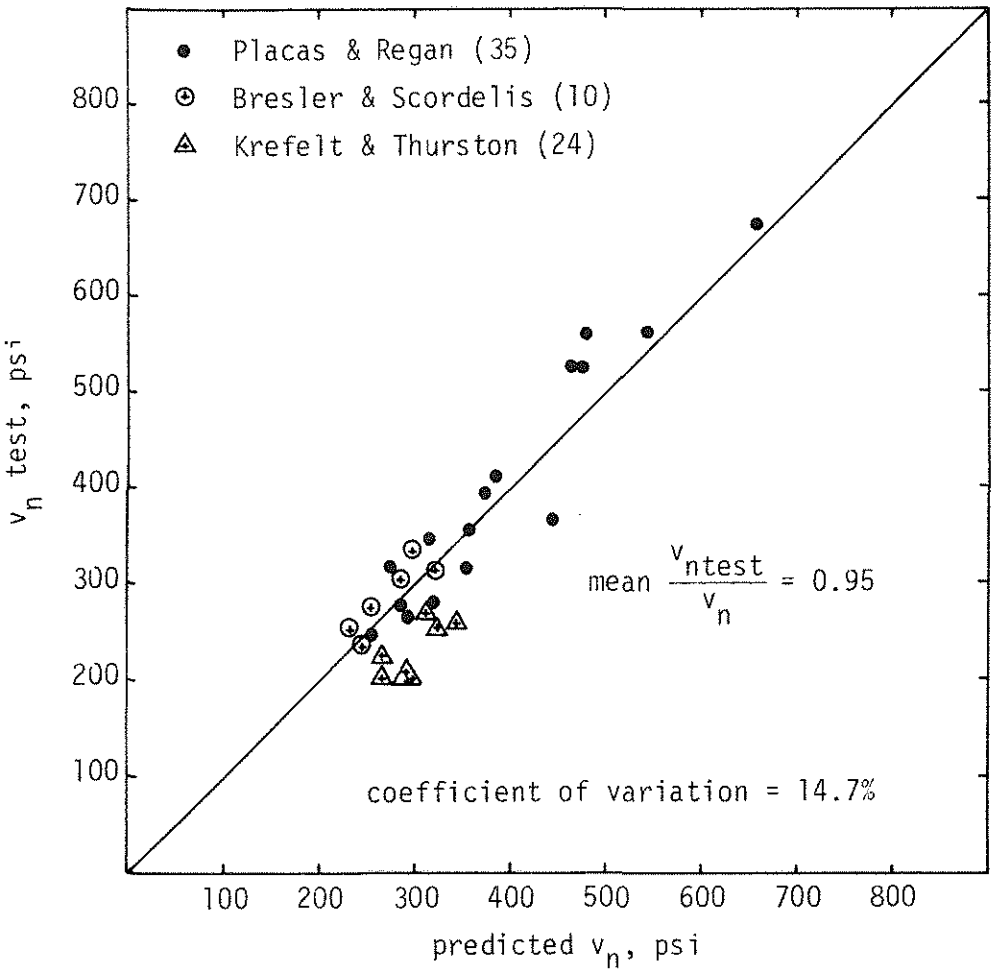

Figure 4.18 Comparison of Predicted and Experimental Nominal Shear Stress for Rectangular Beams with Stirrups.

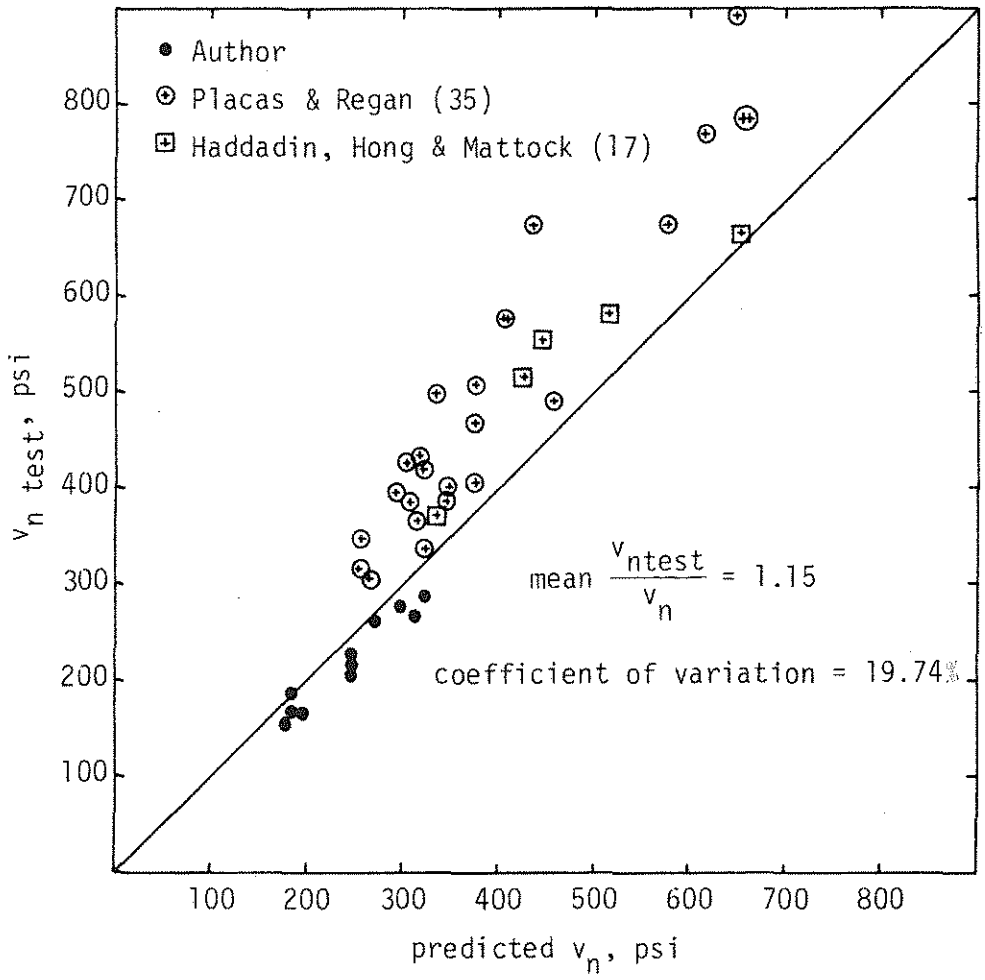

Figure 4.19 Comparison of Predicted and Experimental Nominal Shear Stress for T-Beams with Stirrups.

APPENDIX A

NOMENCLATURE

A_s	area of longitudinal reinforcement
A_{sb}	area of longitudinal reinforcement in equivalent beam under pure bending that produces neutral axis location equivalent to neutral axis in beam under bending and shear
A_v	area of shear reinforcement
a	shear-span
b_w	width of a rectangular beam or web width of a T-beam
C	compression force in the concrete
C_y	resultant of normal stresses for a depth y from the top of the beam
d	effective depth of beam
E_c	modulus of elasticity of concrete ($E_c = 57{,}000\sqrt{f'_c}$)
E_s	modulus of elasticity of steel
F_s	geometric and shear softening factor
f'_c	concrete cylinder strength
f_{cy}	concrete compression stress at a distance y from the top of the beam
f_r	modulus of rupture of the concrete
f'_t	tensile strength of the concrete ($f'_t = 5\sqrt{f'_c}$, assumed)
f_{vy}	yield stress of shear reinforcement
H_x	depth of concrete compression zone at section x
jd	internal moment arm
k	ratio of compression zone to effective depth
kd	depth of concrete compression zone at plane 1-1
K_1	ratio of dowel plus interface shear to total concrete shear ($K_1 = (V_d + V_{ay})/V_c$)
K_2	ratio of shear carried by stirrups to nominal shear ($K_2 = V_s/V_c$)

K_3 variable coefficient

M applied moment

M_u applied moment

M_b moment for the pure bending case

M_x applied moment at section x

n modular ratio ($n = E_s/E_c$)

R_b design cube strength

r effectiveness factor of shear reinforcement ($r = \frac{v_n - v_c}{\rho_v f_{vy}}$)

s stirrup spacing along the axis of beam

$T_i, i=1,2$ tension force in the longitudinal reinforcement at section i

T_{2b} tension force in the longitudinal reinforcement in the pure bending case

V applied shear

V_{ay} interface shear capacity (vertical component of aggregate interlock)

V_c shear carried by the concrete ($V_c = V_{cz} + V_{ay} + V_d$)

V_{cz} shear carried by the concrete compression zone

V_d shear carried by the dowel action of longitudinal reinforcement

V_n nominal (ultimate) shear capacity

$V_{n\ test}$ experimental ultimate shear capacity

V_s shear carried by the shear reinforcement

V_u applied shear

v nominal shear stress

v_{ay} interface shear stress

v_c shear cracking stress (diagonal tension cracking stress)

v_{cz} compression zone "stress" ($v_{cz} = \frac{V_{cz}}{b_w d}$)

v_c^* shear cracking stress for beams without stirrups

$v_{c\,test}$ experimental shear cracking stress

v_d dowel shear stress

v_n nominal ultimate shear stress

$v_{n\,test}$ experimental ultimate shear stress

v_s shear stress carried by the shear reinforcement

w compression strain ratio ($w = \frac{\varepsilon_c}{\varepsilon_u}$)

x distance from plane 1-1 along the longitudinal axis of the beam

Y distance to the neutral axis from the top of the beam

Y_c distance of point of application of resultant, C, from the extreme compressive fiber of the beam at plane 1-1

Y_{cx} distance of point of application of resultant, C, from the extreme compressive fiber of the beam at section x

Y_x distance of neutral axis from the extreme compressive fiber of the beam at section x

y distance from the extreme compressive fiber of the beam

$\bar{y}$ distance of point of application of resultant, C, from the neutral axis

y_x distance of point of application of resultant, C, to the level of flexural reinforcement at section x

z horizontal shear crack projection

α inclination of web reinforcement to longitudinal axis

Δ_s total elongation of longitudinal reinforcement between sections 1-1 and 2-2

ε_c strain in extreme compressive fiber of concrete

ε_{cx} strain in the extreme compressive fiber of the concrete at section x

ε_{cy} strain in concrete at a distance y from the top of the beam

ε_{s2} strain in the longitudinal reinforcement at section 2-2.

ε_{sav} average strain in the longitudinal reinforcement

ε_{sx} strain at the level of the flexural reinforcement at location x

θ inclination of inclined crack

ρ_v ratio of shear reinforcement ($\rho_v = \frac{A_v}{b_w s}$)

ρ_w percentage of longitudinal reinforcement ($\rho_w = \frac{A_s}{b_w d}$)

σ normal applied compressive stress in the concrete

σ_1 principal tensile stress

σ_2 principal compressive stress

τ failure shear stress of the concrete

τ_{av} average shear stress within compression zone at failure

τ_y shear stress at a distance y from the top of the beam

ϕ strength reduction factor (from ACI)

APPENDIX B

STRAIN GAGE INFORMATION

The type and size of the strain gage used in this investigation are shown in Table B.1.

2.4 inch paper backed gages supplied by the Precision Measurement Co. were used to measure concrete strain in all beams except Beams #1 and #2. 1.0 inch paper backed gages supplied by BLH Electronics were used for Beams #1 and #2. The steps of the concrete gage installation were: smoothing the concrete surface with a grinding wheel, bonding the gage to the concrete with Duco cement, and protecting the gage with a layer of Duco cement.

0.03 inch foil gages were used to measure steel strain. This small size was selected in order to make installation possible on the smallest diameter stirrup used (0.132 inches). The steps of foil gage installation were: cleaning and preparing the specimen surface, bonding the gage to the steel surface and waterproofing. All material used for the foil gage installation was supplied by the Micro-Measurements Co. The surface preparation materials were M-Prep Conditioner A and M-Prep Neutralizer 5. The bonding media consisted of M-Bond 200 catalyst and M-Bond 200 adhesive. The waterproofing coat was M-Coat G. For additional information on the material used and detailed information on the procedure of installation of the foil gages see References 28 and 29.

Table B.1 STRAIN GAGES

Beam	Steel Gages Type	Steel Gages Manufacturer*	Concrete Gages Type	Concrete Gages Manufacturer*
#2	FAE-03J-12-S6EL	BLH	A-12	BLH
A00	EA-06-031DE-120	MM	W-240	PM
A25	"	"	"	"
A25a	FAE-031-12-S6EL	BLH	"	"
A50	EA-06-031DE-120	MM	"	"
A50a	FAE-03J-12-S6EL	BLH	"	"
A75	EA-06-031DE-120	MM	"	"
#1	"	"	A-12	BLH
B00	"	"	W-240	PM
B25	FAE-03J-12-S6EL	BLH	"	"
B50	"	"	"	"
C00	"	"	"	"
C25	"	"	"	"
C50	"	"	"	"
C75	"	"	"	"

* BLH = BLH Electronics, Waltham, Mass.
PM = Precision Measurement Co., Ann Arbor, Michigan
MM = Micro-Measurements Co., Raleigh, North Carolina